

Loughborough University

Developing a Dual- Layer System for the Mitigation of Tin Whiskers

PhD Thesis

Dan Haspel

Acknowledgments

I would like to thank Dr Mark Ashworth for his invaluable advice and help throughout my PhD and for generally putting up with me. I would also like to thank my supervisors Prof. Geoff Wilcox, Dr Xujin Bao and Prof. Roger Mortimer for their support and knowledge.

Abstract

There are very few studies that have investigated directly the effect of an oxide film on tin whisker growth, since the 'cracked oxide theory' was proposed by Tu in 1994 ¹. The current work has investigated the effect of using an electrochemically formed oxide and both a molybdate conversion coating and a tungstate conversion coating on tin whisker growth from Sn-Cu electrodeposits on Cu, and compared it with that from a native air-formed oxide. X-ray photoelectron spectroscopy (XPS) has been used to investigate the effect of coating parameters on the thickness and composition of the oxide film. The XPS studies show that the oxide film formed using either of the conversion coating baths was significantly thicker than that produced from the potassium bicarbonate-potassium carbonate bath. Initial observations suggest that both the tungstate-based conversion coatings and the molybdate-based conversion coatings significantly reduced whisker growth by over 80 %, compared with a native air-formed oxide, and provide improved whisker mitigation compared with the electrochemically formed oxides.

The current work has also investigated the potential of using a dual-layer system, comprised of both an electrochemically formed oxide bottom layer and an acrylic conformal coating top layer, for the mitigation of tin whisker growth. The electrochemically formed oxide used in the dual-layer system was produced at 2 V vs. Ag/AgCl while passing a charge of 60 mC cm⁻² and the thickness of the conformal coating was aimed to be between ~5 μm to ~6 μm. This thickness was chosen to enable the study of whisker growth on a shorter time scale and to study the effect the electrochemically formed oxide had when used in conjunction. Initial observations showed that the dual-layer system provided improved whisker mitigation compared with both the electrochemically formed oxides and acrylic conformal coatings when used singularly.

As part of the self-healing work, nanocapsules filled with the reactive agent were needed to be synthesised and the compatibility of them with different solvents needed to be studied. Capsules filled

with the reactive agent were successfully synthesised, however, it was found that the capsules agglomerated and the size of the capsules, in some instances, were too large to be incorporated into a thin conformal coating. Regardless, the capsules were still analysed to check the compatibility with different solvents, to identify a suitable conformal coating mixture that would not dissolve the polymer shell of the capsules. It was observed that the capsules were stable in three out of the five solvents that were analysed, them being isopropanol (IPA), butanone and methylcyclohexane.

Abbreviations

at.%	Atomic Percent
ALD	Atomic Layer Deposition
BE	Binding Energy
CTAB	Hexadecyltrimethylammonium Bromide
CTE	Coefficient of Thermal Expansion
CV	Cyclic Voltammetry
CVD	Chemical Vapour Deposition
DCPD	Dicyclopentadiene
DNT	Dinitrotoluene
DWV	Dielectric Withstanding Voltage
EBS	Electron Back-Scatter Diffraction
EDX/EDS	Energy-Dispersive X-ray Spectroscopy
EMA	Poly(ethylene-alt-maleic anhydride)
EU	European Union
FEGSEM	Field Emission Gun Scanning Electron Microscope
FE-SEM	Field Emission Scanning Electron Microscope
FIB	Focussed Ion Beam
GPTMS	Glycidoxypropyltrimethoxysilane
iCVD	Initiated Chemical Vapour Deposition
IMC	Intermetallic Compound
IPA	Isopropyl Alcohol (Isopropanol)
IPC	Formally known as Institute for Printed Circuits
IPF	Inverse Pole Figure
M (in equations)	Metal

MDI	Methylene Diphenyl Diisocyanate
NASA	National Aeronautics and Space Administration
NMB	Nitromethylbenzene
oCVD	Oxidative Chemical Vapour Deposition
PEDOT	Poly(3,4-ethyenedioxythiophene)
PFOS	Perfluorooctane Sulfonyl Fluoride
piCVD	Photo-initiated Chemical Vapour Deposition
PTFE	Polytetrafluoroethylene (Teflon)
SCE	Saturated Calomel Electrode
SE	Secondary Electron
SEM	Scanning Electron Microscope
S.G.	Specific Gravity
Sn _{met}	Metallic tin
Sn _{ox}	Tin in its oxidised state
TBAF	Tetrabutylammonium Fluoride
TDI	Toluene Diisocyanate
TEOS	Tetraethyl Orthosilicate
TFMG	Thin Film Metallic Glass
R	An organic functional group
RH	Relative Humidity
RoHS	Restriction of Hazardous Substances
TDI	Toluene Diisocyanate
UV	Ultraviolet
VOC	Volatile Organic Compound
wt. %	Weight Percent
XPS	X-ray Photoelectron Spectroscopy

Contents

Acknowledgments	i
Abstract	ii
Abbreviations	iv
Contents	vi
1 Introduction	1
1.1 Post-Electroplating Surface Treatments.....	2
1.2 Self-Healing Polymers.....	3
1.3 Dual-Layer Development.....	4
2 Literature Survey	6
2.1 Tin Whiskers	6
2.1.1 An Introduction to Failure Mechanisms	6
2.1.2 A Brief Introduction to Some Growth Mechanisms	8
2.1.2.1 Stresses – internal and external	8
2.1.2.2 Formation of intermetallic compounds and the interdiffusion between coating and substrate	9
2.1.2.3 Grain size	12
2.1.2.4 Grain shape.....	12
2.1.2.5 Surface oxide	13
2.1.2.6 Tin alloys	14
2.1.2.7 Corrosion induced whisker formation	16
2.1.3 Mitigation Techniques	18
2.1.3.1 Selecting a different type of electroplated tin finish.....	18
2.1.3.2 Depositing a layer between the deposited tin and the substrate	18
2.1.3.3 Thickness of the deposit	19
2.1.3.4 Annealing	19
2.1.3.5 Conformal coatings.....	20
2.1.3.6 Changing the electrolyte used	21
2.1.3.7 Surface treatment (both substrate and electroplated surfaces).....	21
2.1.3.8 Electrochemically formed oxide	21
2.1.3.9 Tin alloys	22

2.2 Electrodeposition of Tin & Tin Alloys	23
2.2.1 Effects of Operating Parameters	24
2.2.1.1 Agitation	24
2.2.1.2 Current density	25
2.2.1.3 Metal ion concentration	26
2.2.1.4 Changing the pH level of the electrolyte	26
2.2.2 Cathode Current Efficiency	26
2.2.3 Forming Hydrogen Gas and the Effects	27
2.2.4 Tin Electrodeposition on Brass	27
2.2.5 Tin-Copper Electrodeposition on Copper	28
2.3 Electrochemical and Naturally Grown Oxides	28
2.3.1 Natural oxide	29
2.3.2 Electrochemically formed oxide	30
2.3.3 Tin oxidation states	30
2.3.4 Cyclic Voltammetry	30
2.4 Conversion Coatings	33
2.4.1 A Brief Background of Molybdate Conversion Coatings	34
2.4.2 A Brief Background of Tungstate Conversion Coatings	34
2.5 Polymeric Coatings	35
2.5.1 A Brief Background of Conformal Coatings in Industry	35
2.5.2 Adhesion	36
2.5.2.1 Adhesion Promoters	37
2.5.3 Application Methods	38
2.5.3.1 Physical Application Methods	38
2.5.3.2 Electrodeposition Application Methods	43
2.5.3.3 Vacuum Deposition	49
2.5.4 Conformal Coatings in the Electronics Industry	52
2.5.4.1 Types of Conformal Coatings	53
2.5.4.2 Required Film Properties	64
2.5.5 Current Practice for Mitigating Whiskers	66
2.5.5.1 Conformal Coatings Used for the Mitigation of Whiskers	66
2.6 Self-healing Coatings	68
2.6.1 Brief Introduction into Self-Healing Coatings	68
2.6.1.1 Concept and Classification of Self-Healing Materials	68

2.6.1.2 Principles of Self-Healing: Physical and Chemical	69
2.6.1.3 Bio-Inspiration	71
2.6.2 Encapsulation Self-Healing	73
2.7 Previous Work	74
2.8 Summary.....	75
3 Experimental Procedure.....	77
3.1 Electroplating of Pure Tin and Tin-Copper Alloy	77
3.1.1 Electroplating of Pure Tin Coatings.....	77
3.1.1.1 Preparation of the electroplating bath.....	77
3.1.1.2 Substrate preparation.....	78
3.1.1.3 Electrodeposition of pure tin.....	78
3.1.2 Electroplating of Tin-Copper Coatings.....	78
3.1.2.1 Preparation of the electroplating bath.....	78
3.1.2.2 Substrate preparation.....	79
3.1.2.3 Electrodeposition of tin-copper.....	79
3.2 Electrochemical Oxidation Studies	79
3.2.1 Preparation of the Electrochemical Oxidation Baths	79
3.2.1.1 Borate buffer solution	79
3.2.1.2 Potassium bicarbonate-potassium carbonate solution.....	79
3.2.2 Post Electrodeposition Sample Preparation.....	80
3.2.3 Cyclic Voltammetry Studies	80
3.2.4 Electrochemical Oxidation of the Electroplated Tin and Tin-Copper	81
3.3 Conversion Coatings Studies	81
3.3.1 Preparation of the Conversion Coating Baths	81
3.3.1.1 Molybdate solution.....	81
3.3.1.2 Tungstate solution	82
3.3.2 Parameters Used for Depositing the Conversion Coatings	82
3.3.2.1 Molybdate conversion coating treatment parameters	82
3.3.2.2 Tungstate coating conversion coating treatment parameters.....	83
3.4 Whisker Growth and Oxide Thickness and Chemistry Studies.....	84
3.4.1 Effect of Oxidation Potential and Charge Passed on the Electrochemically Formed Oxide and Whisker Growth.....	85
3.4.2 12 Month Study of Whisker Growth and Oxide Thickness.....	87

3.4.3	Effect of Electrochemical Oxidation at Higher Potentials on the Oxide Film and Whisker Growth	88
3.4.4	Comparison of Whisker Growth and Oxide Film Thickness and Chemistry at Room Temperature and 55 °C/85 %RH.....	88
3.4.5	Effect of Conversion Coating Parameters and Chemistry on the Whisker Growth and Coating Thickness and Composition	89
3.4.6	Effect of a Dual-Layer Coating has on Whisker Growth	90
3.5	Characterisation Techniques	91
3.5.1	Optical Microscopy	92
3.5.2	Scanning Electron Microscopy.....	92
3.5.3	Focussed Ion Beam Scanning Electron Microscopy.....	92
3.5.4	X-ray Photoelectron Spectroscopy	93
3.5.5	Conformal Coating Thickness	95
4	Electrochemical Oxidation Studies	96
4.1	Cyclic Voltammetry Studies.....	96
4.1.1	Interpretation of the Cyclic Voltammograms.....	97
4.1.2	Selection of Potentials for Electrochemical Oxidation Studies.....	101
4.1.3	Cyclic Voltammetry Using Different Anodic Switching Potentials.....	102
	103	
4.1.4	X-ray Photoelectron Spectroscopy Study of Single Cycles.....	108
4.2	Oxidation Bath Reproducibility	111
4.2.1	Effect of Solution pH on the Thickness and Composition of the Electrochemically Formed Oxide	113
4.2.2	A Comparison of 'Fresh' and 'Aged' Oxidation Baths.....	114
4.2.3	Effect of Increased Electrochemical Oxidation Potentials on Oxide Formation.....	116
4.3	Comparison of Oxide Thickness After Sample Storage at Room Temperature and 55 °C/85 %RH	118
4.4	Whisker Growth Studies.....	120
4.4.1	Effect of Copper Addition on Grain Structure	120
4.4.2	Whisker Growth Studies on Multi-Area Samples	121
4.4.3	Characterisation of Electrochemically Formed Oxide Coatings for Mitigating Whisker Growth	127
4.4.3.1	X-ray Photoelectron Spectroscopy Studies	127
4.4.3.2	Scanning Electron Microscopy of Electrochemically Oxidised Surfaces.....	132
4.4.4	Effect of Increased Oxidation Potentials on Whisker Growth.....	135

4.4.5	Comparison of Whisker Density After Storage at Room Temperature and 55 °C/85 %RH.....	136
4.4.6	Long-Term Whisker Mitigation of Electrochemically Formed Oxides on Both Sn-Cu on Copper and Pure Sn on Brass.....	138
4.4.6.1	Tin-Copper Electrodeposits on Copper.....	138
4.4.6.2	Tin Electrodeposits on Brass.....	141
4.5	Study of Whisker Growth and Oxide Film Thickness Over Time	144
4.6	Further Discussion of Whisker Growth Studies.....	150
5	Investigation of Conversion Coatings as a Whisker Mitigation Strategy.....	152
5.1	Conversion Coating Parameter Studies.....	152
5.1.1	Molybdate Conversion Coating	152
5.1.1.1	Studying the Reproducibility of Forming a Conversion Coating by Immersion.....	152
5.1.1.2	Effect of Immersion Time on the Conversion Coating Thickness	154
5.1.1.3	Effect of Bath pH on the Conversion Coating Thickness	155
5.1.1.4	Application of Conversion Coatings Using Electrochemical Techniques.....	159
5.1.2	Tungstate Conversion Coatings	167
5.1.2.1	Effect of Reverse Current Pulsed Parameters	167
5.1.2.2	Examination of the Reverse Current Pulse Technique for the Formation of Tungstate Conversion Coatings	174
5.1.3	Focused Ion Beam Cross Section Analysis of Intermetallic Growth and Conversion Coating Thickness	176
5.2	Whisker Growth Studies.....	178
5.2.1	Studying the Effect of Molybdate Conversion Coatings on Tin Whisker Growth.....	179
5.2.2	Studying the Effect of Tungstate Conversion Coatings on Tin Whisker Growth	182
5.3	Summary.....	185
5.3.1	Conversion Coating Optimisation	185
5.3.2	Whisker Growth Studies	186
6	Conformal Coating Studies.....	188
6.1	Dual-Layer Whisker Growth Studies.....	188
6.1.1	Effect of Having a Dual-Layer System on Whisker Growth.....	189
6.1.2	Effect of Coating Edge Coverage on Subsequent Whisker Growth	194
7	Conclusions	197
7.1	Post-Electroplating Surface Treatments.....	197

7.1.1	Electrochemical Oxidation	197
7.1.2	Molybdate Conversion Coating	198
7.1.3	Tungstate Conversion Coating	199
7.2	Dual-Layer Trials	200
8	Further Work	201
8.1	Post-Electroplating Surface Treatments.....	201
8.1.1	Electrochemical Oxidation	201
8.1.2	Conversion Coatings	203
8.2	Developing Dual-Layer Systems	204
9	References.....	206
10	Appendix.....	220
10.1	Nanocapsule Production	220
10.1.1	Nano-Capsule Preparation.....	220
10.1.1.1	Analysing the Compatibility of the DCPD Capsules with Different Solvents	222
10.1.2	Results and Discussion.....	222
10.1.2.1	Analysis of the Synthesised Nanocapsules	222
10.1.3	Conclusions	225
10.1.4	Future Work.....	225
10.2	Journal Papers	227
10.3	Conference Presentations	280
10.4	Conference Posters	293

1 Introduction

A tin whisker is commonly a filamentary growth of pure tin which will grow on thin electroplated films to lengths of up to few a millimetres, but most commonly only a few hundred microns ². These whiskers have the potential to cause failure in electronics by shorting the circuit. There are several mechanisms in which electronics can fail due to whisker growth, some mechanisms are listed below:

- The whisker may grow long enough to come into contact with another conductive surface which would then short the circuit when low currents are involved.
- The whisker may melt and volatilise due to high currents running through it, this would then create a conductive gas which causes arcing between the two surfaces, though this is not very common.

In terms of historical context, there have been a great number of observations of tin whisker growth since the 1950s. However, the first observation of metallic whisker growth was reported in 1946 by Cobb ³, where whiskers were growing from cadmium plated tuning capacitors in military radios and short circuiting when the whiskers came into contact with adjacent surfaces. The capacitors were plated in cadmium to improve corrosion resistance. Though it was not until 1951, when Compton *et al* ⁴ from Bell Laboratories reported that other metals such as tin and zinc also form whiskers. The Compton paper focused primarily on tin, as at that time tin and its alloys had become the preferential metals to electroplate electrical components due to their favourable contact resistance, corrosion resistance and solderability.

There are a number of mitigation techniques currently used to combat tin whisker formation and a number of these have been outlined by Osterman ⁵. Such mitigation techniques are:

- Alloying the tin with other elements such as lead or bismuth ⁶, which in the case of lead changes the grain structure to equiaxed so inhibiting the whisker formation ⁷.

- Use a polymeric conformal coating to act as a physical barrier preventing whiskers from growing out of the surface.
- Electroplate a layer between the tin electroplate and the substrate to act as a diffusion barrier between the electroplated layer and the substrate, such as the diffusion of copper which can form a Cu_6Sn_5 intermetallic compound (IMC).
- Anneal the sample after electroplating, so as to relieve internal stresses.

For this work the main strategy for mitigating whisker growth will be to use electrochemical means to generate an enhanced oxide film, whether that be a tin oxide or a mixed oxide film. This is because oxide films are generally extremely thin (ranging from ~20 nm up to ~500 nm) compared with other conventional coating methods, such as conformal coatings; therefore, the addition of an oxide film won't alter the overall dimensions by a significant amount which may be key for some critical components. The latter part of this work will hope to combine two strategies, an oxide film plus a conformal coating, to further enhance whisker mitigation.

1.1 Post-Electroplating Surface Treatments

The first aim to this part of the project was to understand the cyclic voltammograms of pure tin in the standard potassium bicarbonate-carbonate solution and to find out at what potentials certain reactions occur. However, the broad aim of this project was to mitigate whisker growth by means of an electrochemically formed oxide layer. This area was investigated as Tu^{1,8-10} proposed that when an oxide film cracks whiskers are more likely to grow through the crack and that having a thick oxide film would physically stop whiskers and reduce the likelihood of cracking. Electrochemical oxides can, like the polymeric coatings, be seen as physical barriers but unlike the polymeric coatings they are far thinner so not affecting the overall dimensions of the sample, which would be advantageous if high dimensional tolerances are involved. The third aim of this project was to optimise the electrochemical oxidation process by optimising the oxidation solutions and parameters used. This was carried out to produce the most effective electrochemically formed oxides for mitigating tin whisker growth.

To achieve the first aim, continuous cyclic voltammetry was carried out on pure tin in a potassium bicarbonate-carbonate solution and the cyclic voltammograms were then studied. Single cycles were also carried out using different anodic switching potentials, so as to understand where changes would occur. Díaz *et al*¹¹ produced such cyclic voltammograms to determine at what potentials pure tin will oxidise and showed that there two oxidation peaks for tin, one for the oxidation of Sn to Sn(II) and the other for the oxidation to Sn(IV). The cyclic voltammogram will also show regions where passivation will occur, which may also be good for electrochemically forming an oxide film. To achieve the broad aim of mitigating whisker growth, tin-copper was electroplated onto copper substrates, it was then electrochemically oxidised at different potentials. Several tin-copper electroplated samples were also left to develop a naturally air grown oxide layer, to provide a basis for comparison. To achieve the third aim, a study was undertaken to understand the effects of different solution parameters on oxide layer formation, i.e. changing the pH, the concentrations of constituents; another study was undertaken to understand the effect of electrochemically oxidising tin at varying potentials and its effect on the oxide layer.

Two principal characterisation techniques were used to study the samples; scanning electron microscopy (SEM) and X-ray photoelectron spectroscopy (XPS). SEM was used to study the topography of the surfaces and to investigate whisker growth whilst XPS was used for chemical analysis of the oxide layers and to identify any changes in composition with depth. Optical microscopy was also used to evaluate the whisker density.

1.2 Self-Healing Polymers

Self-healing is a fundamental feature that is exhibited by living tissue, whether that be a scratch on human skin or on a plant^{12,13}. Self-healing in materials have been around for over 2000 years¹⁴ since the Romans invented and implemented the use of concrete, which at the time wasn't known for being 'self-healing'. It was observed that the concrete used by the Romans contained a mixture of volcanic rock and lime stone, which when mixed with sea water causes aluminium tobermite to form which

strengthens the concrete enabling the concrete to flex rather than crack when stressed¹⁵. Tittelboom *et al*¹⁶ incorporated fly ash, which is similar to volcanic ash, into the concrete to enable 'self-healing' whereby the material would close up cracks once they form. Now, smart polymeric materials are at the forefront of technology and self-healing polymers are a relatively new class of these smart materials¹⁷. These self-healing polymers possess the ability to either fully or partially recover a functionality that has been damaged by operational use, such as abrasion, corrosion, or thermal degradation. Incorporating a self-healing feature into a material will greatly increase the longevity of the material in service; this will in turn reduce the likelihood of needing to replace any parts that contain a self-healing material. Another advantage of having a self-healing feature is that it will heal damaged areas that can't be detected by the human eye, thus not needing to be inspected as often. However, there will be an increase in production costs due to the implementation of a self-healing feature.

The aim of this part of the project was to produce a self-healing conformal coating based on the use of nano-capsules that will be embedded into current conformal coating. To achieve this, two batches of nano-capsules were produced using emulsion techniques; one batch was filled with dicyclopentadiene (DCPD) and the other batch was filled with the Grubb's catalyst. The DCPD filled nano-capsules were produced using a method described by Brown *et al*¹⁸ and Blaiszik *et al*¹⁹ and the Grubb's catalyst filled nano-capsules were produced using a method described by Jackson *et al*²⁰. These two batches of capsules were then dispersed into a compatible polymer coating and when the coating cracked the DCPD filled capsules would rupture, causing the DCPD to flow into the crack and come into contact with the catalyst. Subsequently, the DCPD would polymerise and 'heal' the crack in the coating.

1.3 Dual-Layer Development

The final aim of this project, was to successfully produce a dual-layered whisker mitigation coating consisting of an electrochemical oxide layer with a self-healing polymeric conformal coating on top. It

is thought that the electrochemical oxide might prevent the majority of whiskers forming, as observed in previous studies^{21,22}, underneath the self-healing coating. The few whiskers that may form will then be mitigated by the self-healing coating. In addition to mitigating whisker growth, the self-healing coating will also be able to heal any physical damage that may occur, i.e. due to handling.

To achieve this, initial trials were conducted whereby an unmodified polymeric coating was used in the dual-layer system. Three trials were carried out to analyse the whisker growth: one trial batch was stored at room temperature; one was stored at 55 °C/85 %RH; and one was used to analyse the whisker growth only at edges and corners. The latter was undertaken because conformal coatings do not have good edge coverage and tend to be thinner compared with flat central areas; however, electrochemically formed oxides are thicker at edges due to presence of increased current densities.

2 Literature Survey

2.1 Tin Whiskers

A tin whisker is a growth of pure tin that is commonly in the form of a filamentary growth, which can grow up to a few millimetres in length, from a thin tin coating (around 0.5-50 μm thick) that has been electroplated onto a substrate ³. The growth of these whiskers can begin very soon after the electroplating of a sample, however the initiation of growth may take years to occur; it is this unpredictability of whiskers that causes concern to reliable operation ⁷. At the current time, there is no one widely accepted mechanism for why and how whiskers grow; though there are number of theories and some commonly agreed factors that affect the growth of tin whiskers.

2.1.1 An Introduction to Failure Mechanisms

Whisker growth can cause major problems in the electronics industry, mainly due to these whiskers growing from one surface and then coming into contact with another, adjacent surface. This contact between the two surfaces can cause a short circuit and result in electronic failure; this is done by the movement of electrons through the whisker from one surface to another. An example of this bridging can be seen in figure 2.1. Circuits can also short by long whiskers falling and landing somewhere that can cause bridging. Both types of failures occur at lower currents.

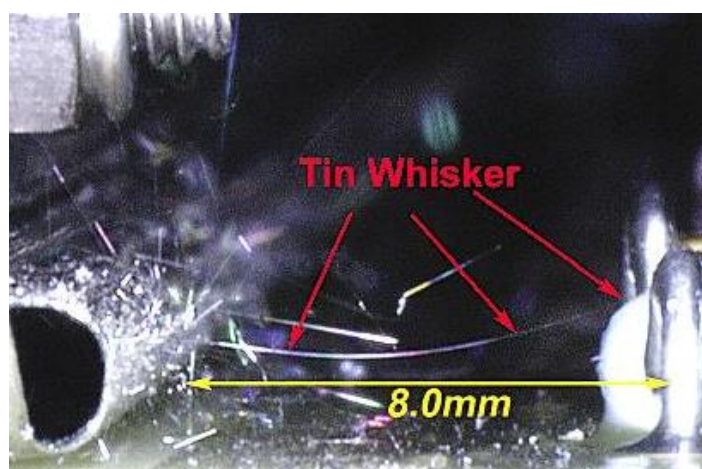


Figure 2.1 Whiskers bridging a gap of 8 mm between two surfaces ²³

At high currents the whiskers can volatilise which causes a conductive metal gas, which in turn can create a metal vapour arc reaction²³. This metal vapour arc can generate such high temperatures that it can melt metals and incinerate polymers. Figure 2.2 shows an example of a metal vapour arc failure. This arc forms when the metal atoms that are vaporized, due to the high electrical potentials, are then ionised in the presence of a strong electrical field; this causes the electrons to flow to the cathode and the ionised metal atoms to flow to the anode. If this occurs at lower pressures then the vaporisation of tin whiskers is increased and less voltage is needed to produce the arc. In 1992, Van Westerhuyzen *et al*²⁴ found that 10 A fuses inside a 30 V relay were blowing out during a thermal vacuum test and was found to be due to a metal vapour arc that was caused by tin whiskers.



Figure 2.2 A relay destroyed by metal vapour arc reaction, induced by tin whiskers²³

Whiskers typically have a diameter between 1-5 μm and most commonly grow to lengths ranging from $\sim 1 \mu\text{m}$ up to $500 \mu\text{m}$ ². It has been observed that whiskers have grown to more than 1 cm, but this is very rare. These whiskers can be straight, kinked, curved or form odd-shaped eruptions, as shown in figure 2.3, which shows the different types of whisker morphologies formed from tin deposits on brass.

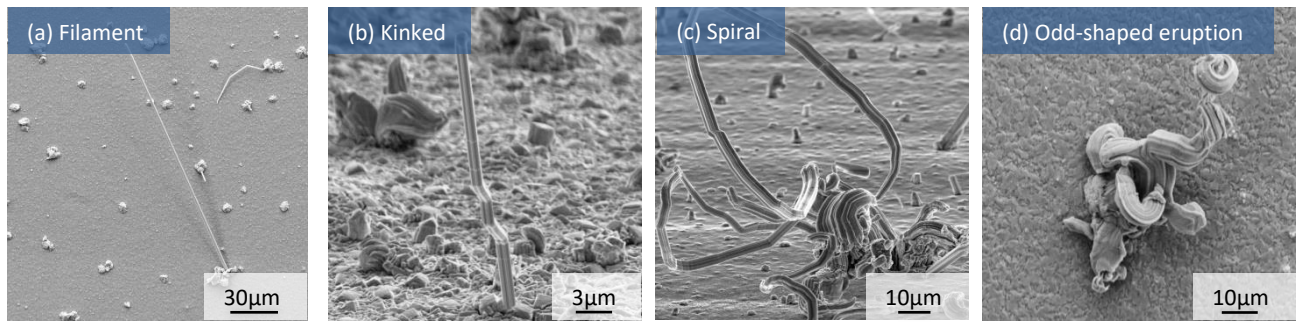


Figure 2.3 SEM micrographs showing examples of tin whisker morphologies (a) a straight whisker, (b) a kinked whisker, (c) a curved whisker and (d) an odd-shaped eruption

2.1.2 A Brief Introduction to Some Growth Mechanisms

An early theory given by Peach²⁵ proposed a dislocation method for whisker growth; this theory stated that tin whiskers grew by a means of tin atoms moving through a screw dislocation that was situated at the centre of the whisker and the moving atoms are thereafter deposited at the end of the whisker. However, not long after Peach's theory was published Koonce and Arnold²⁶ published a paper that voided Peach's original theory; the paper stated that whiskers grew from the bottom and not the top, which were clarified by the first electron micrographs of tin whiskers that were obtained by Koonce and Arnold. This type of growth is still a commonly accepted mechanism for whisker growth. It is widely accepted that whiskers grow due to a form of residual stress in the tin film⁵. Examples of growth mechanisms will now be described.

2.1.2.1 Stresses – internal and external

Williams *et al*²⁷ found that the intrinsic compressive plating stress, which will depend on such factors as the deposit thickness, current density and cathode rotation speed can initiate whisker growth. However, after a certain amount of time the growth ceased; this was because the growth of whiskers and hillocks relieve residual stress, hence if the compressive stress was negated then whiskers would have no driving force for further growth. It was observed by both Yao *et al*²⁸ and Bušek *et al*²⁹ that whisker growth can be increased by applying an external compressive stress on the sample.

Another cause of internal stress can come from the difference in the thermal expansion coefficients between the tin coating and the substrate. This is where upon heating or cooling the substrate expands and contracts, respectively, at a different rate to that of the electrodeposited coating; this will therefore induce stresses on to the electroplated deposit which can cause whiskers to grow, as observed by Shin and Chason³⁰.

2.1.2.2 Formation of intermetallic compounds and the interdiffusion between coating and substrate

Boettinger *et al*⁷ found that after several days a Sn-Cu deposit, which had the highest compressive stress, compared with the pure Sn and Sn-Pb deposits, grew 50 µm hillocks and 200 µm whiskers; the Sn deposit which had a lower compressive stress only grew 20 µm hillocks; and the Sn-Pb, which had the lowest compressive stress, had no growths of any kind. The difference in the compressive stresses came from the rapid precipitation of Cu₆Sn₅ or lead particles within the supersaturated tin grains produced by the electrodeposition.

Tu *et al*⁹ suggested that the stress is generated by the copper diffusing into the tin and the formation of intermetallic compounds (IMCs) at the grain boundaries, which is followed by a volume increase. This volume increase due to the formation of the IMC, causes a compressive stress on the tin grains.

Diffusion through the coating can occur from different directions; for example, both the atoms from the substrate and the atoms from the oxidised surface will diffuse along the grain boundaries and into the coating³¹. This diffusion through the grain boundaries will weaken the cohesion of the coating grains and will induce internal stress by the formation of IMCs and surface oxides³². This is because as intermetallics form, the volume increases, so inducing a stress in the coating. An example of diffusion between the coating and substrate is shown in figure 2.4; as the copper atoms diffuse into the tin coating, they form intermetallics with tin atoms, so increasing in volume and causing stress concentrations. At room temperature the diffusion rate of copper in tin suggests that the mobility of the copper atoms in tin is sufficiently high enough for the intermetallic (Cu₆Sn₅) phase to form at room

temperature³³. Diffusional creep of tin to the base of the whisker can also be caused by stresses that result from a crack in the oxide layer, as suggested by Tu¹, which causes whisker growth to occur.

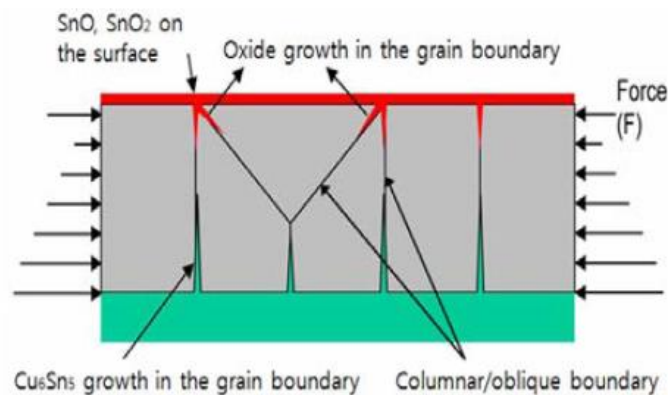


Figure 2.4 Elements from both the surface (oxygen) and substrate (copper) diffusing along the grain boundaries into the coating to form new compounds with the tin in the electroplate³¹

It was observed by Stuttle *et al*³⁴ that when electroplating tin on copper the IMC growth is highly dependent upon substrate texture and not the coating structure and that after 55 days of room temperature storage there is a complete interface coverage of IMC growth. The fast growth of IMC can be attributed to the accelerated speed at which copper diffuses through tin which is $\sim 10^{12}$ faster than the self-diffusion of tin³⁵. This rapid diffusion causes a rapid growth in IMCs which in turn causes internal stresses to initiate very quickly. A similar observation was made by He and Ivey³⁶ whereby large IMCs were found across the entire Sn-Cu interface. In addition to these IMCs found at the interface, it was observed that smaller IMCs were found along the grain boundaries (shown in figure 2.4) and even smaller IMCs were found within the Sn grains themselves. The IMCs at the grain boundaries form in a triangular or wedge shape that point towards the direction of whisker growth causing localised compressive stresses. He and Ivey proposed a three-stage process for the formation of a whisker:

1. Recrystallisation of the tin grains – during the electrodeposition stage vacancies and interstitials will form and as such will cause stresses in the film. Therefore, to overcome this stress recrystallisation will occur and during this stage the strained grains will be completely replaced by unstrained grains.

2. Generation of driving forces – Cu atoms rapidly diffuse into the Sn film forming Cu_6Sn_5 IMCs at the interface, grain boundaries and within the grains. This creates a volume change in the film and generates compressive stresses which provides the driving force for whisker growth. It should be noted that this stage is not entirely discrete from stage 1 and both can occur during the electroplating stage.
3. Mass transport of Sn atoms – some of the recrystallised grains become seeds for whisker formation and Sn atoms from highly stressed regions will move towards these seeds until the driving force disappears.

When electroplating onto brass, not only does copper diffuse into the tin coating but zinc does also, which is also an influence on whisker growth as suggested by Glazunova and Kudryavstev³⁷. Sakuyama and Kutami³⁸ suggested that the zinc in the brass substrate will diffuse along the grain boundaries creating defects in the electroplated surface and influence whisker growth. The zinc will diffuse around the grain boundaries and oxidise at the surface, as shown in figure 2.5.

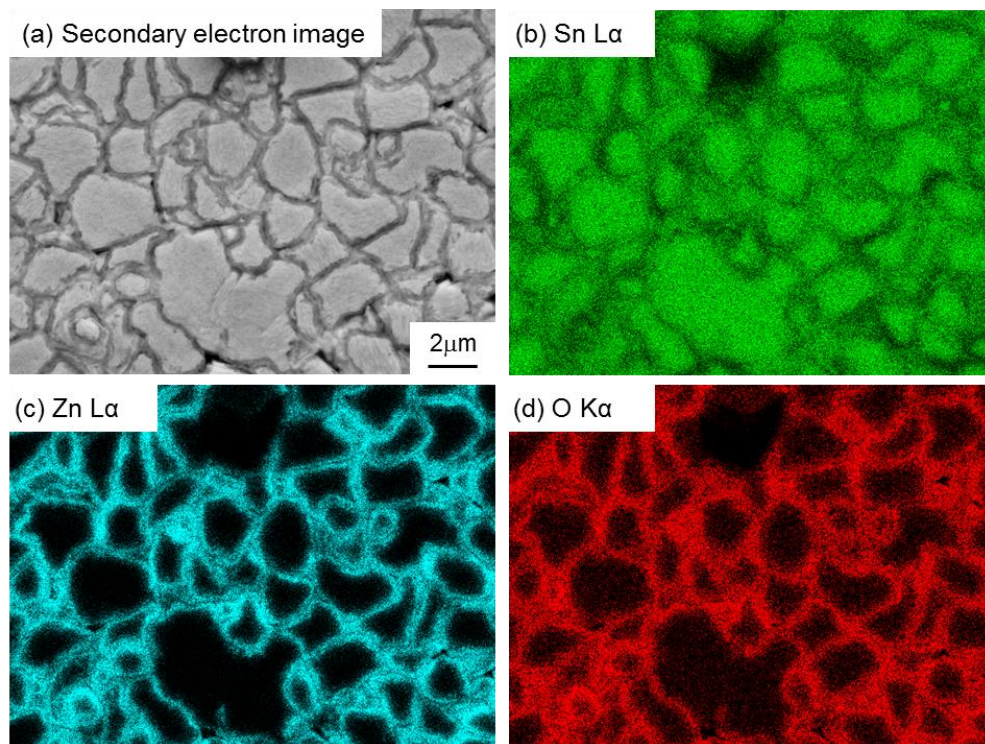


Figure 2.5 SEM micrograph and EDS maps showing the diffusion of zinc to the surface at tin grain boundaries to form zinc oxide a) the surface of tin electroplated onto brass b) EDS map with respect to tin c) EDS map with respect to zinc d) EDS map with respect to oxygen³⁹

2.1.2.3 Grain size

It has been reported that electroplated deposits with smaller grain sizes develop more whiskers⁴⁰. This is because there is an indirect relationship between the grain size and the amount of grain boundaries, i.e. increased number of grain boundaries with decreased grain size. A smaller grain size will increase the rate of grain boundary diffusion and related growth of intermetallics and oxides; this will then increase the internal stresses, which will increase the likelihood of whiskers forming. Additionally, a decrease in grain size will result in smaller grain boundary areas for the whisker formation grain which means that less stress is needed to cause grain boundary sliding and forming of whiskers.

2.1.2.4 Grain shape

Depending on whether the grain structure of the electroplated tin is equiaxed or columnar, there may be a decrease or increase in whisker growth. It was observed by Boettinger *et al*⁷ that by having columnar grains, the rate of whisker formation is increased and by having equiaxed grains, the formation of whiskers is mitigated. This is because with columnar grains, that occurs in pure tin and tin-copper deposits, the compressive stresses must be relieved by whisker or hillock formation; however, when the grain structure is mostly equiaxed, such as when lead is added to the tin deposit, uniform creep is able to occur and rapid stress relaxation may occur which mitigates the formation of whiskers, shown in figure 2.6.

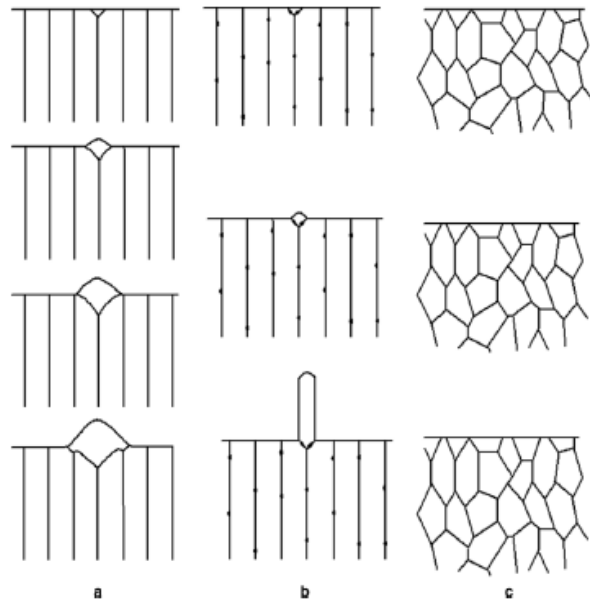


Figure 2.6 Schematic showing how grain shape can affect tin whisker formation a) grain structure in pure tin where the grain boundaries are mobile, b) the grain structure in tin-copper alloys where the grain boundaries are pinned by the intermetallic compounds formed, c) the grain structure in tin-lead alloys where uniform creep is able to occur⁷

2.1.2.5 Surface oxide

When a metal forms a natural oxide layer, an inhomogeneous relaxation occurs at points where the oxide has cracked; this cracked oxide is the cause of whisker formation and Tu¹ suggested that the formation of whiskers, due to the cracked oxide, is similar to that of the extrusion of wire under high pressure, apart from the fact that whiskers grow due to the atomic diffusion of tin atoms and not mechanical flow. A diagram of how a whisker is formed due to the cracked oxide is shown in figure 2.7; it shows that where the crack occurs there is less stress and the tin atoms diffuse to the area of less stress. This is because the crack exposes the native tin surface which generates vacancies in the material; due to the fact that whiskers grow from the base, the crack cannot heal so enabling a continuous generation of vacancies for tin atoms to diffuse to. Tu also suggested that without an oxide layer there would be a homogenous relaxation and there is no long-range diffusion of tin to form whiskers, hence no whiskers will form.

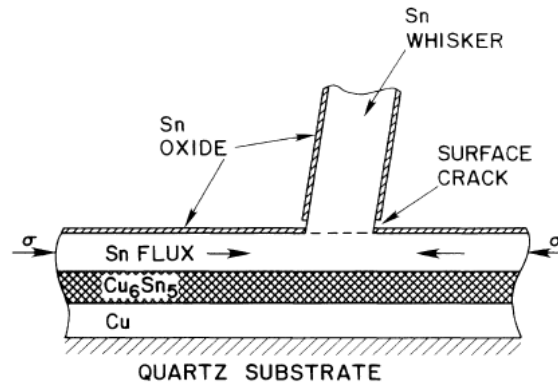


Figure 2.7 Diagram of how a whisker is formed due to the oxide layer cracking and exposing the native tin, allowing the migration of tin atoms to surface crack ¹

Lee *et al* ⁴¹ also showed that having a thin oxide layer is needed for the growth of whiskers due to vacancies penetrating into the tin films through weak points in the oxide layer, thus resulting in the diffusion of tin atoms to these sites and creating a nucleation point for tin whiskers. Su *et al* ⁴² conducted a study by which a dotted pattern was placed on the deposited tin film surface by means of lithography and was subsequently sputtered with a tin oxide. The pattern was then dissolved away to leave areas that had not been covered by the tin oxide layer, thus creating weak points. It was observed that the samples that had a larger number of weak points grew more whiskers and those whiskers grew from the weak points. This was due to the diffusion of tin atoms to these weak points and creating nucleation points. Su *et al* also showed that having fewer weak points will result in fewer whiskers, however, these whiskers will be (on average) longer. It was suggested that the amount of extruded material should be equal regardless of the number of weak points, therefore having longer whiskers on the samples with fewer weak points.

2.1.2.6 Tin alloys

Alloying tin with different elements can affect the growth and formation rate of whiskers; both decreasing and increasing them depending on the alloying addition. Wickham *et al* ⁶ observed that both tin-silver and tin-bismuth alloys reduce the amount of whiskers formed; whilst Kim *et al* ⁴³ reported that alloying tin with bismuth resulted in the growth of more hillocks rather than filament whiskers. Some alloys that promote whisker growth will now be described.

2.1.2.6.1 Tin-copper alloys

Boettinger *et al*⁷ observed that alloying tin with copper will increase the amount of whiskers and hillocks formed. Using copper as an alloy addition to tin electroplating has been shown to increase the amount of whiskers formed^{7,27,44}. It was observed by Illés *et al*⁴⁴ that when tin is oxidised there is a corresponding volume increase of 14 %, depending on which tin oxide is formed, which induces a compressive stress on the plated surface. However, when copper is present in the plating material there is a greater increase in volume when it is oxidised; when copper is oxidised the volume increase can be up to 49 % which will induce a far larger compressive stress and drive the nucleation and growth of whiskers⁴⁵. It was also found that having a high copper content increases the rate of corrosion, which will add an increasing stress to the material hence accelerating the growth of whiskers once formed. Illés *et al* made the assumption that surfaces which contained copper somehow increased the diffusion rate of copper atoms towards the surface, compared with pure tin, which would increase the rate at which whiskers would form due to intermetallic compounds and the copper oxidation.

Williams *et al*⁷ observed that intermetallic compounds (Cu_6Sn_5) were forming within the tin grains and along the grain boundaries, when copper was added to the electrolyte and a tin-copper alloy deposited. These intermetallic compounds increase the compressive stresses within the material resulting in a higher compressive stress compared with pure tin on tungsten. Along with the increased stresses the intermetallic compounds pinned the tin grain boundaries, preventing relaxation of compressive stresses and therefore promoting whisker growth, as shown in figure 2.6.

2.1.2.6.2 Tin-manganese alloys

Chen and Wilcox⁴⁶ observed that adding manganese, as an alloying addition to electroplated tin, accelerated whisker growth and density. It was observed that the mechanism for whisker growth was different to what had been previously suggested for other tin-based alloys; rapid formation of an oxide layer at room temperature was found to be a precursor for whisker growth. Also it was observed in all samples apart from one (deposited at 0.5 A dm^{-2}), that there were no compressive stresses present;

however, it was observed that the samples had tensile stresses and after nearly three months there were still tensile stresses present, therefore whisker formation on tin-manganese did not follow the stress release theory to which there must be a compressive stress present ¹.

2.1.2.7 Corrosion induced whisker formation

In a review conducted by Illés *et al* ⁴⁷ it was reported that the corrosion of tin can induce whisker growth. This is because there are volume changes when tin oxidises, causing compressive stresses in the tin layer which induces whisker growth. It was observed by Schroeder *et al* ⁴⁸ that the majority of the tin whiskers would form at or near corrosion sites and would not grow uniformly across the surface of the sample; this suggested that corrosion may influence whisker growth, however, Schroeder *et al* did not establish a direct relationship between whisker growth and corrosion. A similar observation was made by Obernoff *et al* ⁴⁹ and it was also observed that the corrosion of the tin causes a volume increase in the tin layer which subsequently causes compressive stresses. The authors stated that along with the coefficient of thermal expansion (CTE) mismatch and intermetallic compound (IMC) growth, the oxidation and corrosion of tin induces whisker growth.

Smetana ⁵⁰ theorised that the stress generated by the oxide formation was expected to be significantly less than the stress generated from IMC growth and that the oxide growth might be another compressive stress source which may increase grain boundary diffusion of tin. However, the high humidity would accelerate this effect because the volume of hydrated SnO₂ is significantly greater than non-hydrated SnO₂. Nakadaira *et al* ⁵¹ observed that the corroded layers spread through the tin film and whiskers would form around these corroded islands (similarly observed by Schroeder *et al* ⁴⁸) and the authors theorised that SnO_x had different properties to pure tin. Tin oxide has ~33 % larger molar volume compared to pure tin and SnO₂ is more than four times harder than pure tin. Therefore, the larger and harder tin oxide, caused by corrosion, generates compressive stresses in the tin film.

Interestingly, at a much higher temperature and relative humidity (RH) of 105 °C/100 %RH the strong oxidising environment both induces and mitigates whisker growth, as observed by Illés *et al* ⁵². The

authors observed whiskers growing from cracks in the oxide layer around corrosion spots (similar to what was previously observed ^{48,51}), however, due to the accelerated rate at which the oxide layer grew, the whiskers were also coated in a thick tin oxide layer which prevented them from growing further. This caused periodic appearances of large amounts of short whiskers.

A unique phenomena was observed by Horváth *et al* ⁵³ where copper oxide whiskers would grow from tin-copper alloys plated on copper substrates, under high temperature and RH conditions (105 °C/100 %RH); the authors observed that these whiskers had similar morphological properties to pure tin whiskers. The authors stated a theory as to why these copper oxide whiskers grew, which is as follows:

1. Localised corrosion would occur on the sample in a spot where the water had condensed, causing the tin alloy to oxidise to SnO_x with clusters of Cu_xO within it.
2. During this stage, IMCs would form at the interface to form a layer.
3. Once the water and oxygen reached the IMCs, they would firstly break down and oxidise into their respective hydroxides, then these tin and copper hydroxides would further oxidise to SnO₂ and Cu₂O.
4. As the tin oxides form within the coating, the copper oxide and copper areas are compressed due to the change in volume.
5. These compressed areas are then forced through Cu₂O clusters at the surface, in a whisker shape. This is because the clusters have a much lower hardness than the surrounding SnO₂, therefore being able to break through them. It was observed that these whiskers did not develop on the samples with a pure tin coating because the copper oxide could not break through the harder tin oxide film.

2.1.3 Mitigation Techniques

Much research is dedicated to the mitigation of whisker growth, to prevent failure in electronics due to the whiskers causing short circuits. Currently there are a number of different techniques used to mitigate the growth of whiskers and the following techniques are widely used in industry.

2.1.3.1 *Selecting a different type of electroplated tin finish*

Selecting a matte or stress free tin finish will reduce whisker growth ⁵ as it is known that internal stresses can cause whisker growth ^{5,54}. It has been reported with bright finishes that there is an increased density of whiskers compared with other tin finishes⁵; this could be because of the increased number of additives used in the bright tin finish electroplating bath which would increase the internal stress of the plated material.

2.1.3.2 *Depositing a layer between the deposited tin and the substrate*

A barrier layer which is plated before the electroplated tin can be used as a mitigation technique by reducing the internal stress due to copper-tin intermetallics ^{5,54} but also a barrier coating will prevent zinc, in brass, diffusing through the tin to the surface. Materials such as nickel and silver can be electroplated to act as a barrier between the substrate and the electroplated tin and prevent the formation of Cu_6Sn_5 intermetallics which causes internal compressive stresses ²⁷. Wickham *et al* ⁶ showed in their experiments that firstly plating nickel over the brass before plating the pure tin completely eliminates whisker growth after 1 month and using 5 different aging methods. Dittes *et al* ⁵⁵ conducted similar experiments with nickel and silver under-layers and the intermetallic formations were studied and showed that in both cases the internal compressive stresses were reduced. This is because the intermetallic compounds formed between the under-layer material and the tin undergo a smaller volume change (nickel intermetallic Ni_3Sn_4 and the silver intermetallic Ag_3Sn) compared with copper-tin intermetallics and this will therefore reduce the amount of compressive stress. Zhang *et al* ⁵⁶ also conducted studies of using nickel as a under-layer on copper substrates and it showed that the barrier under-layer significantly reduces the amount of whisker growth. However, Xu *et al* ⁵⁷ observed

that the samples that were subjected to thermal cycling grew whiskers, which would indicate internal stresses that are caused by the difference in the materials' coefficient of thermal expansion (CTE).

Another type of layer than can be used between the tin and the substrate is an amorphous thin film which have been shown to be excellent at acting as a diffusion barrier in integrated circuit applications⁵⁸. In particular, thin film metallic glass (TFMG) films can be used as they have received much recent interest due to their good properties such as high strength, large elastic limits, corrosion resistance and wear resistance^{59,60}. Diyatmika *et al*⁶¹ studied the ternary system of $Zr_{46}Ti_{26}Ni_{28}$ (atomic ratios) TFMG for its ease of fabrication and good thermal stability. It was found that the Sn coating produced on top of this TFMG coating was much smoother than without using the underlay coating. It was observed that after 33 days of room-temperature storage no whiskers were observed on the samples using a TFMG underlay. Both the samples with and without the TFMG underlay had the Sn layer chemically stripped away to study the IMC formation. It was observed that no IMCs were formed on the samples with a TFMG underlay, which proved that the underlay coating successfully blocked any Cu diffusion from the substrate into the Sn.

2.1.3.3 Thickness of the deposit

Thickness of tin plating can also have an effect on the growth of whiskers⁵, having thicker deposits will reduce the effect of internal stresses, due to intermetallic compounds formed from copper diffusion, as the stresses can be dissipated more. Also, when electroplating on brass the zinc has further to diffuse to get to the surface which will therefore slow down the growth of whiskers due to zinc diffusion.

2.1.3.4 Annealing

Annealing can reduce internal stresses in the material and is a process by which the material is heated up to around two thirds of its melting temperature and held for a specific amount of time. Zhang *et al*⁵⁶ assumed that annealing at high temperatures could affect the formation of intermetallics and the experiments that were undertaken suggest that the intermetallics grow uniformly and not

preferentially along the grain boundaries, which causes the formation of a tin-copper intermetallic layer that acts as an under-layer barrier and prevents the further diffusion of elements into the tin. Also Zhang *et al* found that the intermetallics formed at ambient temperatures had a different morphology to those formed at higher temperatures and tended to grow into the grain boundaries causing an increase in stress. Dittes *et al*⁵⁵ showed that after the tin electroplate was annealed the tin layer had coarsened and re-crystallised, therefore able to relieve the stresses caused by the plating process. It was noted that no whiskers were formed on the annealed samples and created an effective diffusion barrier by changing the diffusion mechanism from grain boundary to bulk diffusion when annealing at 150 °C. However, Fukuda *et al*⁶² used the exact same annealing parameters and found that instead of eliminating the whiskers completely there was simply a delay in the formation of whiskers.

2.1.3.5 Conformal coatings

Polymeric conformal coatings can be used as physical barriers to prevent whiskers from creating short circuits^{5,54}. This technique does not prevent the formation of whiskers it only slows the growth rate and also insulating any whisker ends that protrude. A study was conducted by NASA using Uralane 5750^{63,64} as a conformal coating, where one half of the sample was coated in a thicker conformal layer and the other half was coated in a thinner conformal layer. It was observed that whiskers were forming underneath the coating and after two years whiskers had penetrated through the thinner layer whereas whiskers had formed but not penetrated through the thicker layer. This penetration through the thin conformal coatings was also observed by Woodrow and Ledbury⁶⁵, where whiskers penetrated through the thinner conformal layer and not the thicker in all the 6 different coating materials. However, another study by Woodrow and Ledbury⁶⁶ using the same 6 conformal coatings but different atmospheric conditions showed that the experiment with the higher relative humidity (RH) reduces the effectiveness of the conformal coating, where regardless of the thickness, the whiskers penetrated through all the coatings. It was also noted that some coatings were delaminated

by the whiskers. These studies show that conformal coating can be good as a method to slow down growth but eventually the whiskers will penetrate through.

2.1.3.6 Changing the electrolyte used

As it is widely accepted that internal compressive stresses due to tin plating are a significant factor in whisker growth^{30,41}, researchers^{67,68} have been studying the effects of modifying the electrolyte chemistry and additive concentrations. These two factors influence the internal stresses developed during plating, so being able to reduce the internal stresses produced during plating by changing additive concentrations and electrolyte formulation will decrease the number of whiskers formed.

2.1.3.7 Surface treatment (both substrate and electroplated surfaces)

Surface treatments of both the substrate and tin plating have been studied by researchers and have shown that surface treatment can prevent whisker growth. Sukanuma *et al*⁶⁹ observed that treating the tin plating surface, by electroplating thin layers of nickel onto the surface of the tin plating, prevents the formation of whiskers by preventing the atoms that have diffused through the tin layer to form oxides. Whereas, Takeuchi *et al*⁷⁰ surface treated the substrate so as to mitigate whisker growth; the precise surface treatment was micro-etching to roughen the surface of the copper substrate used and it was observed that the plating morphology followed that of the roughened substrate surface. This roughening of the substrate surface proved to mitigate whisker growth by influencing both the growth and nucleation of the electroplated tin and distorting the grain boundaries, which will affect the diffusion of atoms from the substrate.

2.1.3.8 Electrochemically formed oxide

The formation of natural tin-oxide on the plated surface increases the internal stresses in the tin plating and whiskers are more likely to grow where there are cracks in the oxide layer¹, so having an electrochemical oxide that is thicker will dissipate this stress more. There have been several studies^{66,67} that have studied the effects of electrochemically formed oxides as a technique for mitigating whisker growth and suggested that oxides which were electrochemically formed were better at

preventing whisker growth than the native oxide. The results showed that the electrochemically formed oxides were thicker than the respective native oxide and taking into account Tu's theories^{1,8-10}, it may be harder to crack a thicker oxide therefore inhibiting the growth of whiskers by preventing cracks forming.

2.1.3.9 Tin alloys

As mentioned previously tin alloys can both promote and inhibit whisker growth depending on alloying element. Tin-lead alloys are generally the best at mitigating whisker growth and some examples tin-alloy systems will now be described.

2.1.3.9.1 Tin-lead alloys

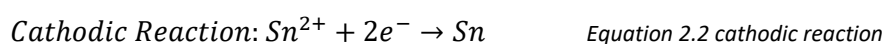
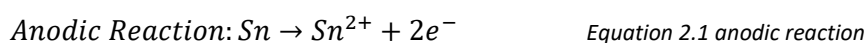
It has been suggested by Arnold⁷³ that adding lead (Pb) will prevent whiskers from growing and this has also been observed in the experiments conducted by Boettinger *et al*⁷. Arnold⁷³ observed that the samples that had been plated with a tin-lead alloy and exposed for a period of 12 years in an atmosphere of 95 % humidity, had all undergone a large amount of surface corrosion, though only a few whiskers were found; it was also observed that only 1 wt.% of lead is needed to mitigate whisker formation. Boettinger *et al*⁷ also observed similar results, that by adding lead as an alloying addition greatly reduces the number of whiskers formed; it was suggested that by adding lead the grain structure changed from columnar, for pure tin, to equiaxed, which increases relaxation and enables uniform creep so reducing the need for a surface eruption to relieve stress. Boettinger *et al* also suggested that with only 2 wt.% of lead added, the volume change that is undergone to obtain an equilibrium mixture of tin and lead phases is -0.13 %; this would suggest that there is very little tensile stress induced and the fact that the stress is tensile would suggest that it would be unlikely for whiskers to grow¹. However, lead can no longer be used as an alloying addition as the element has been banned under EU legislation (RoHS)⁷⁴ due to the toxicity; therefore needing other elements to alloy with tin to reduce whisker formation.

2.1.3.9.2 Tin-bismuth alloys

It was observed by Zhang *et al* ⁷⁵ that alloying tin with small amounts of bismuth would significantly reduce whisker growth compared with using a pure tin finish. The authors also showed that using a tin-bismuth alloy would improve solderability and would be compatible with Sn-37Pb solder joints, as long as the concentration of bismuth did not exceed 6 wt.%.

2.2 Electrodeposition of Tin & Tin Alloys

Tin electroplating is when pure tin is deposited as a plate coating onto a substrate material by using electrochemistry ⁷⁶. This is done by making an electrochemical cell and connecting the two electrodes together by a power supply; the electrode that will be used for depositing the pure tin would be made the anode and the target material would be made the cathode. These two electrodes would be placed in a plating bath containing an electrolyte. Typical electrolytes are often based on either sulphuric acid or methanesulfonic acid (MSA). This electroplating principle works by tin ions migrating from the anode, through the electrolyte and then adsorbing onto the surface of the target substrate to form tin atoms at the surface – this can be shown below by the anodic and cathodic reactions (equations 2.1 and 2.2, respectively) that occur, along with a schematic of the mechanism for cathodic metal deposition, as shown in figure 2.8. At the anode, electrons are taken away which causes pure tin to form tin(II) ions. These ions are then hydrolysed by the electrolyte and travel away from the anode due to fact that both the ions and the anode are positively charged, therefore repelling each other. The ions then move around in the bath and are attracted to the cathode due to its negative charge; near the cathode the ions lose the water molecules and carry on towards the cathode. These ions are then adsorbed onto the surface and gain two electrons to form pure tin. These ad-atoms are then diffused across the surface to the growth point.



Tin is used as an electroplating material in the electronics industry because of its good electrical conductivity, resistance to corrosion and good solderability. This way the substrate material will be protected from the environment, so not corroding; the substrate does need to be conducting so as to be able to electroplate the tin onto it, but the conductive properties do not need to be electronic standard because tin already has good conductive properties.

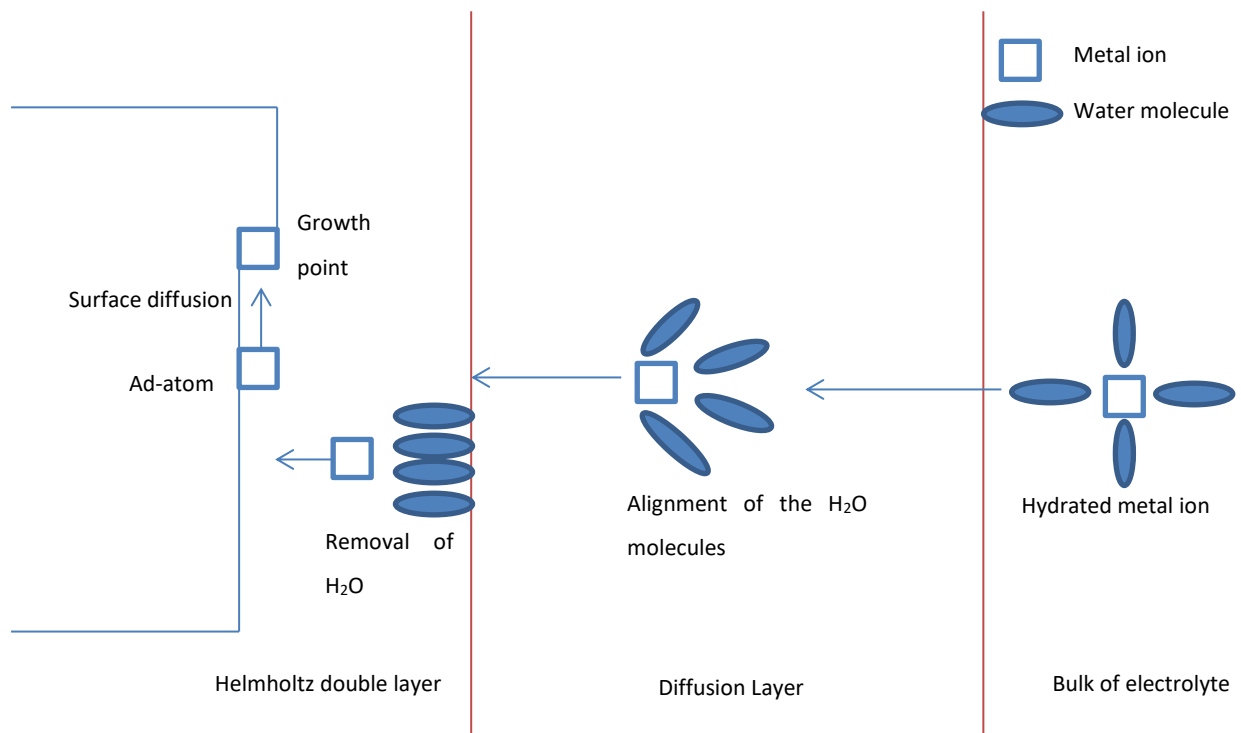


Figure 2.8 The mechanism of cathodic metal deposition. Where the hydrated metal ion migrates towards the substrate surface. During this migration the metal ion becomes dehydrated and is adsorbed onto the surface. ⁷⁶

2.2.1 Effects of Operating Parameters

The electroplating operating parameters can have different effects on the morphology and hence the mechanical properties of the plated material. Such parameters that have an effect will now be described.

2.2.1.1 Agitation

This can be achieved in two ways, either by agitating the electrolyte or physically moving the cathode ^{77,78}. The agitation of the solution will cause the metal ions to constantly move around which will prevent any settling of the salts, it also provides a 'fresh' supply of metal ions to the cathode surface

which decreases the thickness of the diffusional layer. This will then result in a higher concentration of metal ions in the diffusional layer. Agitation will also increase the rate at which plating occurs due to the higher concentration of metal ions. This will increase the roughness of the surface deposited.

Agitation can also sweep away any bubbles that may form at the surface from hydrogen gas evolution, which would otherwise cause pits and porosity in the surface. Higher current densities can also be achieved since the limiting current density has been increased. The grain size of the deposit will also increase with increased rates of agitation.

Agitation by means of mixing the electrolyte using a magnetic stirrer was carried out in a previous work ⁷² and showed to produce very poor surface finishes. It was shown that the uniformity of the deposit is greatly decreased and there is a large variation in both surface morphology and copper content from the leading edge to the trailing edge, as seen in figures 2.9.

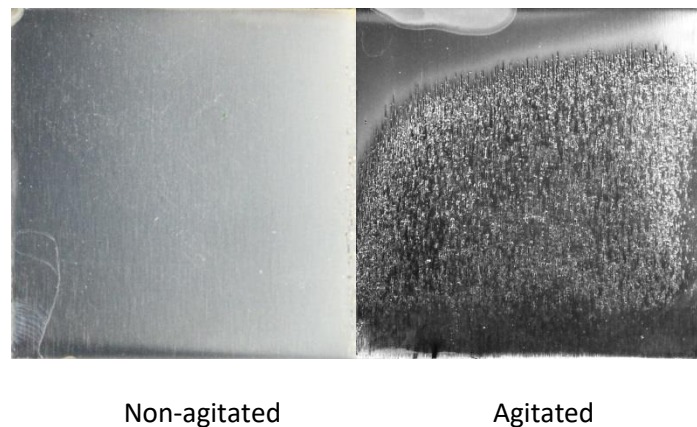


Figure 2.9 Photographs of electroplated Sn-Cu alloy on copper to $\sim 5 \mu\text{m}$ in thickness at 20 mA cm^{-2} showing how agitation changes surface quality with the left image showing an electroplate with no agitation and the right image showing an electroplate with agitation ⁷²

2.2.1.2 Current density

This factor affects how fast plating will occur, higher current densities will result in higher plating rates and lower current densities will result in lower plating rates. However, this is also affected by the limiting current density; hence once the limiting current is approached, any further increase in the current density has little or no influence on the electrodeposition of the particular metal ^{78,79}. As the

current density increases the amount of hydrogen gas evolved is also increased which can leave a poor surface finish.

2.2.1.3 Metal ion concentration

This directly affects the limiting current density of the plating system ⁷⁶. For example, if the concentration of metal ions is doubled the current density is also doubled, which will therefore double the rate of plating that can occur. However, increasing the metal ion concentration will decrease the alkali/acid ion concentration and result in a decrease in throwing power, which can lead to problems of anode passivation. If the substrate is of simple geometry with no holes then this will not be too much of a problem, though the cost is directly linked to the amount of metal salts present in the solution. Increasing metal ion concentration will also increase the grain size of plated material ⁷⁹.

2.2.1.4 Changing the pH level of the electrolyte

The pH of the electroplating solution can affect the rate of reaction but also the current efficiency ⁷⁶. When the electrolyte becomes more acidic the cathode becomes agitated, therefore causing the reaction to speed up; however since acids are hydrogen donors and because the reaction speed has increased, this will result in more hydrogen ions in the solution which are then liberated as hydrogen gas by the electrons oxidising the hydrogen ions instead of the metal ions. Therefore, as the rate of gas generated increases, the current efficiency decreases. The opposite applies to electrolytes that are more alkali; this is due to the number of hydrogen ions present are lower because alkali solutions are hydrogen acceptors. Therefore, any hydrogen ions present will react with the alkali solution to form hydrides, which will increase the current efficiency by preventing the liberation of hydrogen gas.

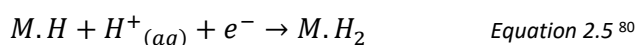
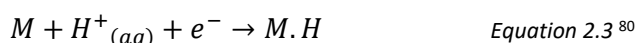
2.2.2 Cathode Current Efficiency

Cathode current efficiency is the efficiency of the current to reduce the metal ions to metal atoms ⁷⁶; if the current efficiency is 90 % then this means that 90 % of the electrons are used to reduce metal ions and the other 10 % of electrons are liberating hydrogen by converting H^+ ions to H_2 gas. This can

happen if the current density is too high, such that there are not enough metal ions for the all the electrons to reduce. Also, the higher the cathode current efficiency the less hydrogen gas is evolved and the more metal will be electroplated.

2.2.3 Forming Hydrogen Gas and the Effects

Hydrogen gas is not immediately produced when reducing the hydrogen ions to hydrogen molecules, initially the hydrogen ions are reduced by the electrons and the atomic hydrogen is adsorbed onto the surface, see equation 2.3 below. These hydrogen atoms can then migrate across the surface to then bond with another hydrogen atom to form a (H₂) hydrogen molecule, see equation 2.4 below. Alternatively, if this mechanism is too slow then hydrogen molecules can be formed by further reduction of hydrogen ions near an already adsorbed hydrogen atom, to which these two atoms will bond to form molecular hydrogen, see equation 2.5 below. The molecular hydrogen is then desorbed from the surface and escapes as gas, see equation 2.6 below. The formation of hydrogen gas can cause irregularities in the plated surface, these irregularities can be seen without any aid of microscopes as thin lines across the sample where the gas has travelled. The gas can also form holes in the surface of plated sample that are visible to the naked eye.



2.2.4 Tin Electrodeposition on Brass

Tin is electroplated on brass to improve the surface properties of the brass material; tin mainly increases the solderability of the sample since brass is not easily soldered to unless a high thermal input is used ⁸¹. Tin is a soft and very ductile material compared with brass and its mechanical properties are insufficient to be used on its own (see table 2.1 for a full comparison). It can be seen

from table 2.1 that the mechanical properties of brass are far greater than those of pure tin, so better suited to a working environment.

Table 2.1 Difference in mechanical properties between brass and pure tin ⁸²

Property	Copper alloy (brass)	Pure tin
Young's Modulus	112 – 148 GPa	41 – 45 GPa
Yield Strength	30 – 500 MPa	7 – 15 MPa
Tensile Strength	100 – 550 MPa	11 - 18 MPa
Compressive Strength	30 – 500 MPa	7 – 15 MPa
Elongation	3 – 50 % strain	55 – 75 % strain
Hardness	44 – 180 H _v	3 – 5 H _v
Fracture Toughness	30 – 90 MPa m ^{1/2}	15 – 30 MPa m ^{1/2}

2.2.5 Tin-Copper Electrodeposition on Copper

Tin-copper is electroplated on copper to accelerate whisker growth ⁶⁷; this enables the study of mitigation techniques over a much shorter time period.

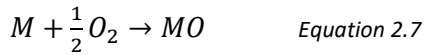
2.3 Electrochemical and Naturally Grown Oxides

An oxide layer can be considered a product of corrosion, where the metal atoms lose electrons; this then enables the metal ions to react with other ions such as oxygen ions (O²⁻) to form oxides or hydroxyl ions ((OH)⁻) to form hydroxides. Oxide layers can also be used to protect the material, depending on the type of oxide that is formed, which will prevent any further corrosion to the substrate. For example with tin, the natural oxide layer is formed from tin(II) species (this forms SnO) and will carry on growing for as long as it is left out in normal atmospheres; however, tin also has another valence species that can be used to form oxides which is tin(IV) species (this forms SnO₂ and Sn(OH)₄) ⁸³.

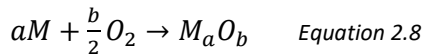
The fundamental difference between an electrochemical oxide layer and a naturally grown oxide layer is that an electrochemical oxide layer is formed putting a current across a sample that is submerged in a specific oxidation bath; and a naturally oxide layer is one that is naturally grown by the material

when left in normal atmospheric conditions. In general electrochemically formed oxide films are thicker than naturally formed oxide layers ⁷¹.

Oxidation equation for divalent metals ⁸⁴ (used for tin(II) species)



Oxidation equation for non-divalent metals ⁸⁴ (used for tin (IV) species)



2.3.1 Natural oxide

For the oxide layer in the natural oxide scenario to increase in thickness via the equations shown previously (equations 2.7 and 2.8), electrons must be conducted to the oxide-gas interface ⁸⁴; this is to enable the reduction of molecular oxygen to oxygen ions. In addition to this occurring, metal ions (M^{n+}) must be able to diffuse away from the metal-oxide interface and/or oxygen ions (O^{2-}) must be able to diffuse away from the oxide-gas interface and toward the metal-oxide interface. Furthermore, this oxide layer acts both similarly to that of an electrolyte for ions to diffuse through but also to an electrical circuit for electrons to be transferred. This growth mechanism can be seen in figure 2.10.

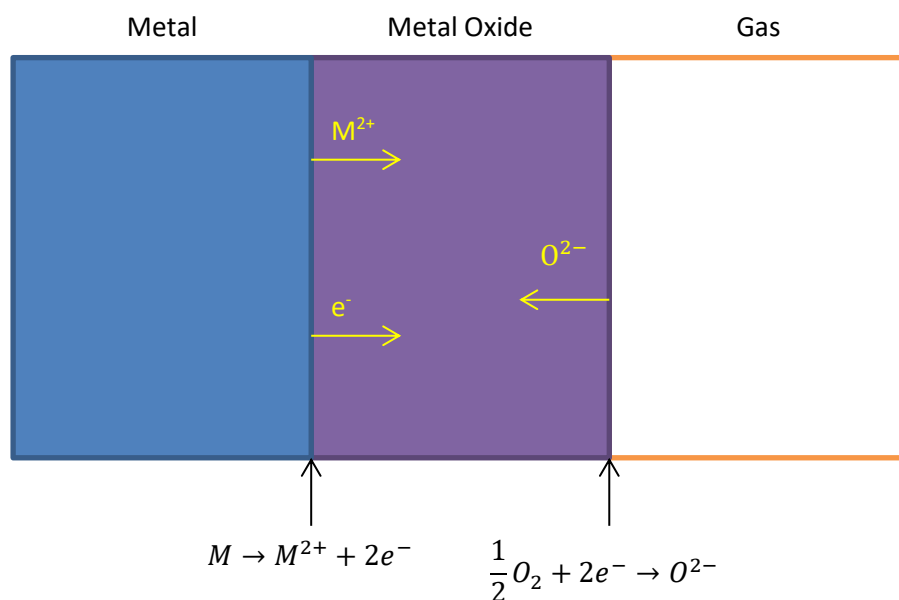


Figure 2.10 A schematic of how natural oxidation occurs. Where oxygen from the air reacts with the metal to form a metal oxide and subsequent oxygen will diffuse through the oxide layer to react with the metal that is diffusing in the opposite direction. ⁸⁴

2.3.2 Electrochemically formed oxide

Electrochemical oxidation can also be known as a process of electrolysis which is conducted in an electrolyte; alkaline electrolytes are the most common and widely used type of electrolytes for oxidising⁸⁵. When metallic tin is submerged in alkaline solutions it will undergo electrolysis and will anodically passivate to form a permanent passive film via the electrochemical oxidation of tin⁸³. A passive oxide film is not to be confused with a native oxide film, as a passive oxide is one formed by a corrosive action like electrolysis in a solution and a native oxide is one formed in the air. Tin can be passivated in alkaline solutions up to around pH12 when maintained anodically; however above pH12 tin will dissolve amphotERICALLY as stannite and stannate⁸⁶. The anodic passivation of the tin is very complex and contains a multistep process and the mechanism and composition of tin oxide is not completely understood.

2.3.3 Tin oxidation states

Tin has two oxidation states, the first one is tin(II) which has the ion representation of Sn^{2+} , this occurs when atomic tin loses 2 electrons from its outer shell and forms an ion with an overall charge of +2. The second is tin(IV) which has the ion representation of Sn^{4+} , this occurs when atomic tin loses 4 electrons from its outer shell and forms an ion with an overall charge of +4.

2.3.4 Cyclic Voltammetry

Cyclic voltammetry is a widely used technique from which information may be obtained about the electrochemical reactions that are occurring in a system, mainly it offers the location of redox potentials^{87,88} – i.e. it can be used to determine at what potentials different reducible and oxidisable species occur. Cyclic voltammetry involves cycling the potential of an electrode that is immersed in an electrolyte and measuring the resulting current. This can be seen as having an initial potential of V_1 that is swept up to a potential of V_2 at a fixed rate and once the potential reaches V_2 the scan is reversed and the potential is swept back down to V_1 – this can be done a number of times or just the

once. However, a two-vertex cycle can be used where V_{start} and V_{end} are the same and 2 potentials are used as ‘turning’ points – i.e. starting at a potential of 0 V, sweeping down to -1.5 V, sweeping up to 1.5 V and finally sweeping back down to 0 V to end the cycle, all vs. a reference electrode (SCE or Ag/AgCl). The rate at which the scan proceeds can affect the intensity of the peaks, as shown in figure 2.11; the faster the scan rate the more defined the peaks are and the slower the scan rate the less defined the peaks are – this could be due to the fact that at faster scan rates there is not enough time for chemical reactions to gain a state of equilibrium, so having a well-defined peak. Generally the peaks that occur in the positive current direction (anodic current peak) represent oxidation reactions and the peaks that occur in the negative current direction (cathodic current peak) represent reduction reactions.

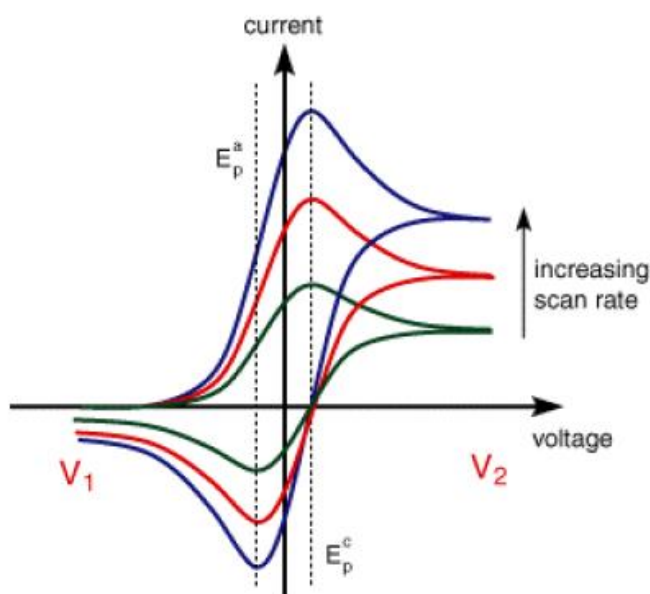


Figure 2.11 Multiple cycle voltammetry scans to show how the scan rate can affect peak current during cyclic voltammetry, with increasing scan rate increasing peak intensity⁸⁷

Both Díaz *et al*⁸³ and Alvarez *et al*⁸⁹ used cyclic voltammetry to determine at which potentials oxidisable and reducible species of tin occur in different buffer solutions. It was suggested, by both authors, that for a borate buffer solution, the first anodic peak corresponded to the oxidation reaction of metallic tin oxidising to form tin (II) species (such as SnO) and the lower second anodic peak corresponded to the oxidation reaction of tin (II) species oxidising to form tin (IV) species (such as

SnO₂). Alvarez *et al* also observed the same two oxidation reactions for a potassium bicarbonate-carbonate solution, additionally it was suggested that the first anodic peak (A₁) can be associated with the active dissolution of tin to tin(II) species⁹⁰, according to equations 2.9 and 2.10. It was suggested that the second anodic peak (A₂) can be associated with the electroformation of tin(IV) species⁹⁰, according to equations 2.11 and 2.12. The broad decreasing side of the second peak was attributed to the dehydration reaction which leads to a more stable tin(IV) species, according to equation 2.13, which then arrives at a low anodic current which corresponds to the passivity region, as shown in figure 2.12.

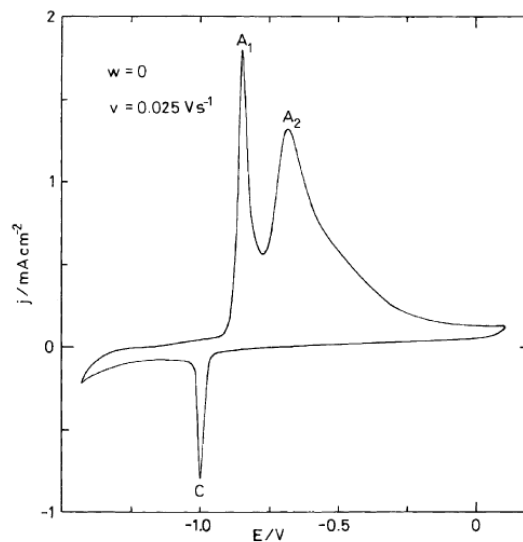
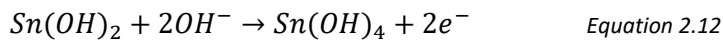
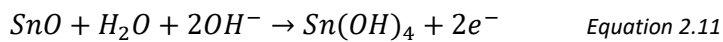
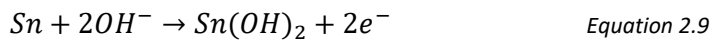


Figure 2.12 A cyclic voltammogram of tin in potassium bicarbonate-carbonate, where A₁ and A₂ correspond to the oxidation peaks tin to tin (II) and tin (IV), respectively. C corresponds to the reduction peak of tin (II) and (IV) oxides to metallic tin⁸⁹

Alvarez *et al*⁸⁹ attributed the cathodic peak (C) to the simultaneous reduction of Sn(II) and Sn(IV) species. However, when two cathodic peaks are present (depending on the anodic switching potential), nucleation processes are involved in the electroreduction of Sn(IV) surface products of

different stability, which was described by Gervasi *et al*⁹¹. Gervasi *et al* suggested that electroreduction of Sn(II)/Sn(IV)-containing surface layers anodically grown on Sn electrodes involved several distinguishable processes. For films that had been formed using an anodic switching potential of -0.8V vs. SCE (just after the first anodic peak, A_2), the electroreduction can be described by the instantaneous nucleation and 3D growth mechanism under diffusion control. For films that had been formed using higher anodic switching potentials, the two cathodic peaks can be associated with the bilayer structure of the oxide film and the electroreduction of the oxide film can be explained mainly as a progressive nucleation and 3D growth process under charge transfer control.

2.4 Conversion Coatings

Conversion coatings are a form of passivation treatment and consist of converting the substrate metal surface from an active to a passive state⁹². A conversion coating can also be thought of as a mixed oxide coating as it consists of a mixture of corrosion products from the substrate metal and reduced species from the ions in the electrolyte. Generally, conversion coatings are significantly thicker than a native air-formed oxide, however, they are prone to cracking and flaking. Which, as suggested by Zhang *et al*⁹³ and da Silva *et al*⁹⁴, may be due to an increase in tensile stress within the coating. The authors suggested that the increase in tensile stress is due to the increased film thickness along with the drying process; whereby the moisture is removed from the coating which causes shrinkage and subsequently generates tensile stresses.

To date there is no published work on the use of a conversion coating to mitigate the growth of tin whiskers, however there has been studies into the use of a conversion coating to mitigate the growth of zinc (Zn) whiskers and in all cases a chromate conversion coating was used⁹⁵. It was reported by Arnold⁹⁶ and Sugiarto *et al*⁹⁷ that the chromate conversion coating only slowed down whisker growth and whiskers would penetrate through the coating. Arnold observed that the zinc whiskers would primarily grow at edges and where cracks developed.

However, there is a restriction on the production of chromate coatings due to hexavalent chromium becoming band under EU law ⁹⁸, due to its high toxicity and carcinogenic properties. Therefore, two different conversions were identified for this project. The conversion coatings identified are a molybdate conversion coating developed by Wilcox *et al* ⁹² and a tungstate conversion coating developed by Van de Leest and Krijl ⁹⁹, both of which are tailored for use with tin.

2.4.1 A Brief Background of Molybdate Conversion Coatings

It was reported by Wilcox *et al* ¹⁰⁰ that at the time, molybdate conversion coatings had not been widely utilised as promoters of conversion coatings, although the authors reported that molybdate conversion coatings were efficient at corrosion resistance in aerated conditions and had relatively low toxicity. The corrosion resistance of the molybdates is due to the formation of a molybdenum oxide film, with the Mo in a range of valency bands. The most common molybdenum oxides are Mo(IV) oxide (MoO_2) and Mo(VI) oxide (MoO_3), however, there are many non-stoichiometric oxides that are present between these two and will take the form of blue or purple solids (also known as 'molybdenum blue') ^{101,102}. Black molybdate coatings can also be produced on tin, as shown by Gabe and Gould ¹⁰³. It was suggested that the black colour would form in the last stages of the molybdate conversion coating process ^{92,101}.

2.4.2 A Brief Background of Tungstate Conversion Coatings

One of the earliest works researching into tungstate conversion coatings was carried out by Robertson in 1951 ¹⁰⁴, who studied tungstate conversion coatings as corrosion inhibitors in cooling water systems. In 2005 da Silva *et al* ¹⁰⁵ studied tungstate conversion coatings that had been produced on Zn-based surface. The authors showed that the formation of the tungstate conversion coatings was similar to chromate, however, the corrosion properties were significantly reduced compared to the chromate coatings. However, for this project corrosion protection is not a necessary property to have. Van de Leest and Krijl ⁹⁹, however, showed that for tungstate conversion coatings on tin, the conversion coating protects the underlying tin from aqueous corrosion and tarnishing. Van de Leest

and Krijl also showed that solderability of the conversion coated tin was sufficient, although not as good as metallic tin.

2.5 Polymeric Coatings

A conformal coating is an organic coating that is applied to a surface to improve the surface properties of the underlying material or for improving the general aesthetics. An organic compound is any compound that is based on carbon (i.e. polymers and elastomers) and these coatings were generally used to improve resistance to the environment, such as corrosion and ultra-violet (UV) degradation¹⁰⁶.

2.5.1 A Brief Background of Conformal Coatings in Industry

These organic coatings can be seen as a complex mixture of chemical compounds and can be grouped into four broad categories¹⁰⁶:

- *Binders*¹⁰⁶ – these are the materials that form the adhesive film which binds the top organic coating and adheres to the substrate material. The binder film must be able to have both good binding properties to the top coat and good adhesive properties. This binder layer governs the properties of the coating film.
- *Volatile components*¹⁰⁶ – these are liquid materials that enable the coating to be fluid enough for application. These liquids subsequently evaporate during and after application. A commonly used term is ‘vehicle’ which is a mixture of both the volatile components and the binder.
- *Pigments*¹⁰⁶ – these are finely divided insoluble solids (such as powders), these solids are dispersed throughout the vehicle and due to their insolubility they will then remain dispersed in the solid coating. Pigments are generally used to give the coating colour and opacity, but can also be used to change the properties of the coating. Not all coatings contain pigments

and are commonly referred as 'clears' or 'clear coatings'; transparent coatings such as clear varnishes are an example of this.

- *Additives*¹⁰⁶ – these are materials that are added in small quantities to change the properties of the coating. Such examples are UV stabilisers, flow modifiers and catalysts for polymerisation reactions when curing.

Majority of organic coatings contain a number of substances from each of these categories, where each of the substances usually comprise of a mixture of compounds¹⁰⁶. There are a limitless number of combinations which means organic coatings can be used for a wide range of applications. There are three main types of organic coatings and these are paints, varnishes and lacquers; however, varnishes and lacquers are generally used for woods and not metals.

2.5.2 Adhesion

Adhesion in organic coatings is a critical property because if the adhesion is poor then the coating won't stay on the substrate and will effectively be useless no matter how good the other properties are. The resistance to the coating delaminating from the substrate can directly be affected by the surface topography, a roughened surface will promote mechanical interlocking¹⁰⁷. If the substrate surface is smooth (figure 2.13a) then only the interfacial attractive forces will be holding the coating and substrate together. Whereas if the surface is rough (figure 2.14b) then the substrate will be mechanically interlocked with the substrate and one would either have to break the substrate or the coating to cause delamination; the total interaction area will be greatly increased therefore increasing the amount of interfacial attractive forces. However, if the coating doesn't penetrate the roughened surface then this can reduce the adhesion compared with having a smooth surface as the interaction area will be smaller than the geometric area and mechanical keying won't be observed. A common way to increase surface roughness would be use an abrasive blasting technique, which fires sand particles at the surface and erode the surface; another way to roughness the surface would be to etch the metal surface in a suitable etching agent, this would produce a finer type roughness.

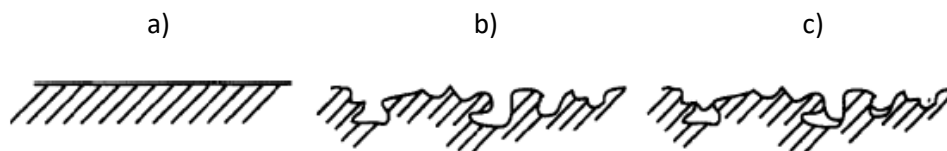


Figure 2.13 Surface geometries and interactions between the coating and the substrate a) a smooth surface, b) a rough surface with complete coating penetration, and c) rough surface with incomplete coating penetration ¹⁰⁷

2.5.2.1 Adhesion Promoters

One way to improve the adhesion properties of the coating is to use adhesion promoters, which are also known as coupling agents; these substances are molecules that are chemically adsorbed to the substrate material to form very thin layers that are commonly mono-molecular ¹⁰⁸, this is shown in figure 2.14. These adsorbed molecules are then able to chemically interact with the organic coating thus providing a strong adherence to the substrate.

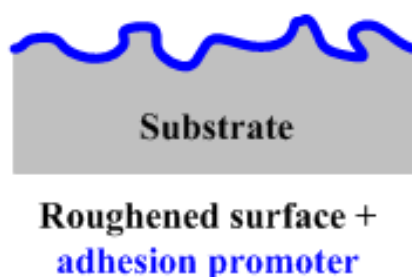


Figure 2.14 Schematic showing how the adhesion promoter forms a very thin layer and follows the surface topography ¹⁰⁸

The molecules that are used as adhesion promoters have chain structures with both ends of the chain having different functional groups ¹⁰⁸. Where one end of the chain will have an inorganic functional group that has a chemical affinity to the substrate material and the other end will have an organic functional group that will be capable of forming a covalent bond with the organic coating material. These adhesion promoters can be either applied straight on to the substrate material as an intermediate layer or can be mixed in with the organic coating before application; when it the adhesion promoter is mixed with the organic coating it will not only improve the adhesion properties to the substrate but also improve the bonding with any reinforcing phase(s) present in the coating.

There are a number of different types of adhesion promoters, these being:

- Organosilanes – these are commonly used to improve the adhesion of the coating to the substrate which contains a hydrolysable group that will react with hydroxyl groups in the inorganic substrate¹⁰⁸ and these molecules then form a polysiloxane polymer on the substrate surface. The organic functional group in the organosilane will form covalent bonds with the organic coating being deposited over it. The most common organosilane used is γ -glycidoxypropyltrimethoxysilane (GPTMS).
- Organotitanates – these are usually used as coupling agents to improve the bonding with the reinforcing phase¹⁰⁸.
- Zirconates – these are similar to the titanates but have improved stability¹⁰⁸.
- Zirconaluminates – these are used as a cost effective replacement to organosilane¹⁰⁸.

2.5.3 Application Methods

There are many different types of application methods for polymeric coatings depending on a number of factors, such as capital costs, operating costs, film thickness and circumstances¹⁰⁹. The application methods can be categorised into two different categories and these are physical methods and electrochemical methods.

2.5.3.1 Physical Application Methods

There are many types of physical methods including brushing and spraying¹⁰⁹, and each method is used depending on the application. These methods include brush, pad, spray and dip applications, which will now be described.

2.5.3.1.1 Brush Application

There are a number of different brushes available: narrow and wide, long and short-handled, and nylon, polyester or hog bristle¹¹⁰. Nylon bristles can be used for water-based coatings but not for some solvent-based coatings as they would swell. Polyester bristles can be used for both water and

solvent-based coatings. Hog bristles can be used for solvent-based coatings but not water-based coatings. The coating is held in place in between the bristles in all brushes and all have a large number of bristles. The coating is applied to surface by the pressure being exerted on the brush forces the coating out from between the bristles and this then splits the layer of coating so that part of the coating is left on the bristles.

The viscosity of the coating is important when using brushes as when the viscosity is too high there will be too much on the brush and it will be hard to apply the coating; when the viscosity is too low there will be too little on the brush, but it will be easier to apply the coating ¹⁰⁹.

2.5.3.1.2 Pad Application

Pad application is similar to brush applications but instead of bristles as the applicator a sheet of fabric is used to apply the coating. The most common pad applicator is a nylon pile fabric that is attached to a foam pad ¹⁰⁹. However, for coatings with a low viscosity (such as varnishes) a pad made from lamb's wool is used. The advantages of using a pad applicator than a brush applicator are that pads can hold more coating material than equivalent width brushes and the coating surface tends to be smoother than when using a brush. However, a disadvantage would be that a tray must be used with pads therefore more wastage is produced and solvents can evaporate.

2.5.3.1.3 Spray Application

This method is widely used and is much faster than using either brush or pad applicators ¹⁰⁹. A main disadvantage to this method is the fact that it is hard to apply the coating exactly where desired, therefore needing areas to be masked where the coating isn't desired. Another disadvantage would be the low efficiency of the method because only a fraction of the coating particles are deposited onto the substrate. There are many different types of spray application but all atomise the liquid coating being used.

The low efficiency of this application method is due to the atomised droplets either bouncing off the substrate or not coming into contact with the substrate¹⁰⁹. The droplets bounce off the substrate due to the eddy currents of air that are formed by the high pressures of the spray applicator. Higher pressures increase the forward velocity of the air therefore more droplets will bounce off the substrate. The two reasons for a number of droplets not coming into contact to the substrate is due to: overspray, which is where the droplets go past the substrate; and fall out, which is where the droplets drop in an arc due to gravity – this problem is particularly affected by distance between spray nozzle and substrate.

2.5.3.1.3.1 Compressed Air Spray Gun

This method of spraying atomises the coating by using fine streams of compressed air and is the oldest type of spraying method¹⁰⁹. This method transfers the coating by driving it through the nozzle by low pressure (1-5 kPa) and the stream of coating is then atomised using fine streams of compressed air (25-50 kPa). The degree of atomisation is dictated by several factors:

1. The viscosity of the coating being applied, where lower viscosities will produce low shear rates and form smaller droplets.
2. The air pressure being used, where higher pressures will form smaller droplets.
3. The diameter of the orifice where the coating is exiting from, where a smaller orifice will form smaller droplets.
4. The pressure forcing the coating through the orifice, where high pressures will form smaller droplets.
5. The surface tension of the coating material, where a lower surface tension will form smaller droplets.

A big disadvantage to using compressed air spray guns is the very low transfer efficiency (percentage of droplets leaving the gun that are then deposited on the substrate) which is 25 %¹⁰⁹. However, if a high volume, low pressure air gun is used then the transfer efficiency can be increased up to 65 %.

This is where the guns are operating at low air pressures (2-7 kPa) and higher air volumes. The increase in efficiency is due to the reduction of droplets being rebounded back off the substrate because of using a lower pressure.

2.5.3.1.3.2 Airless Spray Guns

In this spray method the coating is forced out of the orifice at high pressures (5-35 MPa) and as the coating exits the orifice the pressure is released which then causes cavitation of the particles, thus leading to the atomisation of the coating ¹⁰⁹. The degree of atomisation is dictated by several factors:

1. The viscosity, where decreased viscosities will produce smaller particles.
2. The pressure used, where increased pressures will produce smaller particles.
3. The surface tension of the coating material, where a lower surface tension will produce smaller particles.

Compared with compressed air spraying, this method generally produces larger particles and in general more uniform thicknesses can be achieved using the compressed air method ¹⁰⁹. When using this method, solvents with a higher relative evaporation rate should be used because of the larger sized particles that are produced compared with the compressed air method. However, the advantage over the compressed air method is that the airless method is quicker. Another advantage would be the reduced bounce back due to no air being used to propel the coating, with a transfer efficiency of 40 %.

2.5.3.1.3.3 Electrostatic Spraying

In this method the coating material is electrically charged by, in its simplest form, a wire in the orifice which has an induced charge on it between 50-120 kV ¹⁰⁹. At the end of the wire the discharge causes the air to ionise and as the atomised coating material passes through the ionised gas, the particles are negatively charged. The substrate that is to be coated needs to be electrically grounded, so when the particles coating approach the surface the differential in charge attracts the particles to the surface.

The main advantage for this method is the increased transfer efficiency of 60-85 %; this is because when overspray occurs the particles can be attracted back to the other side of the object being coated. However, if the conductivity of the coating material is poor then this method would be very inefficient as the particles won't be charged sufficiently by the ionised gas. This undercharging would be more common with coatings that contain only hydrocarbon solvents, therefore needing to substitute some of the hydrocarbon solvents for nitroparaffin or alcohol solvents to increase the conductivity of the coating material. Also for coatings that contain a free carboxylic acid group, a tertiary amine can be added to improve conductivity. However, if the conductivity is too high there is a risk of electrical shorting and coatings that are water-based tend to have a higher conductivity than solvent-based. Therefore, to minimise the chance of electrical shorting through the spray of material, the gun should also be grounded.

2.5.3.1.4 Dip Coating

This method is extremely simple by the fact that it's simply the object to be coated being dipped into a tank of the coating material and being pulled back out ¹⁰⁹. Any excess material is subsequently drained off the object and back into the tank. In practice this method does tend to be more complex, due to a difference in film thickness across the object due to excess material drainage and solvent evaporation rate. The film formed tends to be thicker at the bottom of the object than the top because the material flows from top to bottom when withdrawing the object from the tank. Film uniformity can be optimised by carefully controlling the withdrawal rate and the rate of evaporation; therefore if the object is withdrawn slowly enough and the solvent evaporates quickly enough then a uniform film can be achieved. However, in production the object tends to be withdrawn quicker than the optimum speed therefore leading to differences in thickness across the object being coated.

The viscosity of the coating will also affect the thickness of the film as coatings with higher viscosities will form thicker films ¹⁰⁹. The viscosity can also change due to the evaporation of the solvent and as the solvent evaporates more, the viscosity of the coating material increases. Another way for the

viscosity to increase would be due to chemical reactions between individual components in the coating material. Therefore great care is needed when using the dipping technique and if volatile components are used such as oxidising alkyds, then an antioxidant must be added because the oxidising chemical will oxidise which leads to cross-linking. However, the antioxidant must be volatile enough to evaporate in the early stages of curing as it will inhibit the cross-linking when the film cures; also the antioxidant can't be too volatile so as not to rapidly evaporate from the tank.

2.5.3.2 Electrodeposition Application Methods

This method can be a very efficient method for applying high performance coatings ¹⁰⁹. Generally primers are the most common type of coating to be used with this particular method, however there are also a significant amount of uses for single-coat applications. The general principle for this method is relatively simple, where the material is electrodeposited from an aqueous solution onto the substrate. There are two types of electrodeposition systems and these are anionic and cationic. In anionic systems the particles are negatively charged and the substrate is made the anode, to which the particles are precipitated onto the surface by the hydrogen ions (H^+) that are formed there. Whereas, in the cationic system the particles are positively charged and the substrate is made the cathode, to which the particles are precipitated onto the surface by the hydroxide ions (OH^-) that are formed there. In both types the binder is generally a thermoset and the coatings are baked to cure.

These systems must enable all the components in the coating material to be attracted to the substrate electrode at the same rate, because otherwise the composition of the coating material will change over time ¹⁰⁹. Polymer films can be deposited from polymer salt solutions but not from a dissolved polymer as the binder for pigmented coatings. To electrodeposit pigmented coatings well it is necessary to use a vehicle in which the pigments are well dispersed and the cross-linkers are dissolved well. When diluted with water, it will form a stable, electrically charged dispersion of aggregate particles. The pigment being used must be sufficiently wetted by the resin so as not to migrate out of

the aggregates of resin. Also the cross-linking agent must only dissolve in the aggregates and not the water phase.

2.5.3.2.1 Anionic Electrodeposition

The resins that are used in this system must be substituted with carboxylic acid groups (figure 2.15) so the system has a specific acid number ¹⁰⁹. The other components, such as pigments, are then dispersed throughout the resin and the carboxylic acids are partially neutralised using an amine. This substitution is to disable the resin from becoming soluble in water when diluting the coating system, to which the coating is generally diluted down to 10% solids. This then causes the resin to form aggregates in the solution once the coating has been diluted; these aggregates are subsequently stabilised by the salt groups that are attached to the outer surface of the particles, hence improving dispersion in water due to the negative charge.

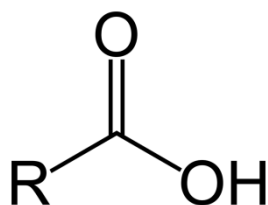
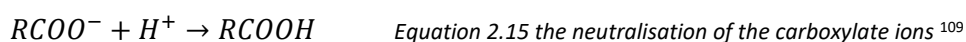


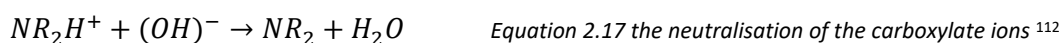
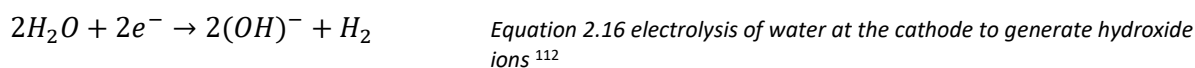
Figure 2.15 Carboxylic acid where R is a functional group ¹¹¹

The primary reactions that occur at the anode can be seen in both equations 2.14 and 2.15, where the first reaction shows the electrolysis of water to generate hydrogen ions ¹⁰⁹. These hydrogen ions subsequently neutralise the carboxylate ions on the resin aggregates. This neutralisation will therefore remove the charge that helps stabilise the aggregates and prevent them from coalescing. This neutralisation causes the surface of the aggregates to be less polar, so there is less swelling of the surface with water therefore the potential stabilisation by entropic repulsion is also reduced. Hence the resin aggregates coalesce on the metal surface and a polymer film will form.



2.5.3.2.2 Cationic Electrodeposition

In this system the resin is substituted with amine groups (figure 2.16) and neutralised with carboxylic acid groups ¹⁰⁹. The substitution of resin for amine groups causes the resin to form insoluble aggregates with a positive charge which in turn improves the dispersion of these aggregates. The primary reactions that occur at the anode can be seen in both equations 2.16 and 2.17, where the first reaction shows the electrolysis of water to generate hydroxide ions ¹⁰⁹. These hydroxide ions subsequently neutralise the amine ions on the resin aggregates. This neutralisation will therefore remove the charge that helps stabilise the aggregates and prevent them from coalescing. This neutralisation causes the surface of the aggregates to be less polar, so there is less swelling of the surface with water therefore the potential stabilisation by entropic repulsion is also reduced. Hence the resin aggregates coalesce on the metal surface and a polymer film will form.



Cationic systems tend to produce coatings with better corrosion resistance for steel than those produced using anionic systems ¹⁰⁹. This is due to the strong interactions between the amine groups, substituted into the resin that then coalesce on the metal, and the substrate which subsequently increases the wet adhesion. However, due to the amine groups remaining in the final cured coating the durability is less than those coatings formed using the anionic systems because they have none.

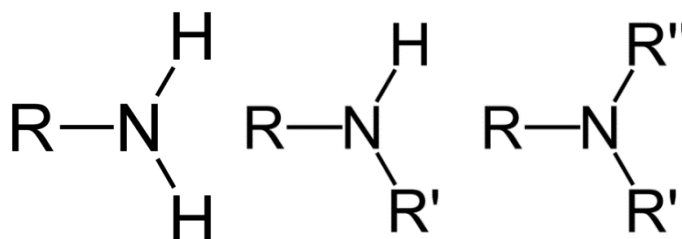


Figure 2.16 Different amine groups that can form in the resin with R representing an organic functional group, (left) primary, (middle) secondary, and (right) tertiary ¹¹³

2.5.3.2.3 Variables That Effect the Electrodeposition

Unlike with the electrodeposition of a metal, the electrodeposition of a polymer doesn't happen instantaneously¹⁰⁹. This is because the concentration of either hydrogen ions for anionic systems or hydroxide ions for cationic systems needs to be sufficiently high enough to enable the neutralisation of the aggregates therefore leading to precipitation on the substrate. After the concentration of neutralising ions is sufficient the rate of deposition is affected by the electrophoresis of the aggregates which is directly related to the voltage that is put into the system. Therefore, a high voltage isn't needed to electrolyse the water but to increase the electrophoresis of the aggregates to the electrode. The deposition rate can also be affected by the weight of coating; a heavier weighted coating will deposit quicker because there is a greater amount coated that is precipitated by the neutralising ion. However, the weight of the coating must be low enough so that there are enough polar salt groups to stabilise the aggregates, otherwise the coating won't be dispersed sufficiently. The deposition rate is also affected by the low molecular weight neutralising chemical groups added to the system as they are also attracted to the electrodes and due to their low molecular weight they will travel faster; therefore the concentration of these chemical groups must be kept low.

Initially the edges will be covered due to the increased current density in those areas and as the film thickness is increased the electrical resistance will also increase, which will reduce the rate of deposition in the initial areas of deposition¹⁰⁹. This will cause a limiting thickness of the coating and after this has occurred the outer flat areas are coated, this is then followed by any recessed and enclosed areas being coated. Therefore, the further back the recess is the longer it will take to fully coat the surface due to coating the recesses last. This time is affected by the throwing power of the system; a good throwing power will decrease the amount of time for recesses to be coated. The throwing power is directly related to the impressed voltage of the system; hence an increased voltage will increase the throwing power. However, having an increased voltage may cause film rupture and if the voltage is sufficiently high then the current will be able to travel through the coating and cause gas to generate underneath the coating which causes bubbling of the coating. Defects will occur at

decreased voltages as the conductivity of the coating increases. It has been reported by Smith and Boyd ¹¹⁴ that as the voltage is increased visible sparks can be seen due to discharging through the film which may cause film rupture.

The throwing power can also be affected by the bath conductivity, where an increased conductivity will give an increased throwing power ¹⁰⁹. However, there is again a limitation to increasing the conductivity because the increased conductivity is due to the increased presence of soluble salts in the bath which will therefore decrease the electrophoresis of the aggregates to the substrate. When these salts are increased the equivalent weight of the aggregates decrease which will therefore decrease the rate at which deposition can occur. Furthermore, from this there will be an increased amount of conductive material being trapped in the film which increases the chance of rupturing. This rupturing (and throwing power) is affected by the viscosity. If the viscosity of the precipitated aggregates is high then the aggregates won't coalesce sufficiently which will lead to a porous film and increased film conductivity which lowers the throwing power. However, if the viscosity is too low then the film formed will be too soft and when electrolysis occurs below the film surface, bubbles will form and easily break through the surface.

2.5.3.2.4 Advantages of Electrodeposition

A good advantage for using electrodeposition is that it can be highly automated which will greatly reduce labour costs ¹⁰⁹ which would be favourable in industry. It was observed by Miranda ¹¹⁵ that using cationic electrodeposition to coat air conditioners with a single epoxy layer, greatly reduces the manpower needed compared with using a flow coated primer and spray application. It was observed that for the previous coating system, 50 people needed to be employed (including post coating, where touch up and repairs are needed); whereas the electrodeposition system only needed one person to operate. This method also reduces the amount of coating being lost due to overspray. One of the major advantages of using this method over other techniques is the complete coverage of the

substrate, assuming the throwing power is sufficient ¹⁰⁹. Therefore, recesses that can't be covered by spraying techniques will be covered by an electrodeposition technique.

Another advantage would be the reduced sagging of the coating once the coating has been heated to cure, which is more common when using spray and dip techniques ¹⁰⁹. This is due to the increased viscosity of the coating upon application. Also, there is less thickness variation which happens when the coating flows down the sample from top to bottom when using a dipping technique.

There is an environmental advantage to using electrodeposition as the solvent content is less which would mean that the VOC (volatile organic compound) emissions is reduced along with the hazard of a fire occurring ¹⁰⁹. Another environmental advantage would be no formation of overspray sludge; also since the solids content of the film deposited is high, only a short flash off time is needed before needing to be cured.

2.5.3.2.5 Disadvantages of Electrodeposition

There is however, a disadvantage to having a highly automated system which is the high capital cost involved, therefore limiting the applicability of highly automated lines to large production operations ¹⁰⁹. Having large production operations would cover the cost of having such a system, whereas smaller production lines would not find this system feasible therefore only needing a much simpler installation.

Even though good uniformity would be classed as an advantage, in this case it can also be classed as a disadvantage, especially with highly pigmented coatings ¹⁰⁹. This is because the coating will follow every contour on the substrate; therefore if the substrate is very rough then the coating applied will also be very rough. It is said that if a coating shows good metal filling the coating will show minimal replication of the contours on the substrate surface. Though, in some cases the defects can be repaired by either sanding or patching the defect with a conventional primer. However, this can be improved by reducing the amount of pigment that is present. This will reduce the viscosity of the coating prior

to cross-linking, which will promote flow and increase the amount of levelling. However, this increase in flow can, in some cases, cause undesirable flow which causes the edges to have a reduced thickness of the coating due to flow away from the edges. Once the cross-linking has occurred the viscosity will increase to a point where no flow will occur.

Another disadvantage would be when the electrodeposited coating is used as an intermediate layer and the fact that the adhesion between the top coat and the intermediate layers is not sufficient enough¹⁰⁹. This is because when using a spray technique, the intermediate layer will be slightly porous which will encourage mechanical interlocking between that layer and the top layer, whereas an electrodeposited layer will be much smoother and have an increased gloss finish which decreases the adhesion. This problem will be amplified when the amount of pigment is decreased to promote levelling, which in turn increases the smoothness and gloss finish. To overcome this problem another layer can be applied on top, which is called a sealer, and then the top coat is applied on top of the wet sealer. This sealer has reduced amounts of solids with relatively strong, slow evaporating solvents. This promotes the solvent to penetrate the primer surface which increases adhesion.

2.5.3.3 Vacuum Deposition

This is where the polymer coating is deposited onto the surface in a gas phase and under vacuum – this can also be known as chemical vapour deposition (CVD) or physical vapour deposition (PVD). When using polymer thin film coatings CVD is most commonly used. There are two types of CVD, these being initiated chemical vapour deposition (iCVD) and oxidative chemical vapour deposition (oCVD)^{116,117}. The method that is CVD is widely used to obtain defect-free, pure inorganic thin film coatings that can have their properties finely tuned. Using iCVD and oCVD enables the advantages of using CVD as an application method while being able to use polymers as the deposited material. Both homopolymer and copolymer coatings can be produced using CVD.

2.5.3.3.1 Initiated Chemical Vapour Deposition (iCVD)

For this particular CVD method, a monomer (the coating required) and an initiator both flow into a vacuum chamber where they then come into contact with electrically heated filaments. The initiator then breaks down into radicals which then starts a free-radical polymerisation of the monomer at the surface of the object being coated ¹¹⁶, this reaction can be shown in figure 2.17. An example of such a reaction is using perfluorooctane sulfonyl fluoride (PFOS) as an initiator to aid the CVD of polytetrafluoroethylene (PTFE). It was found that when PFOS thermally decomposes into radicals, these radicals greatly increases the rate of deposition of the PTFE and it was also found the deposition was more controllable than when an initiator wasn't used.¹¹⁸

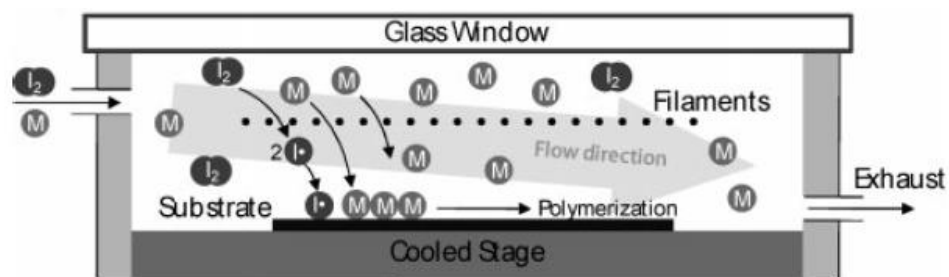
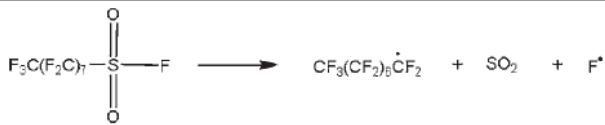
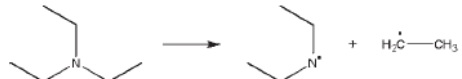
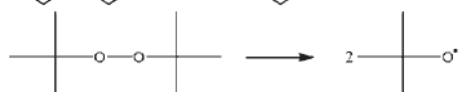

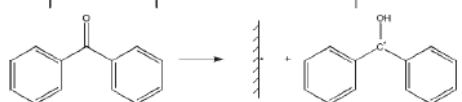


Figure 2.17 Schematic of an iCVD vacuum chamber, showing the initiator breaking down into a free radical (where I_2 is the generator and M is in the monomer) ¹¹⁸

Using wires to heat the initiator gas enables the substrate to keep cool to promote the adsorption of the monomer, by limited the viewing factor for radiative heat transfer ¹¹⁸. Also having a vacuum (low pressure) reduces conduction through any gas phase to the substrate. Another way to decompose the initiators into radicals is to use ultraviolet (UV) irradiation which is also known photoinitiated chemical vapour deposition (piCVD). For this to work the vacuum chamber has no filaments but a viewing window that provides the correct wavelength of UV irradiation so as to excite the initiator gas. The initiators used in piCVD are commonly named photoinitiators and tend to be volatile azo compounds; these can be used with a number of monomers that are used in iCVD. A table of different initiators are shown in table 2.2.

Table 2.2 Examples of initiators, showing their dissociation mechanism, class and dissociation conditions ¹¹⁸

Initiator	Dissociation Mechanism	Class	Dissociation Conditions
Perfluorooctane sulfonyl fluoride	 $\text{F}_3\text{C}(\text{F}_2\text{C})_7\text{SO}_2\text{F} \longrightarrow \text{CF}_3(\text{CF}_2)_7\dot{\text{C}}\text{F}_2 + \text{SO}_2 + \text{F}^\bullet$	Thermal	450–550 °C
Triethylamine	 $\text{N}(\text{CH}_2\text{CH}_3)_3 \longrightarrow \text{N}^+(\text{CH}_2\text{CH}_3)_3 + \text{H}_2\dot{\text{C}}-\text{CH}_3$	Thermal	450–550 °C
Tert-butyl peroxide	 $\text{C}(\text{CH}_3)_3\text{OOC}(\text{CH}_3)_3 \longrightarrow 2 \text{C}(\text{CH}_3)_2\text{O}^\bullet$	Thermal	200–300 °C
2,2'-azobis (2methylpropane)	 $\text{C}(\text{CH}_3)_3\text{N}=\text{N}(\text{CH}_3)_3 \longrightarrow 2 \text{C}(\text{CH}_3)_2\text{O}^\bullet + \text{N}_2$	UV type I photoinitiator	$\lambda = 366 \text{ nm}$ 110 mW/cm^2
Benzophenone	 $\text{C}_6\text{H}_5\text{COC}_6\text{H}_5 \xrightarrow{\text{UV}} \text{C}_6\text{H}_5\dot{\text{C}}\text{O} + \text{C}_6\text{H}_5\text{C}(\text{OH})^\bullet$	UV type II photoinitiator	$\lambda = 254 \text{ nm}$ $60 \mu\text{W/cm}^2$

2.5.3.3.2 Oxidative Chemical Vapour Deposition (oCVD)

This particular CVD method is used to produce conductive polymer coatings by the flowing monomer reacting with an oxidising agent in the vacuum chamber where subsequently a step polymerisation occurs ¹¹⁷, shown in figure 2.18. Conductive polymers (also known as conjugated polymers) tend to be insoluble due to their rigid backbone which causes other application methods to have difficulties when depositing them; however, oCVD can deposit long, rigid chained polymers. An example comparison of this advantage is the deposition of poly(3,4-ethyenedioxythiophene), known as PEDOT, by solution spin-casting and oCVD. In solution spin-casting another chemical (polystyrenesulfonate) needs to be added to increase the solubility and to act as solid-state dopant. However, this added chemical isn't electrically conductive therefore greatly reduces the overall conductivity of the final coating; also the coating uniformity is poor due to wetting effects. In comparison when using oCVD no other chemicals are needed because the monomers required (and their derivatives) are volatile enough and can be easily introduced into the vacuum chamber. This gives the coatings far better conductive properties and the uniformity is vastly improved.

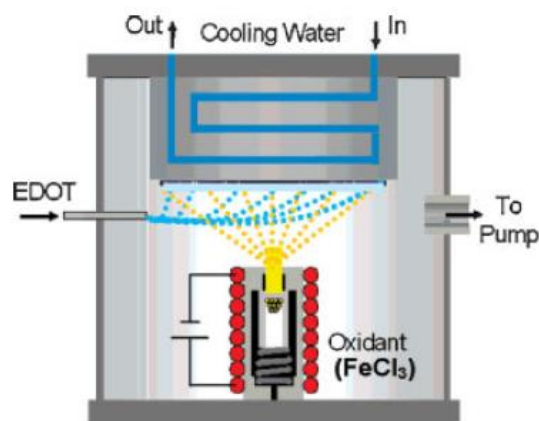


Figure 2.18 Schematic of an oCVD vacuum chamber, showing the oxidant (iron chloride) reacting with the monomer ethyenedioxythiophene (EDOT) ¹¹⁸

The polymerisation method is much different to that of iCVD where the biggest difference is that the chemistry is spontaneous in oCVD and doesn't require an external source to trigger a reaction like with heated filaments in iCVD ¹¹⁸. Initially in oCVD a reaction with an oxidant and the monomer forms a radical cation and subsequently pairs of these radical cations dimerise. These dimers then have a proton removed by further reactions with the oxidants to form neutral conjugated species. The deprotonated dimers then oxidise and further react with other radical cations to form higher order oligomers. Even longer chains are formed through the cycle of formation and oxidation. However, it should be noted that the addition of each monomer requires further reactions with several oxidants. This is much different to iCVD where the initiation radical can cause a large number of monomers to polymerise.

2.5.4 Conformal Coatings in the Electronics Industry

In the electronics industry a conformal coating is a polymeric coating that protects the underlying assemblies which include being protective against heat and solvents ¹¹⁹. They must also be resistant to moisture and humidity, so as to reduce the chance of any current leaking, electrochemical migration, dendrite growth and arcing.

2.5.4.1 Types of Conformal Coatings

According to the IPC (formerly known as Institute for Printed Circuits) standard ¹¹⁹ there are two different liquid groups of coatings, organics and silicones. There are many different coatings that are used but the primary traditional classifications are acrylic, epoxy, silicone, urethane, and poly-para-xylylene, which now be described.

2.5.4.1.1 Acrylics

This type of coating is used as a general-purpose coating, corrosion resistance, enamel for wiring, and wire-coil doping ¹²⁰. They are most commonly made of one-component and have a low-viscosity which can be used for either spray or dip application. Acrylic coatings can be cured rapidly either in air or being baked in an oven, where the coating can reach the optimum physical properties in minutes.

The advantages ^{119,120} of using acrylic based coatings are:

- They are fungus resistant and have a long shelf-life.
- They give off very little heat when curing, which prevents any heat damage to heat-sensitive components.
- They don't shrink during the curing process.
- They have good resistance to humidity.
- They have good adhesion to metals which can be improved by using a nonoxidising alkyd primer.
- The acrylic enamels have very good thermal stability and can be used at intermittent temperatures as high as 260 °C.
- They have good electrical properties at room temperature.
- They have good flexibility which is good when being used for coatings on wires.
- They have low water absorption.
- They have good solderability, though it isn't advised to solder through them.

- They are resistant to water, alcohol, alkalis and acids.
- They are very resistant to oils, greases and chemical fumes.

The disadvantages ¹¹⁹ of using acrylic based coatings are:

- When being used for electrical insulating applications they soften easier at elevated temperatures compared to other polymers. In general, the maximum temperature for acrylics (depending on formulation) is 95-155 °C.
- They aren't very resistant to solvents, which can be shown by the fact they can be easily removed by solvents. Though this may not be such a disadvantage because then the rework and repair method can be used if the substrate needs some form of repairs.
- The electrical properties degrade with increasing temperature and epoxies and silicones are more stable over a larger range of temperatures compared with acrylics.

2.5.4.1.2 Epoxies

These type of coatings are generally based on two components ¹¹⁹ that then react together to form the final chemistry desired. However, single part resin coatings are available, which contain temperature-activated hardeners to cure and set the resin. The temperature that the curing occurs at for these resins are generally higher than 66 °C; however, ultraviolet (UV) curable coatings are available which prevents the need for using higher temperatures. These epoxy resins are primarily based on the high reactivity of the oxilane ring ¹¹⁸; these rings can be seen at either end of the organic functional group, R, in figure 2.19. These epoxy rings will open up and allow polymerisation to occur with the presence of acidic/alkaline compounds or compounds with active hydrogen atoms. This can be shown in figure 2.19, where a diepoxide compound is polymerised by reacting with a compound containing an active hydrogen atom.

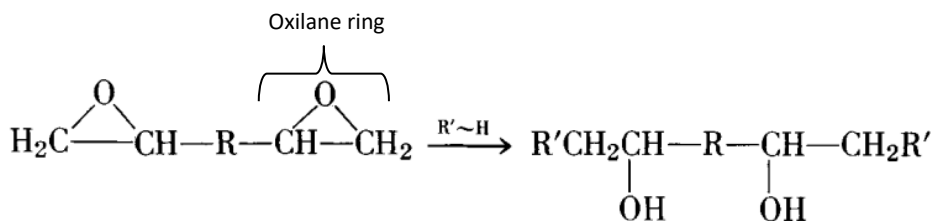


Figure 2.19 Polymerisation reaction of diepoxide (also showing the oxilane ring)¹²⁰

The advantages^{119,120} of using epoxy based coatings are:

- They have excellent adhesion properties to a number of different substrates and under a number of different conditions. This is because epoxies are highly polar and surface-active which enables them to have both good chemical and mechanical bonding properties to the substrate.
- They have excellent resistance to moisture, salt spray, organic solvents and chemicals. The moisture resistance is due to the curing of the epoxy resin, which when properly done will be stable even in boiling water¹¹⁸. When the epoxy is undercured or a non-stoichiometric mix is used, then the moisture absorption will increase, therefore the curing of the epoxy needs to be carefully controlled to obtain the best properties. The salt-spray resistance is also linked with the adhesion properties.
- They have good electrical properties even in high-stress applications. The properties are stable up to temperatures of 150 °C and relative humidity of 95-100 %.
- They have relatively good thermal properties compared to most other coatings (though they are lower than silicone coatings¹²⁰) because they are a thermosetting material, which means that they don't have a melting temperature but a high degradation temperature⁸⁴. In general they are stable up to 150 °C, however, anhydride- and aromatic amine-cured resins can be stable up to 200 °C¹²⁰. Once the operational temperature exceeds these, the coating will begin to degrade along with all of the other properties.
- Being able to cure using UV radiation greatly reduces the curing temperature and time.

The disadvantages¹¹⁹ of using epoxy based coatings are:

- When curing the resin will shrink and may cause damage to the substrate. This means that a buffer material must be used around the components so as to prevent damage due to shrinkage. Also curing at lower temperatures will aid in the prevention of shrinkage damage.
- The curing process can take a prolonged amount of time, especially at lower temperatures which can take days if curing at room temperature. Using higher temperatures will greatly reduce curing time to around a few hours.
- The raw components of the coating have a short shelf-life due to the volatility therefore needing to be used in a short time period.
- Due to being a thermoset, these coatings tend to be less flexible and brittle. This causes them to have poor stress dissipation.

2.5.4.1.3 Silicones

Silicone coatings can be said to be semiorganic due to having a silicon-oxygen structural backbone¹²⁰, as shown in figure 2.20. The physical properties of silicones are very similar to alkanes; however the difference is that silicones have better thermal stability due to the silicon-oxygen backbone¹²¹.

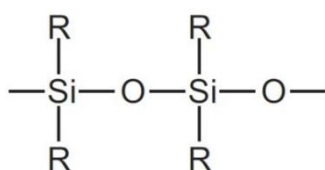
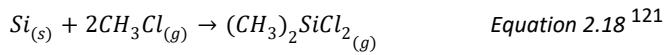


Figure 2.20 Silicon-oxygen backbone of a silicone coating, where R would be an organic group (not necessarily the same one)¹²¹

There are three stages to produce a silicone material; firstly a chlorosilane needs to be produced by reacting silicon with a chloroalkane gas¹²¹ (or any chloro-organic compound). An example reaction can be shown in equation 2.18, where silicon is reacted with chloromethane to produce dichlorosilane. This chemical reaction is done by passing the chloroalkane gas through heated silicon (~500 K) in the presence of a copper-based catalyst (either pure copper or a copper compound), where then the volatile mixture of chlorosilanes distils over.



Once the chlorosilanes are synthesised from silicon they are hydrolysed to form a silanol¹²¹. This is where the previously formed chlorosilane is reacted with water to produce the silanol with an excess chemical of hydrochloric acid, as shown in figure 2.21. In the reaction shown in this figure, a dichlorosilane is hydrolysed to form a disilanol.

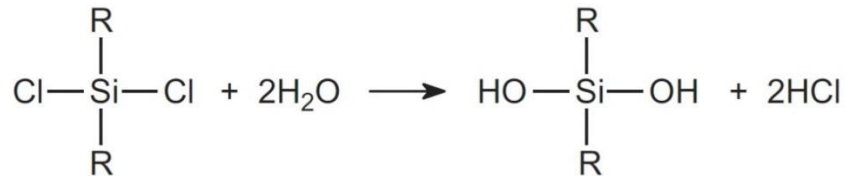


Figure 2.21 Hydrolysis of dichlorosilane to form disilanol¹²¹

These silanols will then spontaneously condense to give linear or cross-linked silicone resins¹²⁰ (siloxane). The reaction is shown in figure 2.22, where a disilanol condenses to a siloxane. Most siloxanes are produced with n being between 20-50, which tend to be too short to be useful and are known as oligomers¹²¹.

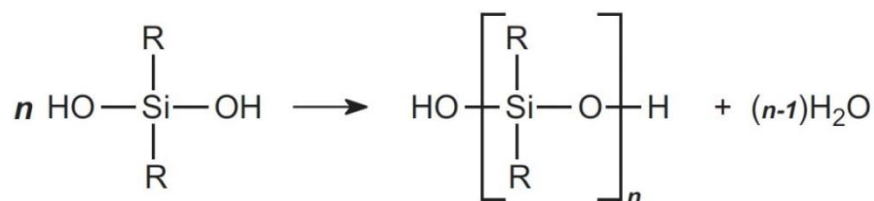


Figure 2.22 Disilanol condensing to form a siloxane¹²¹

Finally the oligomers that are formed condense together in the presence of an acid catalyst to form long chain polymers¹²¹, as shown in figure 2.23. The final number of repeating units tends to be between 2000-4000. To then form silicone gels, elastomers and resins the siloxane chains are then induced to cross-link.

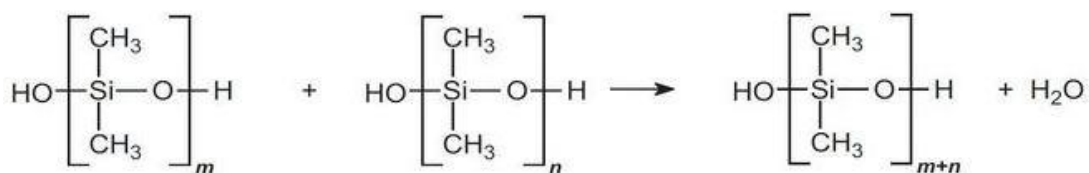


Figure 2.23 Condensation reaction between two oligomers to form a larger siloxane chain¹²¹

The advantages ^{119,120} of using silicone based coatings are:

- They are very good at withstanding extreme temperature cycling and have a wide temperature range of -55 °C to 200 °C. This thermal stability is due to the high bond energy of silicone-oxygen, compared with organics that have carbon-carbon bonds which don't have good thermal stability ¹²².
- They have a high resistance to humidity.
- They are very good insulators and can be used safely up to 180 °C for extended periods of time.
- They have a very low dissipation factor when being used in conduction with high impedance circuitry. The electrical properties are superior to most polymers, including epoxies.
- They are resistant to polar solvents.

The disadvantages ^{119,120} of using silicone based coatings are:

- The curing process should be taken place at or near the maximum operating temperature required for the coating thus possibly causing damage to components.
- Some silicones may migrate to other components and due to their good mould-release properties the adhesion properties may worsen. However, this migration can now be overcome by using solvent-free, non-volatile chemistries.
- The adhesion of silicones is generally low but can be improved by using an intermediate polymer layer, that has good adhesion properties to both the silicone and the component being coated (also known as a primer).

2.5.4.1.4 Polyurethanes

These coatings differ from most polymers because they don't contain any urethane monomers and in almost every case the polymer is created during the manufacturing stage of the object ¹²³. The common reaction between all polyurethanes can be shown in figure 2.24; to which a hydroxyl group

reacts with an isocyanate group to form the common urethane linkage ¹²⁰. The particular reaction shown is between diisocyanate with a diol and the pink atoms in the resulting chemical is known as the urethane linkage and is common to all polyurethanes.

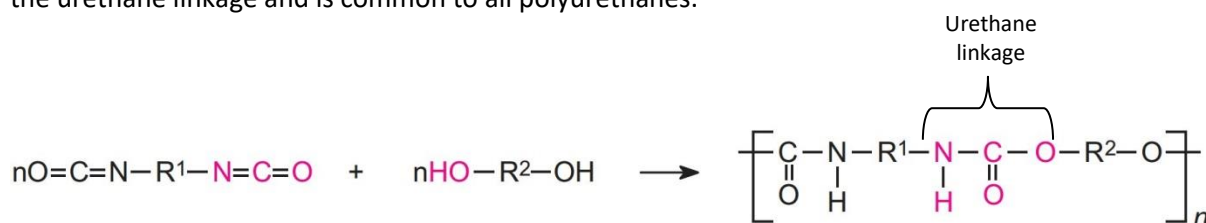


Figure 2.24 Chemical reaction to form polyurethane, showing the urethane linkage in pink ¹²³

The compounds that are the basis for the majority of polyurethanes are di- or polyisocyanates and most widely used is toluene diisocyanate (TDI)¹²⁰; this contains a mixture of the two isomers, as shown in figure 2.25. The TDI compound is produced by initially reacting methylbenzene (toluene) with both nitric and sulphuric acid to form two isomers of nitromethylbenzene ¹²³ (NMB). These NMB isomers are then nitrated further to produce two isomers of dinitrotoluene (DNT). Then the DNT isomers are reduced to form amines and then they are heated with carbonyl chloride to produce the needed diisocyanates. Another common compound is methylene diphenyl diisocyanate (MDI) ¹²⁰. However, they need to be co-reacted due to the high vapour pressures and highly toxic nature of free isocyanate groups (NCO).



Figure 2.25 Structures of both of the isomers for toluene diisocyanate ¹²⁰

These polyisocyanates are then reacted together with a polyol, which is either a hydroxyl-terminated polyether or a hydroxyl-terminated poly-ester ¹²³. Figure 2.26 shows the formation of polyurethane using TDI and a polyol derived from epoxypropane. If the polyol used has more than two hydroxyl groups then the long-chain produced will be linked to other long-chains.

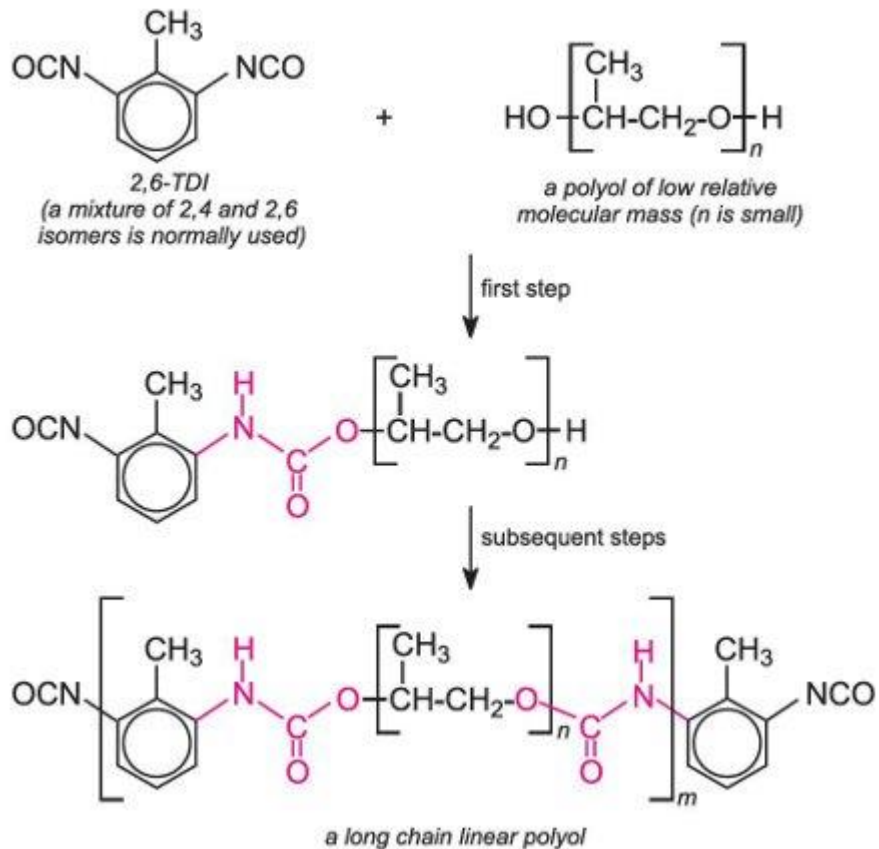


Figure 2.26 Common reaction between TDI and an epoxypropane polyol ¹²³

The advantages ¹¹⁹ of using polyurethane based coatings are:

- Using either single or two-component formulations will give humidity and chemical resistance. However, there is a drawback to having such a good chemical resistance, which is that they can't be removed if rework and repair need to be undertaken. This means it becomes rather difficult and costly to do so.
- They have good dielectric properties as they can withstand increased potentials.
- The newer formulations have resolved the issue of coatings becoming liquid under high humidity and temperatures.
- Two-component formulations have a cure time of 1-3 hours at elevated temperatures.

The disadvantages ¹¹⁹ of using polyurethane based coatings are:

- Even though they can be soldered through, they tend to leave an unwanted residue which will cause poor aesthetics of the coating.
- Single component formulations have a much longer cure time which can span between 3-30 days at room temperature.
- The two-component formulation has an extremely short pot-life ranging from 30 minutes to 3 hours.

2.5.4.1.5 Poly-para-xylelenes (parylenes)

Unlike the other polymeric coatings that are deposited in their liquid phase, this coating system is vacuum vapour deposited ^{119,124}. Due to being deposited in its gas phase, the coating can cover irregular surfaces much better than other polymeric coatings. The most commonly known reaction to produce this coating is by condensing the quinoid highly reactive compound ^{119,124}, shown in figure 2.27.

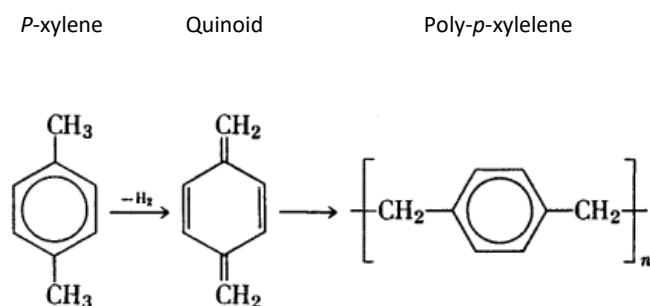


Figure 2.27 Formation of parylene N ¹²⁰

This quinoid compound can be produced initially by the *p*-xylene losing a molecule of hydrogen at elevated temperatures and increasing the pressure from 133.3-666.6 Pa ¹¹⁹, this loss of a hydrogen molecule causes the formation of a paracyclophane ¹²⁴, shown in figure 2.28. The pyrolysis of the paracyclophane then forms the quinoid structure, which can be considered as a diradical. When the quinoid structure comes into contact with the cold metal surface, it will then polymerise by radical-radical coupling to form the desired poly-para-xylene.

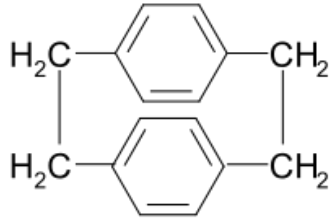


Figure 2.28 Structure of paracyclophane ¹²⁴

There are three widely used different parylenes, shown in figure 2.29, that are used depending on the requirements needed. These are parylene C, parylene N and parylene D. Parylene C is the most commonly used and has a good combination of properties along with having good resistance to moisture, chemicals and other corrosive gases. Parylene N is another widely used parylene and has very good dielectric properties, having a good dielectric strength and a constant that doesn't vary with changing frequencies. Parylene D has the greatest physical strength and electrical properties at elevated properties.

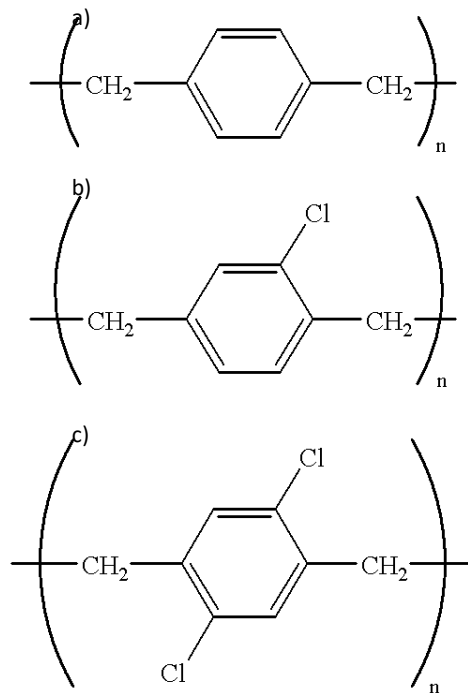


Figure 2.29 Structure of a) parylene C, b) parylene N, and c) parylene D ¹²⁵

The advantages^{119,120} of using parylene based coatings are:

- They have low coefficients of friction. Though not as low as PTFE (Teflon), parylene is similar to nylon with respect to friction.
- They have low moisture permeability. Parylene C has the best permeability properties being similar to that of Teflon.
- They have very good abrasion resistance.
- They have high dielectric strength, volume and surface resistivities. Parylene N has the best electrical properties.
- If the parylene is fluorinated then the parylene coating can maintain its properties up to and in excess of 400 °C. The UV stability is also increased along with lowering the dielectric constant.
- They can produce very uniform coatings that are pinhole and bubble free.
- They have low thermal expansion, therefore reducing risk of damaging any components.
- Due to the polymerisation reaction that occurs by condensation, there are no side reactions or by-products that could contaminate the coating. Thus, this method theoretically produces a pure contaminate-free coating. However, the exact controls must be controlled carefully as some of the paracyclophane may be left unreacted and can be trapped in the coating.

The disadvantages^{119,120} of using parylene based coatings are:

- Even though the polymer itself doesn't decompose until 650-680 °C, the maximum working temperature for a coating part is only 150 °C.
- The unfluorinated compounds have very poor thermal stability in air with parylene only having a stability of 60 °C if being using for ~10 years or 95 °C if being used for ~1000 hours. However, if the environment is inert then this value can be greatly increased to about 200 °C. This is because of oxidation and thermal cleavage readily occurring, which is due to aliphatic

ethylene groups that adjoin the benzene rings. This thermal stability doesn't affect the electrical properties but generally just the physical properties.

- Most parylene derivatives can't be removed by solvents but have to be removed by mechanical or plasma processes. This then makes it hard to repair the substrate if needed. However, parylene E can be removed by solvents which can be copolymerised with parylene C to improve parylene E's electrical properties.

2.5.4.2 Required Film Properties

No one coating can be used for all situations therefore there are different requirements depending on the situation which must be taken into account when choosing what coating to use. Such attributes to be taken into account are: what kind of physical properties are needed for the situation, how do the properties change from published values, how long is the shelf-life and how the properties may change due to the environment the coating will be put in ¹¹⁹. However, there are two main properties that all coatings must do and these are being electrically insulating and provide protection from any environmental damage ¹²⁰.

The electrical requirements can then be split into four sub-categories ¹¹⁹, these are the dielectric withstanding voltage (DWV), the insulation resistance, the Q-resonance and the dielectric constant and dissipation factor.

- The DWV is the measure of how well the coating insulates and resists conducting electricity and is test at high voltages.
- The insulation resistance is the measure of the resistance to electrical flow. There is also moisture resistance which is the same as insulation resistance but when moisture is present. Therefore, if the final product is going to be in an environment with high humidity then the moisture resistance will need to be high.
- The Q-resonance is a measure of how well the material copes with electromagnetic frequencies because these frequencies could alter the dielectric properties.

- The dielectric constant and dissipation factor are the measure of how well the coating material will slow down electromagnetic propagation along with how much of that signal energy is lost. Materials with low dielectric constant and dissipation factors cause little energy of the electromagnetic signal to be lost. Ideally the coating dielectric constant and dissipation factor should be the same as (or as close to as possible) the substrate.

There are a number of different environmental requirements that a coating must comply with ¹¹⁹, these are thermal stability, abrasion resistance, permeability, chemical resistance and compatibility, and general corrosion resistance.

- The thermal stability is how well the properties of the coating materials stay constant at elevated temperatures for a set period of time. High temperatures may cause the coating to soften, if taken above the glass transition temperature, which may cause the coating to slightly change shape. High temperatures can also affect the dielectric properties.
- The abrasion resistance is the resistance to physical attacks such as scratches and indentations.
- The permeability refers to how well the coating prevents water vapour, chemical fumes and particles from flowing through it. This is a key property because even though the coating may not be affected by chemical fumes or water, the underlying substrate may react with them and cause a failure. The permeability is also linked with the chemical resistance as when the coating is attacked by a chemical the permeability increases, allowing easier flow. Therefore, the coating should have low permeability as well as having good chemical resistance.
- The chemical resistance and compatibility are important properties of the coating because the coating may be in contact with harmful chemicals therefore needing to be able to protect the underlying substrate. Along with being resistant, the coating must also be compatible with the specific chemical that it will be contact with, for example if it's fuel then the coating should not react with the fuel as this may cause the fuel to be contaminated.

- The general corrosion resistance is linked to both the permeability and the chemical resistance because if they are both poor then corrosion will occur. Therefore, the coating needs to have good adhesion, no or few voids and an appropriate thickness to aid in corrosion resistance.

It should be noted that there is no requirement for coatings to resist whisker mitigation even though whisker mitigation is a fast growing problem in electronics and is the cause for many failures.

2.5.5 Current Practice for Mitigating Whiskers

Currently the coatings that are used for mitigating whiskers are general conformal coatings for the electronics industry, which so happen to mitigate tin whisker growth as a by-product of what they already do.

2.5.5.1 Conformal Coatings Used for the Mitigation of Whiskers

Polymeric conformal coatings can be used as physical barriers to prevent whiskers from creating short circuits ^{5,54}. This technique doesn't necessarily prevent the formation of whiskers only slows the growth rate and will also insulate any whiskers that protrude. There have been several different studies of how effective different polymeric coatings are. In most cases the whiskers will penetrate through the coating. However, these whiskers won't short circuit when coming into contact with another connection due to the coating on the other connection. Therefore, the whisker has to penetrate through the second coating before causing a failure. This can be seen in figure 2.30.

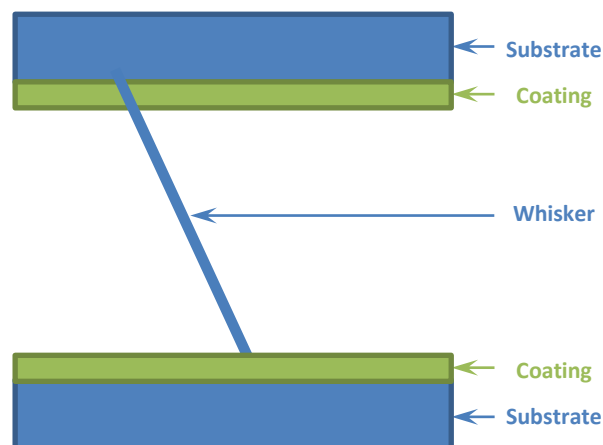


Figure 2.30 Diagram showing a whisker penetrating through one coating and then being stopped by another coating on an adjacent connection to prevent any short circuiting (adapted from S.Han et al¹²⁶)

2.5.5.1.1 Conformal Coating Studies

One study by NASA using Uralane 5750 has been previously described in section 2.1.3.5. Another study was conducted by Han *et al*¹²⁶, where the authors used five polymeric coatings (and one atomic layer deposited (ALD) oxide) to study the effects of different coatings on whisker growth. To accelerate the whisker growth the samples were subjected to different environmental conditions with temperature cycling, temperature/humidity conditions and mixed flowing gases. It was observed that parylene C was the best coating for the mitigation of tin whiskers and also gave the best coating uniformity and coverage. This would be due to how the parylene C coating was applied compared with the other coatings. Both the parylene C and ALD coatings were applied using vacuum deposition, which was previously discussed in section 2.5.3.3, and the other coatings were applied using a spray technique (either by hand or mechanically sprayed). As discussed before, vacuum deposition gives a far superior coverage and uniformity of the sample being coated; whereas spraying the sample will leave some areas being thicker compared to others. It was observed that the edges of all the sprayed coatings were much thinner and more whiskers were found at the edges of the samples. This observation was also true for Woodrow & Ledbury⁶⁵ and Hunt & Wickham¹²⁷, which may suggest that parylene C should be the recommendation when mitigating whiskers. In most cases acrylic coatings are the worst at mitigating whiskers which was also observed by Hong *et al*¹²⁸ and Hunt & Wickham¹²⁷. This would suggest that acrylic coatings should not be used for mitigating whiskers. In all cases the thicker the coating the better the mitigation would be, this would be because the whisker has more coating to break through therefore needing a larger force to penetrate through it. Whereas the force needed to break through a thin coating would be much less.

2.6 Self-healing Coatings

2.6.1 Brief Introduction into Self-Healing Coatings

For a polymer to display self-healing properties it needs to be able to have the ability to transform a physical energy into a chemical and/or physical response – which isn't present in generic polymers¹⁴. Much like in nature, when a scratch on animal skin will trigger the delivery of healing blood platelets¹³, the polymer needs to be able to 'sense' the damaging force, transforming it autonomously into a healing-event¹⁴. To be able to heal the damaged area the system needs to either heal by physical processes alone or a mixture of both physical and chemical processes.

This literature will concentrate on self-healing coatings and not self-healing bulk materials, where the most common strategies for self-healing coatings are micro/nanocapsule embedment; hollow fibre embedment and microvascular systems¹²⁹. There are, however, many more types of self-healing and a number of these can be used for self-healing coatings for the mitigation of tin whisker growth.

2.6.1.1 *Concept and Classification of Self-Healing Materials*

For physical processes, as in nature, the initial damage creates a free interface, which can be seen as a crack, and this turn allows for molecular processes such as swelling, patching or simple molecular diffusion, subsequently leading to crack closing¹⁴. Molecules of varying sizes can also diffuse to this new interface which will lead to a localised change in concentration, which in turn can lead to healing of the crack.

For chemical processes, a combination of both physical and chemical principles is required for healing to occur; because a chemical reaction can only occur when the reactants have come into contact with each other¹⁴. This type of process can be again split into two different types, extrinsic and intrinsic. Where extrinsic self-healing polymers the healing agent needs to be pre-embedded into a matrix; for example, nano-capsules filled with a healing agent and dispersed throughout the polymer matrix, which upon rupturing will release the healing agent. For intrinsic self-healing the polymer uses an

inherent ability to heal, such as using mechanophores that are sensitive to external mechanical forces and uses mechanochemical reactions to self-heal.

2.6.1.2 Principles of Self-Healing: Physical and Chemical

As previously stated there are two types of self-healing principles, physical and chemical, where self-healing can occur by either physical principles alone or by a combination of both physical and chemical processes ¹⁴. For self-healing to be achieved in all cases, the aim is to form crosslinked networks, whether they are generated by covalent or supramolecular chemistry or purely by physical crosslinking via polymer chain entanglement.

Physical self-healing principles are all based on molecular diffusion ¹⁴, where the necessary steps for all physical self-healing principles are interdiffusion and molecular entanglement ^{130,131}. Both of these properties are dependent on both the intermolecular forces and the length of the molecules. Zhang and Rong ¹³⁰ stated that having shorter molecular chains will increase the speed of the molecular diffusion and having longer molecular chains will increase the strength recovery at the interface.

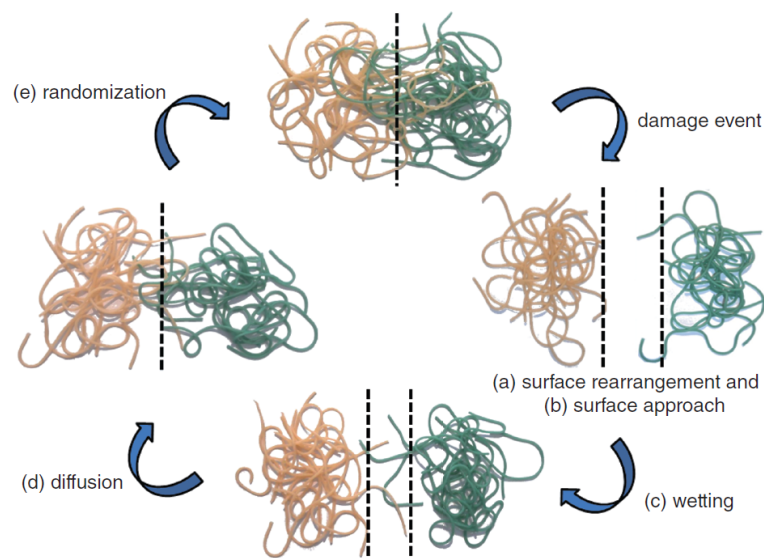


Figure 2.31 Stages of self-healing. (a) Surface rearrangement, (b) surface approach, (c) wetting, (d) diffusion and (e) randomisation ¹⁴

The most well-known and understood physical self-healing principle is molecular interdiffusion and in 1981 a five-stage mechanism was developed by Wool and O'Connor¹³² to understand self-healing by molecular interdiffusion, which is shown in figure 2.31. These stages include surface rearrangement (a), surface approach (b), wetting (c), diffusion (d) and randomisation (e). The first stage of surface rearrangement significantly influences the rate of crack healing due to the topography and roughness created by the crack, whereby a higher surface roughness will increase the rate of diffusion thus increasing the rate of healing¹⁴. This is then followed by the surface approach stage, which is the most crucial stage of self-healing due to the fact that if the surfaces are prevented in coming in contact with each other, then the self-healing process will be terminated¹³³. This stage also determines the mode of self-healing, for example healing in a point or line mode¹³². The third stage of wetting is needed before any self-healing can begin, by either the surfaces themselves or healing agents. This stage then enables the diffusion stage to occur, which is the most important stage for recovering the mechanical properties and is achieved by the entanglement of mobile chains followed by the interpenetration of the undamaged matrix¹⁴. The final stage of randomisation is where the total loss of the crack interfaces is observed and the polymer is now fully healed. This simple model can also be used as a universal mechanism for almost all self-healing concepts, physical and chemical¹³³.

Other physical self-healing principles include:

- Welding – this is where chain entanglements between the two contacting polymer surfaces are formed to enable the restoration of the original mechanical properties of the damaged area¹³⁴. Healing by welding is one of the traditional self-healing methods, along with the aforementioned molecular interdiffusion¹⁴.
- Nanoparticle-based – this is completely different to the previous methods due to fact that this concept doesn't rely on the rejoining of polymer chains; however, this self-healing concept relies on the migration of nanoparticles to the damaged area^{14,133,134}.

Chemical self-healing principles are either based on covalent or supramolecular network formation¹⁴. Covalent network formation, shown in figure 2.32a, is generally irreversible due to the formation of chemical bonds between functional groups. However, supramolecular network formation, shown in figure 2.32b, is reversible due to the involvement of reversible supramolecular reactions such as hydrogen bonding and metal bonding. Both of these two types of network formation can be split into switchable network formation, shown in figure 2.32c, and mechanochemical network formation, shown in figure 2.32d. These categories are, however, often blurred, enabling a number of self-healing methods being assigned to more than one category.

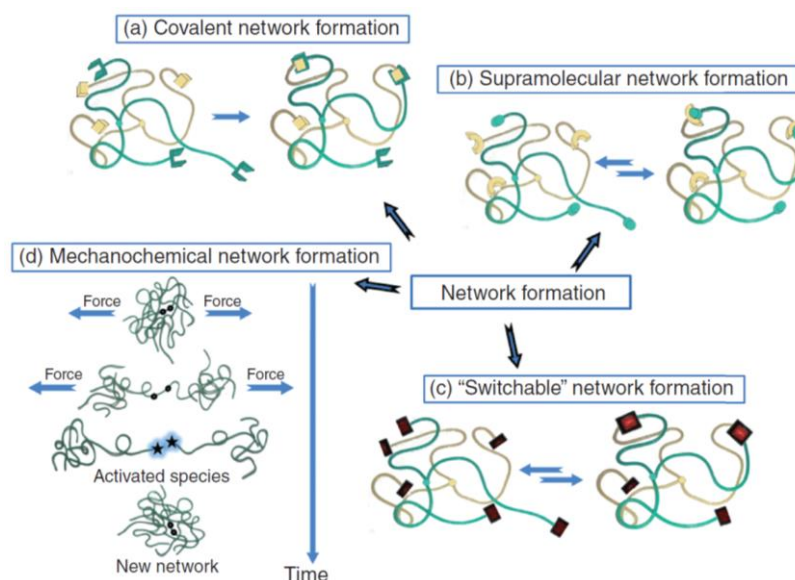


Figure 2.32 Self-healing by different modes of chemical interactions. (a) Covalent network formation, (b) Supramolecular network formation, (c) "switchable" network formation and (d) mechanochemical network formation¹⁴

2.6.1.3 Bio-Inspiration

Bio-inspiration, or biomimicry, is the application of strategies from nature to solve human challenges^{135,136}. There is such a large variation in self-sealing and self-healing mechanisms in nature, the potential for developing biomimetic materials is almost limitless. Synthetic and biological self-healing are extremely similar in the steps each takes to fully heal, however synthetic healing is usually much faster¹³⁷, shown in figure 2.33.

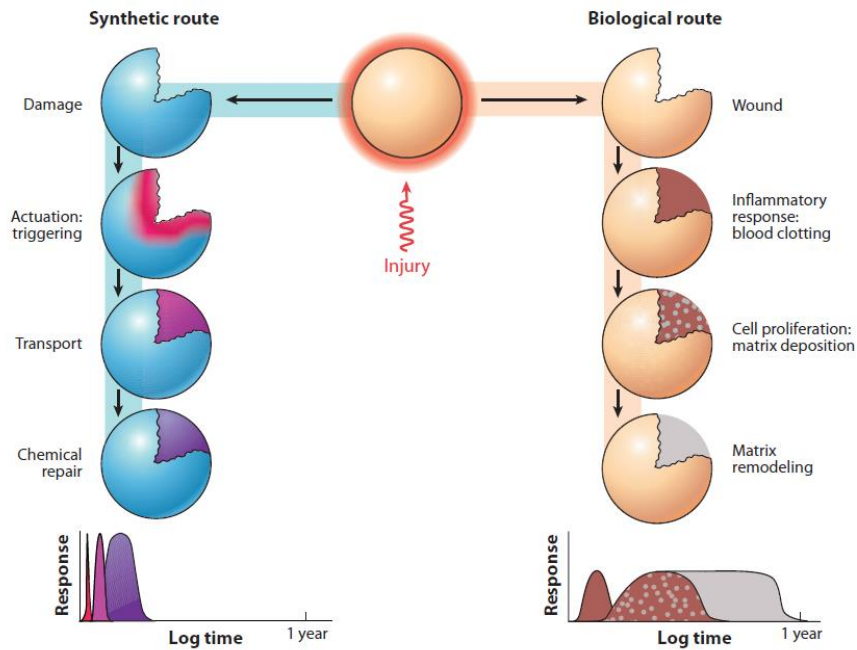


Figure 2.33 Synthetic vs. biological routes for self-healing, showing that both routes are very similar but the synthetic route takes a fraction of the time compared with the biological route ¹³⁷

An example of self-healing in nature is the *Hevea brasiliensis* which uses the encapsulation technique ¹³⁸. This is a latex-producing tree that uses the latex to heal physical damage ¹³⁹. This latex is enclosed in elongated cells, which act as capsules, called laticifers under high pressures. As a result of this high pressure, when the tree is physically damaged the latex is exuded out of these capsules which reacts with the hevein, which is enclosed in lutoids (capsule within a capsule). This hevein is a protein that induces coagulation of the latex, much like a catalyst inducing cross-linking, which closes the wound. This mechanism is also very similar to that observed in *Ficus Benjamin* and other plants in the *Euphorbia* and *Campanula* genera ^{12,138}.

Another example of self-healing in nature is the vascular system which is observed in most animals, as the circulatory system, and some animals and plants, as a noncircular hyperbranched vascular system ¹³⁸. When living tissue is damaged physically, the damage may reach the circulatory system at which point the contents of the system will fill the crack space (bleeding). This is subsequently followed by a fast-sealing mechanism to prevent excessive bleeding, which, in the case for humans, is called haemostasis. During haemostasis, platelets from the blood stream will cross-link through binding

fibrinogens and glycoproteins together, and bind to the collagen from the skin ¹⁴⁰. The red blood cells are then caught in this platelet network, which leads to further coagulation. The fibrinogen is then converted into fibrin which reinforces platelet network by binding the red blood cells together.

Both of these mechanisms of self-healing, are similar, to which a fluid is released upon rupture and reacts with a catalyst to cross-link ¹². However, vascular self-healing can heal the same area multiple times due to being able to allow a continuous flow of healing agents, whereas a encapsulated system can only heal the same area once ¹⁴, this is shown in figure 2.34.

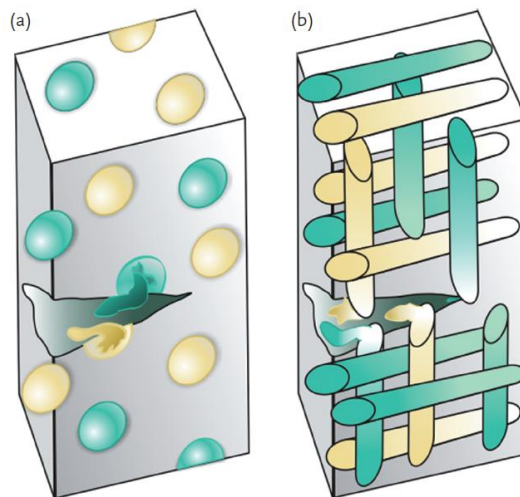


Figure 2.34 Comparing one-time and multiple self-healing. (a) Capsule based self-healing which is a one-time self-healing process and (b) vascular self-healing which is a multiple self-healing process (adapted from Döhler ¹⁴)

2.6.2 Encapsulation Self-Healing

Encapsulation self-healing is also known as compartmentalised self-healing and is considered one of the cheapest type of self-healing ¹⁴¹. This type of self-healing can autonomically heal cracks and was originally proposed by White *et al* ¹⁴², the authors proposed a system whereby a healing agent was encapsulated and dispersed in an epoxy matrix along with a catalyst to initiate the polymerisation to heal cracks. The proposed self-healing method was that upon the rupture of microcapsules the healing agent would pour out filling the crack; the healing agent would then polymerise upon coming into contact with the dispersed catalyst, as shown in figure 2.35.

As previously mentioned in section 2.6.1, this type of self-healing is a one-time self-healing process meaning that if a crack occurs in the same place more than once then no further healing will occur¹³. This is because the entire healing agent in that area has been used up and there is way to resupply that area with more self-healing agent.

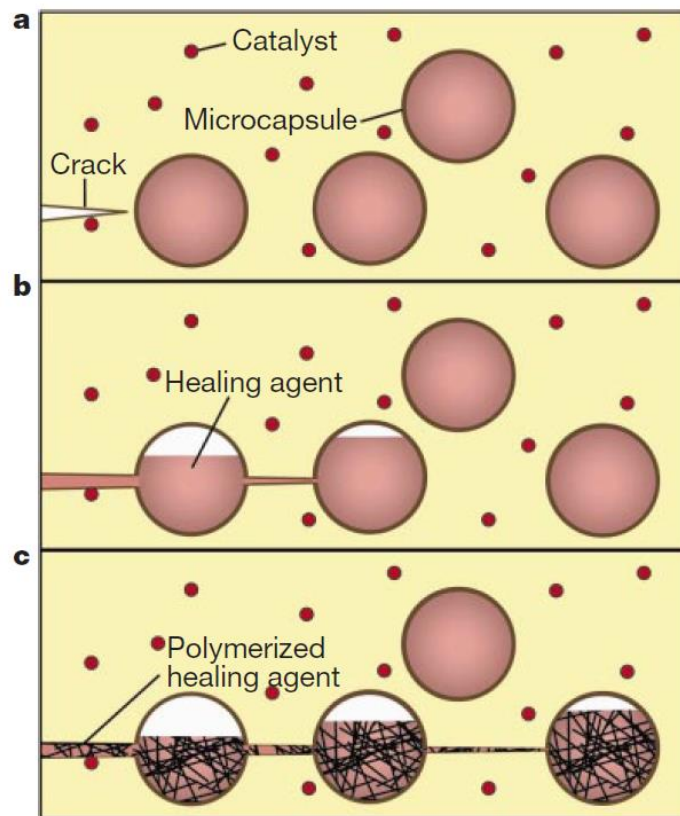


Figure 2.35 Autonomic healing concept as proposed by White et al¹⁴² a) crack is initiated at the damaged site, which at b) propagates further and causes the capsules to rupture whereby the healing agent is released, c) this healing agent then polymerises upon coming into contact with the catalyst and bonds the crack faces

2.7 Previous Work

Previous work prior to this project was undertaken by Wu⁷¹ and Haspel⁷², which was to study the oxide chemistry and whisker growth on electroplated tin and tin-copper coatings. Both copper and brass substrates were electroplated with a tin-copper alloy and pure tin, respectively. Different parameters were used to generate an oxide film in two different oxidising solutions, borate buffer and potassium bicarbonate-carbonate; one set of samples were left to form a natural air formed oxide; the other samples were of electrochemically formed oxide layers that were oxidised at potentials

ranging between $-0.83 - 2.0$ V vs. SCE. The results suggested that electrochemically formed oxide layers became thicker as the oxidising potential increased while oxidising for an equivalent charge passed. The results also suggested that electrochemical oxide layers mitigated whisker growth far better than a native oxide film. The oxide thickness was increased with increasing oxidation time; however this was at the expense of surface dissolution, as shown in figure 2.36.

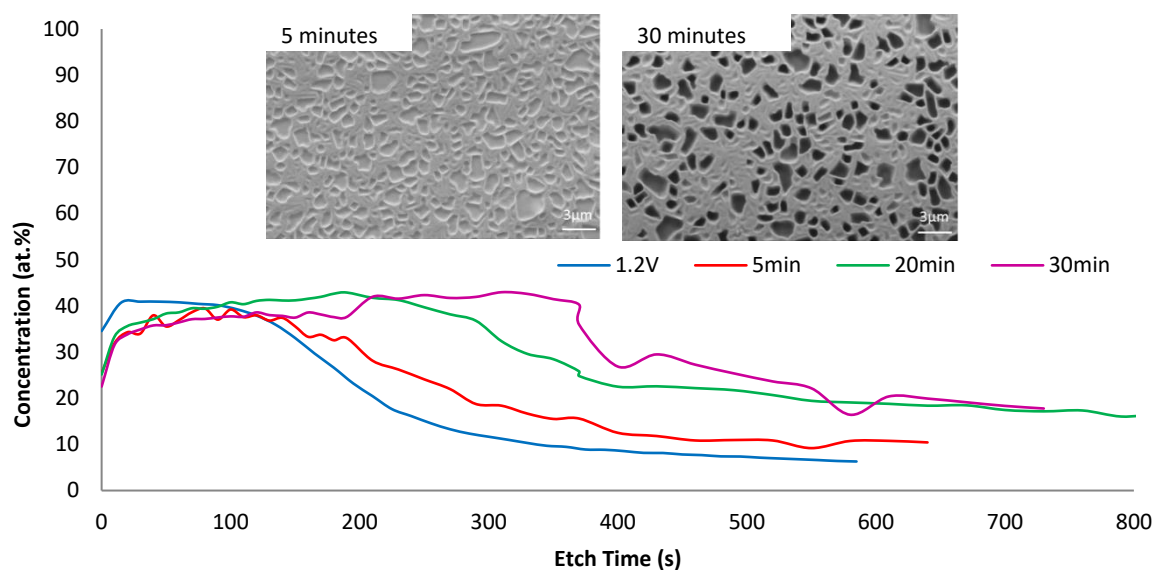


Figure 2.36 XPS depth profile with respect to tin as oxide, showing how tin oxide thickness increases with time when oxidising a potential of -0.66 V and comparing with 1.2 V (blue). The micrographs (inset) shows how the surface morphology changes with increasing oxidation time ²¹

The previous work also showed that electroplating tin-copper on copper would increase the rate of whisker formation and growth ⁷², which was due to the tin-copper intermetallic growth. This intermetallic growth would cause internal stress and this is a known cause of whisker formation ^{7,9}. It should be noted that the oxidation process (electrochemical and naturally formed) of the tin-copper was dominated by tin; this was shown by analysis carried out using XPS which showed that there was no copper present at the surface of the oxide layer.

2.8 Summary

It can be seen from this literature review that there is little research into both the effects of the oxide layer and conformal coating have on tin whisker growth. There currently is no evidence of anyone

attempting to develop a conversion coating, a self-healing conformal coating nor a dual-layer system for the sole purpose of mitigating whisker growth. The research that has been reported, however, is promising and shows that whisker mitigation can be significantly reduced by using either mitigation method. However, both methods have shown to have limitations; for oxide films, the films can become cracked or contain 'weak points' which become sites for whisker growth; and for conformal coatings, whiskers will still grow underneath the coating and the coating is generally thinner at edges which would cause more whiskers to grow at these areas.

In summary there are a high number of factors that will reduce whisker growth rate including: reducing both internal and external stresses in the electroplate ²⁷⁻³⁰; reducing the amount of IMC growth and diffusion between the substrate and the electroplate ^{7,9,37-39}; increasing the grain size of the electroplate ⁴⁰; ensuring the electroplate has equiaxed grains rather than columnar grains ⁷; increasing the tin oxide thickness ^{1,41,42}; alloying tin with elements such as silver, bismuth and lead ^{6,7,43,73}; reducing the corrosion of the tin ^{47,49,52}; replacing bright tin with matte tin to improve internal stresses ⁵; having an intermediate between the tin and the substrate to reduce unwanted Cu_6Sn_5 IMC growth and atom diffusion from the substrate into the tin coating ^{5,6,54-56,61}; increasing the thickness of the tin coating ⁵; annealing the tin coating ⁵⁶; applying a polymeric coating ^{5,54,63-66}; improving the electroplating electrolyte to reduce internal stresses ^{67,68}; and surface treatment of both the substrate and the electroplated surface ^{69,70}.

This project will attempt to fill the gap in the current research of how the oxide film effects the growth of tin whiskers. This project will also study how effective conversion coatings are at mitigating tin whisker growth compared with using an electrochemically formed tin oxide.

3 Experimental Procedure

3.1 Electroplating of Pure Tin and Tin-Copper Alloy

Two different electroplating baths were used in this study, a pure tin electroplating bath was used for both electrochemical studies and whisker growth studies using a brass substrate; and a tin-copper electroplating bath was used for whisker growth studies using a copper substrate.

3.1.1 Electroplating of Pure Tin Coatings

3.1.1.1 Preparation of the electroplating bath

The Tinmac electroplating bath was prepared to electroplate the pure tin; Tinmac is a commercially available pure tin electroplating bath, that produces a bright tin finish and tends to have a high whisker growth. To prepare the Tinmac electroplating bath, tin sulphate, sulphuric acid (S.G. 1.83), Tinmac Stannolyte initial additive, and deionised water were all mixed together. Preparation of the electroplating bath was carried out as follows:

1. 70 ml of sulphuric acid was slowly added to 500 ml of deionised water. This was done whilst the solution was stirred using a magnetic follower and stirring plate. Care should be taken not to add too much at once as this will cause the solution to rapidly heat up.
2. 60 g of tin sulphate was slowly added to the acid and water solution. This was done whilst the solution was stirred using a magnetic follower and stirring plate.
3. The solution was filtered to remove any undissolved salts present in the solution.
4. 40 ml of the Tinmac Stannolyte initial additive was added to the solution. This was done whilst the solution was stirred using a magnetic follower and stirring plate.
5. The solution was topped up to 1 l with deionised water and was continued to mix for at least 20 minutes using the magnetic follower and stirrer plate to ensure full dispersion of the constituents.

3.1.1.2 *Substrate preparation*

The brass and copper substrates were both prepared for electrodeposition in the same way.

1. The samples were submerged and washed in acetone and agitated using an ultrasonic bath for 5 min to remove any dirt/grease from the surface. The coupons were then rinsed using deionised water and dried using a hot-air blower.
2. The samples were masked using a chemically inert tape (0.006 cm thick polyester film tape) to provide an area to be electroplated of either 4 cm² (2 cm x 2 cm) for whisker growth studies, x-ray photoelectron spectroscopy (XPS) studies and electrochemical studies or 1 cm² (1 cm x 1 cm) for electrochemical studies.
3. Immediately prior to electroplating, the samples were immersed in 20 vol.% sulphuric acid (S.G. 1.83) for 1 min to remove any native oxide that had formed on the surface.
4. The samples were then rinsed using deionised water and dried using a hot-air blower.

3.1.1.3 *Electrodeposition of pure tin*

For the electrodeposition of pure tin, a power supply was used. The current density used for the electrodeposition of pure tin on both brass and copper was 20 mA cm⁻²; this gave an electrodeposition rate of ~1 μm min⁻¹. For whisker growth studies the thickness used was 2 μm and for electrochemical and XPS studies the thickness used was 5 μm. The thinner electroplated pure tin coating (2 μm) was used for whisker growth because thinner coatings will promote whisker growth⁵. The thicker electroplated pure tin coating (5 μm) was used for electrochemical and XPS studies to ensure a complete and even coverage of the electroplated tin on the substrate. All electroplating was carried out at room temperature (20°C) and the counter electrode (anode) used was pure tin.

3.1.2 *Electroplating of Tin-Copper Coatings*

3.1.2.1 *Preparation of the electroplating bath*

The same electroplating bath as previously described for pure tin in section 3.1.1.1 was used with an addition of 0.01 mol l⁻¹ of copper sulphate to promote whisker growth. This addition provided the bath

with a source of copper ions to be co-deposited with the tin. This bath became unusable after ~48 hrs due to the precipitation of the tin salts, therefore only 300 ml was made at a time to reduce waste.

3.1.2.2 Substrate preparation

Only copper substrates were used for the electrodeposition of tin-copper. The copper substrates were prepared in the same way as previously described for pure tin electrodeposition in section 3.1.1.2.

3.1.2.3 Electrodeposition of tin-copper

The current density used for electrodeposition was set to 10 mA cm^{-2} ; this gave an electrodeposition rate of $\sim 0.5 \text{ } \mu\text{m min}^{-1}$. All electroplating was carried out at room temperature (20°C) and the counter electrode (anode) used was a titanium mesh with a $1 \text{ } \mu\text{m}$ thick layer of platinum. Immediately after electrodeposition the samples were rinsed with deionised water and dried using a hot-air blower.

3.2 Electrochemical Oxidation Studies

Electrochemical oxidation was used to grow an oxide film on the electroplated tin and tin-copper samples. Two oxidation baths were studied, a borate buffer solution and a potassium bicarbonate-potassium carbonate bath.

3.2.1 Preparation of the Electrochemical Oxidation Baths

3.2.1.1 Borate buffer solution

To prepare the borate buffer solution, 9.55 g of sodium tetraborate and 6.18 g of boric acid were added to 1 l of deionised water⁷¹. The pH was adjusted to ~ 8.4 , using additions of sodium hydroxide.

3.2.1.2 Potassium bicarbonate-potassium carbonate solution

To prepare the potassium bicarbonate-carbonate solution, 75.09 g (0.75 M) of potassium bicarbonate and 6.91 g (0.05 M) of potassium carbonate were added to 1 l of deionised water⁸⁹. The pH was adjusted to the required value, using additions of sodium hydroxide or hydrochloric acid. The acid was added using a pipette drop by drop and after full dispersion the pH of the solution was measured. The target pH range examined for the solution was between pH 7.9-9.9.

3.2.2 Post Electrodeposition Sample Preparation

Electrochemical oxidation and cyclic voltammetry studies were carried out immediately following electrodeposition. Prior to the electrochemical oxidation stage, the samples were electrochemically reduced at a fixed potential of -1.5 V vs. SCE (or Ag/AgCl) until the current levelled off and/or hydrogen bubbles appeared on the surface of the sample. Once bubbles appeared, a pipette filled with the electrolyte was used to blow the bubbles off the sample surface. This reduction process was carried out to reduce any oxide that had formed on the surface.

3.2.3 Cyclic Voltammetry Studies

Cyclic voltammetry was carried out to investigate the electrochemical processes occurring on the surface of the electroplated coating in the borate buffer and potassium bicarbonate-potassium carbonate solutions. Copper substrates with a surface area of 1 cm² and 4 cm² were used for these experiments. The thickness of the pure tin deposits was 5 μm to ensure that samples had a complete covering of tin with no through coating porosity, since this may interfere with the results. For standard cyclic voltammetry the electrode potential was swept from an initial potential of -1.1 V to an anodic limit of 1.5 V, the potential was then reversed and swept to a cathodic limit of -1.5 V and then returned to -1.1 V (all potentials versus SCE) using a linear scan rate of 10 mV s⁻¹. Although, the recorded peaks may be more pronounced if a scan rate of 50 mV s⁻¹ is used, a scan rate of 10 mV s⁻¹ enables smaller peaks to be observed which may be less apparent at a higher scan rate^{87,88}. For single cycles, the same parameters as previously described were used, however different anodic switching potentials were used (-0.75 V, -0.5 V, 0 V, 0.6 V, 1.2 V and 1.5 V all vs. SCE). The data collected for both oxidising solutions was analysed to determine the location of the specific oxidation and reductions peaks.

All studies were conducted using a Solartron SI 1286 Electrochemical Interface at room temperature (20°C) and the counter electrode (anode) used was a titanium mesh with a 1 μm thick layer of platinum.

3.2.4 Electrochemical Oxidation of the Electroplated Tin and Tin-Copper

Electrochemical oxidation was carried out immediately after electrodeposition in either the borate buffer or potassium bicarbonate-carbonate solutions. Initially, the samples were oxidised at three different fixed potentials; two of which corresponded to oxidation peaks identified from the cyclic voltammograms (-0.83 V and -0.66 V vs. SCE) whilst the third potential was 1.2 V vs. SCE (or Ag/AgCl) which had been used in previous work ⁷¹.

To further investigate the oxidation process additional oxidation potentials were selected for study. These potentials were chosen from the active and passive regions on the cyclic voltammograms obtained for pure tin in the potassium bicarbonate-potassium carbonate solution. Electrochemical oxidation potentials from the 1st oxidation peak up to 2.0 V vs. SCE (or Ag/AgCl) were investigated.

All studies were conducted using a Solartron SI 1286 Electrochemical Interface at room temperature (20°C) and the counter electrode (anode) used was a titanium mesh with a 1 µm thick layer of platinum.

3.3 Conversion Coatings Studies

Conversion coatings were investigated as an alternative method to produce oxide films on the surface of electroplated tin and tin-copper to mitigate whisker growth. Two conversion coating chemistries that can be used with tin were identified; these were a molybdate based coating ⁹² and a tungstate based coating ⁹⁹.

3.3.1 Preparation of the Conversion Coating Baths

3.3.1.1 Molybdate solution

The molybdate conversion coating solution used in this study was adapted from the literature ⁹² and was prepared as follows:

1. 10 g of sodium molybdate was added to 1 l of deionised water and mixed until dissolved using a magnetic follower and stirrer plate.
2. The pH was adjusted to the desired level using hydrochloric acid. The range of pH's used in this study were pH 1 to pH 4. This differed from the literature, as the authors used sulphuric acid ⁹².

3.3.1.2 Tungstate solution

The tungstate conversion coating bath was based on that described by Van Der Leest & Krijil ⁹⁹ and was prepared as follows:

1. 10 g of sodium tetraborate was added to 1 l of deionised water and mixed using a magnetic follower and a stirrer plate.
2. Once the sodium tetraborate was fully dissolved, 29.38 g (0.1 M) of sodium tungstate was added and mixed until dissolved using a magnetic follower and a stirrer plate.

3.3.2 Parameters Used for Depositing the Conversion Coatings

3.3.2.1 Molybdate conversion coating treatment parameters

The conversion coating treatment was carried out immediately after electrodeposition. Samples were introduced into the molybdate conversion coating bath, using a scissor stand to raise the bath until the desired electroplated area of the sample was fully immersed. Samples were processed in the molybdate bath by simple immersion, ranging from 1 min to 9 min; potentiostatically at -0.45 to -0.75 V vs. Ag/AgCl for 5 minutes; and by reverse pulsed current using the parameters shown in table 3.1. The thickness and surface morphology of the resultant coatings were investigated using x-ray photoelectron spectroscopy and scanning electron microscopy, respectively.

All electrochemical-based trials were conducted using a Solartron SI 1286 Electrochemical Interface at room temperature (20°C) and the counter electrode (anode) used was a titanium mesh with a 1 µm thick layer of platinum.

Table 3.1 Parameters used for pulsed current molybdate treatment of electroplated tin (modified from Van De Leest and Krijl⁹⁹)

Current Density	Frequency	Number of Square Waves
$\pm 10 \text{ mA cm}^{-2}$	0.5 Hz	30
$\pm 5 \text{ mA cm}^{-2}$	0.5 Hz	30
$\pm 2.5 \text{ mA cm}^{-2}$	0.5 Hz	30
$\pm 2.5 \text{ mA cm}^{-2}$	0.5 Hz	120

3.3.2.2 Tungstate coating conversion coating treatment parameters

Tungstate conversion coatings were applied using a pulsed current technique derived by Van De Leest & Krijl⁹⁹. Three different periodic reverse current densities of $\pm 2.5 \text{ mA cm}^{-2}$, $\pm 5 \text{ mA cm}^{-2}$ and $\pm 10 \text{ mA cm}^{-2}$ were applied for varying numbers of square wave cycles, ranging from 30-300, at a frequency of 0.5 Hz. Three different trials were conducted; one trial was conducted to study the effects of varying the current density while keeping the number of cycles constant and this trial was given the code CD; one trial was conducted to study the effect of varying the number of cycles while keeping the current density constant and this trial was given the code NC; and the final trial was conducted to study the effect of passing an equivalent charge for varying current densities and this trial was given the code EC. The parameters used for coating optimisation trials are summarised in Table 3.2.

All trials were conducted using a Solartron SI 1286 Electrochemical Interface at room temperature (20°C) and the counter electrode (anode) used was a titanium mesh with a 1 μm thick layer of platinum.

Table 3.2 Parameters used for the optimisation of the tungstate coating, (modified from Van De Leest and Krijl⁹⁹)

Experiment	Trial Number	Current Density	Frequency	Number of Square Waves
Comparison of Current Density	CD.1	$\pm 2.5 \text{ mA cm}^{-2}$	0.5 Hz	30
	CD.2	$\pm 5 \text{ mA cm}^{-2}$	0.5 Hz	30
	CD.3	$\pm 10 \text{ mA cm}^{-2}$	0.5 Hz	30
Comparison of Number of Cycles	NC.1	$\pm 5 \text{ mA cm}^{-2}$	0.5 Hz	30
	NC.2	$\pm 5 \text{ mA cm}^{-2}$	0.5 Hz	90
	NC.3	$\pm 5 \text{ mA cm}^{-2}$	0.5 Hz	150
Comparison of Equivalent Charge Passed	EC.1	$\pm 2.5 \text{ mA cm}^{-2}$	0.5 Hz	300
	EC.2	$\pm 5 \text{ mA cm}^{-2}$	0.5 Hz	150
	EC.3	$\pm 10 \text{ mA cm}^{-2}$	0.5 Hz	75

3.4 Whisker Growth and Oxide Thickness and Chemistry Studies

The effect of the electrochemically formed oxides on whisker growth was assessed using 2 μm Sn electrodeposits on brass and 2 μm Sn-Cu electrodeposits on Cu. For each electrochemical oxidation treatment, at least three identical samples were prepared. After electrodeposition and electrochemical oxidation, the samples were stored at room temperature (20°C). The growth of whiskers was studied using both optical microscopy and scanning electron microscopy (SEM). The density of whiskers was measured using an optical microscope. For counting whiskers and calculating whisker density, all counting was carried out manually and a whisker was defined as either a filament-type whisker than can only be seen using the x20 objective lens or a large odd-shaped eruption that had a visible height variation that would be visible when varying the stage Z position. It should be noted that some filament-type whiskers may only be visible when varying the stage Z position back and forth, as some filament-type whiskers may grow perpendicular to the surface and may not be easily visible if the microscope is constantly focused on the sample surface.

However, prior to whisker growth, analysis electron backscatter diffraction (EBSD) was carried out to study the grain structure of both the electroplated pure Sn surface and the electroplated Sn-Cu surface. This was to observe if the addition of Cu would influence the grain structure and subsequently the whisker growth. This was carried out using a JEOL JSM-7800F Field Emission Scanning Electron Microscope (FE-SEM), which was integrated with an Oxford Instruments Nordlys EBSD Detector. For the EBSD camera to collect the electrons, the stage needed to be tilted 70 °.

3.4.1 Effect of Oxidation Potential and Charge Passed on the Electrochemically Formed Oxide and Whisker Growth

Samples with dimensions of 4 cm x 6 cm were prepared, with 3 different areas of treatment that each had dimensions of 4 cm x 1.5 cm, that allowed the effect of oxidation potential and charge passed to be compared against an untreated surface on the same sample as shown by the image in figure 3.1. This was done to eliminate possible sample to sample variations in whisker growth that may occur. The use of these larger samples enabled the electrochemically oxidised areas to be compared with an untreated area on the same sample.

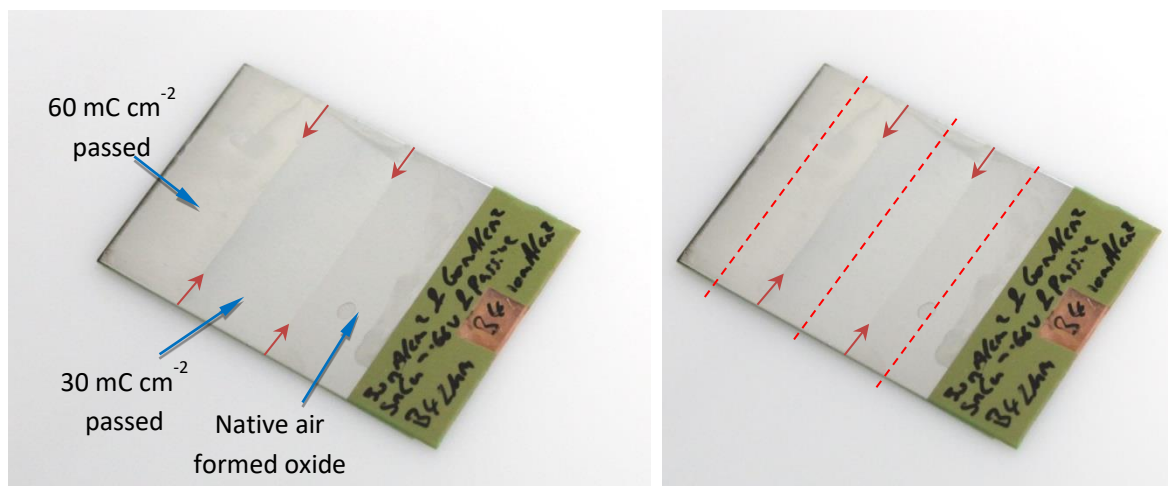


Figure 3.1 (left) An image showing an example of an electroplated test sample treated to produce regions with different charges passed and an area left untreated. (right) An image showing where whisker analysis took place (red dotted lines)

The 4 cm x 6 cm copper coupons were masked to give an electroplated area of 4 cm x 4.5 cm. The masked copper coupons were electroplated using the tin-copper electroplating bath to deposit a tin-copper alloy. Electrochemical oxidation, at selected potentials, was performed on each sample with

two different amounts of charge passed (see figure 3.1). Initially, the bottom ~ 1.5 cm of the sample was immersed into the solution and a charge of 30 mC cm^{-2} was passed. After this the bath was raised ~ 1.5 cm and a further 30 mC cm^{-2} charge was passed, which results in the initial area having a total charge passed of 60 mC cm^{-2} and the second area having a total charge passed of 30 mC cm^{-2} . The sample was then removed from the bath, rinsed with deionised water and dried using a hot-air blower. The uppermost ~ 1.5 cm of the electroplated tin-copper (which was not immersed) was left to develop a native air-formed oxide for comparison. This method can be seen in figure 3.2.

Table 3.3 Parameters used for producing the multiple-area samples, along with the sample identification

Oxidation Potential (vs. SCE)	Sample Identification
1.2 V	A
0 V	B
-0.4 V	C
-0.5 V	D
-0.66 V	E

After ~ 2 months and ~ 14 months of storage at room temperature the samples were analysed using an optical microscope and the number of whiskers were counted; both filament type and large eruption type whiskers were included in the analysis. A total of 46 frames across the centre of each treatment area were analysed (shown by the red dotted lines in figure 3.1) and the number of whiskers in each frame was counted. The total area of the 46 frames was calculated to be $\sim 0.26 \text{ cm}^2$ and the total number of whiskers present in those 46 frames was used to calculate the whisker density.

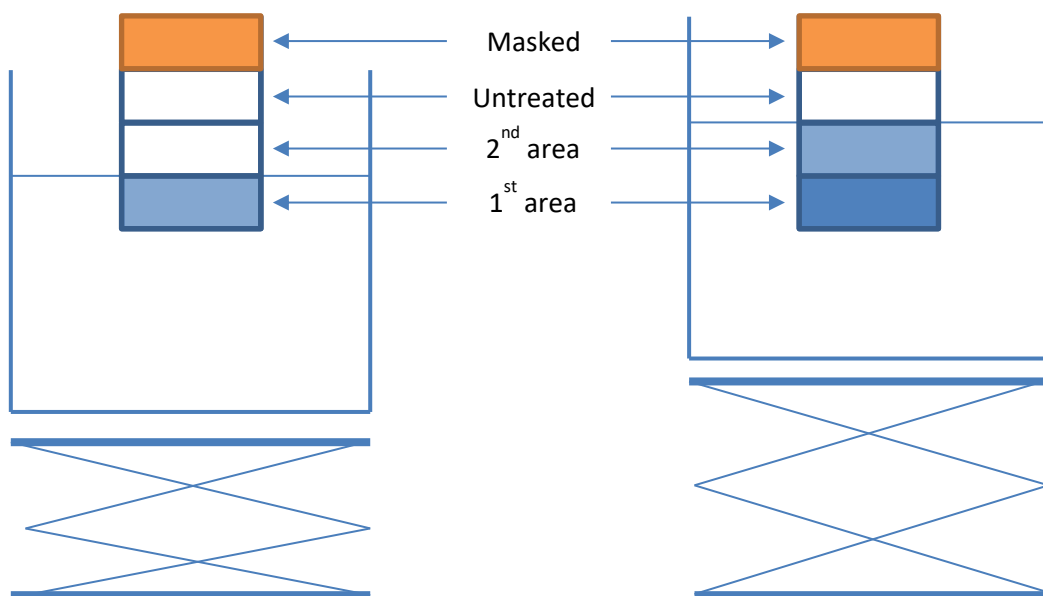


Figure 3.2 Schematics showing how different thicknesses of oxide film can be produced on one sample. The left-hand schematic shows the oxide film being electrochemically formed on the first area only. The right-hand schematic shows the oxide film being electrochemically formed on both the first and second areas whilst the uppermost electroplated area remains untreated.

3.4.2 12 Month Study of Whisker Growth and Oxide Thickness

This study was undertaken to observe how both whisker growth and oxide film thickness evolve with time. Whisker growth and oxide thickness were evaluated after 1 day, 1 week, 2 weeks, 4 weeks, 6 weeks, 2 months, 3 months, 4 months, 6 months, 9 months and 12 months.

For this study, 48 samples were produced and stored at room temperature, 24 were used for whisker growth analysis and the other 24 were used to determine the oxide film thickness. For each set of 24 samples, 12 were electrochemically oxidised at 2.0 V vs. Ag/AgCl (60 mC cm⁻² charge passed) and 12 were left untreated. At each time interval 3 untreated and 3 electrochemically oxidised samples were randomly selected for analysis from the batch of 24 samples. At each time interval, 1 untreated sample and 1 electrochemically oxidised sample were chosen from the other batch of 24 samples and analysed using x-ray photoelectron spectroscopy (XPS) to investigate film composition and thickness. At each analysis point a different sample was used to avoid/eliminate possible artefacts generated by a previous analysis.

Along with the whisker density, the longest apparent whisker length (per frame) was measured to study the effect of time and surface treatment on whisker length. The method used to measure the apparent whisker length is shown in figure 3.3, figure 3.3a shows the actual length of the whisker and figure 3.3b shows the apparent whisker length.

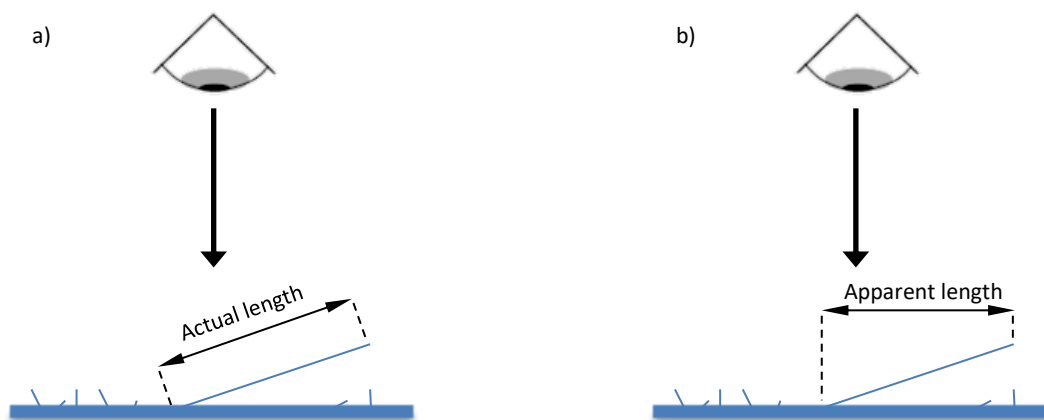


Figure 3.3 Schematic showing how apparent length of whisker is viewed. a) shows the actual length of the whisker and b) shows the apparent length of the whisker

3.4.3 Effect of Electrochemical Oxidation at Higher Potentials on the Oxide Film and Whisker Growth

In an earlier study⁷¹ increased anodic potentials were used to electrochemically oxidise electroplated pure tin on brass. High-resolution XPS scans showed that increasing the electrochemical oxidation potential above 1.2 V vs. SCE further increased the thickness of the oxide film for an equivalent charge passed. Oxidation at 1.2 V, 1.6 V and 2.0 V vs. SCE was therefore carried out in the present study to investigate whisker growth from electroplated tin-copper on copper electrochemically oxidised at those potentials. X-ray photoelectron spectroscopy was also carried out to compare the electrochemically formed oxide film thickness and chemistry.

3.4.4 Comparison of Whisker Growth and Oxide Film Thickness and Chemistry at Room Temperature and 55 °C/85 %RH

Conformal coatings are often cured at elevated temperatures as well as being stored at elevated temperatures and humidity to promote whisker growth. The effect of temperature and relative

humidity whisker growth was assessed using 2 μm Sn-Cu electrodeposits on copper. After electrodeposition and electrochemical oxidation, three untreated samples and three electrochemically oxidised samples were placed in a Memmert Humidity Chamber (HCP153) at 55 °C and 85% relative humidity, whilst three untreated samples and three electrochemically oxidised samples were stored at room temperature (20°C) for comparison. The influence of storage conditions on whisker growth and the thickness and composition of the oxide film was evaluated using optical microscopy and x-ray photoelectron spectroscopy (XPS), respectively. The initial composition and thickness of the oxide film was also analysed within 1-day of sample preparation.

3.4.5 Effect of Conversion Coating Parameters and Chemistry on the Whisker Growth and Coating Thickness and Composition

The molybdate and tungstate conversion coatings described in section 3.3 were investigated to assess the coating produced in terms of quality, composition and thickness (on 5 μm thick electroplated pure Sn on copper) and their ability to mitigate whisker growth (on 2 μm thick electroplated Sn-Cu on copper). The parameters for both conversion coating whisker growth trials are shown in table 3.4. Both whisker growth trials were conducted simultaneously to compare with each other and they were also both compared with electrochemically oxidised Sn-Cu on copper (produced at 2.0 V vs. Ag/AgCl for a charge passed of 60 mC cm^{-2}) and untreated Sn-Cu on copper samples. The coating thickness and composition was analysed using x-ray photoelectron spectroscopy (XPS) and visual analysis of the coatings were analysed using optical microscopy and scanning electron microscopy (SEM). Whisker growth studies were analysed using optical microscopy.

Table 3.4 Whisker growth parameters for both conversion coating trials. All coatings were deposited on 2 μm thick electroplated Sn-Cu on copper

Conversion Coating	Whisker Growth Studies Parameters		
Molybdate Conversion Coating	5 min immersion in $\sim\text{pH } 3$	-0.45 V vs. Ag/AgCl for 5 min in $\sim\text{pH } 3$	-0.6 V vs. Ag/AgCl for 5 min in $\sim\text{pH } 3$
Tungstate Conversion Coating	10 mA cm^{-2} 45 cycles at 0.5 Hz	5 mA cm^{-2} 90 cycles at 0.5 Hz	5 mA cm^{-2} 150 cycles at 0.5 Hz

3.4.6 Effect of a Dual-Layer Coating has on Whisker Growth

A dual-layer coating is that which contains two different coatings and in this study the two coatings were an electrochemically formed oxide (produced 2.0 V vs. Ag/AgCl for a charge passed of 60 mC cm⁻²) and an acrylic conformal coating that was deposited on top of the electrochemically formed oxide. Dual-layer coating trials were conducted because the two types of coatings were expected to complement each other by utilising the strengths of each of the coatings. Used on its own, an electrochemical oxide coating is extremely thin and may still contain 'weak points' or surface damage from handling in the oxide film that whiskers can grow through. The addition of a conformal coating provides an additional level of protection to mitigate any whisker growth from these points. On the other hand, conformal coatings are known to suffer from poor coverage at corners and edges¹⁴³, however electrochemical oxide films are likely to be thicker at edges and corners due to higher current densities present at these regions¹⁴⁴. Additionally, conformal coatings don't generally prevent whiskers from forming and multiple whiskers can be viewed when the coating is stripped off for analysis; however, with an underlying electrochemical oxide film the number of whiskers formed is likely to be reduced.

For the whisker growth studies, four batches of electroplated samples were produced, the first set of samples were untreated and left untreated to develop a native air-formed oxide, the second set of samples were electrochemically oxidised at 2.0 V vs. Ag/AgCl (60 mC cm⁻² charge passed), while the third set had a standard acrylic polymeric coating applied over a native air-formed oxide and the final set of samples had an acrylic polymeric coating applied on top of a Sn-Cu surface that had been electrochemically oxidised at 2.0 V vs. Ag/AgCl (60 mC cm⁻²). Prior to the application of the conformal coating, the tape was removed. The acrylic polymeric coatings were applied using a dip-coating technique with the samples being immersed and then slowly withdrawn at a rate of ~2 cm min⁻¹. This was achieved by clamping the samples in place and raising the coating mixture up to the samples using

a scissor stand. The coating mixture was then lowered at the specified rate by hand. After coating, the samples were then left to cure over a period of 2 days at room temperature (20°C).

Two trials were conducted to study whisker growth, whereby two different coupons were used. For the first trial a standard 2 cm x 4 cm x 0.04 cm copper coupon was used and for the second trial a thicker copper coupon was used, that had dimension of 2 cm x 4 cm x 0.2 cm. In both trials 2 µm thick Sn-Cu was electroplated onto the copper coupons.

Unlike the standard coupons, the thick coupons only had the bottom half taped using chemically inert tape; this left a total area of 9.2 cm² to be electroplated. Prior to electrodeposition the sides were polished using a polishing wheel and 800 grit SiC paper. This was to ensure flat, smooth surfaces on the sides. After the conformal coating was applied the samples were placed copper end down into prepared polystyrene slots to cure.

The first trial was conducted to evaluate the effect of a dual-layer coating on the whisker growth and the second trial was conducted to evaluate the effect of a dual-layer coating on the whisker growth at the edges.

Acrylic coatings were chosen because researchers in the lab had previously investigated conformal coatings and chose to study acrylic coatings in more depth. At the time of this research, the researchers in the lab were investigating into improving acrylic conformal coatings, therefore the acrylic coating system was chosen for this work.

3.5 Characterisation Techniques

A range of different characterisation techniques were used to analyse the samples. Optical and electron microscopes were used to study whisker density, whisker morphologies and surface topography. X-ray photoelectron spectroscopy (XPS) was used to analyse the chemical composition of the untreated, electrochemically oxidised and conversion coated surfaces. Depth profiles were also acquired to determine the thickness and in-depth compositional changes.

3.5.1 Optical Microscopy

The whisker density on electroplated Sn-Cu samples was analysed using a GX Microscopes L3030 using a x20 objective lens. The whisker density was determined by counting filament type whiskers and large eruptions in up to 20 randomly selected areas across the whole sample (not including the area at the edges of the sample). Each area studied had an area of 0.00567 cm². For each area studied the whiskers were counted and the whisker density per frame was calculated. The whisker density for each sample was then calculated and used to obtain an average whisker density.

The morphology of the conversion coated Sn-Cu samples was analysed using a Leica DMI8 optical microscope at magnifications ranging from 100-1,000x.

3.5.2 Scanning Electron Microscopy

The surface topography and whisker growth morphologies of the electroplated samples were analysed using a Carl Zeiss (Leo) 1530 VP Field Emission Gun Scanning Electron Microscope (FEGSEM) equipped with an Oxford Instruments X-Max 80 mm² Detector operating in secondary electron (SE) mode. Typically, an accelerating voltage of 10 kV was used, with a working distance of ~12 mm, an aperture size of 30 µm and high current mode.

3.5.3 Focussed Ion Beam Scanning Electron Microscopy

The effect of an electrochemical oxide film on the microstructural evolution of the electrodeposited Sn and Sn-Cu alloys was investigated by means of cross-sections that were prepared by focussed ion beam (FIB) milling using a FEI Nova 600 Nanolab Dual Beam FIB-SEM. Ion beam milling was carried out at a 52 ° tilt angle with a 30 kV gallium ion beam. Initial trench milling was carried out at 20 nA and the final face milling was carried out at 3 nA with a tilt angle of 53.5 °. Ion beam images were acquired using the gallium ion beam at a current of 30 pA, with a tilt angle of 0 °

ImageJ was used to calculate the percentage of intermetallic compound (IMC) growth within the electroplated coating. This was carried out by importing the ion beam image produced during FIB-SEM analysis into ImageJ. This image was then cropped so only the electroplated coating was visible. The image was then converted into 8-bit and then converted to binary; this made the IMC white and the electroplated tin coating black. Subsequently a histogram was produced showing how many pixels were white and how many were black. A simple equation was then used to calculate the percentage of IMC growth, which is shown in equation 3.1.

$$\frac{\text{Number of white pixels}}{\text{Number of white pixels} + \text{Number of black pixels}} \times 100 \quad \text{Equation 3.1 – Calculation used to determine percentage of IMC growth}$$

3.5.4 X-ray Photoelectron Spectroscopy

The electrochemically oxidised samples, conversion coated samples and untreated samples were analysed using a Thermo-Scientific K-Alpha X-ray Photoelectron Spectrometer using an aluminium K-alpha source, to determine the thickness and composition of the surface oxide. For each sample, survey scans were conducted to quantify the surface composition and high resolution scans were used to accurately determine the binding energies of the peaks. The parameters used to acquire these scans are shown in table 3.5.

X-ray photoelectron spectroscopy (XPS) was also used to obtain depth profiles through the oxide layer to investigate how the elemental distribution varied with depth and also to determine the thickness of the oxide layer. Sputtering using an argon ion beam was carried out between each analysis at a constant etch rate for a specified time. After each sputter period a snapshot scan was obtained (parameters shown in table 3.5), which although is less accurate than a high resolution scan it allows depth profiles to be acquired more quickly and with sufficient accuracy to quantify the elements present at that depth. The parameters used for sputter depth profiling are given in table 3.6. The sputter time taken to reduce the initial oxygen content by 50% was used to compare the oxide film

thickness between different samples. This is because the etch rate stated by the software is in respect to tantalum oxide and will not be not be the true rate for the oxide films. Each element and compound have different etch rates, therefore to obtain an accurate etch rate a known thickness can be sputtered to determine the etch rate, with respect to the tantalum oxide etch rate stated by the software.

Table 3.5 Parameters to use with XPS for high resolution scans, snapshot scans and survey scans

Type of scan	Scan step ev	Pass energy ev	No. of Scans	Scan Size µm	Scan range eV	
High Resolution Scan	0.1	20	10	400	Sn	505-479
					O	545-525
					C	298-279
					Cu	965-925
Snapshot Scan	0.00	150	5	400	Sn	505-479
					O	545-525
					C	298-279
					Cu	965-925
Survey Scan	1	150	10	400	1350-0	

The depth profiling was stopped once the oxygen content had become less than 0.5 at.%. A low ion beam energy was used for the untreated and electrochemically oxidised due to their oxide films being relatively thin ⁷¹. A much higher ion beam energy was used for analysing the conversion coated samples since their surface oxides were generally much thicker ⁹². The higher ion beam energy was also used to analysis the electrochemically oxidised samples for comparison. This is due to results being obtained using the high ion beam energy can't be compared with those obtained at the low ion beam energy.

Table 3.6 Parameters used for XPS depth profiling for all types of surface finishes

Type of coating	Ion beam energy eV	Current	Tantalum oxide etch rate nm s ⁻¹
Electrochemical and native oxide	200	Low	0.01
Conversion coating and electrochemical oxide	1000	High	0.28

3.5.5 Conformal Coating Thickness

The thickness of the applied conformal coatings was measured using a Fischer Dual-Scope coating thickness measurer. Prior to use the instrument was calibrated using the provided calibration foils. For each conformal coated sample 10 readings were taken in the same location and the average was calculated, together with the standard deviation. The measured coating thicknesses were tabulated for comparison.

4 Electrochemical Oxidation Studies

An electrochemical oxidation treatment was applied to electroplated tin coatings to form oxide films that are thicker than a native air-formed oxide and mitigate whisker growth. Studies were conducted to analyse the composition and thickness of the oxide film and to assess the whisker growth. Trials were also conducted to reproducibility of forming these enhanced oxide coatings. This chapter will present and discuss the results obtained for the electrochemically oxidised samples.

4.1 Cyclic Voltammetry Studies

Cyclic voltammetry was used to study the electrochemical stability of the oxidation bath and to identify the positions of the oxidation and reduction peaks^{87,88} for 5 μm electroplated tin on copper, in a potassium bicarbonate-carbonate oxidation bath. A cyclic voltammogram may be used to identify the potentials at which electrochemical reactions occur within a specified potential range; the voltammograms may then be used to identify suitable potentials at which electrochemical oxidation can be carried out.

On the first cycle (figure 4.1) two large oxidation peaks are present at -0.83 V and -0.66 V (both vs. SCE); however, on every subsequent cycle three oxidation peaks of reduced intensity were present at -0.84 V, -0.78 V and -0.67 V (all vs. SCE). It was also apparent that the reduction peak at \sim -1.3 V vs. SCE in the first cycle, shifted to \sim -1.2 V vs. SCE on subsequent cycles. Also, the broad reduction peak at \sim -0.5 V vs. SCE increased in intensity in each subsequent cycle. The formation of three oxidation peaks has not previously been reported in the published literature.

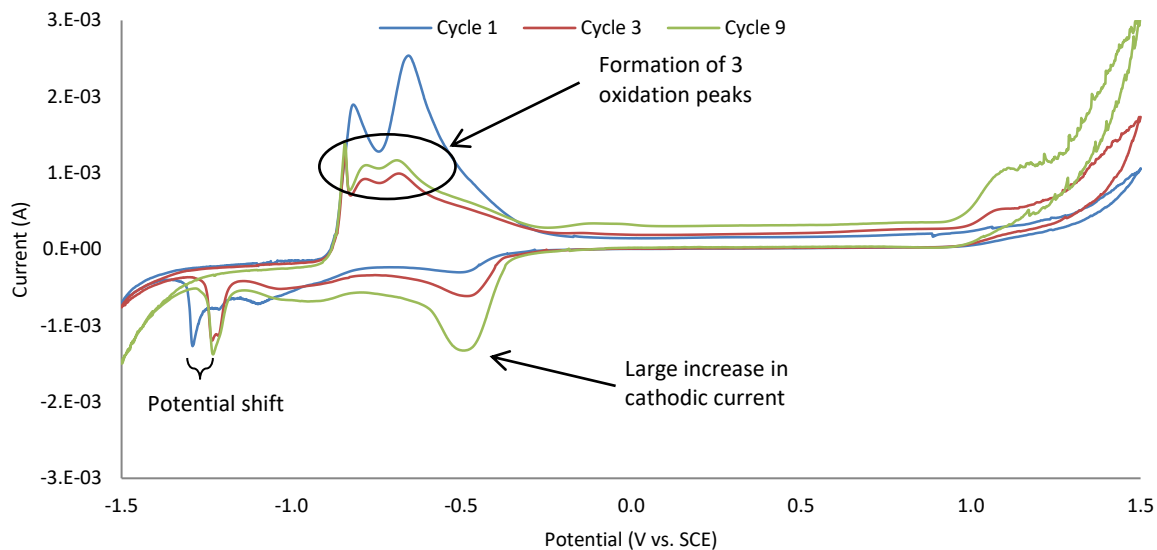


Figure 4.1 Cyclic voltammograms of electroplated tin on copper with a thickness of $5\ \mu\text{m}$ in a potassium bicarbonate-carbonate oxidation bath at a scan rate of $10\ \text{mV s}^{-1}$. These voltammograms show that the subsequent cycles differed significantly from the first.

To fully understand the electrochemical reactions occurring during cyclic voltammetry, further experiments were carried out. These included; cyclic voltammetry using different anodic reversing potentials and anodic potential sweeps up to defined upper potential limits followed by x-ray photoelectron spectroscopy (XPS) of the surface of the oxidised tin.

4.1.1 Interpretation of the Cyclic Voltammograms

This study was used to determine the locations and attribute electrochemical reactions of the anodic and cathodic peaks on the voltammogram. The cyclic voltammogram in figure 4.2 is the first cycle shown in figure 4.1 and shows two well defined peaks (1 & 2) and a plateau region starting at a potential of $\sim -0.15\ \text{V vs. SCE}$. It was suggested by Drogowska *et al*⁹⁰ that there are three different potential regions present when tin is oxidised in bicarbonate solutions; these are a short active dissolution region (peaks 1 and 2), the active to passive transition (the broad region where the current decreases from peak 2 to the plateau region), and a large passivity region (the plateau region). It has been previously suggested^{89,90} that the first two anodic peaks can be attributed to the oxidation of metallic tin to tin(II) (peak 1) and tin(II) to tin(IV) (peak 2).

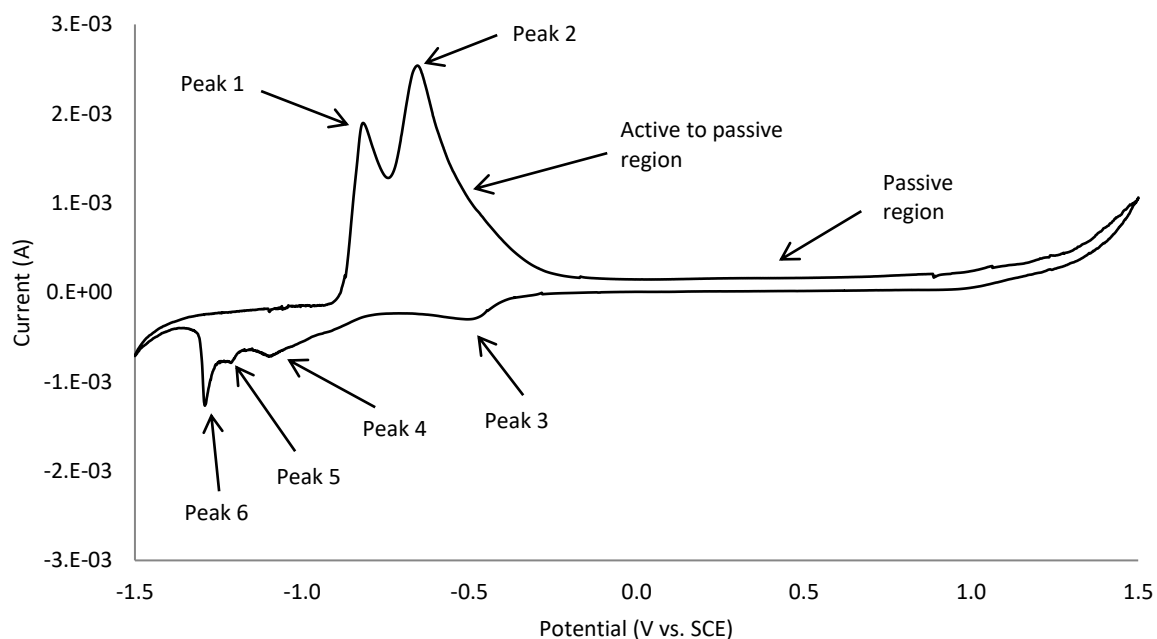


Figure 4.2 A single cycle voltammogram of electroplated tin on copper with a thickness of $5 \mu\text{m}$ in a potassium bicarbonate-carbonate oxidising bath at a scan rate of 10 mV s^{-1} , showing the different regions and oxidation and reduction peaks.

The first anodic peak (1) was attributed to the oxidation of tin to tin(II) species by active dissolution and the second anodic peak (2) has been attributed to the electrochemical formation of tin(IV) species and the oxidation of the previously formed tin (II) species. The broad decrease from the second anodic peak (2) to the plateau region can be attributed to the dehydration of the tin(IV) species to a more stable configuration, e.g. dehydrating $\text{Sn}(\text{OH})_4$ to SnO_2 and water. The large plateau region has been attributed to the passivity of tin. It was suggested by Drogowska *et al* that the reactions occurring at peak 1 could be associated with a prepassive region where stannous oxide and hydroxide form the majority of the species by a dissolution-precipitation process; since this layer is not strongly passivating, as the potential becomes more positive a second anodic peak (peak 2) is observed that may be attributed to the formation of $\text{Sn}(\text{OH})_4$ which subsequently dehydrates to its most stable species of SnO_2 .

The cyclic voltammogram shown in figure 4.2 shows multiple cathodic peaks, which may suggest that multiple reduction processes occurred. Alvarez *et al*⁸⁹ observed only one reduction peak at a potential of -1.0 V , which was attributed to the simultaneous reduction of Sn(II) and Sn(IV) species. However, it

was noted that multiple reduction peaks may be present when using increased anodic reversing potentials (as used in this study). Gervasi *et al*⁹¹ suggested that the reduction process involved several processes, which can be attributed to peaks 3 to 6.

However, it was observed that after the initial scan, voltammograms obtained in the subsequent cycles differed significantly during a continuous cyclic voltammetry experiment with multiple cycles; this is illustrated in figure 4.3, which shows the 9th cycle (the same as what is shown in figure 4.1). The main difference being an additional anodic peak appearing.

Figure 4.3 shows the cyclic voltammogram from the 9th cycle, which shows one well defined anodic peak (peak 1a), followed by two peaks (peaks 2a and 3a) and a broad active to passive region, there is then a passive region commencing at ~ -0.15 V vs. SCE. During the cathodic sweep there is a well-defined broad peak (peak 4a) and a well-defined narrow peak (peak 6a) with an ill-defined broad peak in between (peak 5a). The 9th cyclic voltammogram (figure 4.3) shows three reduction peaks that are not observed by Alvarez *et al*⁶⁰, but the authors noted that additional reduction peaks may occur depending on the anodic switching potential. The additional reduction peaks that were observed in the present study may have been due to the use of an anodic switching potential of 1.5 V vs. SCE compared to 0.1 V used by Alvarez *et al*. Peaks A and A2 (figure 4.2 and 4.3, respectively) may correspond to the reduction of Sn(II) and Sn(IV) species that are formed by the reactions during the anodic sweep, as suggested by Alvarez *et al*. However, as there are three reduction peaks present, a multiple stage nucleation processes is likely to be involved in the electrochemical reduction of tin(IV) species of different stabilities, as suggested by Gervasi *et al*⁹¹.

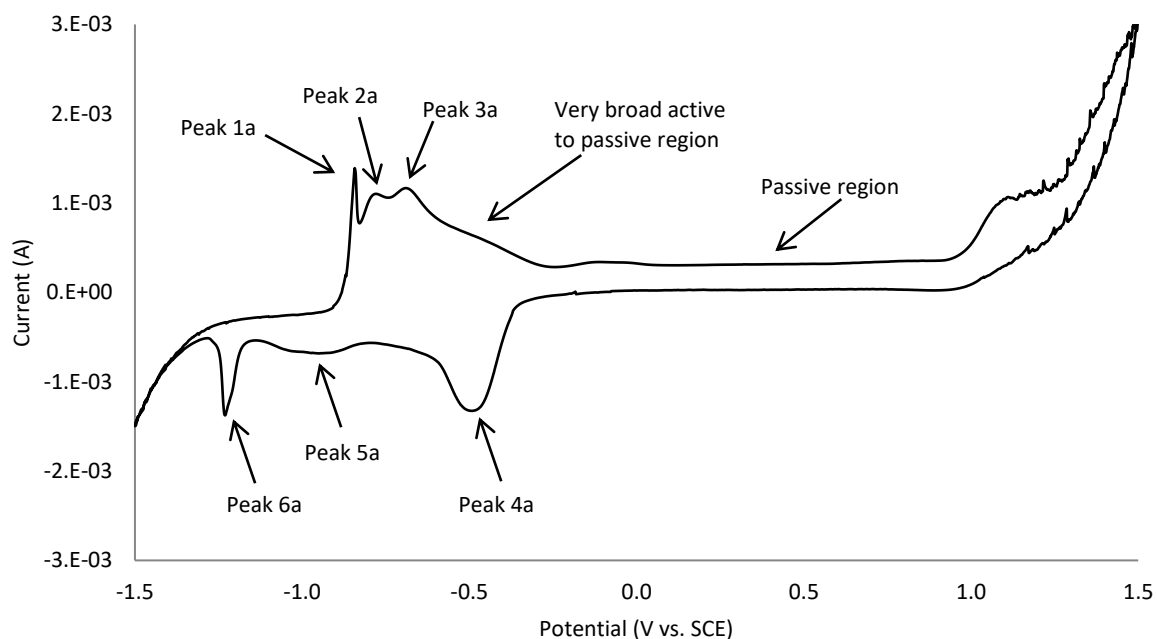


Figure 4.3 The 9th cyclic voltammogram of electroplated tin on copper with a thickness of $5\ \mu\text{m}$ in a potassium bicarbonate-carbonate oxidising bath at a scan rate of $10\ \text{mV s}^{-1}$, showing the different regions and oxidation and reduction peaks.

Both peak 6 (figure 4.2, $-1.29\ \text{V vs. SCE}$) and peak 6a (figure 4.3, $-1.23\ \text{V vs. SCE}$) may be associated with the reduction of both tin species, as suggested by Alvarez *et al*⁸⁹. As mentioned earlier there may be a multiple stage nucleation and growth process for the electrochemical reduction of Sn(IV) species of varying stabilities, whereby the Sn(II)/Sn(IV) species undergo a phase transformation to form metallic Sn⁹¹. However, the increase in cathodic current for peak 4a (figure 4.3) compared with peak 3 (figure 4.2) may suggest that a reduction process is occurring and not just a nucleation process. In a later publication, Gervasi *et al*¹⁴⁵ observed three reduction peaks, whereby the first cathodic peak was associated with the reduction of the Sn(II) oxide film, the second cathodic peak was associated with the reduction of the initially formed Sn(OH)₄ passive film and the third cathodic peak was associated with the reduction of dissolved anodic dissolution products generated at the third anodic peak. The authors suggested that the Sn(OH)₄ species can become increasingly more difficult to reduce, which could be the reason for the change in cathodic sweep when increasing the number of cycles.

Peak 1a (-0.84 V vs. SCE) and peak 3a (-0.69 V vs. SCE) in figure 4.3 may be attributed to the same reactions as peaks 1 (-0.82 V vs. SCE) and 2 (-0.66 V vs. SCE) in figure 4.2 respectively. The development of the third peak may be attributed to an intermediate reaction from peak 1a to peak 3a. However, Gervasi *et al*¹⁴⁵ suggested that the peak 3a is associated with the formation of soluble Sn(IV) ions that may form complexed species; this is then followed by a second passivation reaction forming a multilayer of Sn(OH)₄. Gervasi *et al* suggested that peak 2a is associated with the direct oxidation of Sn to a thin layer of Sn(IV) hydroxide. The Sn(OH)₄ that is produced following the third anodic peak is extremely insoluble and will evolve into a more thermodynamically stable SnO₂ film with time and increasing anodic polarisation.

4.1.2 Selection of Potentials for Electrochemical Oxidation Studies

The voltammogram shown in figure 4.4 was obtained from a freshly electroplated pure tin deposit on copper and is identical to the voltammograms shown in figures 4.1 and 4.2, with the addition of where each oxidation potential was identified. Cyclic voltammetry was conducted using a standard potassium carbonate-bicarbonate electrolyte. Peaks 1 and 2 were the first two potentials chosen for electrochemical oxidation studies. However, oxidation at peak 1 does not necessarily mean that a stable Sn(II) oxide film is produced; this is because Sn(II) will readily oxidise to Sn(IV) in normal atmospheric conditions because Sn(IV) is more stable than Sn(II)¹⁴⁶.

Figure 4.4 shows the location of the potentials selected for electrochemical oxidation studies (blue dots). These chosen potentials were -0.6 V, -0.5 V, -0.4 V, 0 V and 1.2 V (all vs. SCE). The oxidising potentials of -0.4 V, -0.5 V and -0.6 V vs. SCE were chosen as they all occurred in the broad trailing slope following the second oxidation peak, which was attributed to an active to passive region; 0 V vs. SCE was chosen as a potential as it occurred on the part of the voltammogram corresponding to the beginning of the passive region; and 1.2 V vs. SCE was chosen because it had previously been shown to produce a thick oxide compared to a native oxide^{21,71,72}.

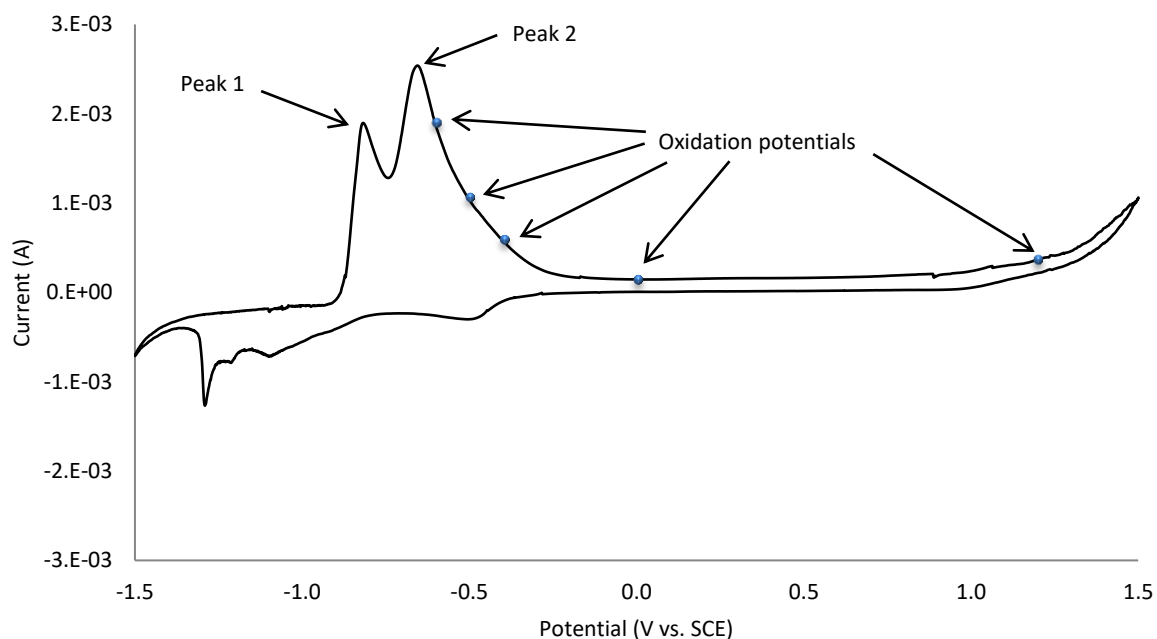


Figure 4.4 A single cycle voltammogram of electroplated tin on copper with a thickness of $5\ \mu\text{m}$ in a potassium bicarbonate-carbonate oxidising bath at a scan rate of $10\ \text{mV s}^{-1}$, showing each oxidation potential used to produce enhanced oxides

4.1.3 Cyclic Voltammetry Using Different Anodic Switching Potentials

Alvarez *et al*⁸⁹ did not observe three anodic peaks nor multiple cathodic peaks and as the anodic limit used by Alvarez *et al* was $0.1\ \text{V vs. SCE}$ the anodic limit used in a previous study⁷² was $1.5\ \text{V vs. SCE}$ and, it may be inferred that an electrochemical reaction was occurring between $0.1\ \text{V}$ and $1.5\ \text{V vs. SCE}$. Therefore, to investigate where this electrochemical oxidation reaction occurs, consecutive cyclic voltammetry was carried out using different anodic switching potentials. The results of these experiments are shown in figures 4.5 – 4.10. All the cyclic voltammograms used a cathodic switching potential of $-1.5\ \text{V vs. SCE}$. Table 4.1 shows the positions and the intensities of the oxidation and main reduction peaks for the 1st, 3rd and 9th cycles of the cyclic voltammograms using different anodic switching potentials.

Table 4.1 Peak potentials and peak currents for the 1st, 3rd and 9th cycles for each different switching potential for the cyclic voltammograms obtained for pure Sn on Cu in the potassium bicarbonate-potassium carbonate solution. An * indicates that an ill-defined shoulder is present.

Switching Potential	Oxidation Peak 1		Oxidation Peak 2		Oxidation Peak 3		Reduction Peak	
	Potential (V vs. SCE)	Current (A)	Potential (V vs. SCE)	Current (A)	Potential (V vs. SCE)	Current (A)	Potential (V vs. SCE)	Current (A)
-0.75 V	1 st cycle	1.92E-3	-	-	-	-	-0.907	-1.87E-3
	3 rd cycle	2.22E-3	-	-	-	-	-0.908	-2.31E-3
	9 th cycle	2.84E-3	-	-	-	-	-0.905	-2.44E-3
-0.5 V	1 st cycle	2.24E-3	-0.668	2.54E-3	-	-	-0.916	-4.03E-3
	3 rd cycle	3.96E-3	-0.676	2.62E-3	*	-	-0.918	-4.25E-3
	9 th cycle	4.45E-3	-0.679	2.72E-3	*	-	-0.919	-4.07E-3
0 V	1 st cycle	2.16E-3	-0.668	2.47E-3	-	-	-0.976	-1.57E-3
	3 rd cycle	3.95E-3	-0.682	2.77E-3	*	-	-0.974	-1.68E-3
	9 th cycle	4.34E-3	-0.684	2.86E-3	*	-	-0.975	-1.78E-3
0.6 V	1 st cycle	2.80E-3	-0.649	2.53E-3	-	-	-1.06	-2.19E-3
	3 rd cycle	3.29E-3	-0.665	3.43E-3	*	-	-1.06	-1.90E-3
	9 th cycle	3.32E-3	-0.665	3.65E-3	*	-	-1.06	-1.75E-3
1.2 V	1 st cycle	2.54E-3	-0.643	2.38E-3	-	-	-1.24	-2.27E-3
	3 rd cycle	1.24E-3	-0.761	1.04E-3	-0.680	1.23E-3	-1.21	1.28E-3
	9 th cycle	1.33E-3	-0.761	1.16E-3	-0.681	1.38E-3	-1.22	1.14E-3
1.5 V	1 st cycle	1.90E-3	-0.655	2.54E-3	-	-	-1.29	-1.27E-3
	3 rd cycle	1.25E-3	-0.783	9.23E-4	-0.667	9.68E-4	-1.23	-1.19E-3
	9 th cycle	1.39E-3	-0.788	1.09E-3	-0.689	1.17E-3	-1.23	-1.38E-3

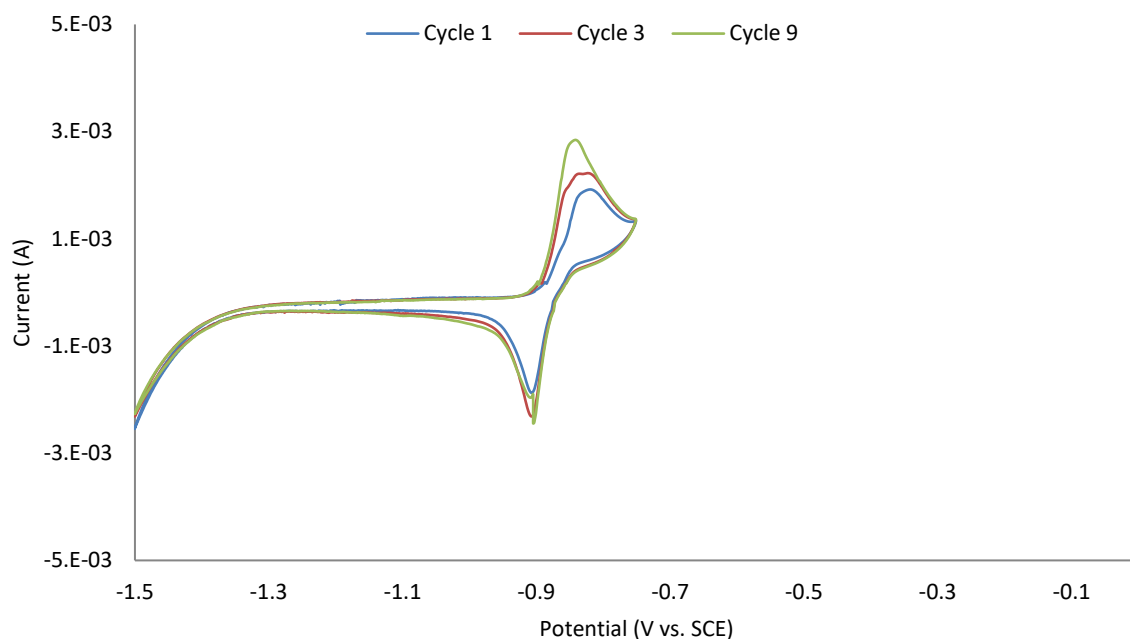


Figure 4.5 Cyclic voltammograms of electroplated tin on copper with a thickness of $5 \mu\text{m}$ in a potassium bicarbonate-carbonate oxidation bath with an anodic switching potential of -0.75 V vs. SCE and at a scan rate of 10 mV s^{-1}

The total cathodic charge passed and the total anodic charge passed for the anodic switching potentials of -0.75 V vs. SCE (figure 4.5) looks similar which may suggest that the oxide produced during the anodic sweep is completely reduced during the cathodic sweep. This similarity in the cathodic and anodic charges passed was observed for every cycle, which would suggest that when cycled up to an anodic potential of -0.75 V vs. SCE , the electrochemical reactions are reversible. It was observed that after the first cycle, the anodic peak, at -0.82 V vs. SCE , significantly increases in intensity while the intensity of the cathodic peak only increases slightly (table 4.1). The anodic peak also shifts slightly shifts in potential from -0.82 V to -0.84 V vs. SCE (table 4.1).

The total cathodic charge passed and the total anodic charge passed for the anodic switching potentials of -0.5 V vs. SCE (figure 4.6) looks similar in the first cycle. However, the anodic charge passed significantly increased after the first cycle while the cathodic charge passed stayed constant. In addition a slight shoulder appeared between the two oxidation peaks, which would suggest that an additional oxidation reaction occurred after the first cycle.

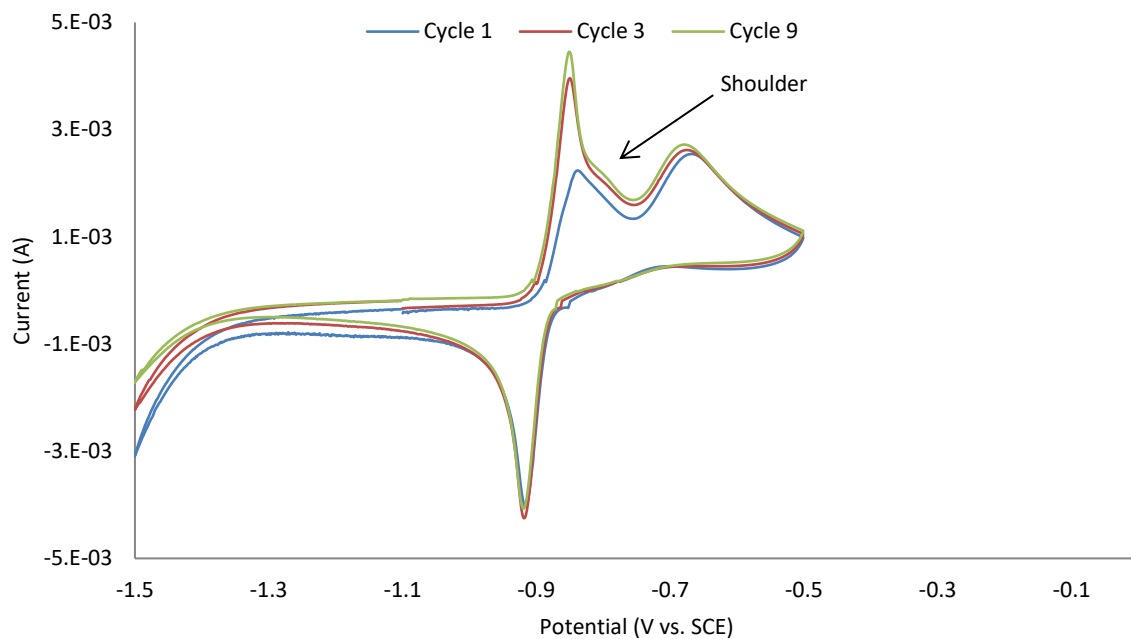


Figure 4.6 Cyclic voltammograms of electroplated tin on copper with a thickness of $5 \mu\text{m}$ in a potassium bicarbonate-carbonate oxidation bath with an anodic switching potential of -0.5 V vs. SCE and at a scan rate of 10 mV s^{-1}

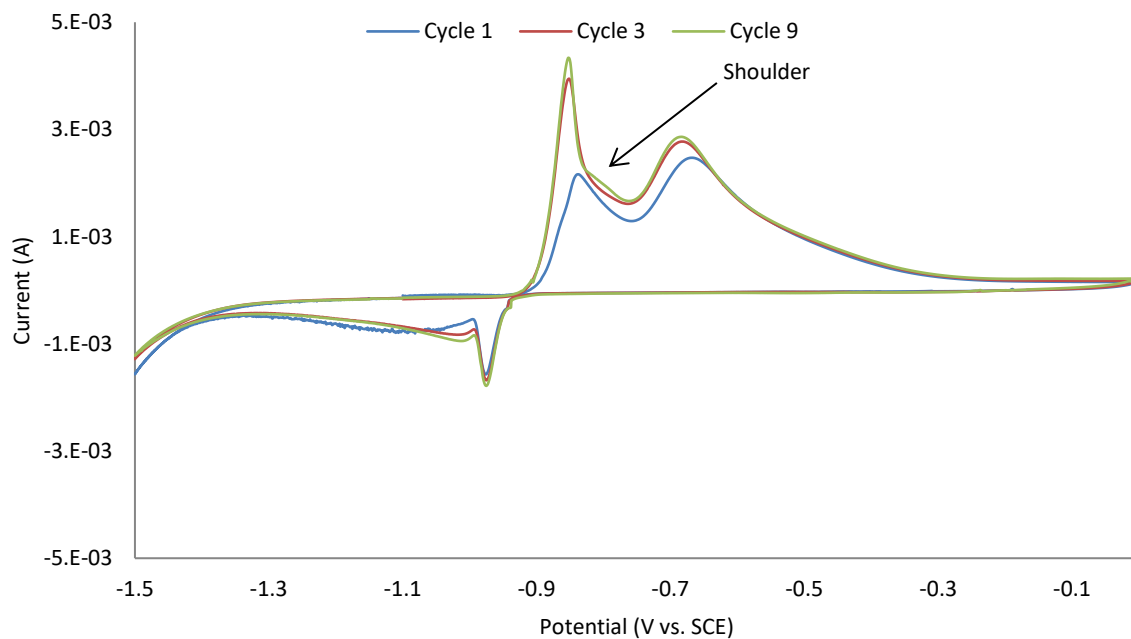


Figure 4.7 Cyclic voltammograms of electroplated tin on copper with a thickness of $5 \mu\text{m}$ in a potassium bicarbonate-carbonate oxidation bath with an anodic switching potential of 0 V vs. SCE and at a scan rate of 10 mV s^{-1}

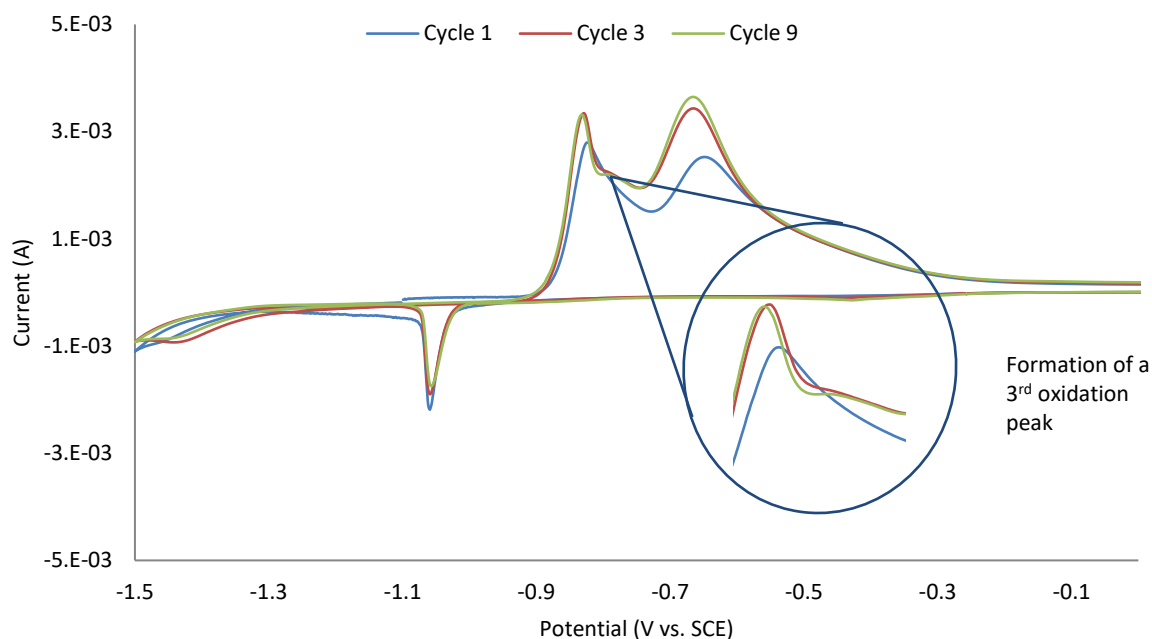


Figure 4.8 Cyclic voltammograms of electroplated tin on copper with a thickness of $5\ \mu\text{m}$ in a potassium bicarbonate-carbonate oxidation bath with an anodic switching potential of $0.6\ \text{V vs. SCE}$ and at a scan rate of $10\ \text{mV s}^{-1}$

The total cathodic charge passed and the total anodic charge passed for anodic switching potentials of $0\ \text{V vs. SCE}$ and above (figures 4.7 – 4.10) are not equal. The cathodic charge passed is significantly less than the anodic charge passed, which would suggest that the oxide produced during the anodic sweep is not completely reduced during the cathodic sweep. A similar observation was also made by Alvarez *et al*⁸⁹, who suggested that a stable tin(IV) oxide was formed that couldn't be fully reduced during the cathodic sweep. It can also be seen that the reduction peak in figures 4.9 and 4.10 shifted to more positive potentials after the initial cycle (table 4.1). This may suggest that an oxide is produced during the anodic sweep that cannot subsequently be reduced, i.e. the process is irreversible. It was also observed that when using switching potentials of $0\ \text{V}$ and $0.6\ \text{V vs. SCE}$ (figures 4.7 and 4.8) that a small anodic peak began to form between peaks 1 and 2.

For anodic switching potentials of $1.2\ \text{V}$ and $1.5\ \text{V vs. SCE}$ (figure 4.9 and 4.10) the additional oxidation peak is clearly present, there is also a reduction in the intensity of reduction peaks after the initial cycle. An anodic switching potential of $1.5\ \text{V vs. SCE}$ also showed the presence of two additional reduction peaks, one at $-0.5\ \text{V}$ and another much broader peak at $\sim -0.95\ \text{V vs. SCE}$ (figure 4.10).

If the position of the main reduction peak (~ -1 V vs. SCE) is compared for figures 4.5 to 4.10, it can be seen that the peak shifts to more negative potentials as the anodic switching potential is increased (table 4.1). The additional reduction peak, at -0.5 V vs. SCE, increases in intensity as the number of cycles increases (figure 4.10); this additional reduction peak may have appeared to counteract or may be connected with the additional oxidation peak observed after the first cycle.

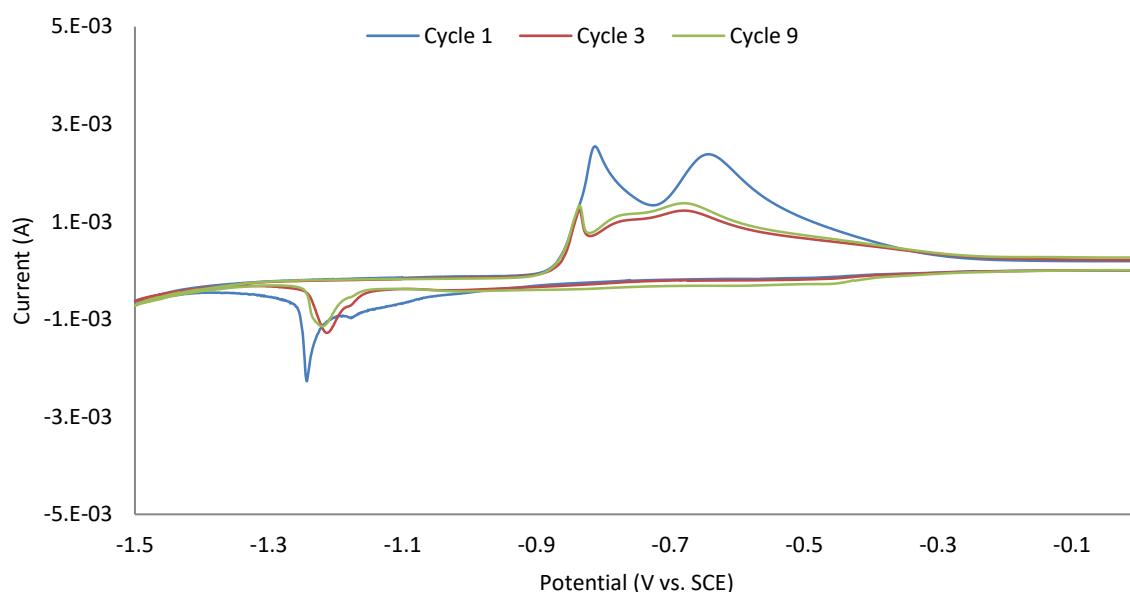


Figure 4.9 Cyclic voltammograms of electroplated tin on copper with a thickness of $5 \mu\text{m}$ in a potassium bicarbonate-carbonate oxidation bath with an anodic switching potential of 1.2 V vs. SCE and at a scan rate of 10 mV s^{-1}

The shoulders present in figures 4.6 to 4.8 are not very well defined. This may, in part, be attributed to the scan rate of 10 mV s^{-1} used in these studies; a faster scan will increase the intensity of the peaks⁸⁷, however a slower scan rate may identify smaller peaks that a fast scan rate may miss. The shoulder in figure 4.9 is more clearly defined than the other shoulders, however, the maximum current is still not well defined in figure 4.10 since the peak overlaps the area created by the two adjacent peaks.

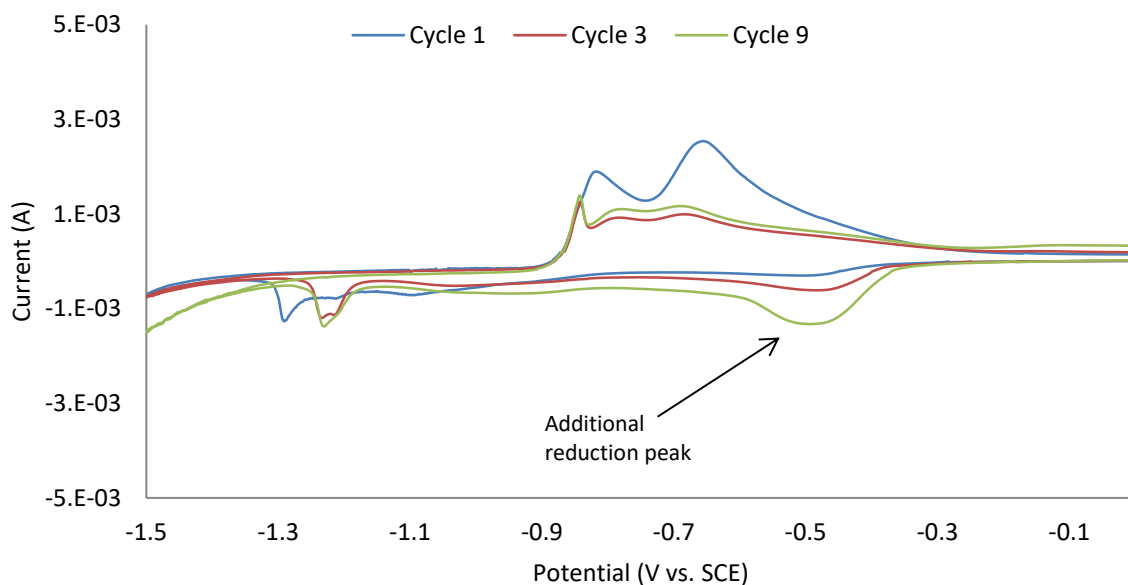


Figure 4.10 Cyclic voltammograms of electroplated tin on copper with a thickness of 5 μm in a potassium bicarbonate-carbonate oxidation bath with an anodic switching potential of 1.5 V vs. SCE and at a scan rate of 10 mV s^{-1}

4.1.4 X-ray Photoelectron Spectroscopy Study of Single Cycles

To more fully understand the irreversible reaction that is occurring during cyclic voltammetry, x-ray photoelectron spectroscopy (XPS) analysis was carried out to investigate the oxide film present after single cyclic sweeps carried out using the same sweep parameters and anodic limits as those shown in figures 4.5 – 4.10. The surface oxide present on each sample was then studied using XPS high resolution scans within 24 h of the single cycle.

Figure 4.11 a and b show the raw data obtained using XPS for a native air-formed oxide and an electrochemically formed oxide produced at a potential of 2.0 V vs. Ag/AgCl, respectively. For both scans the left peak represents tin as oxide and the right peak represents tin as metal as the peak binding energies fit within published ranges¹⁴⁷. The raw data by itself needed to be split into its individual components to enable them to be quantified. To do this, a peak fitting function was carried out to best fit individual peaks to create an envelope that best matches the original scan. This was carried out for each high resolution scan, an example of which is shown in figure 4.11 c and d. Figure 4.11c shows a high resolution scan of the Sn3d5 peak for a native air-grown oxide, whilst figure 4.11d shows a high resolution scan for the Sn3d5 peak for an electrochemically formed oxide produced at

2.0 V vs. Ag/AgCl. The blue lines represent the original scan obtained by XPS and the red lines are the envelope obtained after performing a peak fit. Figure 4.11a shows that two oxide peaks are needed to fit the envelope for the native air-formed oxide, whereas only one tin oxide peak is needed to fit the envelope for the electrochemically formed oxide (figure 4.11b); this suggests that the oxide film on the native air-formed oxide may contain a mixture of two tin oxide species. The narrow peak on the right in both figure 4.11a and 4.11b represents tin as metal and they both show that only one peak is needed to fit the envelope. It can be seen from figure 4.11 that there is much more tin oxide formed when it is formed electrochemically compared with a native air-formed oxide.

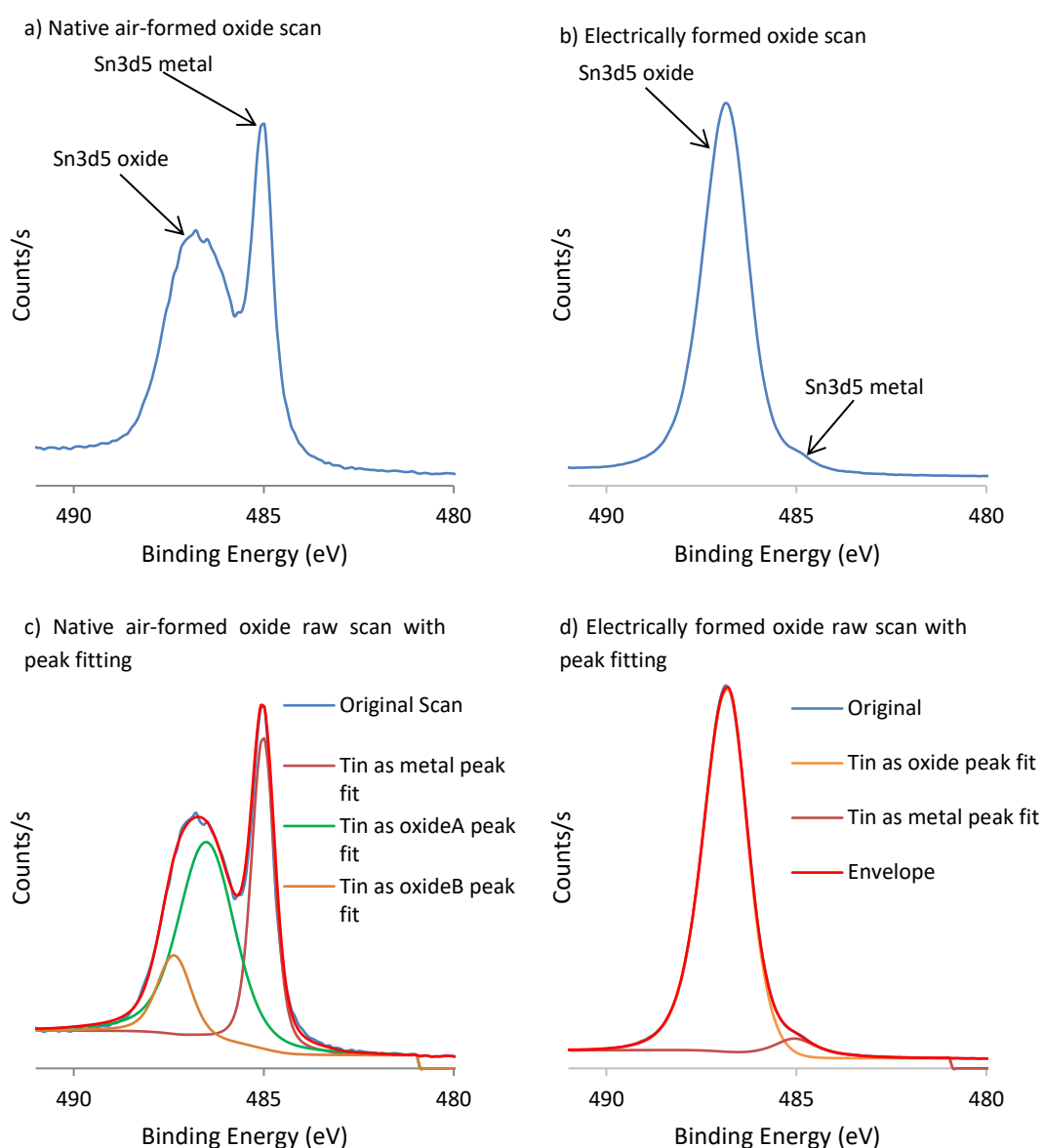


Figure 4.11 XPS high resolution scan of the Sn 3d5 peak, of a) a native air formed oxide and b) an electrochemically formed oxide produced at 2.0 V vs. Ag/AgCl, both on electroplated tin on copper samples that had been left for ~24 hr. With the corresponding peak fittings shown in c) for the native air-formed oxide and d) for the the electrochemically formed oxide

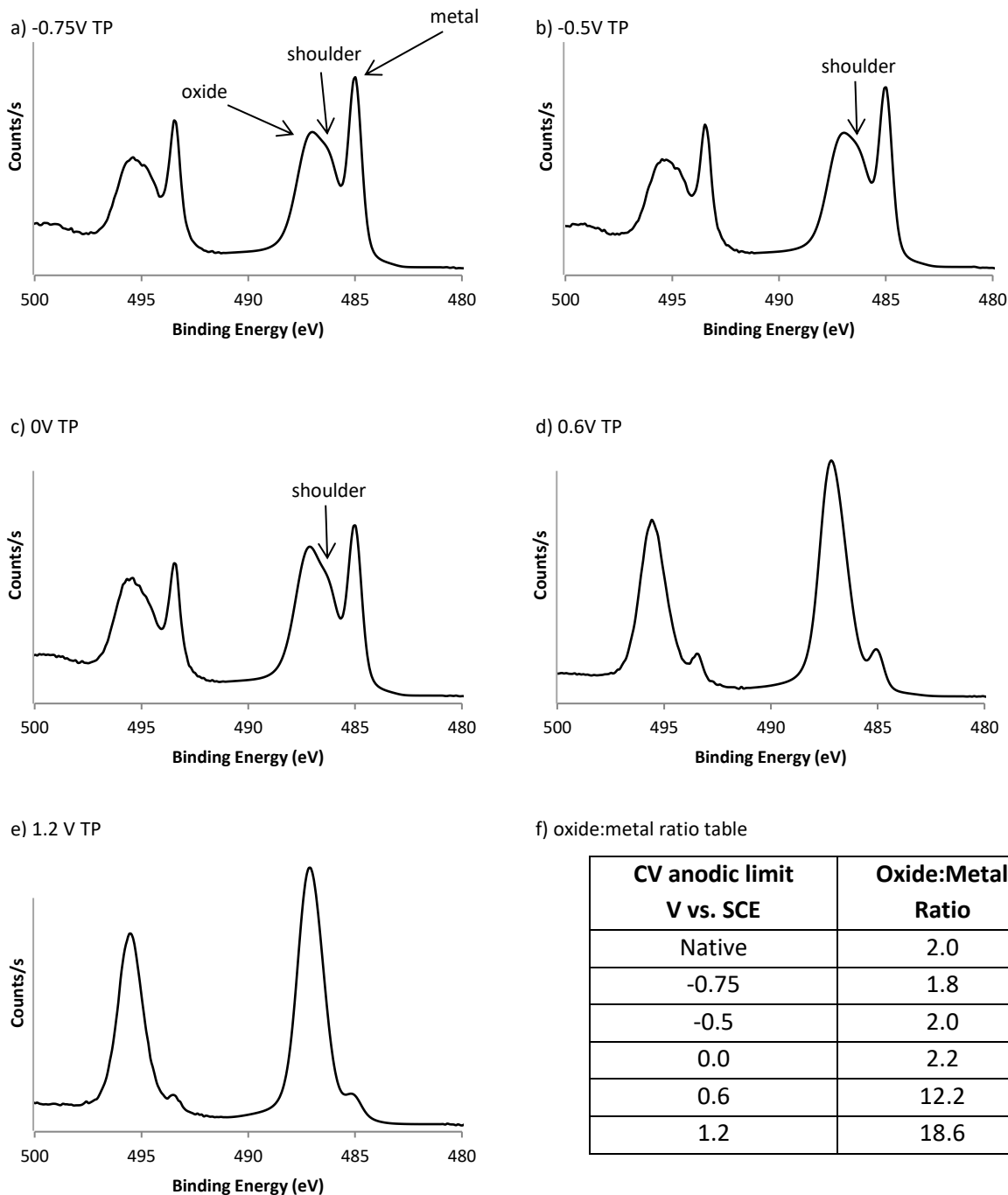


Figure 4.12 XPS high resolution scans of the Sn3d peaks for electrochemically oxidised electroplated pure tin on copper formed after a single cycle with an anodic switching potential of a) -0.75 V vs. SCE b) -0.5 V vs. SCE c) 0 V vs. SCE d) 0.6 V vs. SCE e) 1.2 V vs. SCE and f) a table showing the oxide to metal ratio for each high resolution scan and a native air-formed oxide

The XPS high resolution scans for each single cycle are shown in figure 4.12. It is seen from the high resolution Sn3d5 scans, that sweeping anodically to limits of -0.75 V and -0.5 V vs. SCE results in an oxide similar in thickness to a native air-formed oxide (figure 4.11), although there is a distinct

shoulder present in both scans shown showing that the oxide coating may be comprised of at least two tin oxides with different binding energies, which could mean that the oxide coating may contain both tin(II) and tin(IV) oxides (figures 4.12 a and b). This may suggest that the oxide produced during the anodic sweep is completely reduced during the cathodic sweep and subsequently a native air formed oxide was subsequently formed after removal from the oxidising bath. This would be consistent with the cyclic voltammograms shown in figures 4.5 and 4.6, as both show to have cathodic areas that are similar in size to the anodic area. However, anodically sweeping to an anodic limit of 0 V vs. SCE results in an oxide slightly thicker than that of a native air formed oxide, Again, this is consistent with the cyclic voltammograms shown in figures 4.7 to 4.9, as they all show that the cathodic area is much smaller than the anodic area. This suggests that the oxide produced during the anodic sweep is only partially reduced during the cathodic. Sweeping to anodic limits of 0.6 V and 1.2 V vs. SCE results in thick oxide films with similar intensity ratios of tin oxide to tin metal to those of electrochemically oxidised tin surfaces observed in previous studies^{21,71,72}. This suggests that the oxide formed during the anodic sweep is not reduced on the cathodic sweep.

4.2 Oxidation Bath Reproducibility

Prior to analysis of the electrochemically formed oxides, depth profiling of a native air-formed oxide was carried out to serve as a benchmark for comparison. An x-ray photoelectron spectroscopy (XPS) depth profile measured on the native air-formed oxide present on electroplated pure tin (5 μm) on copper, 1 day after electrodeposition, is shown in figure 4.13. The graph shows the concentration of oxygen, metallic tin (Sn_{met}), tin in the oxidised state (Sn_{ox}) and carbon as a function of argon ion sputter time. As shown in figure 4.12, two Sn_{ox} peaks are sometimes needed to fit the Sn_{ox} signal, however the depth profile in figure 4.13 (and all future depth profiles) shows only one Sn_{ox} depth profile which was because the two Sn_{ox} depth profiles were combined to form one Sn_{ox} depth profile. The initial analysis, as shown by the data points at 0 s sputter time, was carried out prior to any sputtering.

After the second sputter level (20 s) the carbon content drops to ~0 at.%, which shows that carbon is only present at the surface, most likely as a contaminant. At the surface, both the oxygen and Sn_{ox} contents are similar (~30 at.%), which suggests that the oxide at the surface is SnO. After the first 10 s sputter the Sn_{ox} content increases, which was most likely due to the decrease in carbon content, before gradually decreasing on subsequent scans. The Sn_{met} content increases with sputter time and reaches a plateau after 120 s sputter time, this plateau may suggest the point at which the interface between the oxide and the underlying metal surface lies. The oxygen content progressively reduces with sputter time, reaching ~0 at.% at 120 s. However, the Sn_{ox} content never reaches zero which did not correlate, as no oxygen signal was detected after 120 s sputter time. This was most likely due to the ion beam preferentially sputtering oxygen¹⁴⁸ and the constant detection of Sn_{ox} may be due to atomic mixing induced by the ion beam¹⁴⁹. Relating the tantalum oxide (Ta₂O₃) etch rate of 0.01 nm s⁻¹ with the depth profile shown in figure 4.13, it was observed that the oxide was very thin, which was established in previous work^{21,72}.

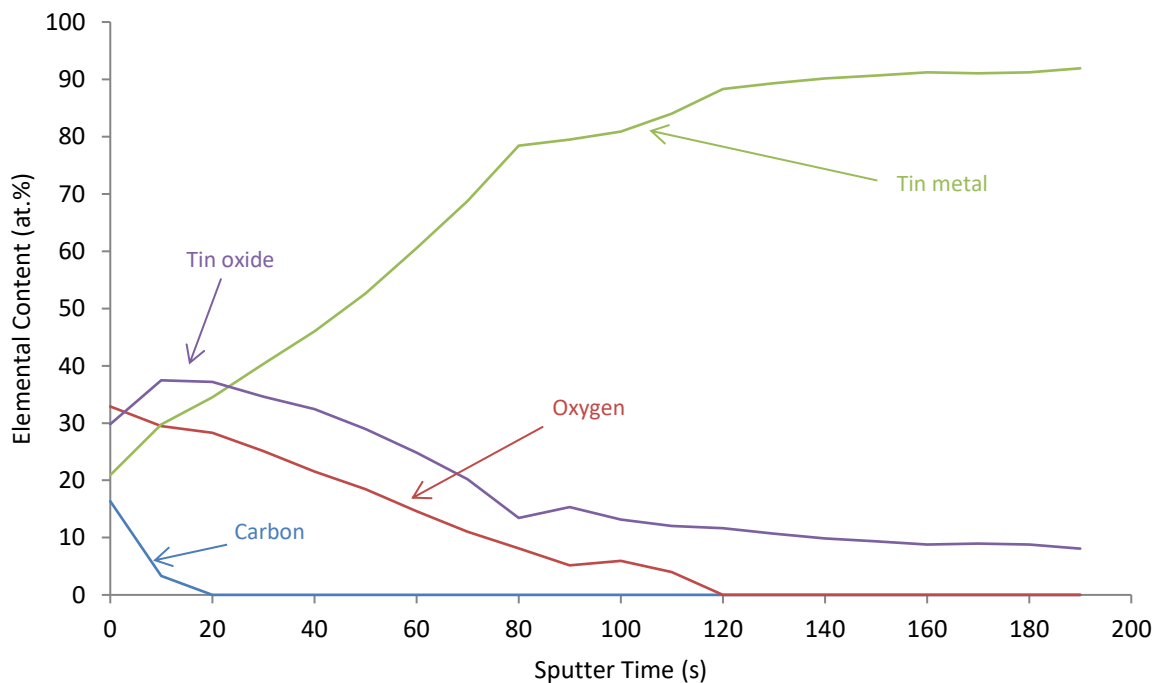


Figure 4.13 XPS depth profile through a native air formed oxide on an electroplated tin on copper surface

4.2.1 Effect of Solution pH on the Thickness and Composition of the Electrochemically Formed Oxide

This study was undertaken to determine whether or not the pH of the oxidising bath had an influence on the thickness and composition of the electrochemically formed oxide. Figure 4.14 shows the Sn_{ox} profiles for samples electrochemically oxidised at 1.2 V vs. SCE in baths with the pH adjusted to 7.9, 8.9 and 9.9, respectively. Also included for comparison is the Sn_{ox} profile for a native air-formed oxide. It is seen that electrochemical oxidation at a potential of 1.2 V vs. SCE results in the formation of a much thicker oxide compared a native air-formed oxide. Figure 4.14 also shows that the pH (within the range of 7.9-9.9) has no effect on the Sn_{ox} content of the electrochemically formed oxide.

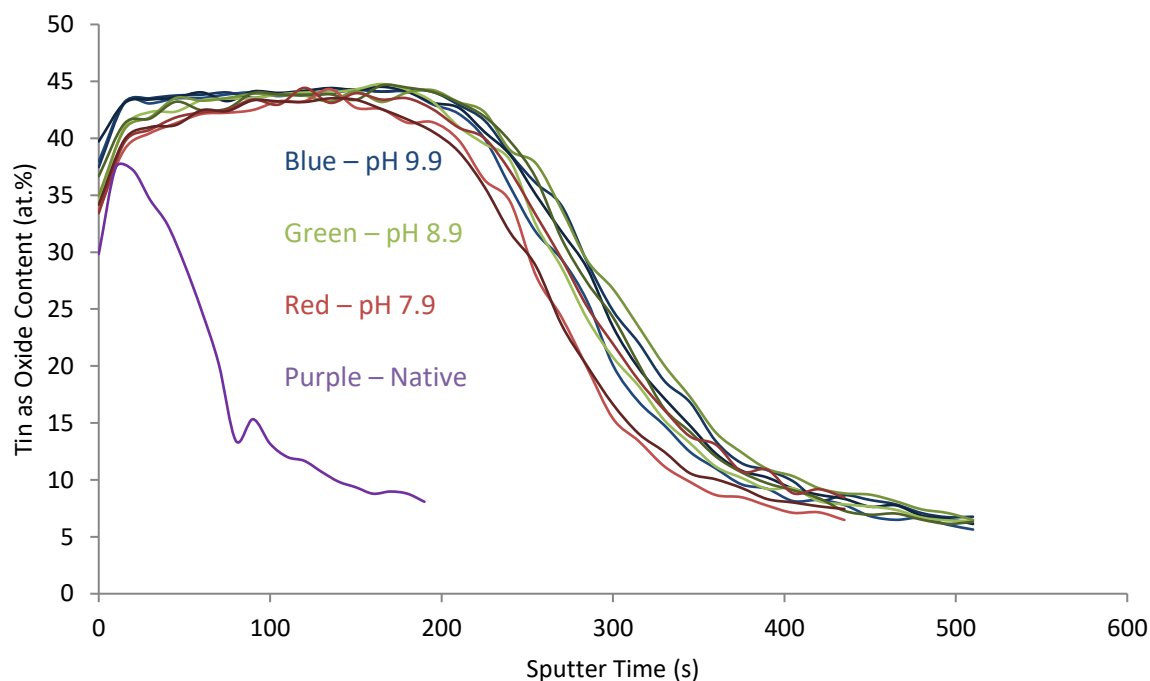


Figure 4.14 XPS depths profile showing the effect of bath pH on the tin as oxide content for samples electrochemically oxidised at 1.2 V vs. SCE. An XPS depth profile of a native air-grown oxide is shown for comparison (purple)

The depth profiles in figure 4.15 shows that the corresponding oxygen content was also unaffected by the pH of the oxidising bath, which suggests that the electrochemically formed oxides all have similar stoichiometries, i.e. the pH has no effect on the oxide chemistry. These results suggest that the pH of the oxidising solution does not need to be adjusted, provided its pH lies within the range studied. This study also shows that the process is reproducible as all samples had similar depth profiles.

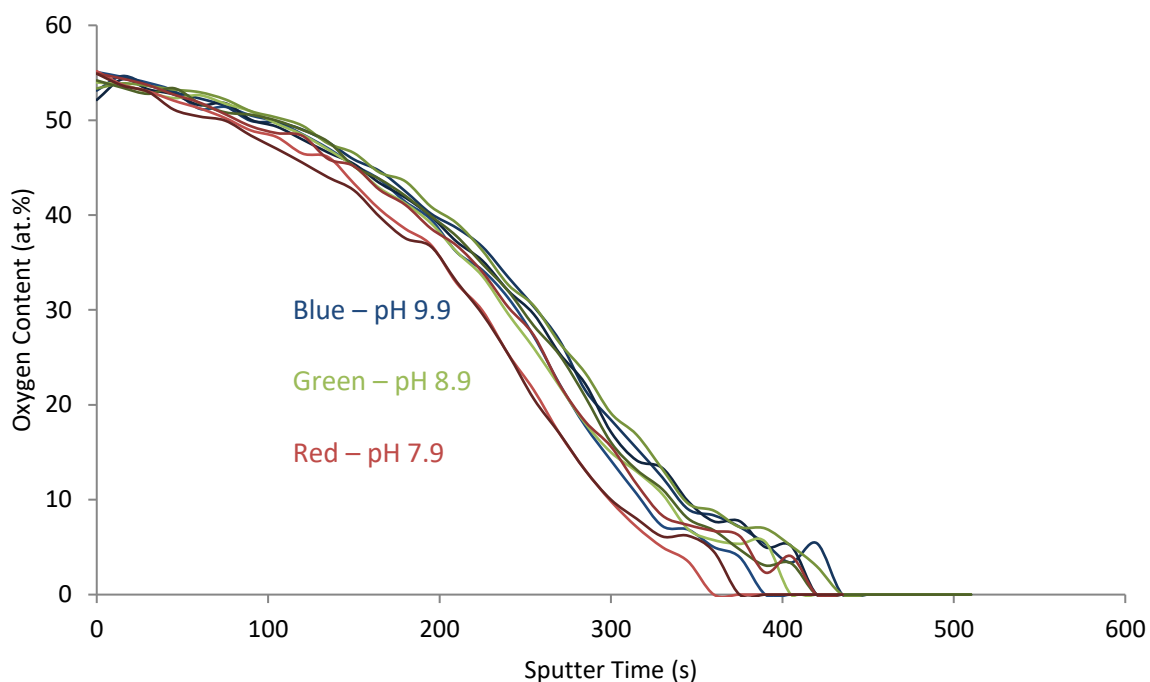


Figure 4.15 XPS depths profile showing the effect of bath pH on the oxygen content for samples electrochemically oxidised at 1.2 V vs. SCE

4.2.2 A Comparison of 'Fresh' and 'Aged' Oxidation Baths

This study was undertaken to determine whether the bath used for electrochemical oxidation degrades over time and influences the thickness and composition of the electrochemically formed oxide layer. The 'aged' solution was ~4 weeks old and had previously been used on ~6 samples whilst the new solution was freshly prepared the same day it was used. Electrochemical oxidation was carried out at 1.2 V vs. SCE on electrodeposited pure tin samples. Sn_{ox} depth profiles from samples oxidised in the 'fresh' and 'aged' baths are shown in figure 4.16, together with a Sn_{ox} profile for a native air-formed oxide.

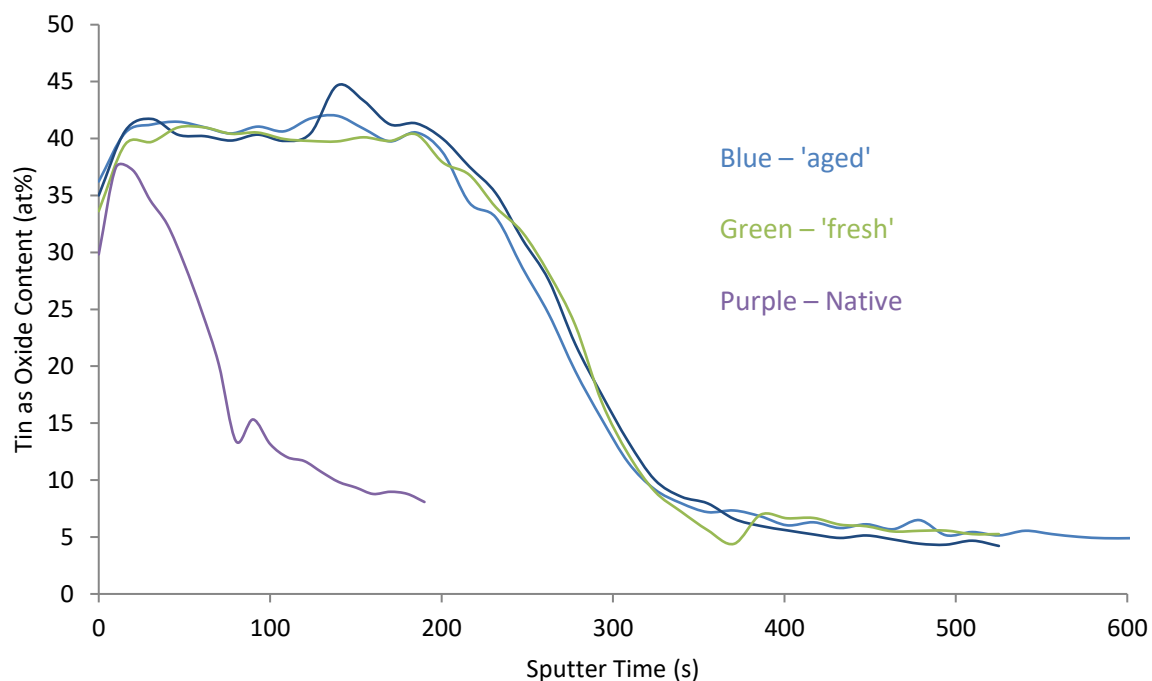


Figure 4.16 XPS depth profile of electrochemically oxidised electroplated tin using 'aged' (blue) and 'fresh' (green) solutions and at a potential of 1.2 V vs. SCE, with respect to tin as oxide. An XPS depth profile of a native air-grown oxide is shown for comparison (purple)

Figure 4.16 shows that all of the Sn_{ox} depth profile for the electrochemically oxidised samples are similar, which indicates that the 'aged' bath is stable and produces electrochemical oxides that are similar in thickness to those obtained from the freshly prepared bath.

Oxygen depth profiles from samples oxidised in the 'fresh' and 'aged' baths are shown in figure 4.17. The curves in figure 4.17 are similar which suggests that the electrochemically formed oxides all have similar stoichiometry, i.e. the use of an 'aged' bath has no effect on the chemistry of the electrochemical oxide layer.

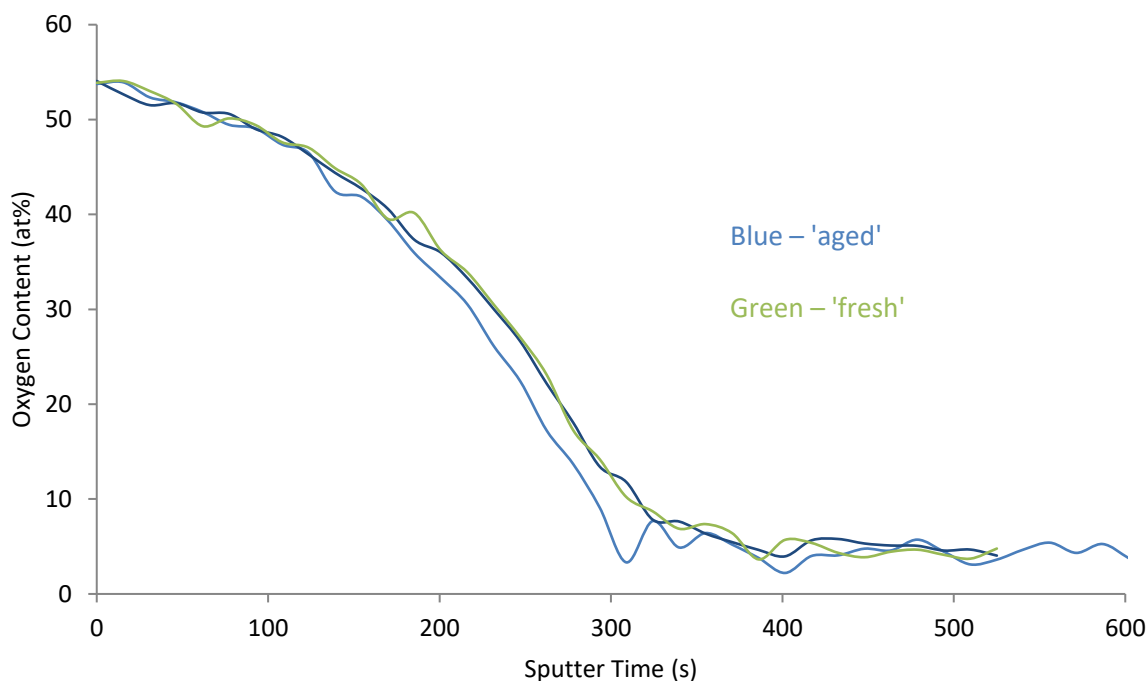


Figure 4.17 XPS depth profile of electrochemically oxidised electroplated tin using 'aged' (blue) and 'fresh' (green) solutions and at a potential of 1.2 V vs. SCE, with respect to oxygen

4.2.3 Effect of Increased Electrochemical Oxidation Potentials on Oxide Formation

The aim of this study was to investigate electrochemical oxidation at potentials greater than 1.2 V vs. SCE, Wu ⁷¹ had previously shown that electrochemical oxidation at potentials greater than 1.2 V vs. SCE, using a borate buffer bath, resulted in the formation of a thicker oxide for electroplated pure tin on brass. The high resolution Sn3d scans obtained by Wu showed that as the potential was increased above 1.2 V vs. SCE the relative intensity of the metal peak reduced, which suggested that the thickness of the electrochemically formed oxides increased with increased potentials. However, no depth profiling was performed to confirm that the oxide thickness increased rather than a more uniform oxide layer being developed.

Figure 4.18 shows high resolution scans of the Sn3d peak for electrochemically formed oxides at 1.2 V, 1.6 V and 2.0 V vs. SCE. The peaks at binding energies of ~495 eV and ~487 eV represent Sn3d3 oxide and Sn3d5 oxide, respectively. The peaks at binding energies of ~493 eV and ~485 eV represent Sn3d3 metal and Sn3d5 metal, respectively. Figure 4.18 shows that as the electrochemical oxidation

potential increases the tin metal peak decreases in intensity, consistent with an increase in oxide film thickness. There was also a small binding energy shift in the oxide peak for samples electrochemically oxidised at 2.0 V vs. SCE; which may indicate that a different oxide species was produced. However, examination of the binding energies of the carbon peaks it was noted that there was a shift in the carbon peak from 285 eV (1.2 V vs. SCE) to 284.8 eV (2.0 V vs. SCE), which would account for the shift in tin oxide peak from 487 eV (1.2 V vs. SCE) to 486.8 eV (2.0 V vs. SCE).

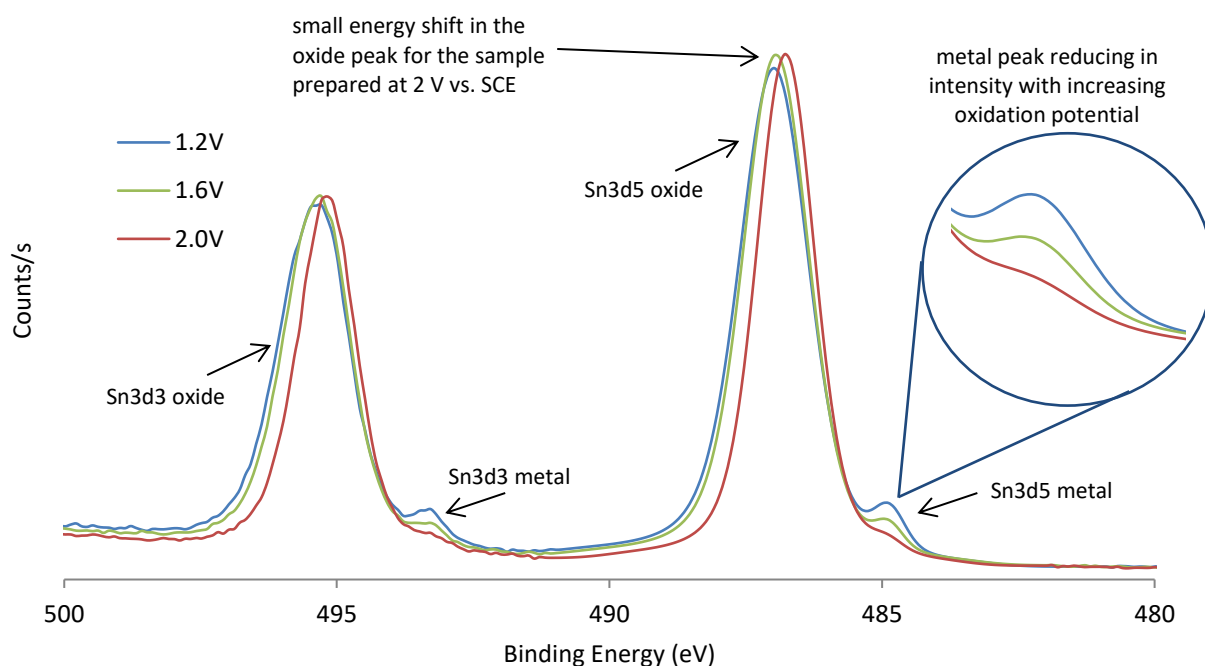


Figure 4.18 XPS high resolution scans of the Sn3d peak after oxidation at 1.2 V (blue), 1.6 V (green) and 2.0 V (red) vs. SCE. The inset XPS profile shows the Sn3d5 metal peaks and how increasing the oxidation potential will decrease the intensity of the metal peak

Figure 4.19 shows the Sn_{ox} XPS depth profiles for samples electrochemically oxidised at 1.2 V, 1.6 V and 2.0 V vs. SCE, respectively. Also included for comparison is the Sn_{ox} XPS depth profile for a native air-formed oxide. The depth profiles for Sn_{ox} shown in figure 4.19 indicate that the oxide film thickness increases when the electrochemical oxidation potential is increased from 1.2 V to 2.0 V vs SCE. The figure shows that electrochemical oxidation at a potential of 2.0 V vs. SCE increases the oxide thickness by ~75% compared with electrochemical oxidation at a potential of 1.2 V vs. SCE. Another advantage of electrochemical oxidation at higher potentials is a reduction in the time required to pass an

equivalent charge. For example, electrochemical oxidation at 2.0 V vs. SCE was ~20 times faster than electrochemical oxidation at 1.2 V vs. SCE. This suggests that electrochemical oxidation at 2.0 V vs. SCE is an optimum potential (of those studied) for producing the thickest electrochemically formed oxide layer, in the potassium bicarbonate-carbonate bath.

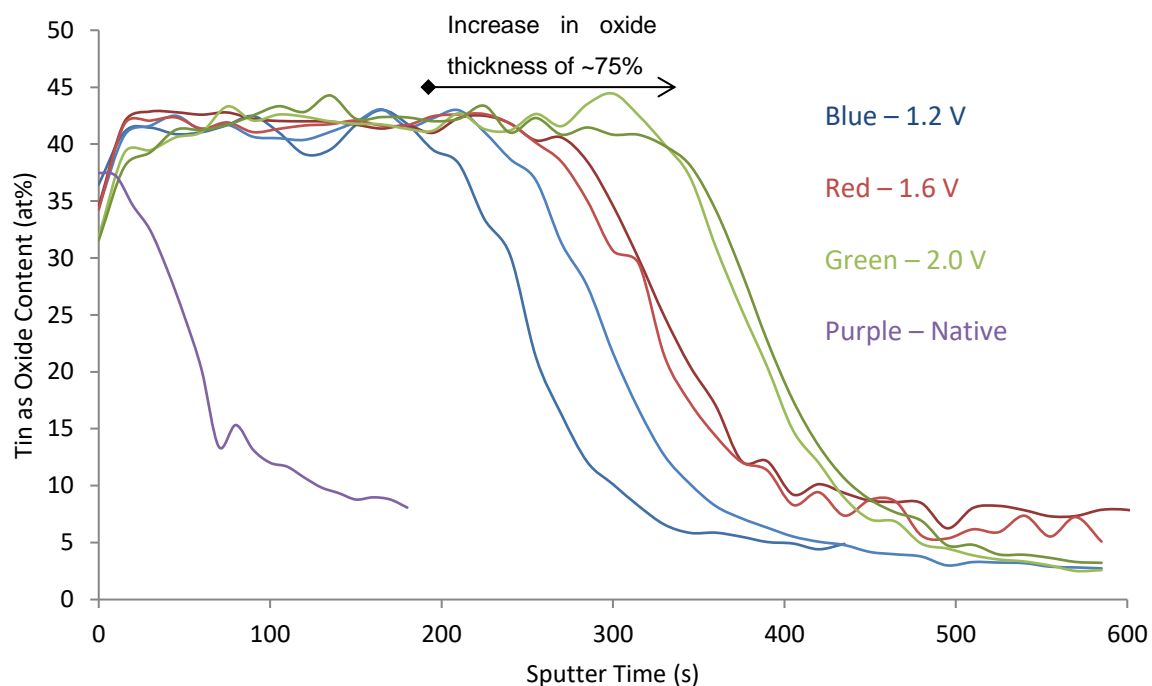


Figure 4.19 XPS depth profile of electrochemically oxidised electroplated tin at varying potentials, with respect to tin as oxide. Showing that increasing the oxidation potential will increase the oxide thickness. An XPS depth profile of a native air-grown oxide is shown for comparison (purple)

4.3 Comparison of Oxide Thickness After Sample Storage at Room Temperature and 55 °C/85 %RH

The aim of this study was to investigate the effect of storage at elevated temperature and relative humidity on both native air-formed and electrochemically formed oxides. This was carried out because whisker growth studies were planned for samples having both electrochemically oxidised surfaces and a polymeric conformal coating. Polymers are often cured at elevated temperature and stored at elevated temperatures and relative humidity to accelerate whisker growth.

Figure 4.20 shows the oxygen depth profiles for six samples; three of which were left to develop a native air-formed oxide and three of which were electrochemically oxidised at a potential of 2 V vs.

SCE, for a charge passed of 60 mC cm^{-2} . The dashed lines the oxygen depth profiles that were obtained within 24 hrs of electrodeposition whilst the solid lines show the oxygen distribution after a storage time of ~ 9 weeks.

Figure 4.20 shows that a native air-formed oxide stored at room temperature increases in thickness by $\sim 400\%$ after ~ 9 weeks of storage. In comparison, a ~ 9 -week-old electrochemically formed oxide has a thickness comparable to a 1 day old sample. In contrast, the oxide film thicknesses for both the native air-formed and the electrochemically formed oxides significantly increased after storage at $55^\circ\text{C}/85\% \text{RH}$ for ~ 9 weeks. This suggests that whisker mitigation for both a native air-formed oxide and electrochemically formed oxide may be improved when stored at elevated temperature and humidity, compared with room temperature storage. However, stresses may be introduced by oxidation at elevated temperatures which may affect whisker growth. The whisker density analysis is discussed later in section 4.4.

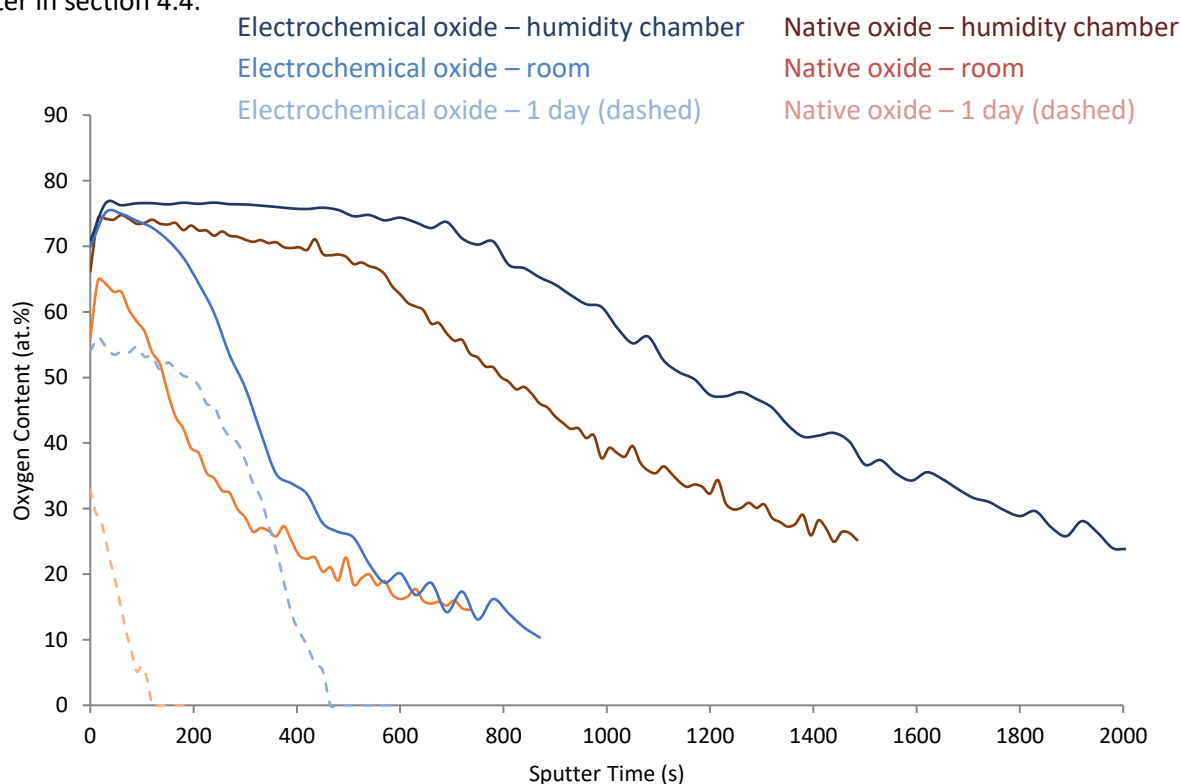


Figure 4.20 XPS depth profiles of electroplated tin samples, with respect to oxygen content, after 1 day and ~ 9 weeks of room temperature storage. The red lines represent the samples that had a native oxide and the blue lines represent the samples with an electrochemically formed oxide produced at 2.0 V vs. SCE . The dotted lines represent samples that were analysed within 24 hr of room temperature storage, for comparison.

4.4 Whisker Growth Studies

Whisker growth studies were carried out on samples that had been electrochemically oxidised at different potentials, to determine which provided the greatest whisker mitigation.

4.4.1 Effect of Copper Addition on Grain Structure

To promote whisker growth for electroplated tin on copper, copper was added to produce a Sn-Cu alloy electrodeposit with a Cu concentration of ~ 1 wt.%⁷². However, the grain structure of the Sn-Cu electrodeposit has not been previously analysed. The addition of copper may affect the grain structure, which may in turn affect whisker growth. It was reported that a change in grain size will affect whisker growth⁴⁰, with an increase in grain size reducing whisker growth. It was also reported that specific grain orientations will promote whisker growth and others that will prevent whisker growth^{150,151}.

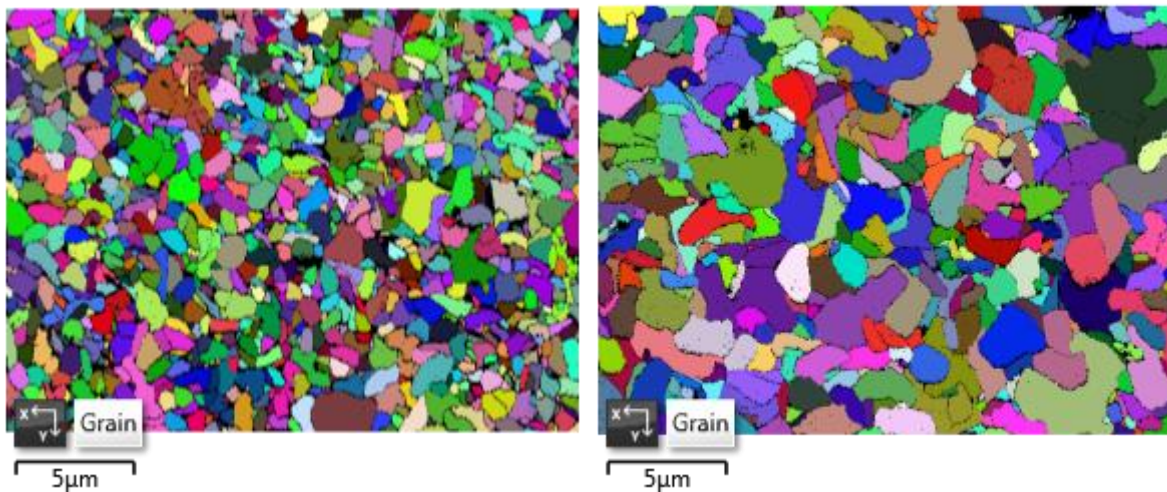


Figure 4.21 EBSD euler colour maps showing the grain structure of electroplated $2 \mu\text{m}$ (left) pure Sn on Cu and (right) Sn-Cu on Cu

Figure 4.21 shows electron back scattered diffraction (EBSD) micrographs, which illustrate the grain size and shape of both an electroplated $2 \mu\text{m}$ pure tin deposit on copper (figure 4.21a) and an electroplated $2 \mu\text{m}$ Sn-Cu deposit on copper (figure 4.21b). Comparing both of the EBSD micrographs, it is shown that the sample with the addition of copper has larger grains, although the overall shape

of the grains has not significantly changed. This increase in grain size should mitigate whisker growth, as suggested by Boguslavsky & Bush⁴⁰.

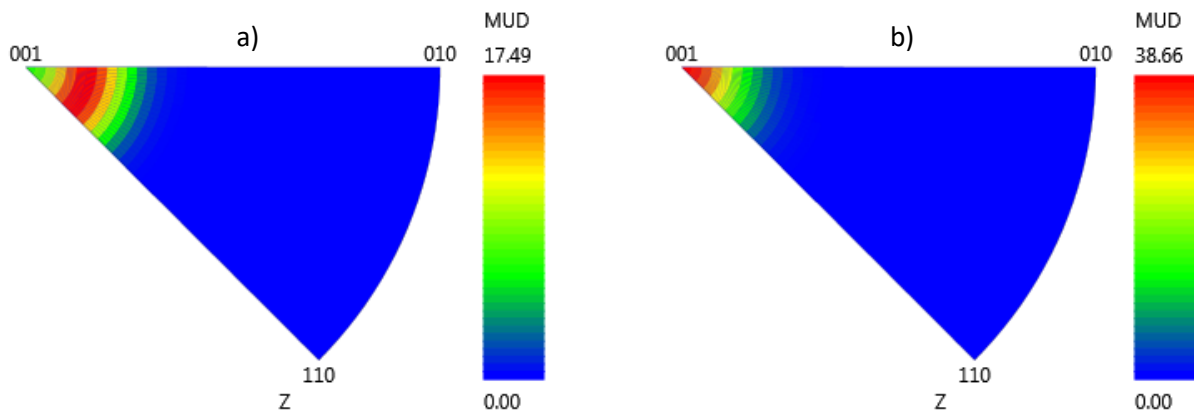


Figure 4.22 Folded inverse pole figures showing the grain orientation of electroplated 2 μm a) pure Sn on Cu and b) Sn-Cu on Cu

Figure 4.22 shows the folded inverse pole figures, which illustrates the grain orientation of both an electroplated 2 μm pure tin deposit on copper (figure 4.22a) and an electroplated 2 μm Sn-Cu deposit on copper (figure 4.22b). Comparing both of the inverse figures, it is shown that both samples have the same preferred grain orientation of 001, which suggests that there will be no effect on whisker growth due to grain orientation. However, the figure does show that the pure tin has an overall preferential orientation of 001, but also slightly orientated in both the 010 and 110 planes, which is shown in figure 4.22a by the fact the distribution is slightly shifted away from 001.

The results shown in both figures 4.21 and 4.22 shows that any increased whisker growth will be due to the addition of copper and the formation of intermetallic compounds (IMCs) and not because there might have been a change in grain structure.

4.4.2 Whisker Growth Studies on Multi-Area Samples

Whisker growth studies were carried out on the samples that each contained three oxide films; one area was left untreated to form a native air-formed oxide (blue) and the other two areas were electrochemically oxidised at the specified potential, with one area having a total charge passed of 30 mC cm^{-2} (red) and the other area having a total charge passed of 60 mC cm^{-2} (green). Figure 4.23a

shows the whisker density for individual areas on each sample after ~2 months of room temperature storage and figure 4.23b shows the whisker density for each area on each of the same samples after ~14 months of room temperature storage.

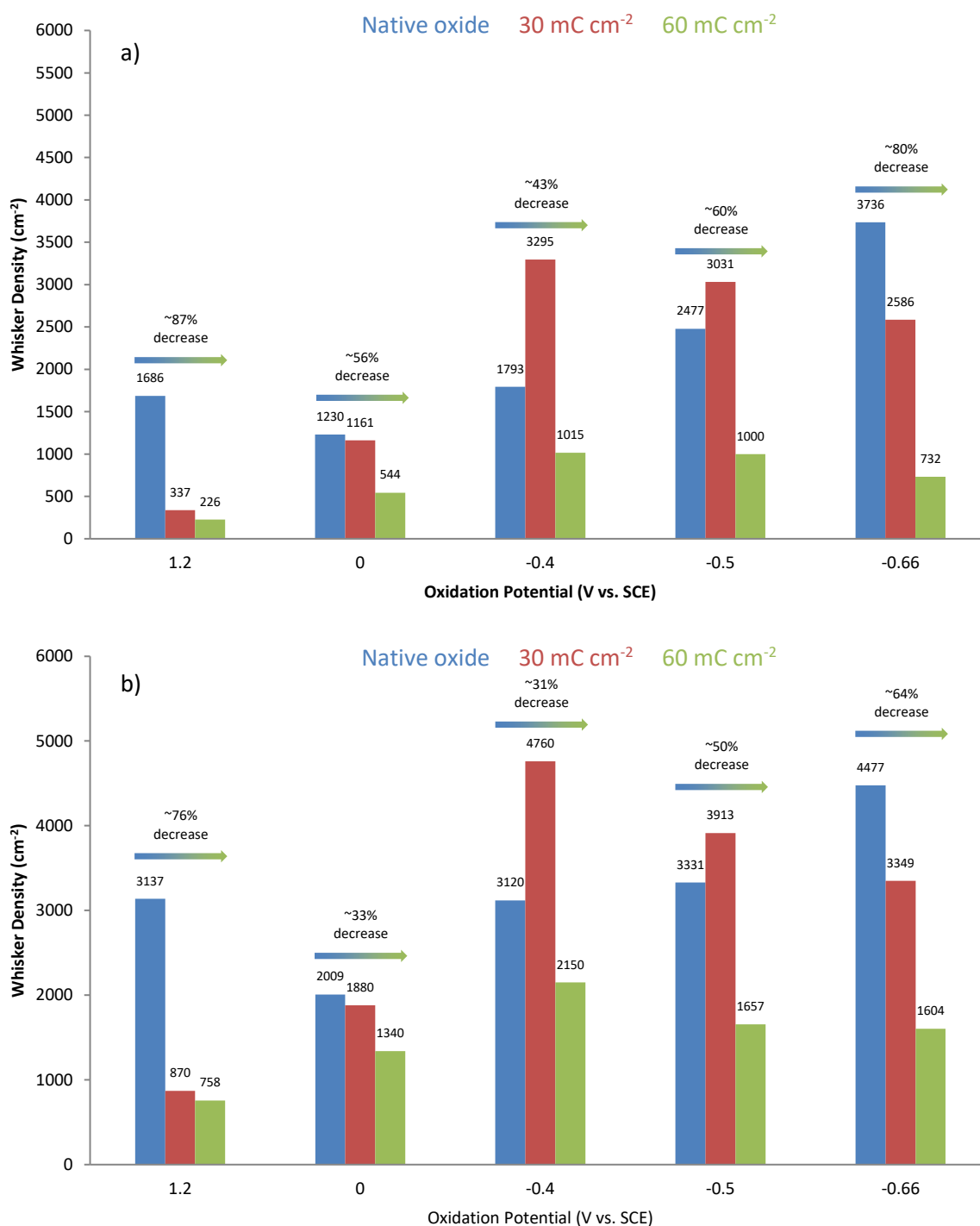


Figure 4.23 a) a graph to show the whisker density on electrochemically oxidised tin samples at different potentials that had been left for ~2 months and b) a graph to show the whisker density on electrochemically oxidised tin samples at different potentials that had been left for ~14 months. The blue bars represent the native oxide; the red bars represent a charge passed of 30 mC cm⁻²; and the green bars represent a charge passed of 60 mC cm⁻². The arrows show the reduction in whisker density using a charge passed of 60 mC cm⁻², compared with the untreated area.

The first observation to make is that there is a significant difference in the whisker densities for the native oxides, ranging from $\sim 1200 \text{ cm}^{-2}$ to $\sim 3700 \text{ cm}^{-2}$ after ~ 2 months of storage (figure 4.23a) and from $\sim 2000 \text{ cm}^{-2}$ to $\sim 4500 \text{ cm}^{-2}$ after ~ 14 months of storage (figure 4.23b). There are several possible explanations for this difference:

- The tin-copper electroplating bath was not being replenished with fresh metal ions due to the use of an inert counter electrode, therefore the concentration of tin and copper ions in the electroplating bath may be depleted with repeated use. The depletion of metal ions is acceptable as long as the ratio of the metal ions remains constant, however if the ratio changes then the concentration of elements may change in the electroplated coating. Although there should not have been a significant difference in the electroplated surfaces for the number of samples being produced. However, there is a correlation between samples B1-B4 with whisker density progressively increasing from the 1st sample to the 4th, which may be due to the order in which the samples were electroplated. Equally the tin and copper ions may be being electrodeposited at different rates, causing a change in ratio in the coating which may affect whisker growth.
- Whisker growth can be unpredictable and there is no standard incubation period before whisker growth will occur. For example, whiskers may begin to grow within 24 hrs of electroplating, or they may not start to grow until weeks after electroplating. The varying incubation period can also be accounted for by sample to sample variation.
- Sample B5 (0 V vs. SCE) was prepared four days after the others, which may account for it having a different whisker density; the tin-copper electroplating bath used in this work is unstable, and over time the tin sulphate will precipitate out. The addition of copper sulphate in the bath accelerates the rate at which the tin sulphate precipitates out. Therefore, the chemistry of the tin-copper electroplating bath may have changed between the day the bath was prepared and the day electrodeposition was carried out on sample B5.

- Whisker growth was not evaluated for all the samples on the same day. This may, in part, account for the increased whisker growth shown by the samples that had more time in storage, i.e. the samples that had more time to grow whiskers. However, the difference in storage time is not great and is unlikely to have significantly affected the whisker density.

The difference in whisker density measured for the native oxide film shows sample to sample variations in whisker density across different samples can occur. In the current study, this is (partly) compensated for by having the native oxide and the electrochemically oxidised regions on the same sample, i.e. whisker growth in the different regions can be compared on the same sample which eliminates potential compositional differences and storage times.

Comparing the sets of data in figure 4.23 it can be seen that for the different electrochemical oxidation potentials, the percentage reduction in whisker density, compared with the native air-formed oxide, has decreased over time. This may suggest that as time increases the ability of the electrochemically produced oxides to mitigate whisker growth reduces. However, at both time intervals the electrochemical oxidation potential of 1.2 V vs. SCE (60 mC cm⁻² charge passed) is the most effective at mitigating whisker growth. For both time intervals, the electrochemical oxidation potentials of -0.5 V and -0.66 V (both vs. SCE) both significantly reduce whisker growth at a total charge passed of 60 mC cm⁻². However, at both time intervals, both -0.4 V and -0.5 V (vs. SCE) increase whisker density for a total charge passed of 30 mC cm⁻².

For a charge passed of 30 mC cm⁻², it might be expected that the electrochemical oxide film would bring about a reduction in whisker density because electrochemically formed oxides are generally much thicker than native air-formed oxides (as discussed previously). Whilst this is true for electrochemical oxidation at 1.2 V, 0 V and -0.66 V vs. SCE (figure 4.23). However, electrochemical oxidation at potentials of -0.4 V and -0.5 V vs. SCE increased the whisker density, which can be seen in both sets of data in figure 4.23. This may be because the electrochemically formed oxide film is

weaker than a native air-formed oxide and may have more weak points at which cracks can develop (this will be discussed in section 4.4.3.1).

For 60 mC cm^{-2} charge passed, all of the electrochemically formed oxide films significantly reduced the whisker density compared with the corresponding native oxide film. The reduction in whisker density, between the electrochemically oxidised and untreated areas, for samples electrochemically oxidised at potentials of -0.4 V and -0.5 V vs. SCE may suggest that a minimum threshold of charge must be passed before a stable oxide is formed that is able to reduce whisker growth.

Based on the results shown in figure 4.23 the two best electrochemical oxidation potentials for mitigating whisker growth are 1.2 V and -0.66 V vs. SCE; after ~ 14 months of room temperature storage both potentials reduced whisker density by over 60% (for a charge passed of 60 mC cm^{-2}) compared with the corresponding native air-formed oxide. For a charge passed of 30 mC cm^{-2} , electrochemical oxidation at a potential of 1.2 V vs. SCE for resulted in the greatest reduction in whisker density. Figure 4.23 shows that, for this potential, increasing the charge passed to 60 mC cm^{-2} from 30 mC cm^{-2} only brought about a small further reduction in the whisker density.

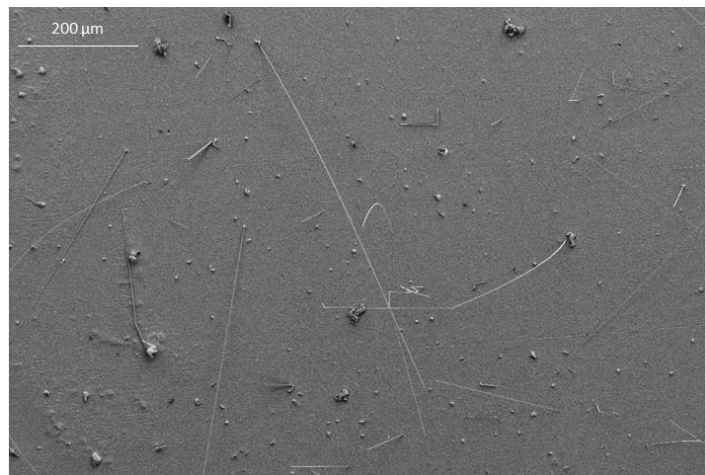


Figure 4.24 SE micrograph of whisker growth on an untreated area on electroplated $2 \mu\text{m}$ Sn-Cu on Cu after ~ 7 months of room temperature storage

Figure 4.24 shows the whisker growth on an area left untreated for ~ 7 months of room temperature.

It was observed that there a high density of whisker growth for all the untreated areas and there was a high density of long filament-type whiskers, as shown in figure 4.24. Figure 4.25 shows whisker growth on each area that had been electrochemically oxidised on each of the multiple area samples.

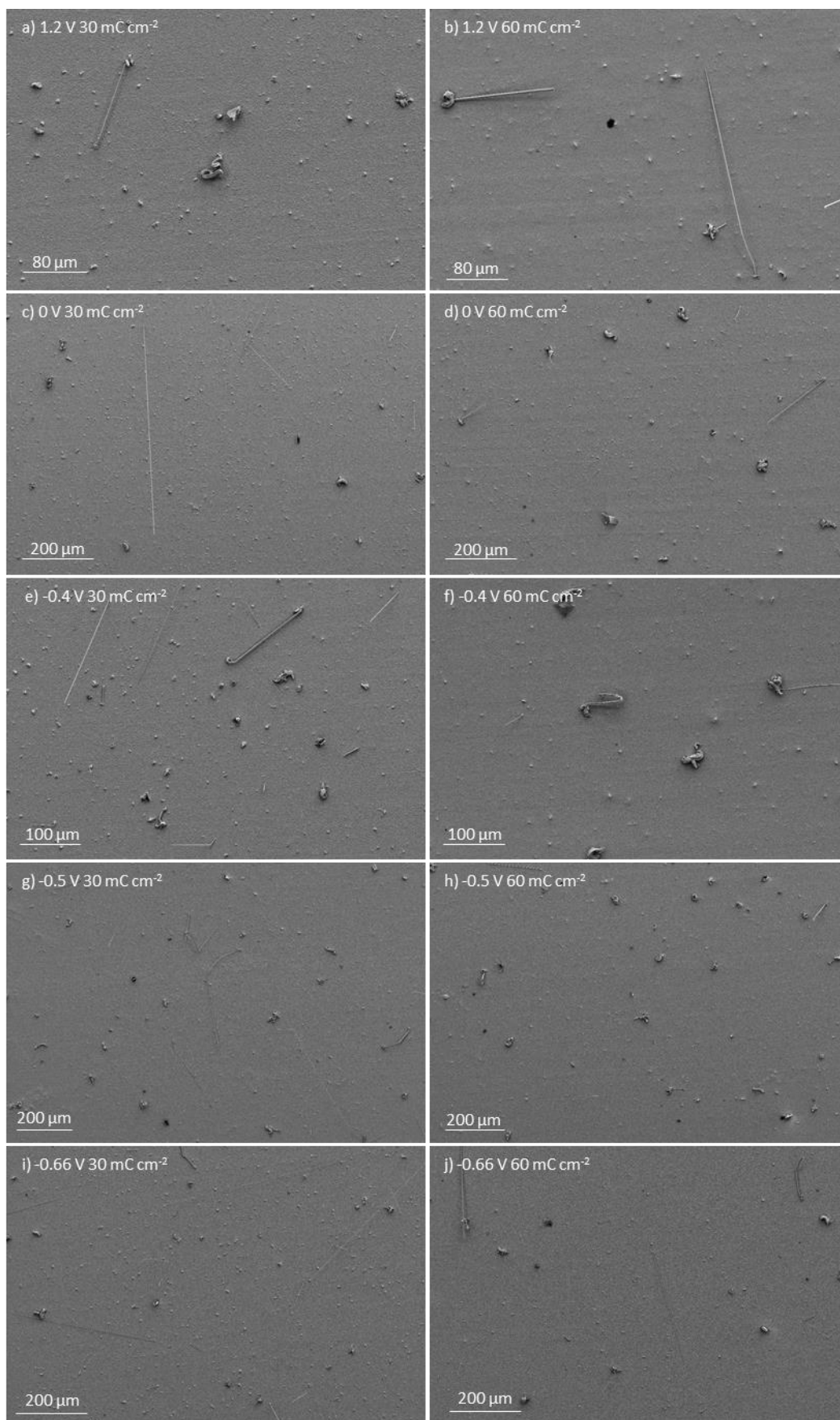


Figure 4.25 SE micrographs showing whisker growth on electroplated 2 μm Sn-Cu on Cu after ~7 months of room temperature storage on the electrochemically oxidised samples at varying potentials (all vs. SCE)

4.4.3 Characterisation of Electrochemically Formed Oxide Coatings for Mitigating Whisker Growth

4.4.3.1 *X-ray Photoelectron Spectroscopy Studies*

Due to the significant variations in whisker densities for the native air-formed oxide areas on the different samples and the surprising results showing an increase in whisker growth for some of the electrochemically oxidised samples in the areas where 30 mC cm^{-2} charge was passed, XPS analysis was carried out. High resolution scans were carried out on each area for each sample to study the surface composition; these are shown in figure 4.26.

Comparing the high resolutions scan shown in figure 4.26 with that shown in figure 4.11a the native air-formed oxide films thicken over time and are similar in thickness to an electrochemically formed oxide. Table 4.2 shows the oxide to metal ratio for each area on each sample, whereby the oxide to metal ratio was calculated by using the surface concentrations. It can be seen that for the samples produced at 0 V and -0.66 V vs. SCE, the electrochemically formed oxides are similar in thickness to their native air-formed oxide counterpart. The electrochemically formed oxides produced at 1.2, -0.4 and -0.5 V vs. SCE have a much thicker oxide layer, compared to their native air-formed oxide counterpart.

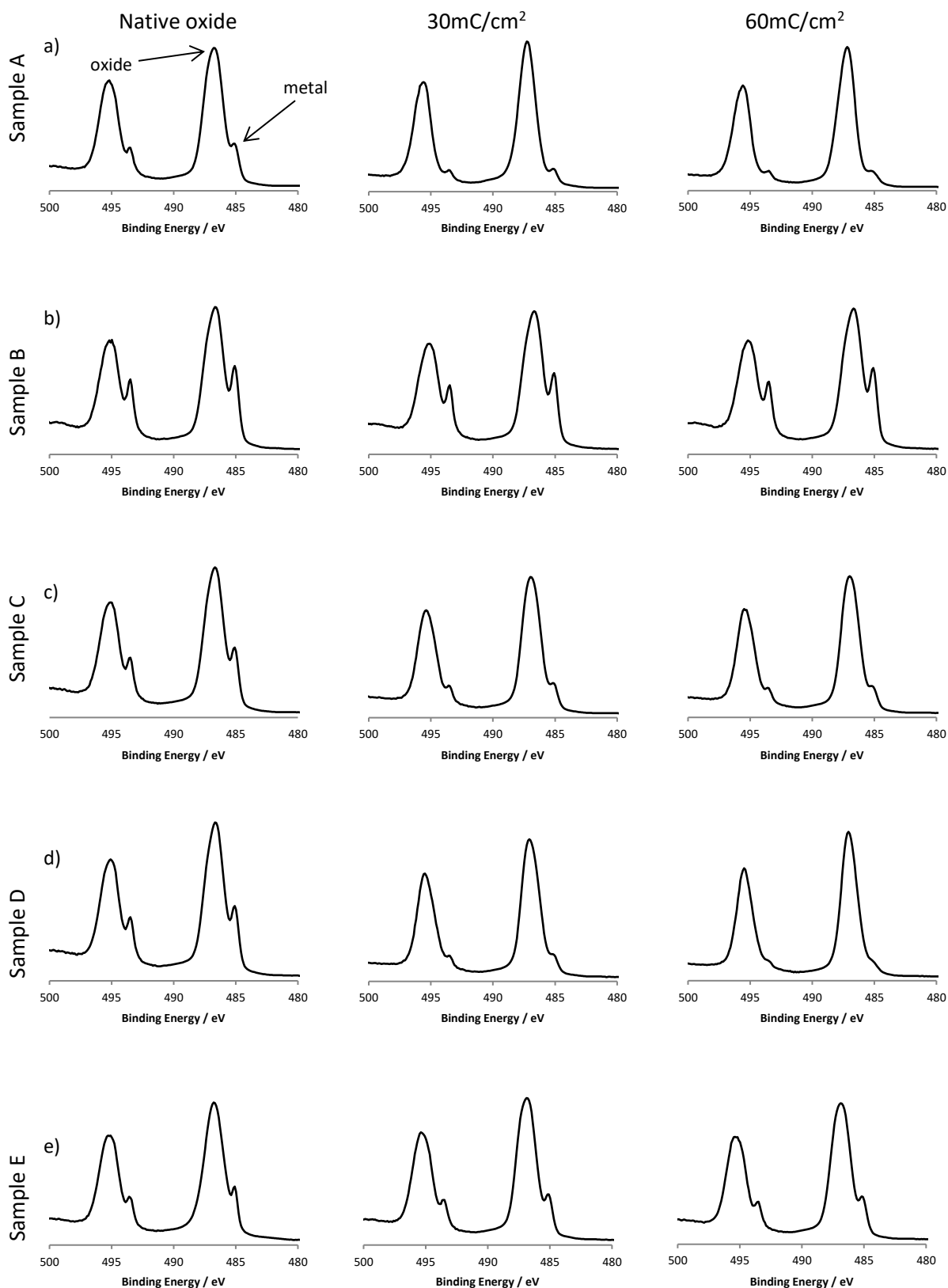


Figure 4.26 XPS high resolution scans of the Sn3d peaks recorded from electroplated pure tin on copper samples with multiple areas of treatment that had been stored at room temperature for ~ 3 months. All samples have one area that had no treatment and two areas that had been electrochemically oxidised in a standard potassium bicarbonate-carbonate solution. The left-hand scans are all native air-formed oxides, the middle scans have a charge passed of 30 mC cm^{-2} and the right-hand scans have a charge passed of 60 mC cm^{-2} . Each row indicates a multiple-area sample a) 1.2 V (sample A) b) 0 V (sample B) c) -0.4 V (sample C) d) -0.5 V (sample D) and e) -0.66 V (sample E), all vs. SCE.

Table 4.2 Tin as oxide to tin as metal ratios for each treatment area on the samples shown in figure 4.22

Electrochemical Oxidation Potential (V vs. SCE)	Native Oxide	30 mC cm ⁻²	60 mC cm ⁻²
1.2	10.7	26.6	19.9
0	4.8	5.2	4.9
-0.4	7.2	15.2	16.3
-0.5	6.8	22	27
-0.66	10.8	10.1	10.1

The results for the samples electrochemically oxidised at -0.4 V and -0.5 V vs. SCE in figure 4.26 do not explain the whisker density results shown in figure 4.23. Since both samples possess oxide films that are thicker than the native air-formed oxide regions, which would be expected to impart improved whisker mitigation.

In view of these somewhat unexpected results, additional samples were electroplated and electrochemically oxidised (using a total charge passed of 30 mC cm⁻²), at the potentials used for whisker growth studies (section 4.1.4), to investigate the initial chemical composition of the oxide films within 24 h of electrochemical oxidation. Figure 4.27 shows the high resolution Sn3d scans obtained from the surface of the electrochemically oxidised samples (using a total charge passed of 30 mC cm⁻²) within 24 h of electrochemical oxidation. A table showing the ratio of the surface Sn_{ox} concentration to Sn_{met} concentration is also given in figure 4.27. The Sn_{ox} to Sn_{met} ratios show that electrochemical oxidation at a potential of 1.2 V vs. SCE produced the thickest tin oxide. This directly relates to results shown in figure 4.23 on the basis that the sample electrochemically oxidised at 1.2 V vs. SCE showed the greatest reduction in whisker density. Unexpectedly electrochemical oxidation at a potential of -0.66 V vs. SCE produced a comparatively thin tin oxide coating, shown by the large metal peak (figure 4.23), which is not consistent with the whisker growth results shown in figure 4.23.

The high resolution Sn3d scans of the surfaces electrochemically oxidised at potentials of 0 V, -0.4 V, -0.5 V and -0.66 V vs. SCE all give comparatively low tin oxide to tin metal ratios; however, compared

to the results discussed in section 4.1, they are all thicker than a 1 day old native air-formed oxide (figure 4.11a), which doesn't correlate to the whisker density data shown in figure 4.23. The high resolution scans shown in figure 4.27 show that electrochemical oxidation at these four potentials produces an oxide layer that is significantly thicker than a native air-formed oxide, with the exception of the electrochemically formed oxide produced at -0.5 V which has a similar high resolution scan to a native air-formed oxide, but is still slightly thicker; therefore, it may be expected that the electrochemical oxide layer should provide improved whisker growth mitigation. However, for the samples that were electrochemically oxidised at 0 V, -0.4 V and -0.5 V vs. SCE the whisker density results shown in figure 4.23 indicated that whisker growth was either unchanged (0 V vs. SCE) or increased (-0.4 V and -0.5 V vs. SCE) for the electrochemically oxidised samples (using a total charge passed of 30 mC cm^{-2}). Therefore, there could be other factors influencing the structure and/or the chemistry of the electrochemically formed oxide layers. For example, the electrochemically formed oxide layer may be porous or non-uniform or comprised of a different type of oxide.

As the whisker density was increased for the samples that were electrochemically oxidised at potentials of -0.4 V and -0.5 V vs. SCE at a charge passed of 30 mC cm^{-2} , it could be suggested that these two electrochemically formed oxide layers have an increased number of weak points which would cause cracking. Alternatively, the electrochemically formed oxide may have a different structure (decreased density, increased porosity) to that produced at 1.2 V vs. SCE which may cause the oxide film to have reduced physical properties.

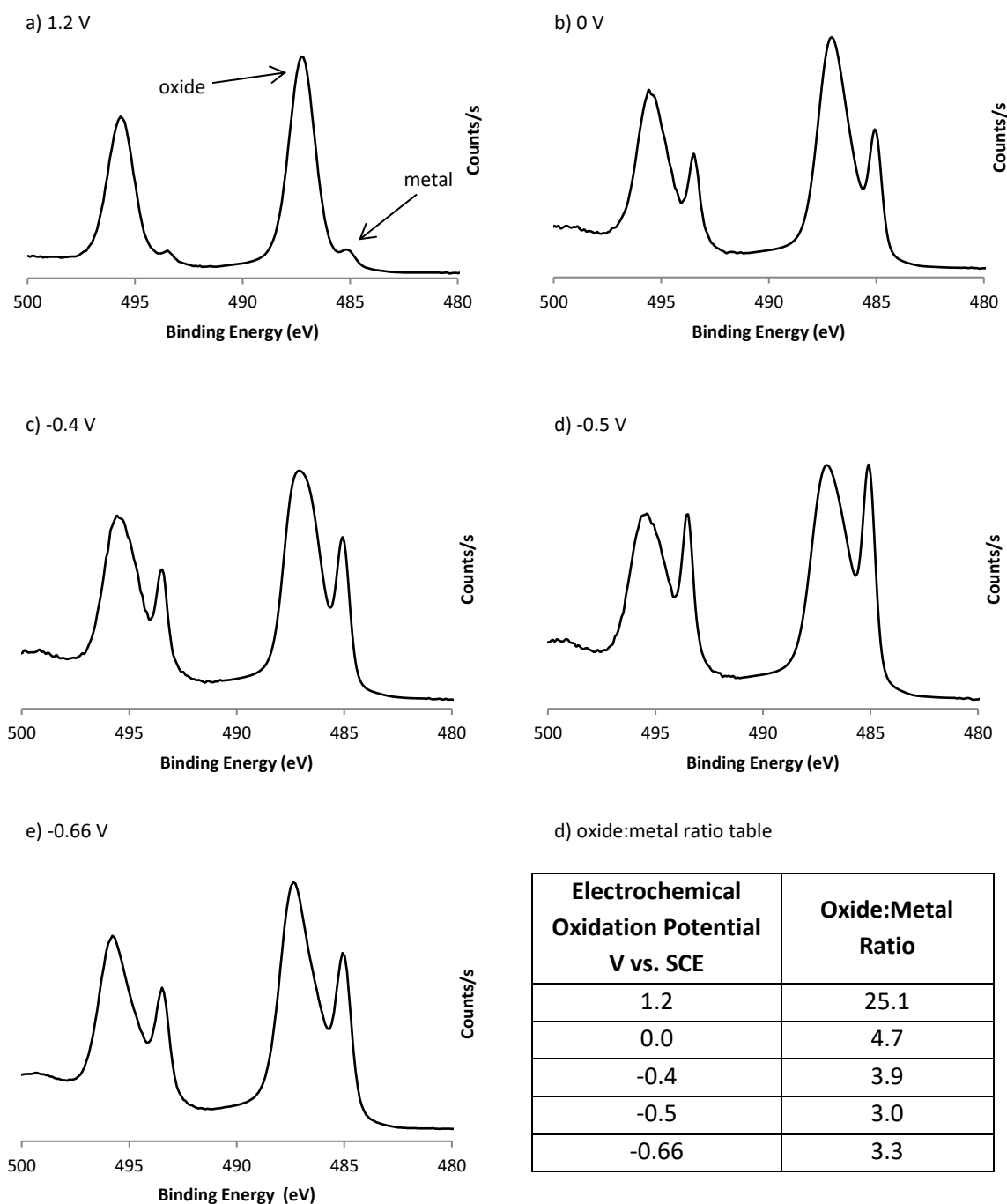


Figure 4.27 XPS high resolution scans, with respect to tin, of oxidised electroplated pure tin on copper samples that had been left for ~24 hr. All have been electrochemically oxidised in a standard potassium-bicarbonate solution and had a charge passed of 30 mC cm^{-2} with formation potentials of a) 1.2 V vs. SCE b) 0 V vs. SCE c) -0.4 V vs. SCE d) -0.5 V vs. SCE e) -0.66 V vs. SCE and d) a table showing the ratio of tin as oxide to tin as metal for each of the potentials

Comparing figures 4.11a, 4.26 and 4.27, it is observed that all the oxide films, with the exception of that electrochemically formed at 1.2 V vs. SCE, have thickened over time regardless of whether they were formed naturally or electrochemically. This suggests that over time, the thickening of the oxide

films may help to enhance the ability of the oxide film to mitigate tin whisker growth, depending perhaps on the nature of the oxide growth. This will affect the incubation period prior to the onset of whisker growth, i.e. if a sample has an initially thin oxide film then whiskers may grow sooner than from a sample that possess a thicker oxide film. As shown in figure 4.26, the electrochemically formed oxide produced at 1.2 V vs. SCE does not increase in thickness after ~3 months of room temperature storage which may suggest that the oxide is different in another way than the other electrochemically formed oxides and native air-formed oxide, i.e. it may have fewer defects or may have increased uniformity. The time dependency for both whisker growth and oxide film is discussed in section 4.5.

4.4.3.2 Scanning Electron Microscopy of Electrochemically Oxidised Surfaces

Scanning electron microscopy was carried out to study the surface morphology of the electrochemically formed oxides and to compare them with that of a native air-formed oxide. Figure 4.26 shows a representative secondary electron (SE) micrograph of the surface of a tin-copper electrodeposit on copper. The micrograph shown in figure 4.28 serves as a benchmark for comparison with the electrochemically formed oxides.

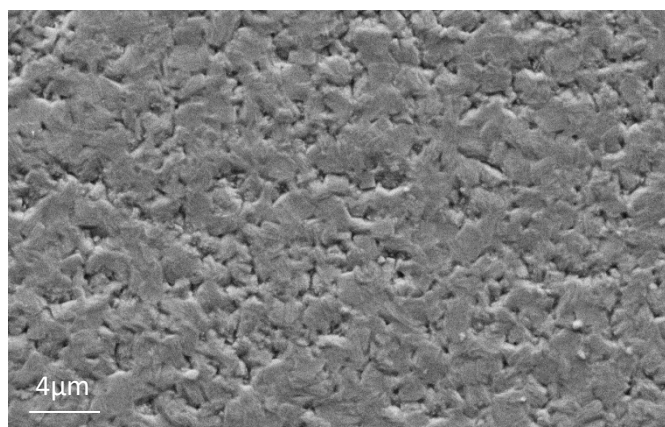


Figure 4.28 SEM micrograph showing the surface morphology of a sample left to develop a native air-formed oxide for ~24 hr

Figure 4.29 shows SE micrographs of the surface of electrochemically oxidised tin-copper electrodeposits at each potential used for oxide formation and whisker mitigation (in section 4.4.2) for both charges passed of namely 30 mC cm^{-2} and 60 mC cm^{-2} . It can be seen from figure 4.27 that the surface morphology of samples electrochemically oxidised at potentials of 1.2 V, 0 V and -0.4 V vs.

SCE, for a charge passed of 30 mC cm^{-2} , is comparable to that of a native air-formed oxide (figure 4.28). For the sample that had been electrochemically oxidised at potentials of 1.2 V, 0 V, -0.4 V vs. SCE for a charge passed of 60 mC cm^{-2} (figure 4.29 b, d and f, respectively), the surfaces seem slightly different to those produced for a charge passed of 30 mC cm^{-2} (figure 4.29 a, c and e, respectively). This difference being a small etch effect, whereby it would appear that the surface has become slightly rougher in texture and the grains also appear more well-defined. The micrographs shown in figure 4.29 b, d and f are all similar in appearance. The etching effect on the surfaces are illustrated by the white circled areas on the micrographs. For the samples shown in figure 4.29(g and h), the surfaces appear to have an increased roughness compared with the surfaces shown previously in the figure; whereas for the samples shown in figure 4.29(i,j), the surfaces appear to have pores which are illustrated by the yellow circles. The pores show clear evidence of surface dissolution, which was more apparent when electrochemical oxidation was carried out when increasing the total charge passed. The dissolution observed in figure 4.29(i,j) may be preferential dissolution of individual grains because the size of features are similar to the grain size of the tin-copper coating.

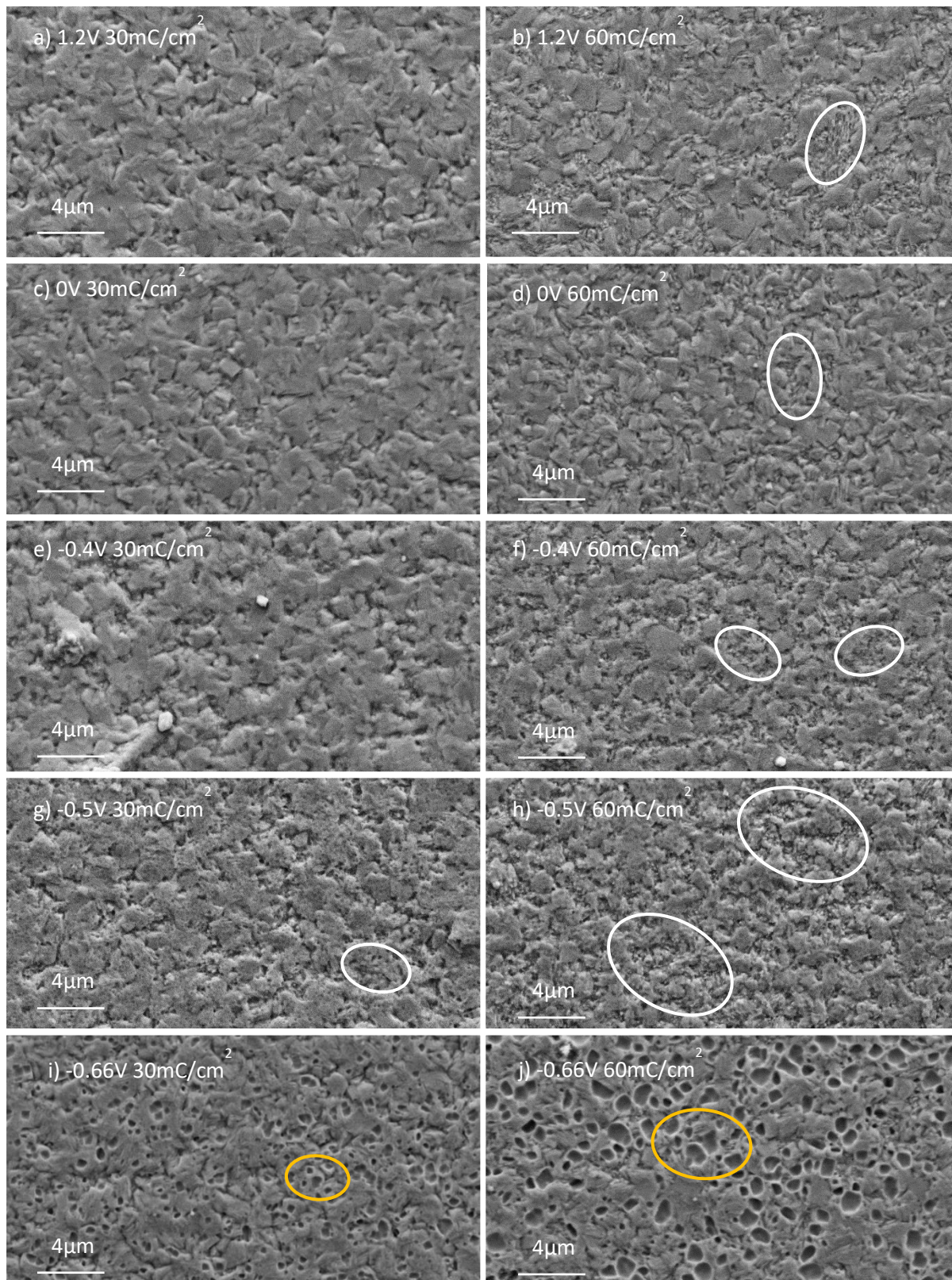


Figure 4.29 SE micrographs showing the effect of electrochemical oxidation on the surface morphology at varying potentials (all vs. SCE), where white circles illustrate areas of an etching effect and the yellow circles illustrate areas of dissolution

4.4.4 Effect of Increased Oxidation Potentials on Whisker Growth

In section 4.2.3 it was shown that increasing the electrochemical oxidation potential above 1.2 V vs. SCE resulted in an increased oxide film thickness, for an equivalent charge passed, which would suggest that increased electrochemical oxidation potentials would further improve the mitigation of whisker growth compared with treatment at 1.2 V vs. SCE. Figure 4.30 shows the whisker densities for electrochemically formed oxides produced at 1.2 V, 1.6 V and 2.0 V vs. SCE for both 30 mC cm⁻² charge passed and 60 mC cm⁻² charge passed; whisker growth on samples left to develop a native air-formed oxide are also shown for comparison. For each treatment three samples were analysed (and the average whisker density was calculated together with the standard deviation).

It can be seen from figure 4.30 that each of the electrochemical oxidation potentials used to produce the oxide film significantly reduced whisker density compared with a native air-formed oxide. Figure 4.30 also shows that the reduction in whisker density is similar for each of the electrochemical oxidation potentials, although, the electrochemical oxidation at 2 V vs. SCE for a charge passed of 60 mC cm⁻² did give the lowest average whisker density. This suggests that these parameters provide the most effective whisker mitigation. The improvement in whisker mitigation is most likely due to the increased oxide film thickness, as shown in section 4.2.3.

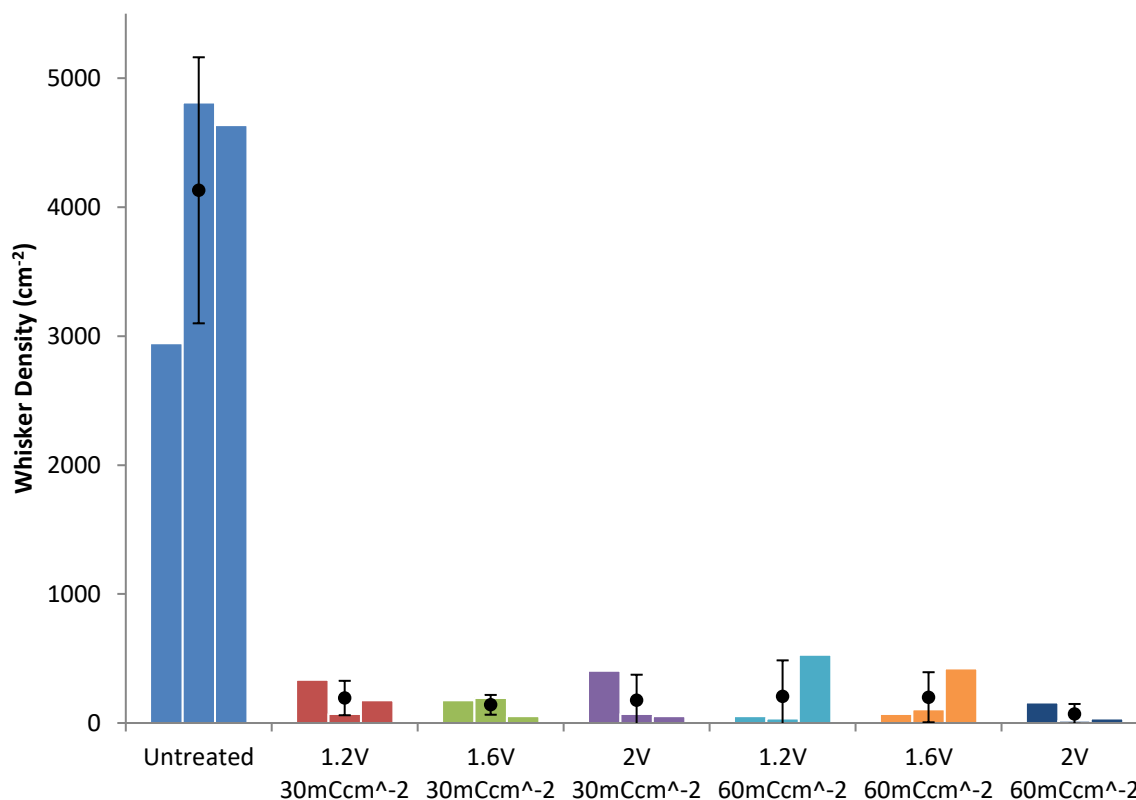


Figure 4.30 Data showing whisker density for electrochemically formed oxides in potassium bicarbonate-carbonate bath and untreated electroplated 2 μm tin-copper on copper samples after ~ 9 months at room temperature. It should be noted that the second '2 V 60 mCcm⁻²' sample had 0 visible whiskers. With the error bars representing the standard deviation between samples

4.4.5 Comparison of Whisker Density After Storage at Room Temperature and 55 °C/85 %RH

The aim of this study was to investigate storage at room temperature or at an elevated temperature and relative humidity on whisker growth for both electrochemically oxidised and untreated samples. This was carried out because it was envisaged that a combined electrochemically formed oxide and polymeric conformal coating would be investigated; furthermore, conformal coated samples would generally be stored in a humidity chamber at 55 °C/85 %RH to promote whisker growth. The study on how storage at elevated temperature and relative humidity affected the oxide films, discussed in section 4.3, showed that storing both the untreated and electrochemically oxidised samples at 55 °C/85 %RH resulted in an increase in the thickness of the all oxide films. This may suggest that storage at 55 °C/85 %RH would result in improved whisker mitigation for both the untreated and electrochemically oxidised samples – depending on the when the whiskers grew and the quality of the oxide.

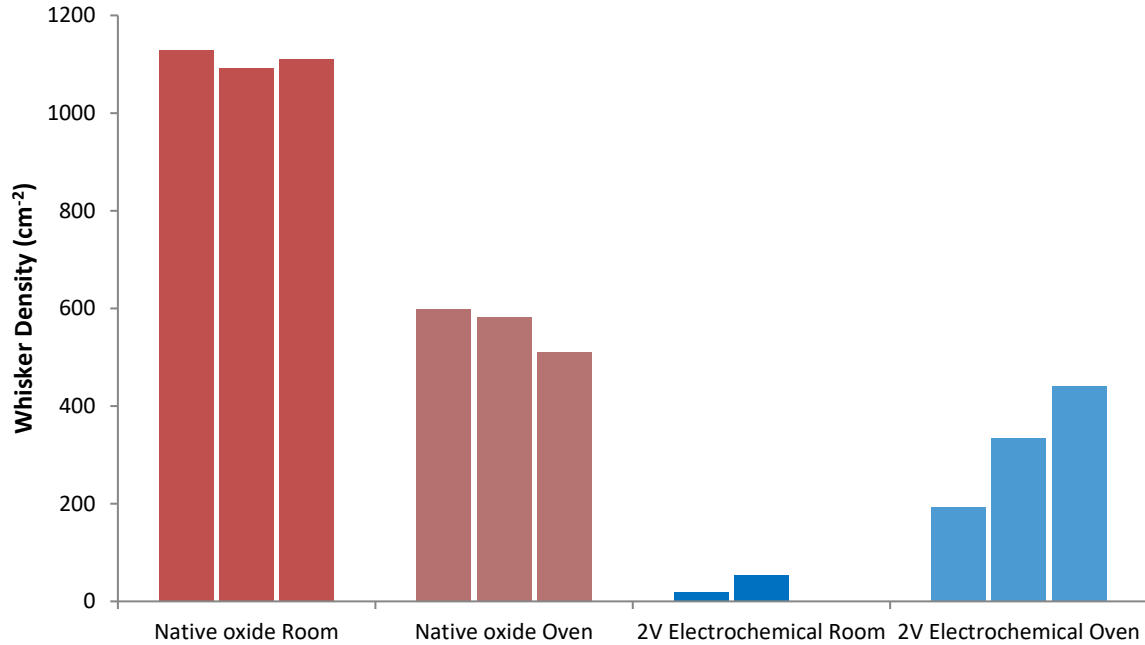


Figure 4.31 Data showing whisker density for electrochemically formed oxides (blue) and untreated (red) electroplated tin-copper on copper samples after ~6 weeks of room temperature and humidity chamber storage. It should be noted that the third '2 V Electrochemical Room' sample had 0 visible whiskers.

Figure 4.31 shows the whisker densities for both the untreated and the electrochemically oxidised (at a potential of 2 V vs. Ag/AgCl for a total charge passed of 60 mC cm⁻²) samples after ~6 weeks of room temperature and a humidity chamber storage. For the samples that had been left to develop a native air-formed oxide, the whisker density was reduced by ~50 % for the humidity chamber stored samples, which could have been due to the significant increase in oxide thickness as shown in section 4.3. However, there may be other factors that influenced whisker growth, such as a change in intermetallic compound (IMC) growth, the 'quality' of the oxide may have changed, or the stress in the coating may have changed. However, for the samples that had been electrochemically oxidised, the whisker density was increased for the samples stored in the humidity chamber, which at first glance may be contradictory to the results shown in section 4.3. The latter showed that the electrochemically formed oxide thickness significantly increased when stored in the humidity chamber. This suggests that storage of the electrochemically oxidised samples in the humidity chamber impairs the ability of the oxide film to mitigate whisker growth, i.e. may cause the oxide film to become porous or non-uniform and/or it may cause the oxide film to become more brittle. Therefore, it would be suggested that dual-

layer samples should not be stored/cured in the humidity chamber as the storage conditions will compromise the electrochemically formed oxide.

4.4.6 Long-Term Whisker Mitigation of Electrochemically Formed Oxides on Both Sn-Cu on Copper and Pure Sn on Brass

This section presents and discusses the long-term whisker density results for both Sn-Cu electrodeposits on Cu and pure Sn on brass. Focused ion beam scanning electron microscopy (FIB-SEM) and x-ray photoelectron spectroscopy (XPS) were also used to investigate the mechanisms that bring about whisker mitigation for both systems. Electroplated pure tin deposits on brass were studied, in addition to Sn-Cu deposits on copper, to determine whether the same mechanism was responsible for the observed reduction in whisker growth brought about by electrochemical oxidation. The results obtained in this section will establish an understanding as to how whisker mitigation is achieved, i.e. whether the oxide layer is acting simply as a physical barrier to prevent whisker growth.

4.4.6.1 Tin-Copper Electrodeposits on Copper

The effect of an electrochemically formed oxide and its subsequent effect on long-term whisker growth was evaluated for 2 μm Sn-Cu deposits on copper oxidised in both the borate buffer and potassium bicarbonate-carbonate solutions. Figure 4.32 shows the change in average whisker density over ~ 3 years of room temperature storage. The data shows that after ~ 3 years of room temperature storage there remains an order of magnitude reduction in whisker growth for the electrochemically formed oxides compared with the whisker density for the native air-formed oxides. Figure 4.32 also shows that there is a rapid increase in whisker growth within the first 180 days of storage, after which the rate of whisker growth significantly reduces. For the untreated samples, this may have been due to the thickening of the native air-formed oxide (as discussed in section 4.4.3), which would enhance the whisker mitigation effect. However, this may not be the case for the electrochemically formed oxides, as it was shown in section 4.4.3 that the thickness of oxides formed electrochemically at 1.2 V

vs. SCE does not increase with time. Therefore, there must be some other factor, such as the IMC formation, affecting the rate at which the whiskers grow, which will be discussed later in section 4.5.

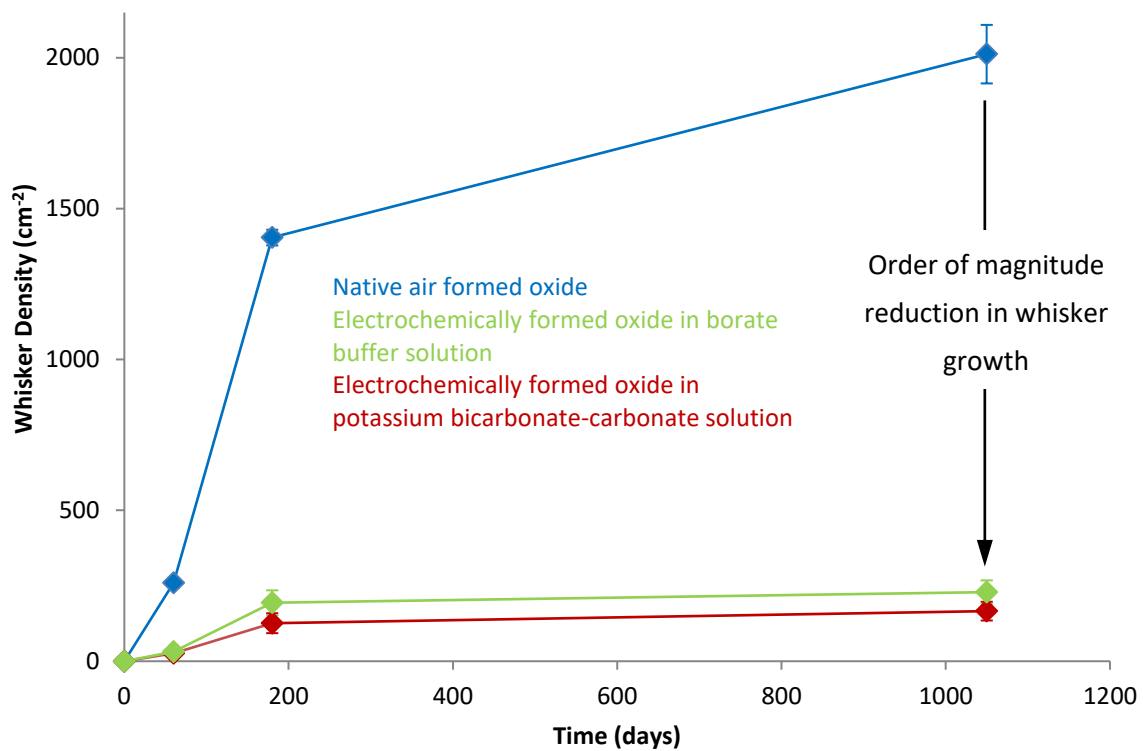


Figure 4.32 A graph showing the effect of electrochemical oxidation on 2 μm thick Sn-Cu electrodeposits on copper in two different electrolytes has on whisker growth after ~3 years of room temperature storage. With the error bars representing the standard deviation between samples

To further understand the mechanism by which whisker mitigation is accomplished for the electrochemically oxidised samples, FIB-SEM analysis was carried on Sn-Cu electrodeposits on Cu after storage at room temperature for ~24 months.

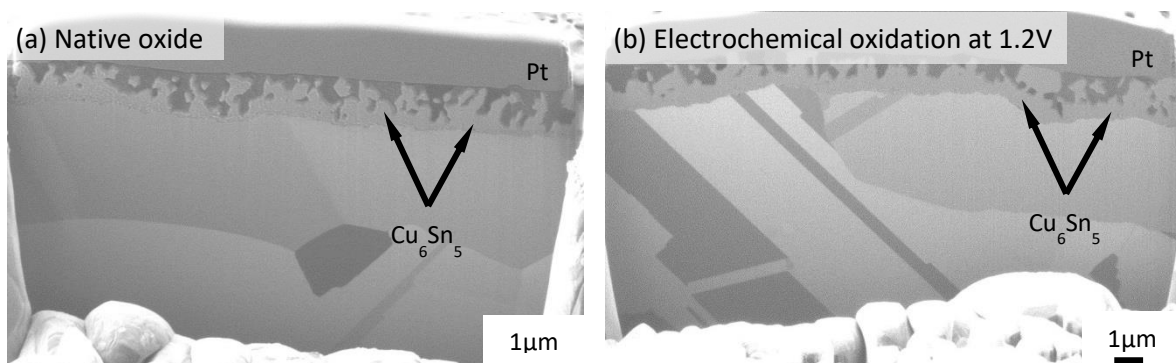


Figure 4.33 Ion beam images of FIB cross-sectioned 2 μm Sn-Cu electrodeposits on Cu after ~24 months of storage at room temperature, a) native air-formed oxide and b) oxide formed electrochemically at a potential of 1.2 V vs. SCE in potassium bicarbonate-carbonate solution

Figure 4.33 shows ion beam images of FIB cross-sections obtained from two Sn-Cu on Cu samples after storage at room temperature for 24 months; the first was left to develop a native oxide (figure 4.33a) and the second was electrochemically oxidised at 1.2 V vs. SCE in potassium bicarbonate-carbonate solution (figure 4.33b). It can be seen that extensive intermetallic formation has occurred in both samples, i.e. the presence of the electrochemical oxide has had no observable effect on intermetallic growth, which is considered to be the primary driving force for whisker growth in these samples^{7,9,32}. This suggests that the reduced whisker growth observed for the electrochemically oxidised Sn-Cu deposits on copper results from the thicker electrochemical oxide (as demonstrated in sections 4.1 and 4.2) providing an enhanced physical barrier to the growth of whiskers rather than a reduction in the driving force for whisker growth.

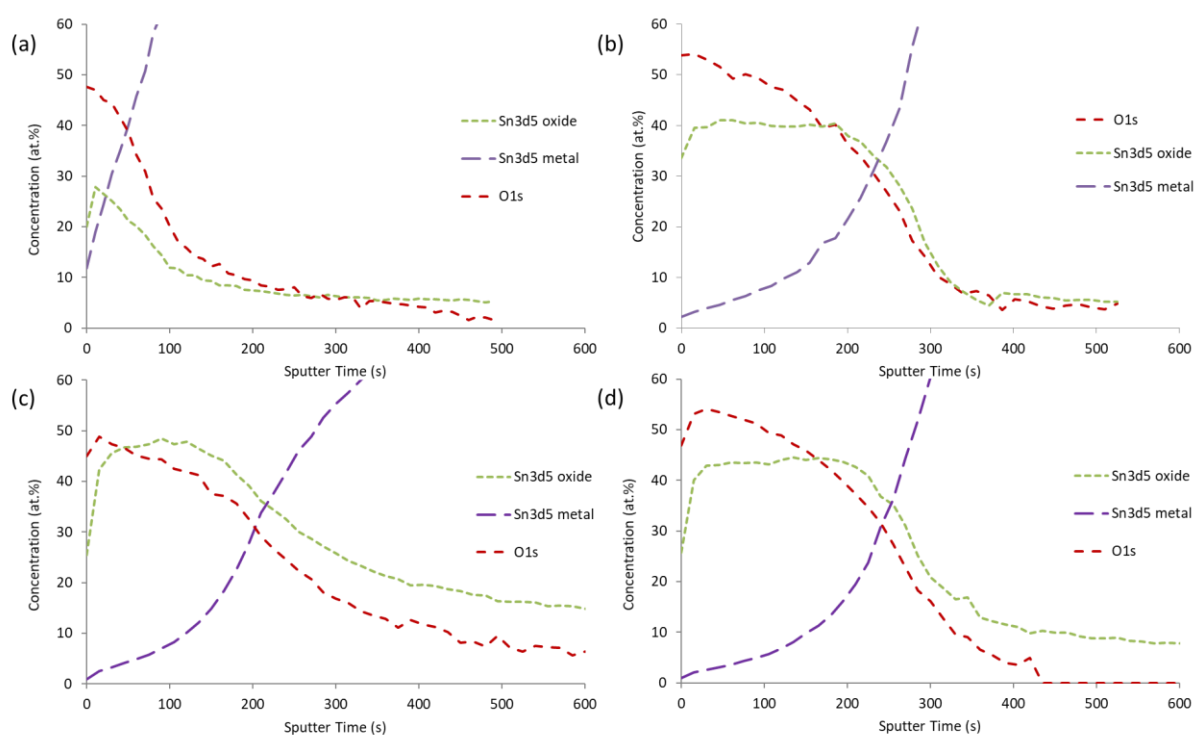


Figure 4.34 XPS depth profiles for Sn-Cu electrodeposits on Cu: a) 1 day old native oxide, b) 1 day old oxide formed electrochemically at a potential of 1.2 V vs. SCE in potassium bicarbonate-carbonate solution, c) native oxide after ~24 months storage, and d) oxide formed electrochemically at a potential of 1.2 V vs. SCE in potassium bicarbonate-carbonate solution after ~24 months storage (the C1s profile has been removed)

The oxide films on the electrodeposited surfaces were also analysed after ~24 months of room temperature storage, to observe how they might have changed with time. XPS depth profiles obtained from the surface of these samples are shown in figure 4.34, together with a native air-formed oxide

and an electrochemically formed oxide analysed within 24 hrs of electrodeposition. After storage at room temperature for ~24 months, the Sn oxide thickness has greatly increased for the sample left to develop the native oxide and is approaching the thickness of the 24 month old electrochemically oxidised sample. The more gradual reduction in oxygen content with depth for the sample with the native oxide after ~24 months storage (figure 4.34b) indicates that significant inward diffusion of oxygen into the electrodeposit has occurred. In comparison, the oxygen content drops off more rapidly for the electrochemically oxidised sample. This suggests that the electrochemical oxide film may act as a diffusion barrier to prevent the inward movement of oxygen into the electrodeposit.

Comparing the depth profiles in figure 4.34, the thickness of the electrochemically formed oxide after ~24 months is similar to that measured for equivalent samples analysed within 24 h of electrochemical oxidation. However, the thickness of the native air-formed oxide after ~24 months is comparable to the thickness of the electrochemically formed oxide. The increase in oxide thickness with the time observed for the untreated samples may influence the propensity to grow whiskers, but will depend on many factors such as composition, film density and uniformity, generation of stresses, incubation time, etc. How whisker density and oxide film changes will be discussed in section 4.5.

4.4.6.2 Tin Electrodeposits on Brass

The long-term effect of electrochemical oxidation on whisker growth was evaluated for 2 μm pure Sn deposits on brass oxidised in borate buffer solution at potentials of 1.2 V, 1.6 V and 2.0 V vs. SCE. Table 4.3 shows the measured whisker densities for pure Sn electrodeposits on brass that had been stored at room temperature for ~36 months. Table 4.3 shows that whisker growth was dramatically reduced by each of the electrochemical oxidation treatments. Furthermore, as the applied oxidation potential was increased, the whisker density was further decreased. The slight reduction in whisker growth at the higher oxidation potentials can be attributed to the increased oxide film thickness that was achieved by electrochemical oxidation at the higher potentials²¹, which was also shown in figure 4.18. Table 4.3 also shows that the number of frames (out of 60) where no whiskers were observed was

considerably higher for the electrochemically oxidised samples and increased slightly with increasing oxidation potential. The large number of frames with no whiskers present gives rise to the high standard deviation for the measured whisker density, for the electrochemically oxidised samples.

Table 4.3 Whisker densities for electrochemically oxidised 2 μm Sn electrodeposits on brass after ~ 36 months of storage at room temperature

Oxidation potential V vs. SCE	Average number of whiskers per cm^2	Number of frames with no whiskers (out of 60)
Native	1489 \pm 681	0
1.2 V	9 \pm 21	50
1.6 V	7 \pm 18	51
2.0 V	5 \pm 16	54

To determine the whisker mitigation mechanism for pure Sn electrodeposits on brass, FIB-SEM analysis was carried out on oxide covered Sn electrodeposits on brass after storage at room temperature for ~ 30 months.

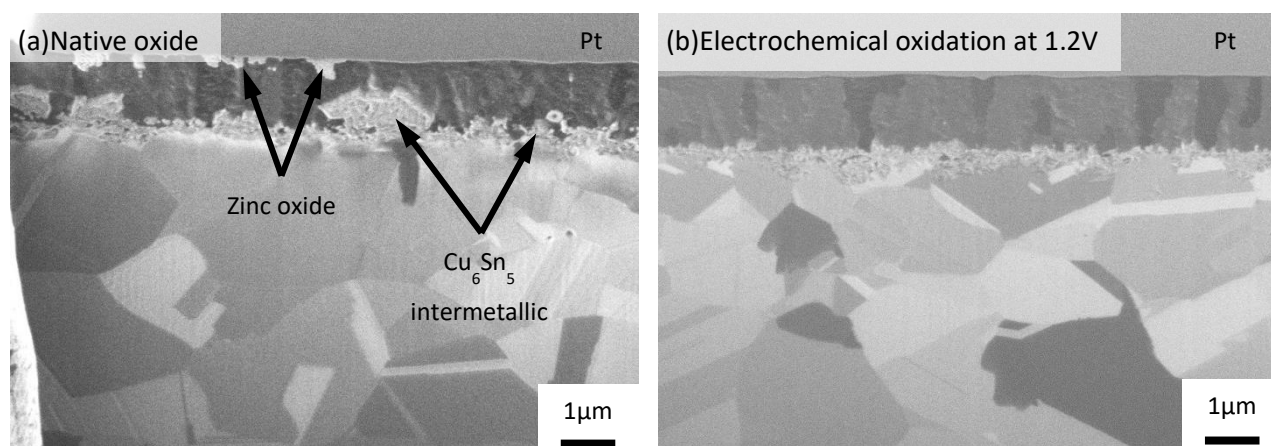


Figure 4.35 Ion beam images of FIB cross-sectioned 2 μm Sn electrodeposits on brass after ~ 30 months of storage at room temperature, a) native air-formed oxide and b) oxide formed electrochemically at a potential of 1.2 V vs. SCE in borate buffer

Figure 4.35 shows ion beam images of FIB cross-sections of the two electroplated Sn on brass samples, with the first left to develop a native oxide (figure 4.35a) and the second with an electrochemical oxide formed at 1.2 V vs. SCE in the borate buffer (figure 4.35b). Figure 4.35a shows both zinc oxide formation, at the deposit surface ³⁹, and Cu_6Sn_5 intermetallic formation at the Sn-brass interface.

Ashworth *et al*³⁹ reported that zinc diffusion occurred from the brass substrate, through the electrodeposit, to the deposit surface where it formed zinc oxide. Stuttle *et al*³⁴ reported that copper-tin IMCs (Cu_6Sn_5) would form at the interface between the electrodeposit and the substrate. Therefore, it can be assumed that the areas pointed out in figure 4.35a are zinc oxide and Cu_6Sn_5 . Both zinc oxide and Cu_6Sn_5 IMC are likely to cause whisker growth^{7,9,21,32,39}, by generating internal stresses within the electrodeposited coating. In comparison figure 4.33b suggests that no zinc oxide formation has occurred at the surface of the electrochemically oxidised electrodeposit and only limited intermetallic formation has occurred at the Sn-Cu interface even after ~30 months of storage. The intermetallic formation in the sample with the electrochemically generated oxide seems to be more evenly distributed and without the large areas seen in the sample with the native oxide.

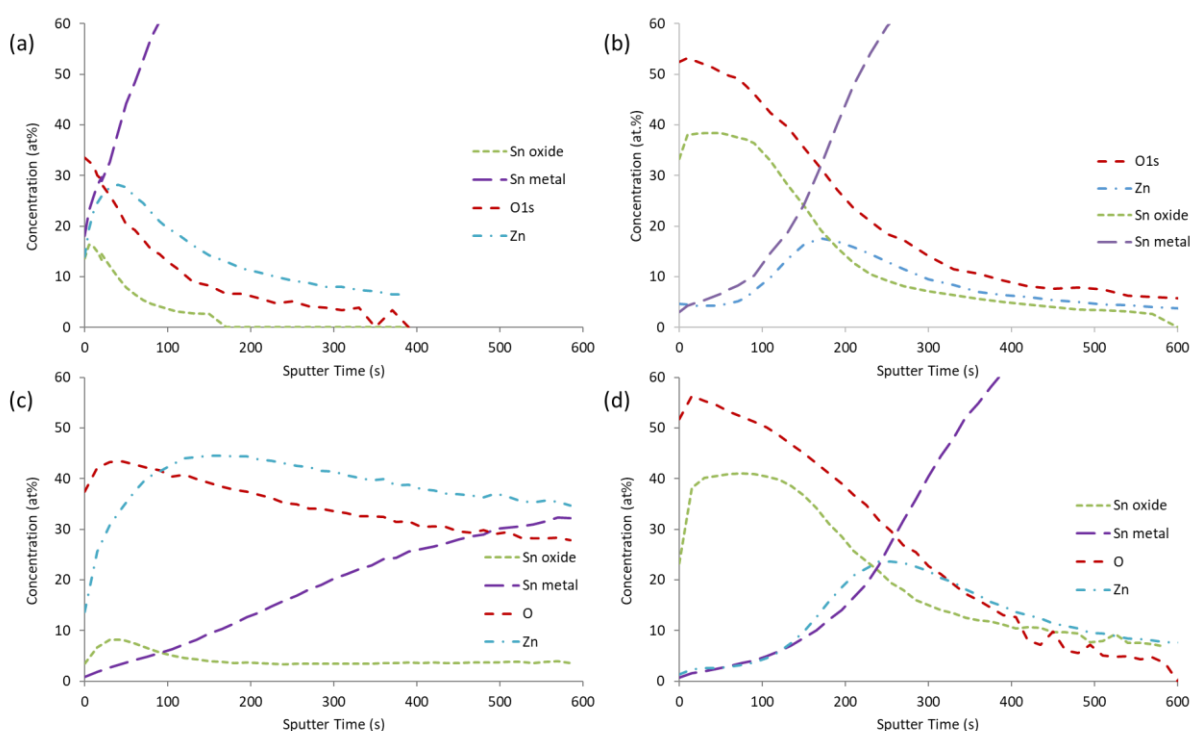


Figure 4.36 XPS depth profiles for 2 μm Sn electrodeposits on brass: a) 1 day old native oxide, b) 1 day old oxide formed electrochemically at a potential of 1.2 V vs. SCE in borate buffer solution, c) native oxide after ~30 months storage at room temperature, and d) oxide formed electrochemically at a potential of 1.2 V vs. SCE in borate buffer after ~30 months storage (the C1s profile has been removed)

XPS depth profiles obtained from pure electroplate Sn on brass are shown in figure 4.36. Comparison of the samples left to develop native oxides after 1 day (figure 4.36a) and ~30 months (figure 4.36b) shows that the concentrations of zinc and oxygen present at the deposit surface have greatly

increased over 30 months, which has led to the extensive formation of zinc oxide at the surface. By comparison, zinc diffusion to the surface of the electrochemically oxidised deposit has been prevented by the presence of the thicker Sn oxide film, which was produced shortly after the deposition of the Sn²¹. Since high zinc concentrations are built up in the Sn electrodeposit beneath the Sn oxide, but FIB analysis suggests that no zinc oxide is present within the electrodeposited coating, it may be inferred that the electrochemically formed Sn oxide is preventing the inward diffusion of oxygen atoms into the electrodeposit and the diffusion of zinc atoms to the oxide surface, thus suppressing Zn oxide formation.

These results demonstrate that the electrochemically formed oxide acts as a diffusion barrier and prevents the formation of zinc oxide at the electrodeposit surface, which reduces the development of internal stresses. The effect of the electrochemical oxidation treatment on the development of the Cu₆Sn₅ intermetallic is, perhaps, more surprising, since it was not expected that a difference in oxide formation mechanism would have an influence on the Cu₆Sn₅ intermetallic growth, therefore being able to act as both a diffusion barrier and a physical barrier to mitigate whisker growth.

4.5 Study of Whisker Growth and Oxide Film Thickness Over Time

Whisker growth from 2 µm tin-copper deposits on copper has been evaluated over a period of ~220 days. Three randomly selected samples (from each batch of 12) were analysed using optical microscopy at each time interval and the average whisker density calculated for both the electrochemically oxidised (at a potential of 2 V vs. Ag/AgCl and a total charge passed of 60 mC cm⁻²) and untreated groups of samples. Figure 4.37 shows that, for both sets of samples, the whisker density increases progressively with time, however, the presence of the electrochemically formed oxide significantly reduces the rate at which whiskers form compared with untreated samples that were left to develop a native air-formed oxide.

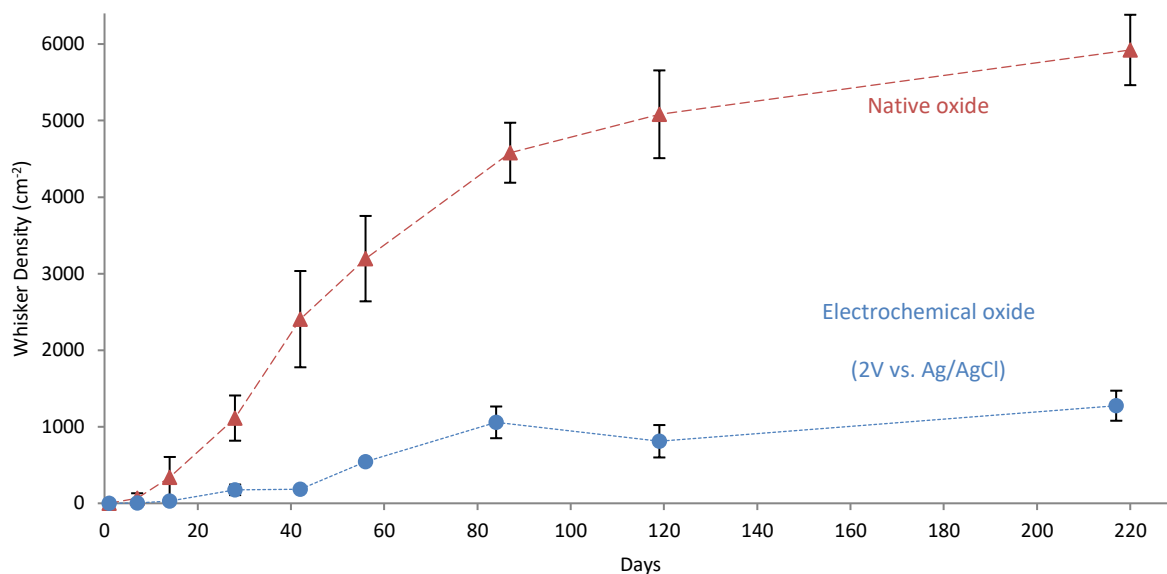


Figure 4.37 Data comparing the evolution of whisker density with room temperature storage time for electroplated Sn-Cu samples left untreated with those electrochemically oxidised at 2 V vs. Ag/AgCl. With the error bars representing the standard deviation between samples

Figure 4.37 shows that whisker growth was observed on the untreated samples after only 7 days and rapidly increased between 14 and 84 days of storage; after which the whisker formation rate reduced. Although, the rate of whisker formation may have reduced prior to this time because whiskers may have already been present, however, they may have been too small to observe at the time of identification, therefore only observing them once they had become sufficient in size to be view. In comparison, the electrochemically oxidised samples showed an increased incubation period prior to the onset of whisker growth whereby the first whisker were observed at, with no significant increase in whisker density until the analysis after ~56 days storage. For both sets of samples there was a reduced rate of whisker initiation after ~84 days. For the untreated samples the majority of whiskers were formed between ~24-84 days and for the electrochemically oxidised the samples the majority of whisker were formed between ~42-84 days.

The data shows that the whisker density for the electrochemically oxidised samples reduces after 120 days compared with the analysis at 84 days. This would have been because at each time interval 3 random samples were chosen from the batch of 12 samples, therefore it was most likely different

samples were analysed. This also shows that there is a significant variation in whisker densities between samples.

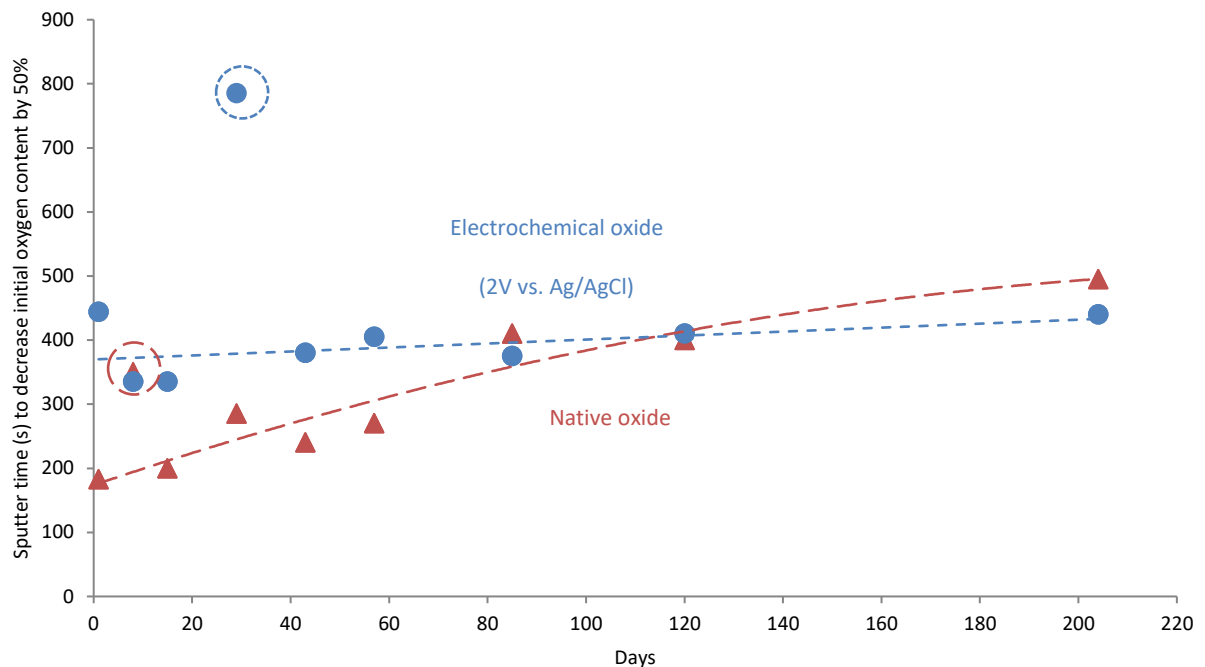


Figure 4.38 Data comparing the evolution of oxide thickness, measured using XPS, with room temperature storage time for electroplated Sn-Cu samples left untreated with those electrochemically oxidised at 2 V vs. Ag/AgCl. Outliers are circled and not included in the trendlines

Figure 4.38 shows how the oxide thickness, for both the native air-formed oxide and the electrochemically formed oxide, changes with time. The two circled points in the figure (8 days for the native air-formed oxide and 29 days for the electrochemically formed oxide) have been omitted to calculate the line of best fit; this is because they are considered to be anomalies due to lying significantly outside of the general trend of results. These anomalies may have occurred due to sample-sample variations in oxide formation or human error during the processing stages. The data in figure 4.38 shows that the thickness of the oxide on the untreated samples steadily increases over time and becomes similar in thickness to that of the electrochemically oxidised samples after ~84 days of storage. Figure 4.38 also shows that the thickness of the oxide on the electrochemically oxidised samples remains relatively consistent over time with very little change over a period of 204 days. The increase in oxide thickness for the untreated samples may contribute to the reduced rate of whisker initiation and growth observed after ~84 days. However, the reduced rate of whisker growth may also

be due to a reduced rate of intermetallic compound (IMC) formation, which is a known driving force for whisker growth due to increased compressive stresses in the coating^{2,33,41}. Stuttle *et al*³⁴ showed that after 1 day, IMC growth was observed for 5 μm electroplated pure Sn on Cu, and after 55 days almost the entire copper surface was covered in IMC growth. This suggests that significant IMC growth will have occurred within the first 84 days, which may potentially result in a reduced driving force for whisker growth beyond this point; however, the IMCs may continue to grow along the grain boundaries within the tin-copper coating. The coating used in this paper was a Sn-Cu alloy, which may promote a more rapid formation of IMC due to the presence of copper within the coating itself. The increased incubation period prior to the onset of whisker growth for the electrochemically oxidised samples may be attributed to the increased thickness of the oxide film, compared with the untreated samples.

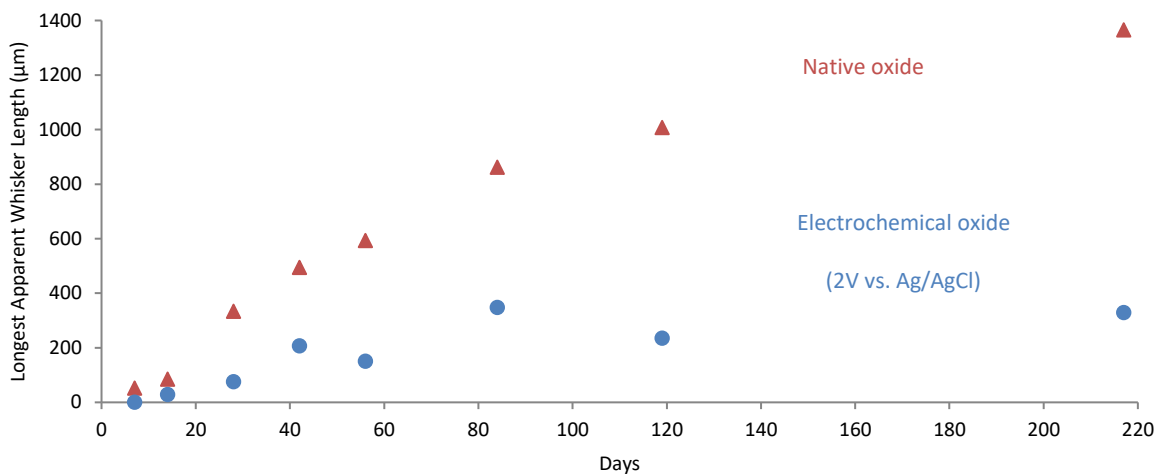


Figure 4.39 Data showing how the longest apparent whisker length changes with room temperature storage time for both untreated and electrochemically oxidised (2 V vs. Ag/AgCl, 60 mC cm^{-2}) electroplated Sn-Cu deposits on Cu

For each frame used to determine whisker density, the longest apparent length of whisker was also measured at each time interval and is plotted in figure 4.39. For the untreated samples, the results indicate that the largest whisker length increases gradually over the 220 days of storage but that the rate at which the whiskers grow progressively reduces with time. Compared with the untreated samples, the length of the longest whisker is significantly reduced for the electrochemically oxidised samples throughout the period analysed, with little apparent increase in whisker length between ~80

and ~220 days, i.e. the electrochemical oxidation treatment not only reduces whisker density but also significantly reduces the maximum length of the whiskers that are present.

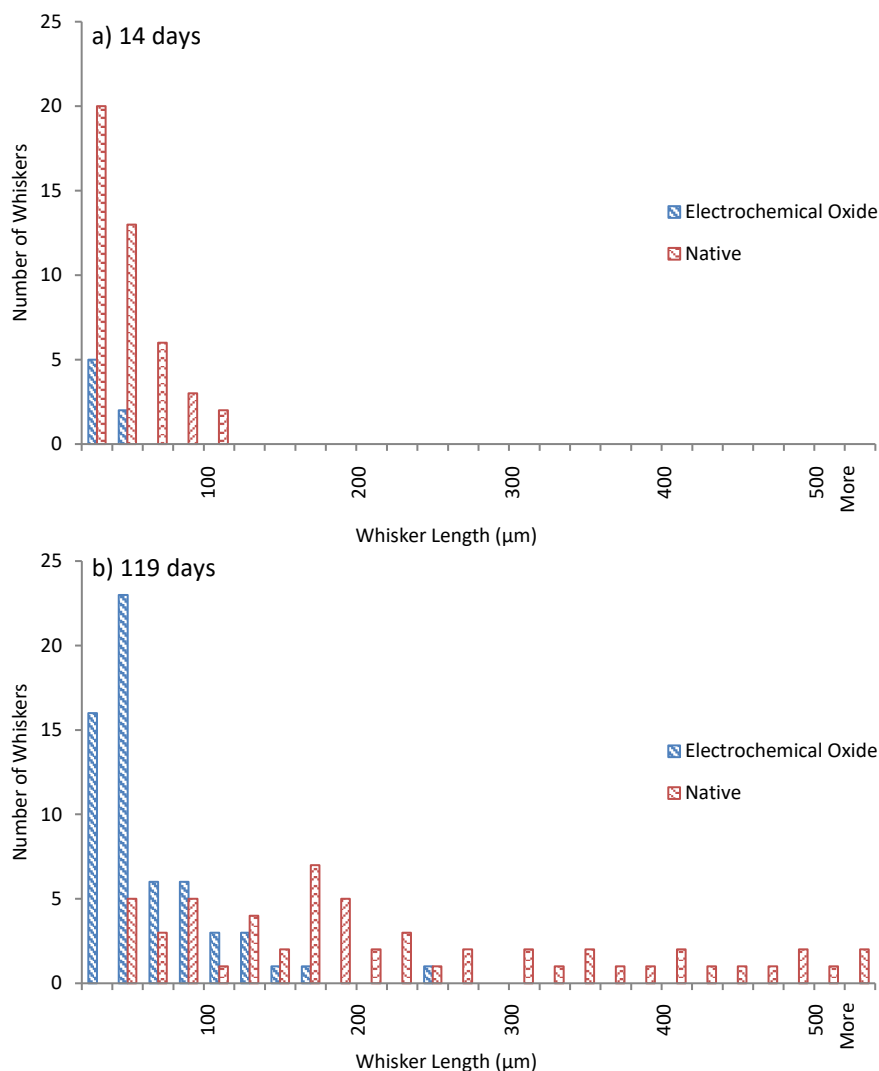


Figure 4.40 Data showing whisker distributions on both untreated (orange) and electrochemically oxidised samples (blue) stored at room temperature after (a) 14 days and (b) 119 days of storage for Sn-Cu deposits on Cu

Figure 4.40 shows the change in the distribution of the longest whisker per frame for both electrochemically oxidised (2 V vs. Ag/AgCl , 60 mC cm^{-2}) and untreated samples, between 14 days and 119 days of room temperature storage. After 14 days (figure 4.40a), all the measured whiskers were less than $100\text{ }\mu\text{m}$ in length for both the untreated samples and the electrochemically oxidised samples. Figure 4.40a also shows that not only were far fewer whiskers present on the electrochemically oxidised samples compared with the untreated samples, but they were all less than $40\text{ }\mu\text{m}$ in length. After 119 days (figure 4.40b), the whisker distribution for the untreated samples has shifted to much

greater lengths and each frame analysed contained a whisker greater than 20 μm in length. The whisker length distribution for the untreated samples shows that the majority of the longest whiskers were greater than 100 μm in length after 119 days, whereas after 14 days, no whiskers were greater than 100 μm in length. In comparison, for the electrochemically oxidised samples, the majority of the longest whiskers were still less than 40 μm in length, although the maximum whisker length had increased compared with data after 14 days of room temperature storage. Figure 4.40b shows that the whisker lengths on the electrochemically oxidised samples were greatly reduced compared with the untreated samples, thereby significantly reducing the risk of the whiskers bridging a gap between components or connections and causing a short circuit. The reduction in the number of long filament whiskers may, at least in part, be due to the increased incubation period for the electrochemically oxidised samples.

Additionally, the results may suggest that the presence of the electrochemically formed oxide also influences the rate at which the whiskers grow once the whisker has penetrated the oxide layer. It might be expected that when a whisker penetrates through the oxide film it would have a similar rate of growth as the untreated samples; this is because if the thicker electrochemically formed oxide was purely acting as a physical barrier, then once the barrier is overcome the whisker would be expected to have the same growth rate as that from a sample with a thinner native air-formed oxide, assuming the same driving force for growth exists. However, this is not the case (figure 4.39), therefore, the electrochemical oxide also appears to be having an influence on the driving force for whisker growth as well as inhibiting whisker initiation. It was shown previously that for Sn-Cu deposits on Cu, IMC growth didn't appear to be significantly influenced by the presence of the electrochemical oxide²². In the absence of an oxide film, the surface of the tin serves as a source for vacancies to facilitate tin diffusion through the coating, to support the growth of whiskers¹⁵². However, the presence of a sufficiently thick oxide may impede diffusion of tin atoms by reducing the number of available surface vacancies⁹, therefore slowing the rate at which whiskers may grow. This may suggest that whisker growth on the electrochemically oxidised samples is diffusion limited and because the native air-

formed oxide film is much thinner than the electrochemically formed oxide, the oxide film may not reduce the number of available surface vacancies for tin diffusion to occur; therefore, whiskers will grow faster if only a thin native air-formed oxide is present.

4.6 Further Discussion of Whisker Growth Studies

The studies discussed in the previous sections show that an electrochemical oxidation at a potential of 2.0 V vs. SCE, with a charge passed of 60 mC cm^{-2} , provides the most effective whisker mitigation. Compared with a native air-formed oxide, whisker density was reduced by $\sim 92 \%$ (after ~ 9 months as shown in figure 4.30). The work discussed in sections 4.4.1 and 4.4.3, showed that when increasing the electrochemical oxidation potential past 1.2 V vs. SCE and increasing the amount of charge passed there was only a small further reduction in whisker growth. This may suggest that any further increase in the electrochemical oxidation potential, past 2.0 V vs. Ag/AgCl and any further increase in the total charge passed, past 60 mC cm^{-2} , may only result in a minor reduction in whisker growth.

The reduction in whisker density on the electrochemically oxidised samples can be attributed to the presence of a thicker oxide film compared with that developed on samples left to form a native air-formed oxide. This increase in thickness will also reduce the risk of cracks as suggested by Tu^{1,8-10}, which are known nucleation sites for whisker growth. This relates to the observations made by Su *et al*⁴², who showed that having an increased number of 'weak points' would increase whisker density. The work discussed in section 4.5 suggests that the electrochemically formed oxide also significantly reduces the maximum and average whisker length, which would reduce the risk of a whisker bridging a gap between electronic components and causing a short circuit.

The electrochemically formed oxides, produced at -0.4 V and -0.5 V vs. SCE, that increased whisker growth (section 4.4.2) may correlate with Tu's cracked oxide theory^{1,8-10}, where having a cracked oxide would cause whiskers to grow; therefore having a weaker oxide with more weak points for cracks to occur will increase whisker density, regardless of the thickness. The oxide films produced at

these potentials, for a charge passed of 30 mC cm^{-2} , may have reduced physical properties, therefore being more prone to cracking than the other oxide coatings. This was also shown by Su *et al*⁴² and this increase in the number of weak points in the electrochemically formed oxide layer may be the reason for an increased whisker density.

5 Investigation of Conversion Coatings as a Whisker Mitigation Strategy

Conversion coatings were applied to electrodeposited pure Sn and Sn-Cu coatings in order to produce oxide coatings that were thicker than those achieved using electrochemical oxidation. Two different conversion coating systems were investigated: one produced from a sodium molybdate based solution and one from a sodium tungstate based solution. Studies were conducted to investigate both the composition and thickness of the conversion coating and their ability to mitigate whisker growth. This chapter presents and discusses the results obtained from these studies.

5.1 Conversion Coating Parameter Studies

The influence of conversion coating formation parameters on composition, thickness and structure was investigated for each conversion coating.

5.1.1 Molybdate Conversion Coating

Key parameters were varied to determine their influence on the conversion coating. These parameters were: immersion time; the pH of the bath; and the effect of using electrolytic techniques. Initially, the coating was produced using an immersion technique with the sample immersed for a specified time. To investigate the influence of electrolytic methods, both potentiostatic and reversed pulsed current techniques were used.

Reproducibility was also studied by using a fresh batch of solution for each sample compared to processing multiple samples in the same batch of solution.

5.1.1.1 *Studying the Reproducibility of Forming a Conversion Coating by Immersion*

This study was carried out to study the reproducibility of conversion coatings produced following immersion in a fresh bath as well as those produced from a solution used to process multiple samples. Figure 5.1 shows x-ray photoelectron spectroscopy (XPS) molybdenum depth profiles for samples

conversion coated in a fresh batch of solution each time, whilst figure 5.2 shows the XPS molybdenum depth profiles for conversion coated sample in the same solution one after the other. The same parent batch of solution was used for each trial. The pH of the solution was 2.25 and the immersion time for each sample was 3 min. It was noted during this trial that the first and second samples were visually the same but were visually different from the rest of the samples, therefore only sample 1 was analysed using XPS.

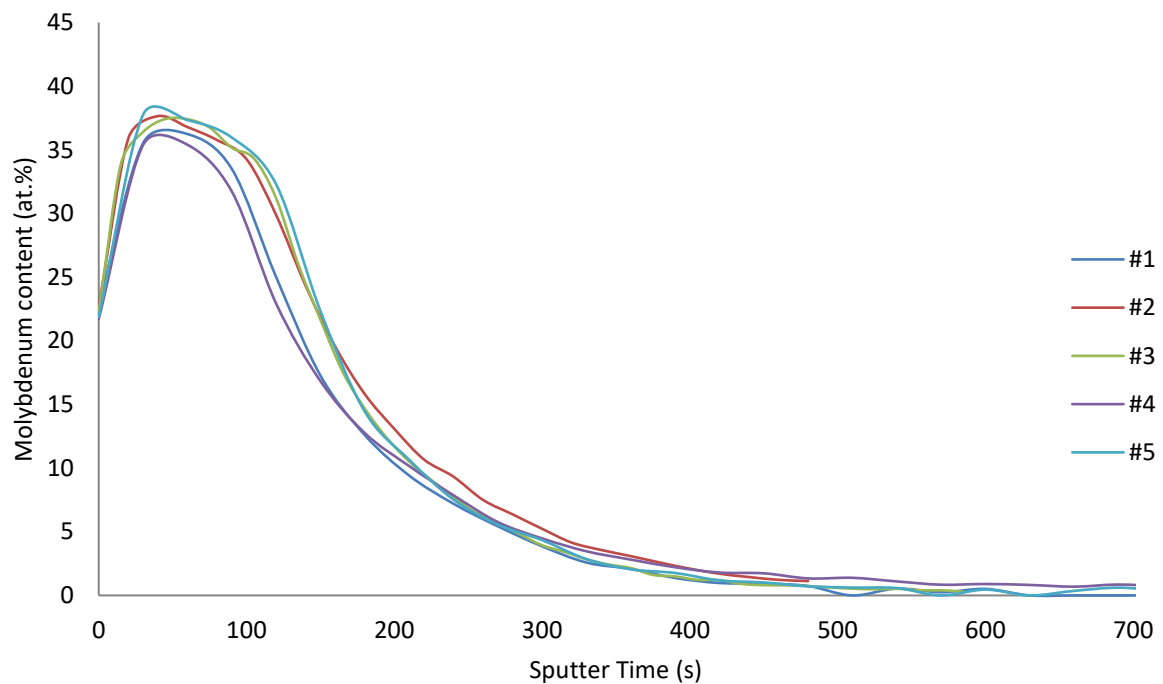


Figure 5.1 XPS depth profiles showing the molybdenum content of immersion molybdate conversion coatings on pure electrodeposited tin using a fresh batch of solution for each sample with the numbers representing the sample number, which also corresponds to the order the samples were produced.

The XPS depth profiles in figure 5.1 show that samples produced using a fresh batch of solution (each time) all had a similar coating thickness, this showed that there was consistency in producing the conversion coatings. In comparison, the molybdenum depth profiles in figure 5.2 indicate that for samples processed (one-after-another) in the same batch of solution, there is a difference between the first two samples processed and those that followed, i.e. the thickness of the first two samples is less than those from sample 3 onwards. This was assumed because, visually, samples 1 and 2 looked the same and were visually different from the subsequent samples, which may suggest that samples 1 and 2 were of the same thickness but different from the subsequent samples. This suggests that the

solution needs to process two 2 cm x 2 cm samples to produce consistent (and thicker) conversion coatings. This may be because the solution needs to gain a state of equilibrium before thicker coatings can be consistently produced. It can also be seen that the coating thickness of sample 1 in figure 5.2 is comparable to those shown in figure 5.1.

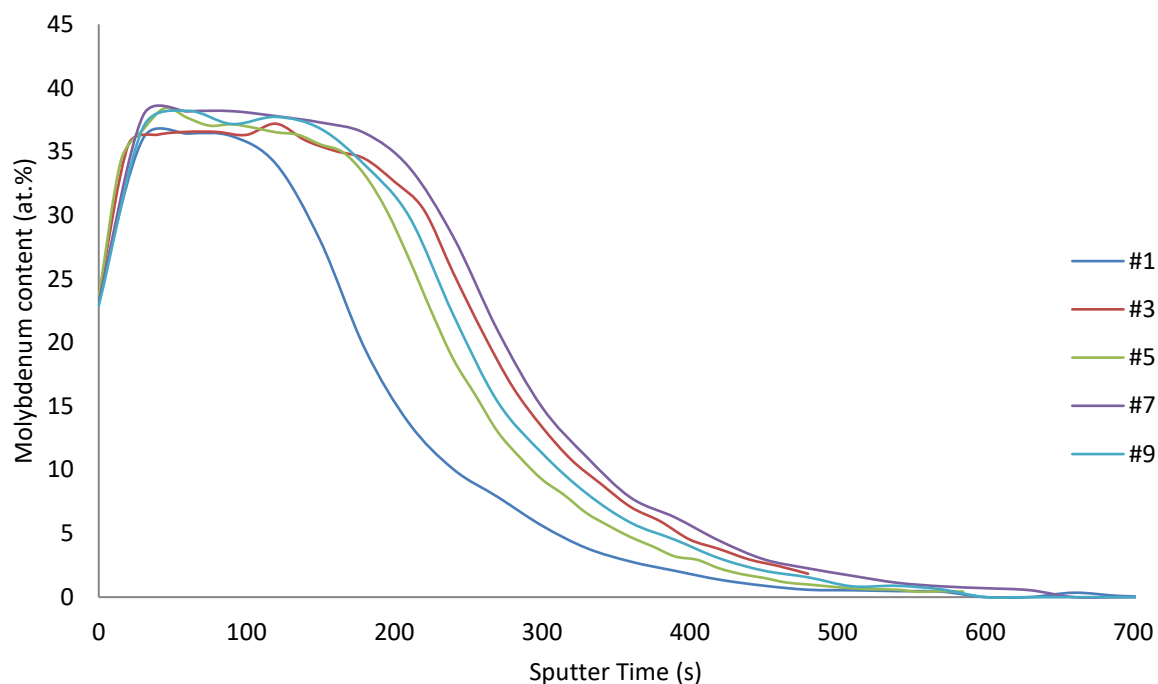


Figure 5.2 XPS depth profiles showing molybdenum content of immersion molybdate conversion coatings on pure electrodeposited tin using the same batch of solution for all samples with the numbers representing the sample number, which also corresponds to the order the samples were produced.

5.1.1.2 Effect of Immersion Time on the Conversion Coating Thickness

The effect of immersion time on the thickness and composition of conversion coatings formed on the electrodeposited tin has been investigated and compared with the electrochemically formed tin oxides. Figure 5.3 shows the x-ray photoelectron spectroscopy (XPS) oxygen depth profiles for the conversion coatings produced at different immersion times, together with the oxygen depth profile of a tin oxide electrochemically formed at 2 V vs. SCE for a charge passed of 60 mC cm^{-2} (refer to section 4 for the electrochemically formed oxides). The XPS depth profiles show that even at the shortest immersion time (1 min) the conversion coating thickness is far greater than that formed by electrochemical oxidation. Figure 5.3 also shows that as immersion time increases, the thickness of the conversion coating also increases.

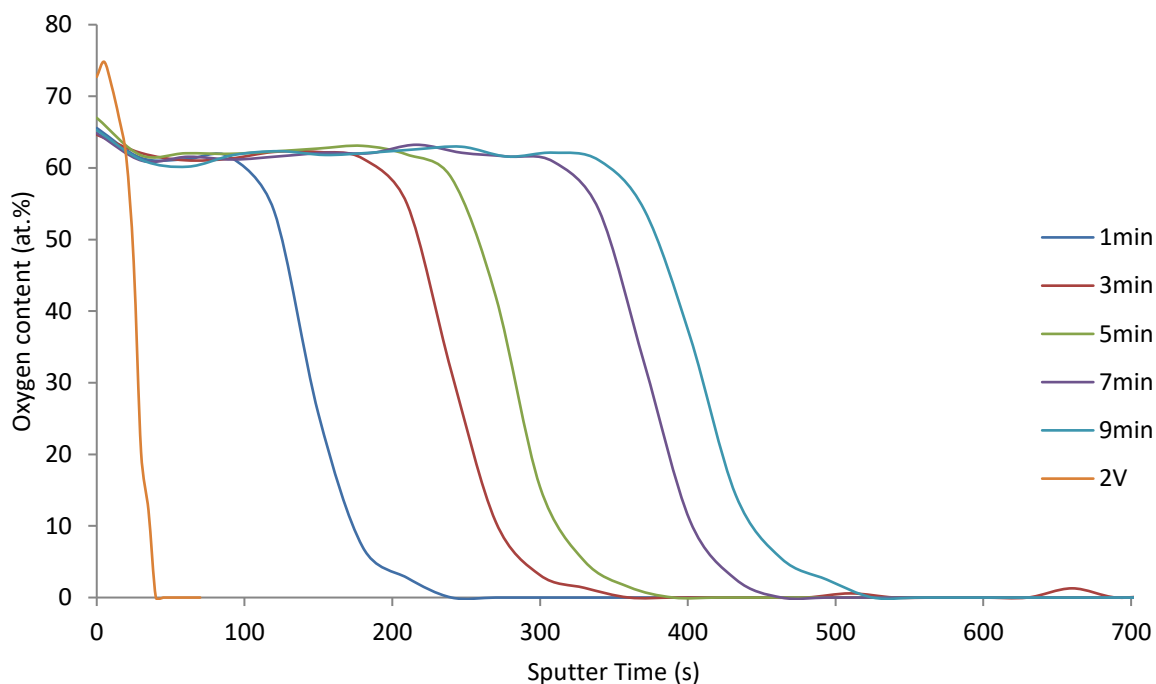


Figure 5.3 XPS depth profiles showing oxygen content of molybdate conversion coating on pure electrodeposited tin for different immersion times. An electrochemical oxide formed at 2 V (60 mC cm^{-2} charge passed) is included for comparison, which is labelled as '2V'.

Table 5.1 shows the sputter time taken for the oxygen content to reduce by 50 %, which is used to compare the relative thickness of the coatings. It can be seen that the thinnest molybdate conversion coating is almost $\sim 5.5x$ thicker than the electrochemically formed oxide produced at 2 V vs. SCE (for a charge passed of 60 mC cm^{-2}) and the thickest molybdate conversion coating is $\sim 15.5x$ thicker than the electrochemically formed oxide. This significant increase in coating thickness, compared with an electrochemically formed oxide, may suggest that even the thinnest molybdate coating could provide enhanced whisker mitigation.

Table 5.1 XPS oxygen depth profile summary showing the sputter time to reach 50 % of the surface oxygen content from data shown in figure 5.3

	2 V vs. SCE	1 min	3 min	5 min	7 min	9 min
Sputter time to 50 % oxygen surface content	26 s	144 s	240 s	280 s	370 s	406 s

5.1.1.3 Effect of Bath pH on the Conversion Coating Thickness

The effect of bath pH on the thickness of the conversion coating formed on the electrodeposited tin has been investigated. Figure 5.4 shows the x-ray photoelectron spectroscopy (XPS) depth profiles for

both molybdenum and tin oxide for the molybdate coated tin samples produced at an immersion time of 5 min using different bath pH. It can be seen in figure 5.4a that there is a clear plateau region for coatings produced at pH 2 and pH 3; however, no plateau region was at for either pH 1 or pH 4. The XPS depth profiles in figure 5.4a show that as the pH of the solution is reduced from pH 4 to pH 2 the thickness of the conversion coating increases. The depth profile for the conversion coating produced at pH 1 shows a reduced molybdenum content at the surface, however, the molybdenum content reduces at a slower rate compared to the other pH levels.

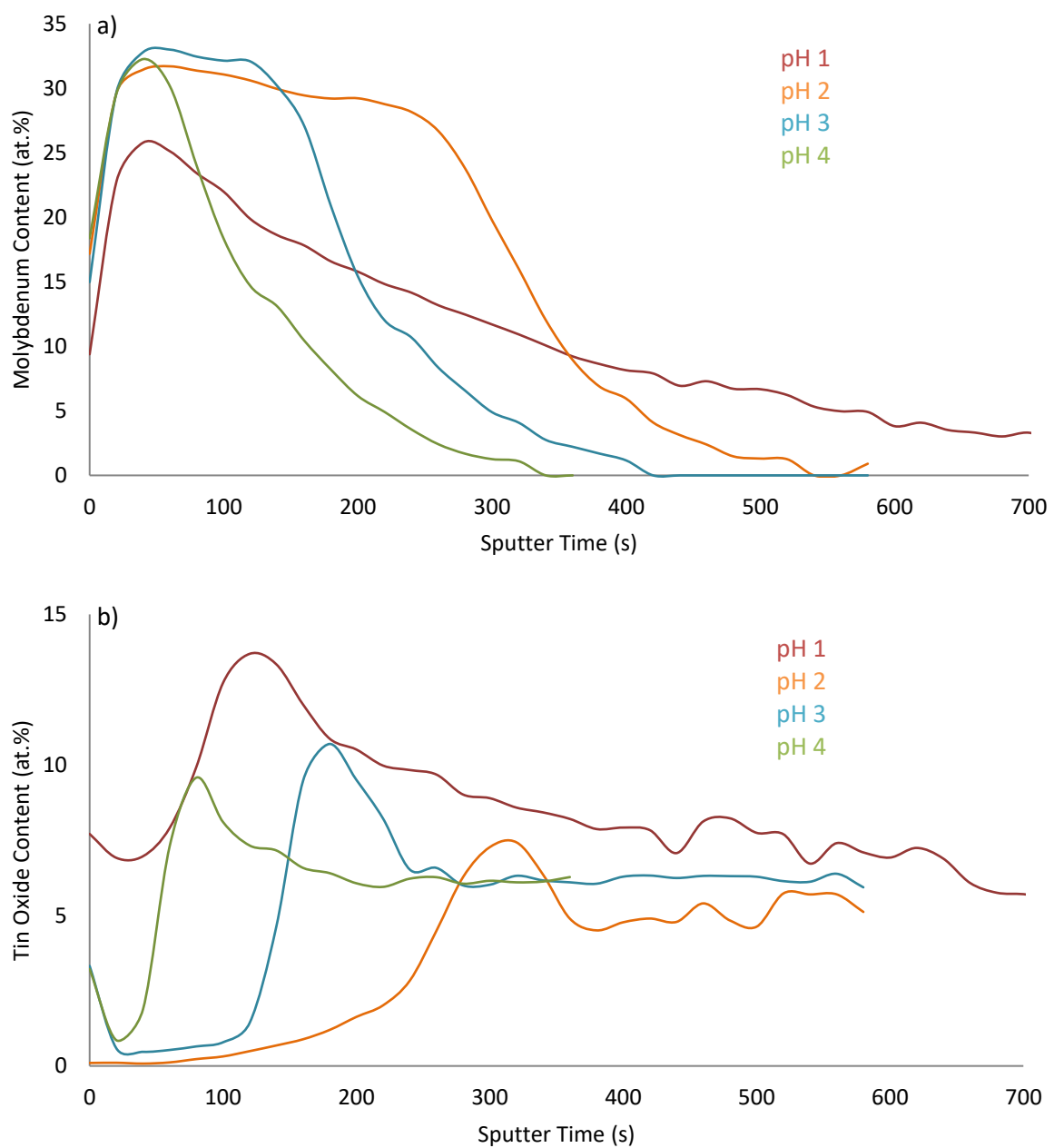


Figure 5.4 XPS depth profiles showing (a) molybdenum content and (b) tin as oxide content of molybdate conversion coated pure electrodeposited tin for different levels of pH for an immersion time of 5 min.

Figure 5.4b shows the XPS depth profiles for the tin oxide concentration for the molybdate conversion coatings produced at an immersion time of 5 min using different levels of bath pH. The tin oxide profiles shown all display a peak at a depth that corresponds approximately to the point where the molybdenum content begins to reduce, which suggests that beneath the molybdate conversion coating there is a tin oxide coating present. Figure 5.4b also suggests that the conversion coating produced at pH 1, may be thicker than that produced at pH 4 but thinner than those produced at pH 2 and pH 3; this is shown by the positioning of the tin oxide peak. However, the pH 1 depth profile shows an increased peak concentration of tin oxide compared with the other pH's and that the molybdenum signal extends to increased sputter times (figure 5.4a). This suggests that although the conversion coating produced at pH 1 has a lower molybdenum content throughout the coating, the conversion coating itself may be thicker and comprised of a mixture of both molybdenum and tin oxides. These results suggest that as the pH is reduced the bath becomes more aggressive, which may cause an increase in tin dissolution and result in the growth of a mixed oxide conversion coating with an increased amount of oxides present.

Figure 5.5 shows depth profiles for the oxygen concentration of molybdate conversion coatings produced at an immersion time of 5 min using different levels of bath pH. It is shown that from pH 4 to pH 2, the thickness in the coating is reduced. However, the coating produced at pH 1 has an oxygen profile that steadily reduces with increased sputter time, rather than having a well-defined plateau region. This may suggest that the conversion coating produced at pH 1 has a different chemical composition to the other conversion coatings.

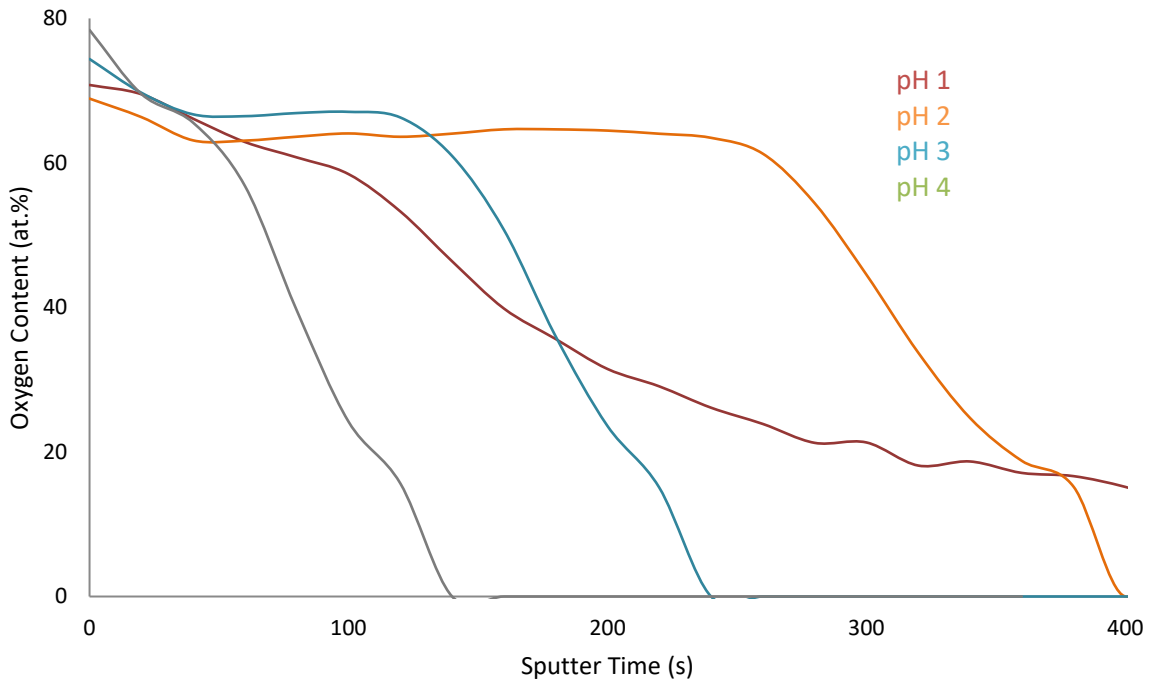


Figure 5.5 XPS depth profiles showing oxygen content of molybdate conversion coated pure electrodeposited tin for different levels of pH for an immersion time of 5 min.

Table 5.2 shows the sputter time taken for the oxygen content to reduce by 50 % along with the sputter time taken to reach the maximum tin oxide content. For the samples produced in baths ranging from pH 2 to pH 4, the sputter time taken for the oxygen content to reduce by 50 % is the same as that taken to reach the point at which the tin oxide is at its maximum content. However, the sputter times aren't comparable for the sample produced in the pH 1 bath; which may be due to the increased amount of mixed oxide being deposited that occurred (shown in figure 5.4).

Table 5.2 XPS oxygen depth profile summary showing the sputter time to reach 50 % of the surface oxygen content from data shown in figure 5.5

	pH 1	pH 2	pH 3	pH 4
Sputter time to 50 % oxygen surface content	181 s	319 s	178 s	80 s
Sputter time to max. tin oxide content	120 s	320 s	180 s	80 s

Analysis of the sputter times taken to reduce the original oxygen content by 50 % (table 5.2) shows that the thickest conversion coating was produced in the pH 2 bath, with the thinnest conversion coating being produced at pH 4. Table 5.2 also shows that the conversion coatings produced in the pH

1 and pH 3 baths have very similar thicknesses, even though figure 5.4a shows that the molybdate content for the pH 1 sample was reduced compared to the other samples. This increased amount of mixed oxide deposition for the conversion coating produced in the pH 1 bath may be due to competing deposition and dissolution reactions. Due to the high acidic level, there may be tin dissolution occurring while the molybdate conversion coating is being deposited.

5.1.1.4 Application of Conversion Coatings Using Electrochemical Techniques

The effect of electrochemical techniques on the thickness of conversion coatings formed on electrodeposited tin has been investigated; both potentiostatic and reverse current pulse techniques were used to form conversion coatings. Coatings produced potentiostatically were at potentials of -0.45 V, -0.6 V and -0.75 V (all vs. Ag/AgCl). The conversion coatings that were produced using a reverse current pulse technique used current densities ranging from $\pm 2.5 \text{ mA cm}^{-2}$ to $\pm 10 \text{ mA cm}^{-2}$ for between 30 to 120 square waves (the parameters are summarised in table 3.1 in section 3.3.2.1). The same parent solution was used for all the samples at pH 3.1, i.e. the parent bath was divided into two volumes, one was used for producing conversion coatings potentiostatically and the other was used for producing conversion coatings using a reverse current pulse technique. For each bath two immersion samples were used to 'condition' the solution.

Figure 5.6 and 5.7 shows the x-ray photoelectron spectroscopy (XPS) depth profiles for the electrochemically produced molybdate conversion coatings together with those from a 5 min immersion and electrochemical oxidation at 2 V vs. SCE for a charge passed of 60 mC cm^{-2} . All the conversion coatings are significantly thicker than the electrochemically formed oxide (figure 5.6h and figure 5.7h). For the conversion coatings that were produced potentiostatically, as the potential increased cathodically the thickness of the conversion coating also increased. For the conversion coatings that were produced using a reverse current pulse technique, as the reverse current was increased, the conversion coating thickness was increased; also, increasing the number of square waves increased the conversion coating thickness.

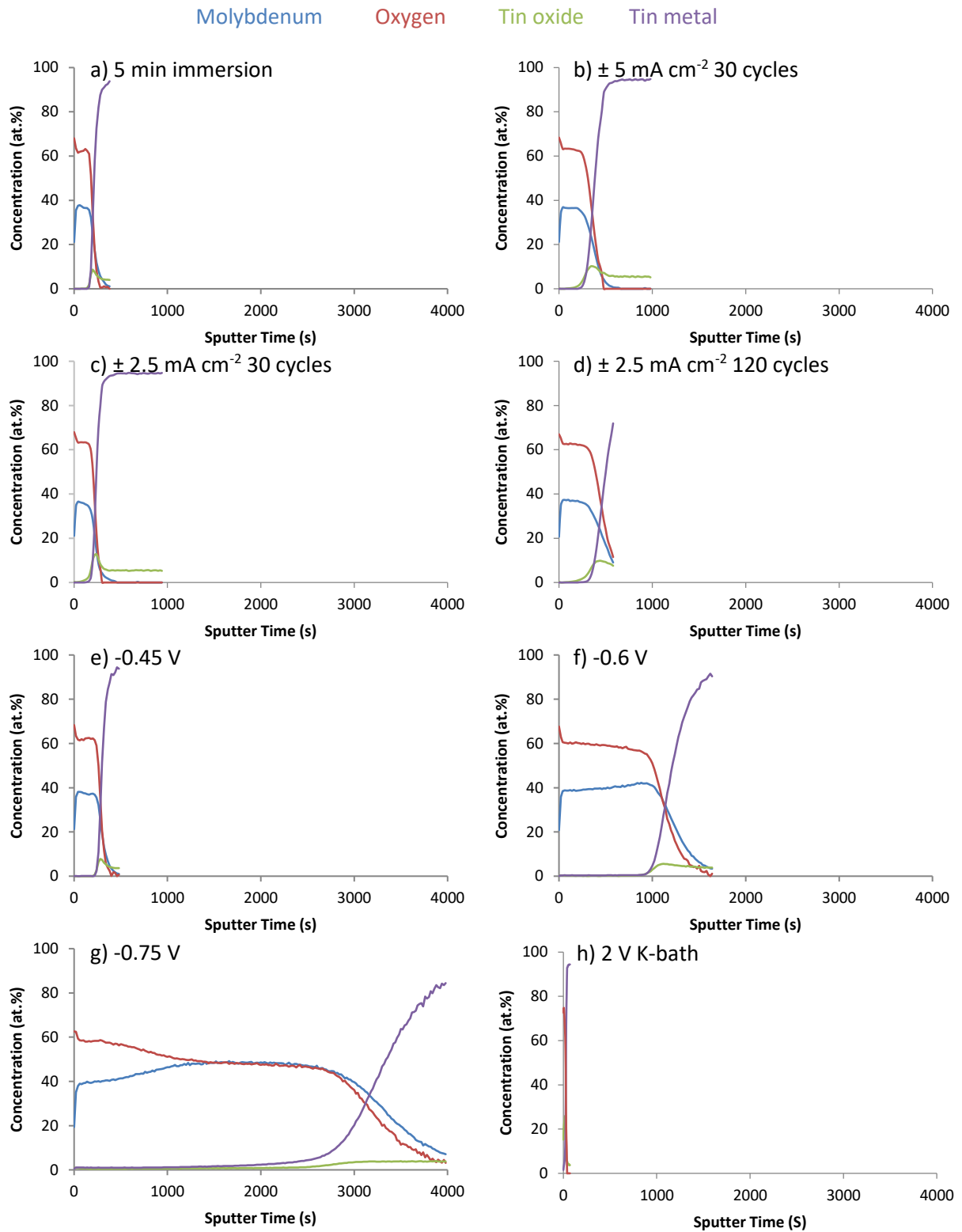


Figure 5.6 XPS depth profiles (without the carbon profile) of molybdate conversion coatings on pure electroplated tin (using the same x-axis scale), produced in a bath at pH 3.1 a) 5 min immersion, b) $\pm 5 \text{ mA cm}^{-2}$ for 30 cycles, c) $\pm 2.5 \text{ mA cm}^{-2}$ for 30 cycles, d) $\pm 2.5 \text{ mA cm}^{-2}$ for 120 cycles, e) -0.45 V vs. Ag/AgCl for 5 min, f) -0.6 V vs. Ag/AgCl for 5 min, g) -0.75 V vs. Ag/AgCl for 5 min, and h) an electrochemically formed oxide produced at 2 V vs. SCE for a charge passed of 60 mC cm^{-2} .

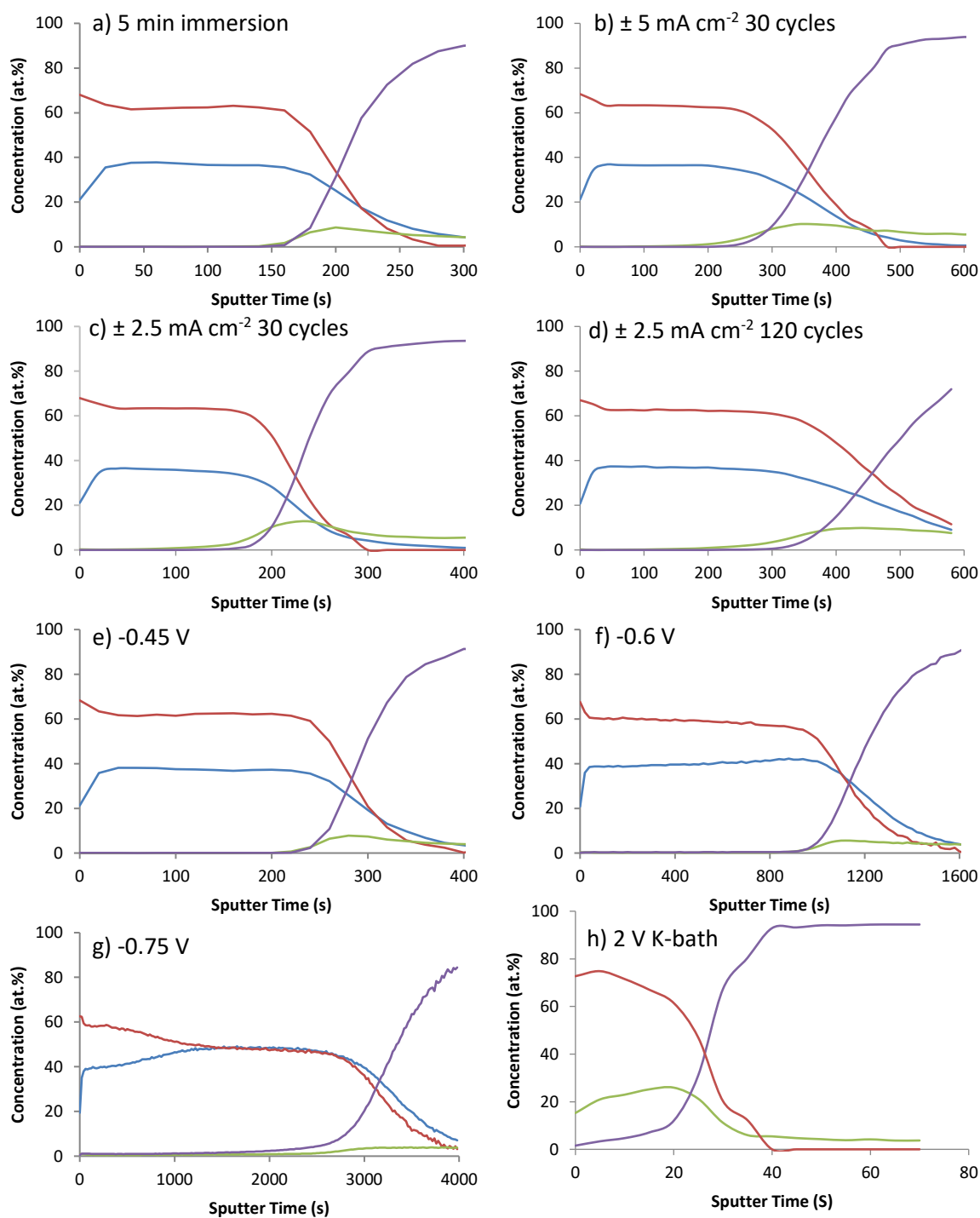


Figure 5.7 XPS depth profiles (without the carbon profile) of molybdate conversion coatings on pure electroplated tin (using different x-axis scales), produced in a bath at pH 3.1 a) 5 min immersion, b) $\pm 5 \text{ mA cm}^{-2}$ for 30 cycles, c) $\pm 2.5 \text{ mA cm}^{-2}$ for 30 cycles, d) $\pm 2.5 \text{ mA cm}^{-2}$ for 120 cycles, e) -0.45 V vs. Ag/AgCl for 5 min, f) -0.6 V vs. Ag/AgCl for 5 min, g) -0.75 V vs. Ag/AgCl for 5 min, and h) an electrochemically formed oxide produced at 2 V vs. SCE for a charge passed of 60 mC cm^{-2} .

The results show that a 5 min immersion technique forms the thinnest conversion coating compared to the electrochemical techniques; the thickest conversion coating was formed by a potentiostatic treatment of -0.75 V vs. Ag/AgCl for 5 min. All of the depth profiles show that the conversion coatings

are comprised of molybdenum and oxygen with a region enriched in tin oxide present at the interface between the conversion coating and the tin metal (as shown in section 4.1.1.2). These results show that using electrochemical techniques only affects the thickness of the resultant conversion coating and not its chemical composition, as shown by the ratios between the oxygen and molybdenum content and the shape of the depth profiles.

The XPS depth profiles in figure 5.7 show that the stoichiometry of the molybdate coatings change between the surface (prior to sputtering) and the rest of the conversion coating. Figure 5.7 f&h show that the stoichiometry of the conversion coatings significantly changes with increasing sputter time through the thickness of coating. To investigate what this change may correspond to in terms of the coating chemistry, the Mo3d peak binding energy was analysed; this was carried out to study how the oxidation state of molybdenum changes with increasing sputter times.

Figure 5.8 shows the XPS depth profile for a conversion coating formed by a 5 min immersion (figure 5.7a) and a potentiostatic treatment of -0.75 V vs. Ag/AgCl for 5 min (figure 5.7c), along with the corresponding graphs showing the Mo3d peak binding energy as a function of sputter time (figure 5.7 b&d). The change in oxidation state is shown in the previous figures, which plot the binding energy of the molybdenum peak, extracted from the 'snapshots' used to produce the depth profile, as a function of sputter time. It can be seen from figure 5.7 that the peak binding energy reduces with increasing sputter times.

For the majority of the samples, the molybdenum peak binding energy decreases significantly from ~232 eV at the surface, prior to sputtering, to ~229 eV in the remainder of the conversion coating which again decreases to ~227.5 eV at the same sputter time at which the tin as oxide content is at its maximum, which may also correspond to the interface between the conversion coating and the tin oxide coating. For all the samples, the molybdenum peak binding energy at the unsputtered surface corresponds to Mo(VI) oxide (MoO_3)¹⁴⁷ and the molybdenum peak binding energy for the remainder of the coating corresponds to Mo(IV) oxide (MoO_2)¹⁴⁷. The molybdenum peak binding energy at the

interface corresponds to metallic Mo¹⁴⁷. Similar changes in oxidation state for molybdenum between the unspattered outer surface and the remainder of the conversion coating has been observed previously^{153–155}.

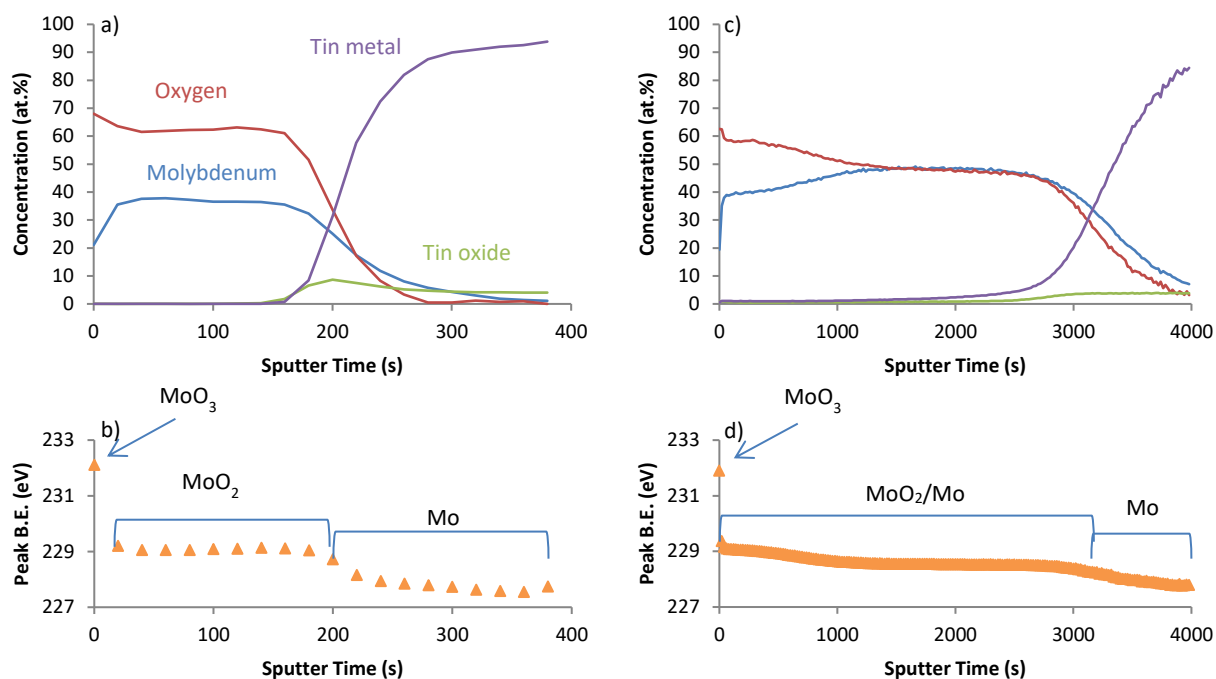


Figure 5.8 XPS depth profiles obtained from molybdate conversion coatings showing the elemental distribution (top) and Mo3d peak binding energy (bottom): (a) & (c) 5 minutes immersion and (b) & (d) produced potentiostatically at -0.75 V vs. Ag/AgCl for 5 minutes. The pH of the conversion coating bath was 3.13.

For the sample immersed for 5 min (figure 5.8a), the oxygen and molybdenum contents for the bulk of the conversion coating (62 at.% and 37 at.% respectively) suggest that the stoichiometry of the coating corresponds, somewhat, close to MoO₂; whilst the outer surface of the conversion coating, prior to sputtering, may correspond close to MoO₃ (68 at.% for oxygen and 21 at.% for molybdenum). Similar results were obtained for each of the electrochemically formed conversion coatings shown in figure 5.7 b-e. The molybdenum peak binding energy at the unspattered outer surface was 232.11 eV, which lies within the reported binding energy range given in the literature for MoO₃ (231.7-233.60 eV)¹⁴⁷, which is consistent with the chemical composition shown in figure 5.8a; whilst that within the remainder of the coating (229.04-229.21 eV) lies within the reported range given in the literature for MoO₂ (228.8-232.0 eV)¹⁴⁷, which is consistent with the chemical composition shown in figure 5.8a. The binding energy data implies that the molybdenum was further reduced to metallic Mo at the

approximate position of the oxide-metal interface. The presence of metallic Mo in the coating is unlikely since the coating is a molybdate coating and not a metallic coating; it's also known that metallic Mo cannot be deposited from aqueous solutions¹⁵⁶ and the solution used in this work is aqueous. The presence of metallic Mo is most likely due to sputter induced reduction caused by the ion beam used to conduct the depth profiling analysis¹⁵³⁻¹⁵⁵.

However, for samples electrochemically formed at -0.6 V and -0.75 V vs. Ag/AgCl for 5 min, the oxygen and molybdenum contents change with increasing sputter times. A similar trend was observed in the binding energy of the molybdenum peak as previously discussed, however, there is a gradual reduction in the oxygen content up to ~1000 s of sputter, from ~60 at.% at the unspattered surface to ~50 at.% at sputter times greater than 1000 s; beyond 1000 s the oxygen content remains constant, which would suggest a stoichiometry of MoO. The gradual reduction in oxygen content that was observed could be due to prolonged argon ion sputtering causing reduction of the molybdenum oxide¹⁵³⁻¹⁵⁵. Molybdenum reduction, probably as a result of the prolonged sputter, is also reflected in figure 5.8d which shows that the molybdenum peak binding energy continually reduces throughout the thickness of the coating. The molybdenum peak binding energy at the unspattered outer surface is 231.9 eV which lies within the reported binding energy range given in the literature for MoO₃ (231.7-233.6 eV)¹⁴⁷, which is consistent with the chemical composition shown in figure 5.8c. The molybdenum peak binding energy within the remainder of the conversion coating (229.37-228.32 eV) overlaps with reported range given in the literature for MoO₂ (228.8-232.0 eV)¹⁴⁷ and the peak binding energy for metallic Mo¹⁴⁷.

Table 5.3 shows that all of the molybdate conversion coatings are significantly thicker than the thickest electrochemical oxide that has been produced (discussed in chapter 4). Table 5.3 also shows that there is a significant thickness difference between the two samples produced at the most cathodic potentials (-0.6 and -0.75 V vs. Ag/AgCl) and the rest of the samples. It is also evident that the molybdenum content within the conversion coating lies within the range of 36 at.% to 40 at.% for all

the samples, with the exception of that produced at -0.75 V vs. Ag/AgCl where the Mo content increases progressively through the bulk of the coating.

Table 5.3 Showing the sputter time to reach 50 % of the surface oxygen content and the molybdenum content within the plateau region of the depth profiles for molybdate conversion coatings, along with an electrochemically formed oxide for comparison.

Conversion coating formation parameters	Sputter time to 50% original oxygen content	Molybdenum content within the plateau region
5 min immersion	200 s	~37 at.%
$\pm 5 \text{ mA cm}^{-2}$ 30 cycles	340 s	~36.5 at.%
$\pm 2.5 \text{ mA cm}^{-2}$ 30 cycles	215 s	~36 at.%
$\pm 2.5 \text{ mA cm}^{-2}$ 120 cycles	440 s	~37 at.%
-0.45 V 5min	280 s	~37 at.%
-0.6 V 5min	1085 s	~40 at.%
-0.75 V 5min	3095 s	~40-48 at.%
Electrochemically formed oxide at 2V 60 mC cm ⁻² (potassium bath)	27 s	N/A

This may be due to sputter induced reduction of the molybdenum oxide^{153–155}, which may also cause preferential sputtering of the oxygen. It was reported by Simpson *et al*¹⁴⁸ that the argon ion beam in XPS will preferentially sputter oxygen, which would cause the detection of metallic molybdenum to occur. However, other factors may affect the results obtained during a depth profile such as the ion beam energy, which causes the depth resolution to reduce as the ion energy increases¹⁴⁹. This deterioration in resolution is caused by the ion beam mixing the atoms within the sample at greater depths due to the increased ion energy, as increasing the energy of the ion beam will cause the ions to penetrate further into the sample. The ion beam can also induce roughness on the surface of the sample which is due to different elements sputtering at different rates, this roughness will cause elements at different depths to be detected.

5.1.1.4.1 Optical Studies of the Molybdate Conversion Coatings

Optical microscopy was carried out to study the structure of the molybdate coatings. The results show that for the thinner coatings (5 min immersion and -0.45 V vs. Ag/AgCl for 5 min) there is no visible cracking and were generally blue in colour, as illustrated in figure 5.9 a&b. This shows that the coatings are homogeneous without many 'weak points'; this may suggest that the coatings will mitigate tin whisker growth.

However, for the coatings produced electrochemically at a potential of -0.6 V and -0.75 V vs. Ag/AgCl for 5 min, there is a high density of cracking which is illustrated in figure 5.9 c&d, respectively. Comparison of the two samples shows there is a much higher density of cracking on the sample produced at -0.75 V vs. Ag/AgCl for 5 min which may be related to the increased conversion coating thickness. The observed cracking for both samples may be due to increased tensile stress induced by the increased film thickness and/or the drying process, as suggested by Zhang *et al*⁹³ and da Silva *et al*⁹⁴. During the drying process the moisture is removed from the coating, which causes the coating to shrink; this shrinkage generates tensile stresses related to the coating thickness, within the coating which can subsequently cause cracking. This cracking may suggest that these conversion coatings may not effectively mitigate tin whisker growth, even though both conversion coatings are considerably thicker than an electrochemically formed oxide. This is because the cracks will most likely become sites at which whiskers could easily penetrate the coating.

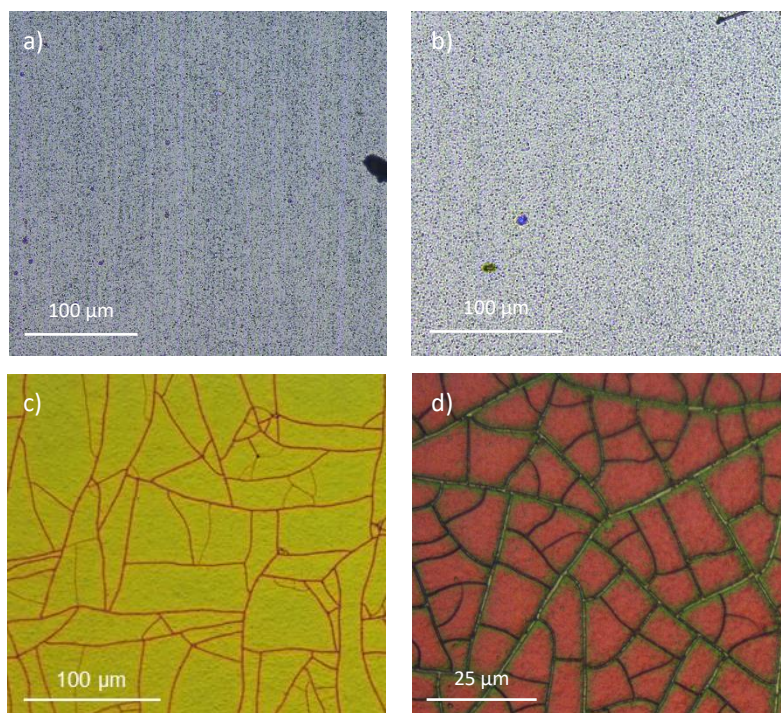


Figure 5.9 Optical micrographs of molybdate conversion coatings produced at a) 5 min immersion, b) $-0.45\text{ V vs. Ag/AgCl}$ for 5 min, c) $-0.6\text{ V vs. Ag/AgCl}$ for 5 min and d) $-0.75\text{ V vs. Ag/AgCl}$, all on pure electroplated Sn after ~ 2 months of room temperature storage.

5.1.2 Tungstate Conversion Coatings

Several parameters were investigated to optimise the coating in terms of thickness and structure; the reproducibility was also studied. The processing method used was based on the reverse current pulse technique described by Van De Leest & Krijl⁹⁹. The parameters that were varied were: the reverse current density (trial numbers CD.1-3); the number of cycles (trial numbers NC.1-3); and equivalent charge passed at different current densities (trial numbers EC.1-3).

5.1.2.1 Effect of Reverse Current Pulsed Parameters

The effect of processing parameters on the conversion coating thickness, structure and reproducibility have been investigated using x-ray photoelectron spectroscopy (XPS) and optical microscopy. Figure 5.10 shows XPS depth profiles for each of the tungstate conversion coatings.

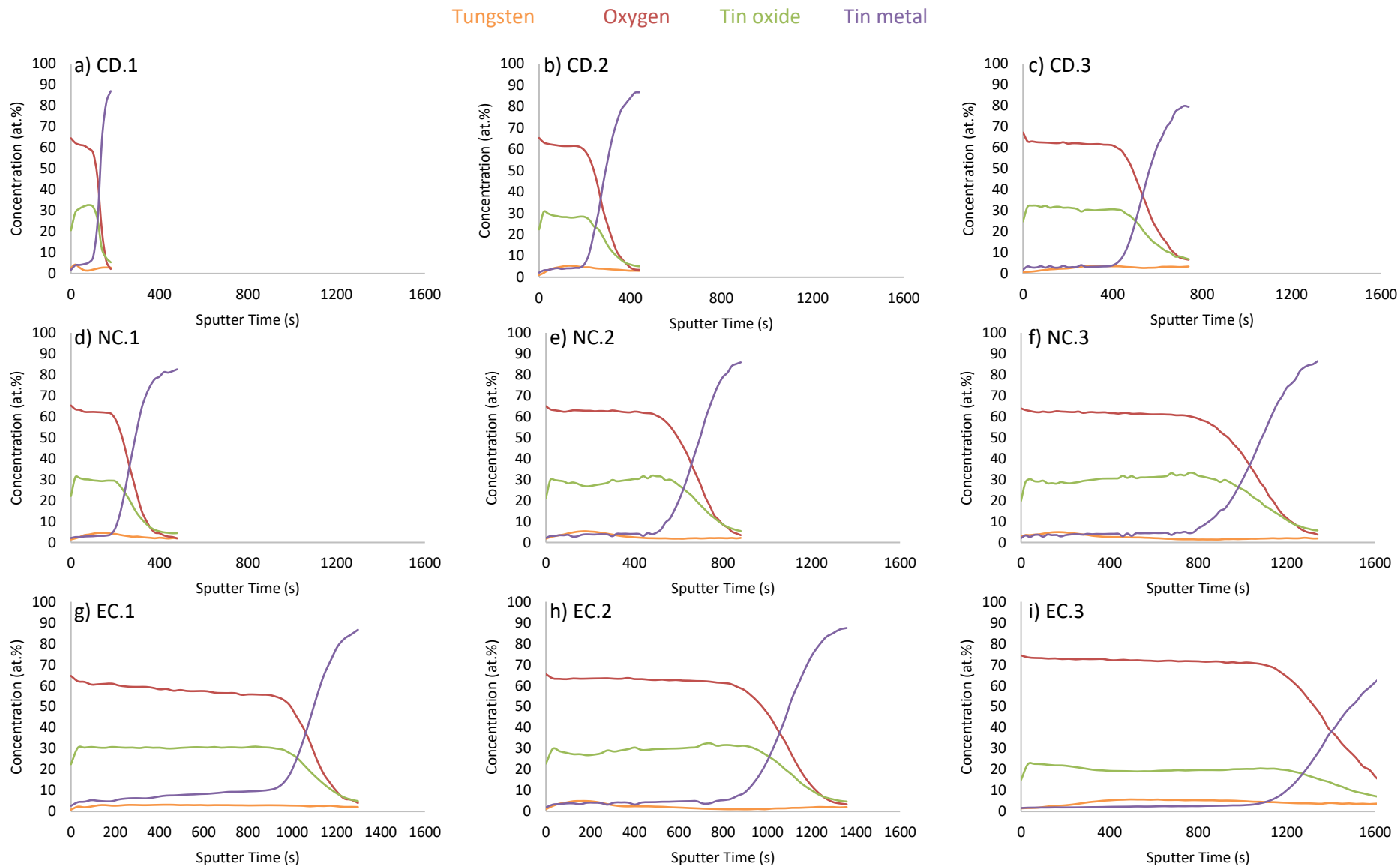


Figure 5.10 XPS depth profiles for tungstate conversion coatings formed by a pulsed current method at a) $\pm 2.5 \text{ mA cm}^{-2}$ for 30 cycles, b) $\pm 5 \text{ mA cm}^{-2}$ for 30 cycles, c) $\pm 10 \text{ mA cm}^{-2}$ for 30 cycles, d) $\pm 5 \text{ mA cm}^{-2}$ for 30 cycles, e) $\pm 5 \text{ mA cm}^{-2}$ for 90 cycles, f) $\pm 5 \text{ mA cm}^{-2}$ for 150 cycles, g) $\pm 2.5 \text{ mA cm}^{-2}$ for 300 cycles, h) $\pm 5 \text{ mA cm}^{-2}$ for 150 cycles and i) $\pm 10 \text{ mA cm}^{-2}$ for 75 cycles.

The depth profiles in figure 5.10 show that the coatings consist mainly of tin oxide with only a small amount of tungsten present throughout the thickness of the coating; the tungsten content increases with increased sputter time to ~4 at.%, which then steadily decreases after reaching its maximum. The tin present as an oxide stays constant throughout the bulk of the conversion coating at ~30 at.% and the oxygen content remains ~64 at.%, this stoichiometry suggests that the tin oxide is SnO₂. All the depth profiles measured from the tungstate conversion coated samples are similar in appearance, irrespective of processing parameters, and the results are summarised in table 5.4. It can be seen that as the current density is increased (trials CD.1 to CD.3) the thickness of the conversion coating is also increased, which is to be expected given that the total charge passed is greater.

Table 5.4 also shows that as the number of cycles increases the thickness of the conversion coating increases (trials NC.1 to NC.3). It might be expected that passing an equivalent charge, at different current densities (trials EC.1 to EC.3), would result in conversion coatings of similar thickness, however, EC.3 (processed at $\pm 10 \text{ mA cm}^{-2}$) was significantly thicker than EC.1 and EC.2 (processed $\pm 2.5 \text{ mA cm}^{-2}$ and $\pm 5 \text{ mA cm}^{-2}$, respectively), which were similar in thickness. This may arise from oxide formation at $\pm 10 \text{ mA cm}^{-2}$ being more efficient at developing a thicker oxide layer than at either $\pm 2.5 \text{ mA cm}^{-2}$ or $\pm 5 \text{ mA cm}^{-2}$. However, it will also depend on the electrochemical reactions occurring at different currents; different reactions may occur at different currents. This will also affect oxide formation and thickness.

Table 5.4 also indicates good reproducibility; trials CD.2 and NC.1 used the same coating parameters and the sputter times to reach 50 % of the original oxygen content at the surface are almost identical at 280 s and 275 s, respectively. Trials NC.3 and EC.2 also used the same parameters and required very similar sputter times to reach 50 % of the original oxygen content at the surface. These results show that the reverse current pulse technique used in this work is able to produce consistent conversion coating thicknesses.

Table 5.4 Summary of XPS depth profile measurements for tungstate conversion coated pure Sn electrodeposited samples.

Trial Number	Parameters		Sputter Time to 50% Original Oxygen Content
	Current Density	Number of Cycles	
CD.1	$\pm 2.5 \text{ mA cm}^{-2}$	30 cycles	130
CD.2	$\pm 5 \text{ mA cm}^{-2}$	30 cycles	280
CD.3	$\pm 10 \text{ mA cm}^{-2}$	30 cycles	550
NC.1	$\pm 5 \text{ mA cm}^{-2}$	30 cycles	275
NC.2	$\pm 5 \text{ mA cm}^{-2}$	90 cycles	680
NC.3	$\pm 5 \text{ mA cm}^{-2}$	150 cycles	1060
EC.1	$\pm 2.5 \text{ mA cm}^{-2}$	300 cycles	1085
EC.2	$\pm 5 \text{ mA cm}^{-2}$	150 cycles	1085
EC.3	$\pm 10 \text{ mA cm}^{-2}$	75 cycles	1410

Although a higher current density is able to produce a thicker coating for an equivalent charge passed (table 5.4), there is a limit to how much charge can be passed before the coating quality deteriorates. Figure 5.11 shows photographs of tungstate conversion coatings produced using $\pm 10 \text{ mA cm}^{-2}$, figure 5.11 (a,c,e,g), and $\pm 5 \text{ mA cm}^{-2}$, figure 5.11 (b,d,f,h), for different numbers of cycles. Figure 5.11 shows that the tungstate conversion coatings produced at $\pm 10 \text{ mA cm}^{-2}$ for 30 cycles (figure 5.11a), $\pm 5 \text{ mA cm}^{-2}$ for 60 (figure 5.11b), 90 (figure 5.11h) and 150 (figure 5.11d) cycles all appear to be homogeneous, i.e. the coating is uniform and contains no visible defects. Whereas, the other four samples, figure 5.11 (c,e-g) all appear to have a less consistent conversion coating, with the two least consistent conversion coatings being produced at $\pm 10 \text{ mA cm}^{-2}$ 150 and 90 cycles (figure 5.11c and figure 5.11e, respectively).

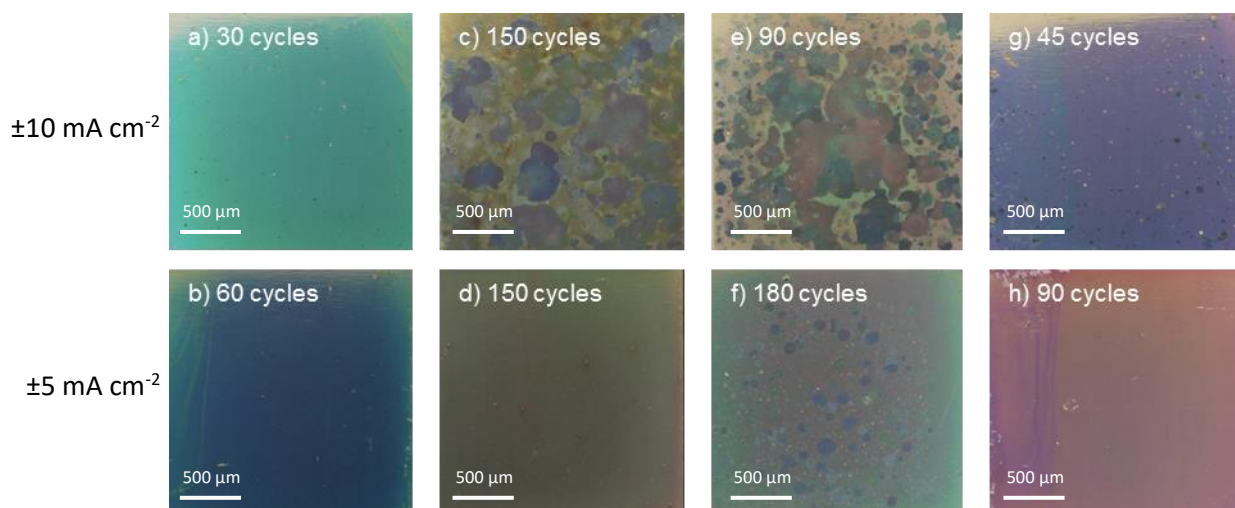


Figure 5.11 Photographs of tungstate conversion coatings showing the coating form and colour. The samples on the top row were processed using a current density of $\pm 10 \text{ mA cm}^{-2}$ and the bottom row using a current density of $\pm 5 \text{ mA cm}^{-2}$, a) 30 cycles, b) 60 cycles, c) 150 cycles, d) 150 cycles, e) 90 cycles, f) 180 cycles, g) 45 cycles and h) 90 cycles. All coatings were deposited onto $5 \mu\text{m}$ pure Sn.

At the higher current density ($\pm 10 \text{ mA cm}^{-2}$), more gas bubbles (most likely hydrogen gas during the cathodic half-cycle and oxygen gas during the anodic half-cycle) were observed to be formed at the sample surface, compared with at the lower current density ($\pm 5 \text{ mA cm}^{-2}$), which may have hindered or prevented the formation of the oxide coating and resulted in regions where the coating had either fully flaked off, to expose the underlying tin, or are thinner than the rest of the coating; such regions can be considered as 'weak points'. Visual examination of the conversion coated samples suggests that for a current density of $\pm 10 \text{ mA cm}^{-2}$ there is a limit of ~ 45 cycles before the coating quality is reduced, whilst the limit for a current density of $\pm 5 \text{ mA cm}^{-2}$ is between 150 and 180 cycles. These results, along with the results shown in table 5.4, indicate that thicker coatings may be produced at lower current densities since increased charge may be passed before the coating quality deteriorates. Figure 5.11 shows that for an equivalent charge passed, the quality of the conversion coating can be improved by reducing the current density.

Figure 5.12 shows XPS depth profiles for the oxygen content in the tungstate conversion coatings for samples produced at $\pm 10 \text{ mA cm}^{-2}$ for 45 cycles (purple) and $\pm 5 \text{ mA cm}^{-2}$ for 150 cycles (blue), it is evident that the sample produced at the higher current density is thinner than the sample produced at the lower current density.

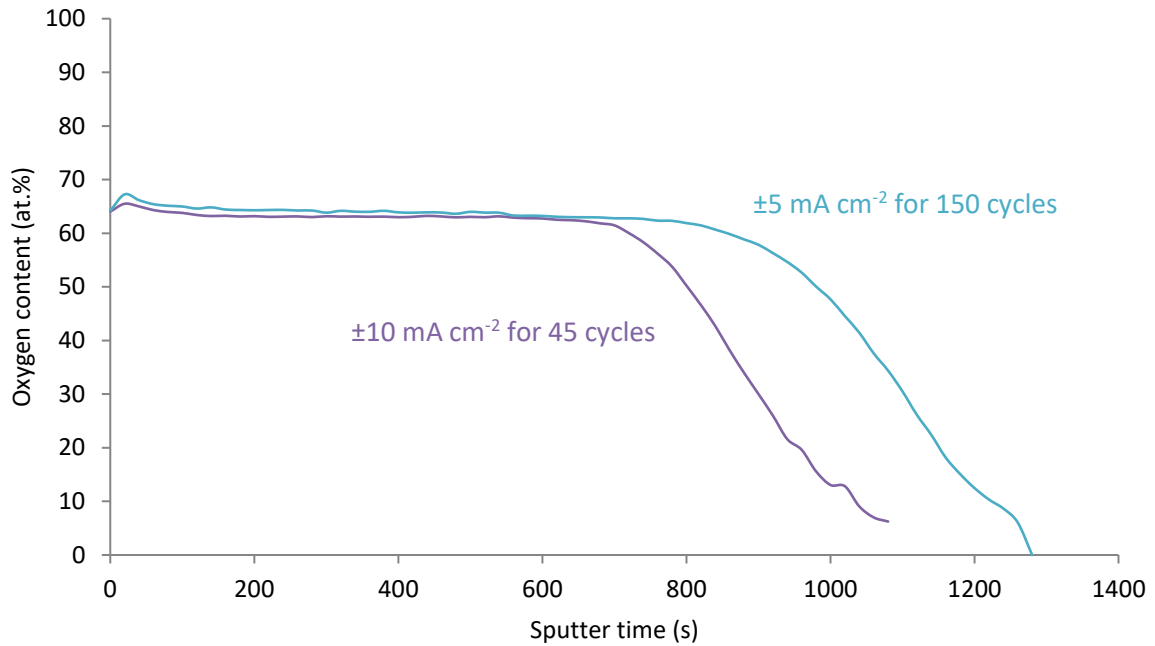


Figure 5.12 XPS depth profiles of oxygen content in tungstate conversion coatings on electrodeposited pure tin on copper produced at $\pm 10 \text{ mA cm}^{-2}$ for 45 cycles (purple) and $\pm 5 \text{ mA cm}^{-2}$ for 150 cycles (blue).

Optical microscopy was carried out on selected tungstate conversion coated samples. Figure 5.13 shows the appearance of the coatings ~3 months after deposition, for samples processed at $\pm 10 \text{ mA cm}^{-2}$ for 45 cycles, $\pm 5 \text{ mA cm}^{-2}$ for 90 cycles and $\pm 5 \text{ mA cm}^{-2}$ for 150 cycles. Examination of the images in figure 5.11 suggests that the cycle limit for samples processed at $\pm 10 \text{ mA cm}^{-2}$ is < 45 cycles, however, figure 5.13a reveals that a high number of defects are present in the coating. In comparison the tungstate coating produced at $\pm 5 \text{ mA cm}^{-2}$ for 90 cycles (figure 5.13b) showed no such defects. Defects were, however, present on the tungstate coating produced at $\pm 5 \text{ mA cm}^{-2}$ for 150 cycles (figure 5.13c), though far fewer than were observed on the sample produced at $\pm 10 \text{ mA cm}^{-2}$ for 45 cycles (figure 5.13a). The impact of these defects on the ability of the coating to mitigate whisker growth is discussed later in section 5.2.2.

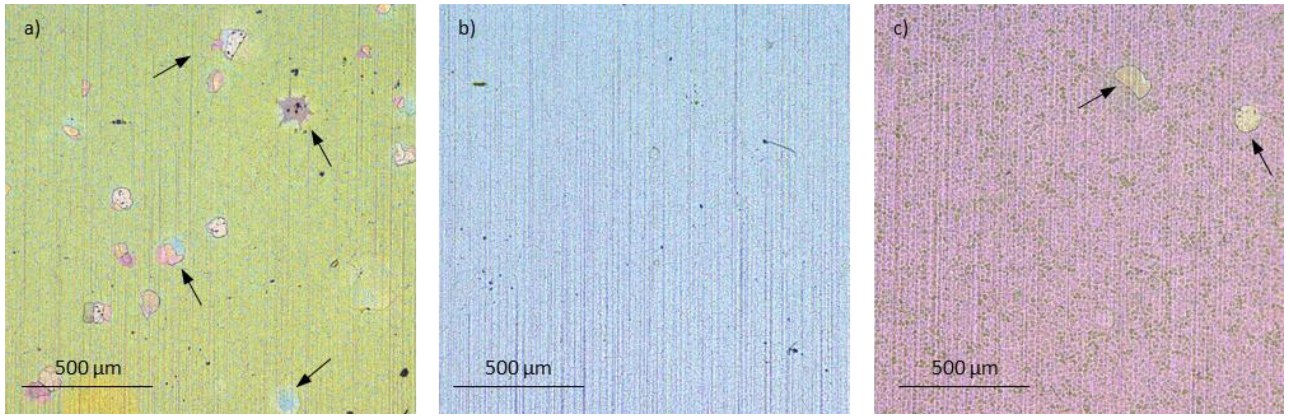


Figure 5.13 optical images of tungstate conversion coatings on $2\ \mu\text{m}$ Sn-Cu ~ 3 months after deposition: a) $\pm 10\ \text{mA cm}^{-2}$ 45 cycles, b) $\pm 5\ \text{mA cm}^{-2}$ 90 cycles and c) $\pm 5\ \text{mA cm}^{-2}$ 150 cycles. The black arrows are pointing out 'weak points'.

SEM analysis was carried out on the tungstate conversion coated samples to study the surface morphology of the coating in more detail. Figure 5.14 shows the appearance of the coating for samples processed using different conditions; figure 5.14 a&b, which were processed at $\pm 10\ \text{mA cm}^{-2}$ for 30 cycles and $\pm 5\ \text{mA cm}^{-2}$ for 60 cycles, respectively, both showed a uniform surface with no evidence of cracking. In comparison samples processed at $\pm 10\ \text{mA cm}^{-2}$ for 90 and 150 cycles (figure 5.14 c&d respectively), both showed a surface with a large number of cracks and areas, which varied in size, where the coating was either thinner or completely removed to expose the underlying Sn (as shown in figure 5.14e, $\pm 10\ \text{mA cm}^{-2}$ for 90 cycles). Compared with the cracking on the molybdate samples (figure 5.9), that on the tungstate conversion coated samples was much finer, in terms of crack width, (figure 5.14 c&d) and not visible under the optical microscope at an objective magnification of x20.

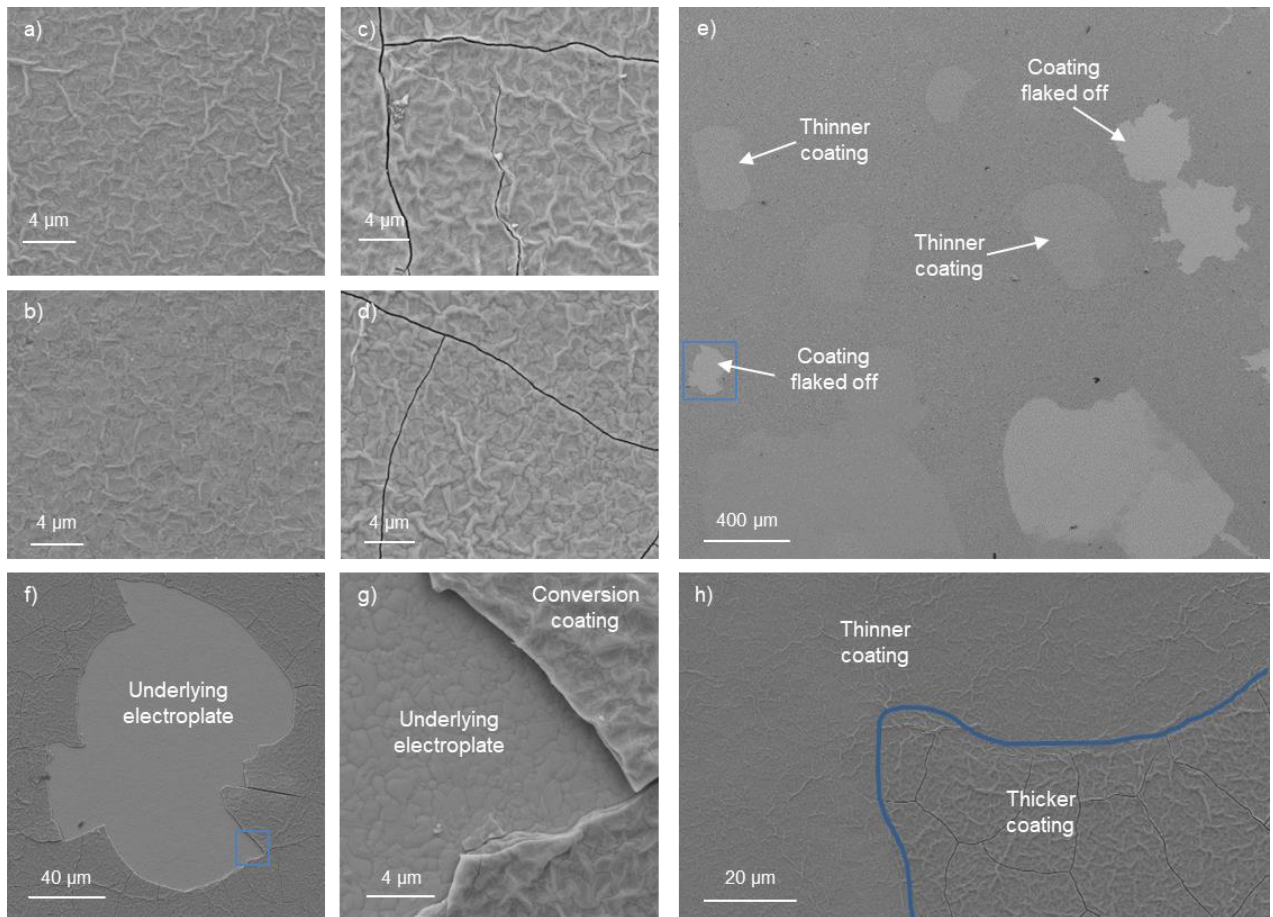


Figure 5.14 SE micrographs of tungstate coatings on 5 μm pure Sn. a) ±10 mA cm⁻² 30 cycles, b) ±5 mA cm⁻² 60 cycles, c) ±10 mA cm⁻² 90 cycles, d) ±10 mA cm⁻² 150 cycles, e) ±10 mA cm⁻² 90 cycles showing examples of 'weak points' in the coating, f) ±10 mA cm⁻² 90 cycles showing the flaked off coating within the blue box in (e), g) ±10 mA cm⁻² 90 cycles showing the area within the blue box in (f) and h) ±10 mA cm⁻² 90 cycles showing areas where the conversion coating is thinner

5.1.2.2 Examination of the Reverse Current Pulse Technique for the Formation of Tungstate Conversion Coatings

Figure 5.15 illustrates a single cycle for each of the four different reverse current pulse experiments that were used to investigate the influence of the positive and negative current pulses on the deposition of the conversion coatings. Each of the four square waves were performed for 30 cycles using a reverse current density of ±10 mA cm⁻² and were as follows: reducing the duration of the negative pulse by 50 % (half -ve); reducing the duration of the positive pulse by 50 % (half +ve); positive pulse only (+ve only); and negative pulse only (-ve only).

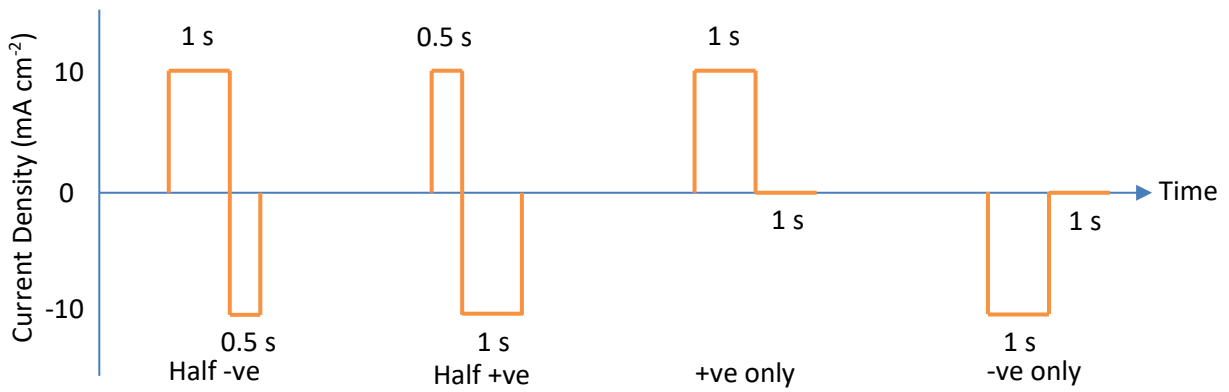


Figure 5.15 A schematic depicting each pulse study. Whereby 'Half -ve' is 1 s anodic and 0.5 s cathodic; 'Half +ve' is 0.5 s cathodic and 1 s anodic; '+ve only' is 1 s anodic and 1 s at 0 mA cm⁻²; and '-ve only' is 1 s cathodic and 1 s at 0 mA cm⁻².

Table 5.5 shows the measured tungsten content at the coating surface together with the sputter time taken to reduce the original oxygen content by 50 %, both using x-ray photoelectron spectroscopy (XPS). It can be seen from table 5.5 that the square waves that passed a net positive charge (Half -ve and +ve only) produced the thickest conversion coatings. Comparison of the sputter time taken to reduce the original oxygen content in table 5.5 with that in table 5.4 shows that reducing the negative pulse duration by 50 % will produce a conversion coating similar in thickness to that produced using the standard pulse durations (table 5.4, CD.3).

Table 5.5 The surface tungsten content and the sputter time taken to reduce the original oxygen content by 50 % for the different pulse studies.

	Half -ve	Half +ve	+ve only	-ve only
Tungsten content at the surface	3.0 at. %	1.9 at. %	1.9 at. %	3.5 at. %
Sputter time taken to reduce original oxygen content	540 s	190 s	323 s	10 s

Table 5.5 also shows that using a negative pulse only produces a coating with the highest tungsten content at the surface prior to sputtering, however, the resulting conversion coating was much thinner compared with the other conversion coatings. Comparing the results shown in table 5.5 with the those shown in table 5.4 suggests that both positive and negative pulses, for equal duration, are required to produce the thickest conversion coating with the highest tungsten content. However, table 5.5 does show that reducing the holding time for the negative cathodic half-cycle will produce a coating with a similar thickness to a coating produced using equal anodic and cathodic half-cycles.

5.1.3 Focused Ion Beam Cross Section Analysis of Intermetallic Growth and Conversion Coating Thickness

Focused ion beam (FIB) cross-sections were produced to study both the intermetallic compound (IMC) growth in the Sn-Cu coating and the thickness of the conversion coatings, which are shown in figure 5.16. Figure 5.16a shows an ion beam image of the cross-section of an electroplated 2 μm Sn-Cu coating on pure copper together with a molybdate conversion coating that had been produced at -0.6 V vs. Ag/AgCl for 5 min. Figure 5.16b shows an ion beam image of the cross-section of an electroplated 2 μm Sn-Cu coating on pure copper with a tungstate conversion coating that had been produced at $\pm 10 \text{ mA cm}^{-2}$ for 45 cycles. Figure 5.16c shows a binary image of the electroplated coating for the molybdate conversion coated sample shown in figure 5.16a. Figure 5.16d shows a binary image of the electroplated coating for the tungstate conversion coated sample shown in figure 5.16b. The cross-sections were imaged using the ion beam rather than the electron beam, so as to obtain a good contrast between the different structural components, e.g. IMC growth and conversion coating. The ion beam images obtained from these cross-sections were then analysed using ImageJ to estimate the percentage of IMC growth. The results from ImageJ show that for the molybdate sample after ~ 19 weeks of room temperature storage (figure 5.16a), the IMC growth accounted for $\sim 60\%$ of the electroplated coating; and for the tungstate sample after ~ 24 weeks of room temperature storage (figure 5.16b), the IMC growth accounted for $\sim 50\%$ of the electroplated coating. The equations for calculating the percentage of IMC growth for the molybdate conversion coated sample and tungstate conversion coated sample are shown in equations 5.1 and 5.2, respectively:

$$\frac{17885}{17885+11854} \times 100 \approx 60\%$$

Equation 5.1 – Calculation used to determine percentage of IMC growth for the molybdate conversion coated sample shown in figure 5.16a. With the equation representing the number of white pixels divided by the total number of pixels.

$$\frac{18125}{18125+17995} \times 100 \approx 50\%$$

Equation 5.2 – Calculation used to determine percentage of IMC growth for the tungstate conversion coated sample shown in figure 5.16b. With the equation representing the number of white pixels divided by the total number of pixels.

Comparison with cross-sections prepared from untreated Sn-Cu electrodeposited coatings (shown in figure 4.30a) shows that the conversion coatings have little effect on the IMC formation. This would suggest that the tungstate and molybdate conversion coatings mitigate whisker growth simply by acting as physical barrier in a similar way as the electrochemically formed oxides. The micrographs in figure 5.16 can also be used to estimate the thickness of the conversion coatings. The thickness of the molybdate conversion coating produced at -0.6 V vs. Ag/AgCl for 5 min was measured at ~300 nm and the thickness of the tungstate conversion coating produced at $\pm 10 \text{ mA cm}^{-2}$ for 45 cycles was measured at ~240 nm.

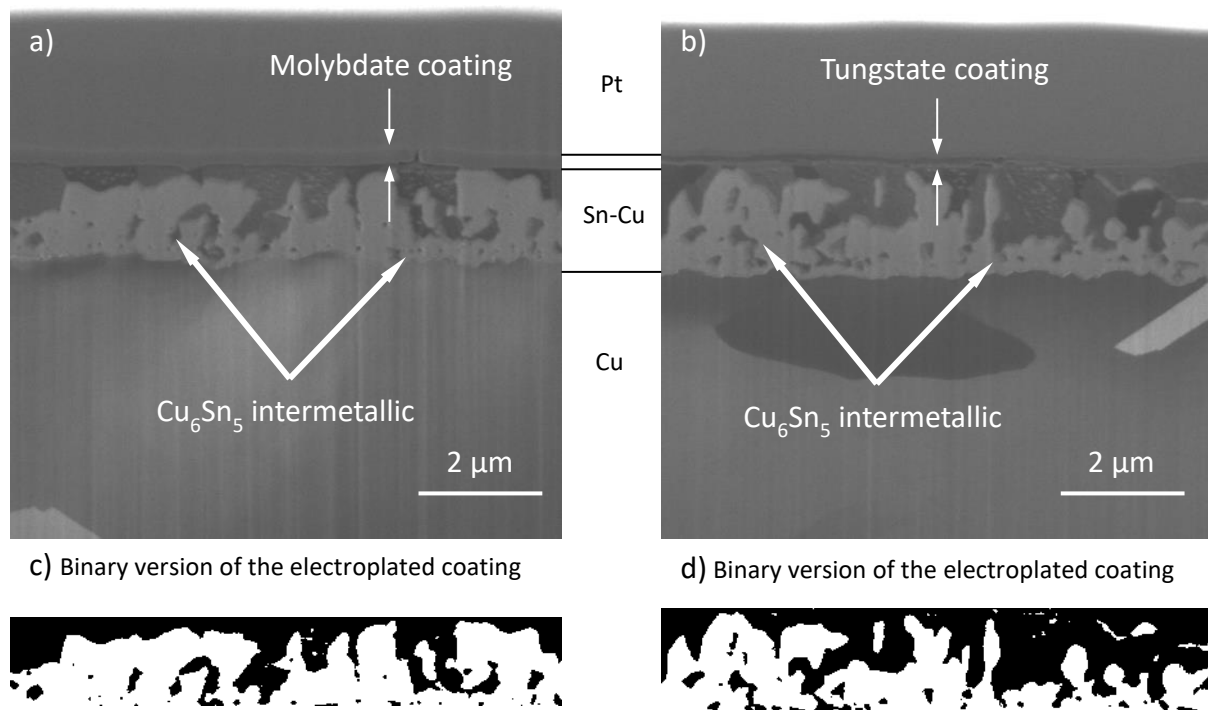


Figure 5.16 Ion beam images of FIB cross-sections of 2 μm Sn-Cu electrodeposits on Cu, a) with molybdate conversion coating produced at -0.6 V vs. Ag/AgCl for 5 min after 19 weeks of room temperature storage and b) with tungstate conversion coating produced at 10 mA cm^{-2} for 45 cycles after ~24 weeks of room temperature storage. Both c) and d) are binary versions of the electroplated coatings for the molybdate and tungstate conversion coated samples, respectively, to calculate the percentage of IMC growth.

The ratio between the molybdate conversion coating thickness and the tungstate conversion coating thickness (1:0.80) is very similar to the ratio between the corresponding sputter times taken to reach 50 % of the original oxygen content (1:0.82). Using the tantalum etch rate quoted for XPS (0.28 nm s^{-1}), an estimated thickness can be calculated. For the molybdate conversion coating, the sputter time taken to reach 50 % of the original oxygen content was 1085 s (table 5.3) which corresponds to a depth of 304 nm and for the tungstate conversion coating, the sputter time taken to reach 50 % of the original oxygen content was 890 s (figure 5.12) which corresponds to a depth of 249 nm. Both of these calculated values are very similar to the measured values obtained from the cross-sections. Therefore, the sputter time taken to reach 50 % of the original oxygen content can be used for comparing coating thicknesses.

5.2 Whisker Growth Studies

Whisker growth studies were carried out on molybdate and tungstate conversion coated samples, produced using different process parameters, to determine which conversion coating provided the greatest whisker mitigation. The whisker density results from these samples are compared to those obtained from samples electrochemically oxidised at a potential of 2 V vs. Ag/AgCl for a charge passed of 60 mC cm^{-2} (section 4.5). The whisker density results for the electrochemically oxidised samples that will be used for comparison, with the whiskers results of the conversion coated samples, are shown in figure 5.17. The orange dotted lines in figure 5.17 represent the time intervals at which the molybdate conversion coated samples were analysed and the purple dotted lines represent the times at which the tungstate conversion coated samples were analysed.

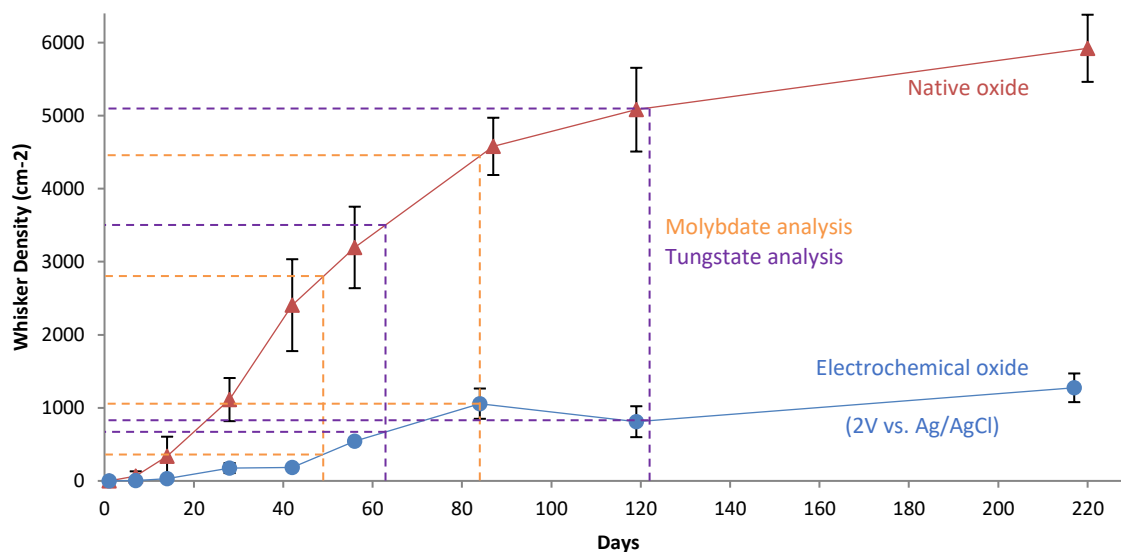


Figure 5.17 Data comparing the evolution of whisker density with storage time for untreated electroplated Sn-Cu samples with those electrochemically oxidised at 2 V vs. Ag/AgCl (60 mC cm⁻² charge passed). The orange dotted lines indicate the time intervals at which the molybdate conversion coated samples were analysed and the purple dotted lines indicate the times at which the tungstate conversion coatings were analysed.

5.2.1 Studying the Effect of Molybdate Conversion Coatings on Tin Whisker Growth

For whisker growth studies, molybdate conversion coatings were produced using three different conditions: 5 min immersion was chosen due to its simple method, -0.45 V vs. Ag/AgCl for 5 minutes was chosen as it was slightly thicker than a simple immersion, and -0.6 V vs. Ag/AgCl for 5 minutes was chosen as the coating was much thicker and had a similar thickness to one of the tungstate conversion coatings ($\pm 5 \text{ mA cm}^{-2}$ for 150 cycles) that were also investigated. Whisker growth was evaluated after 7 and 12 weeks of storage at room temperature in twenty random areas distributed across a sample, and the whisker densities for each coating treatment were calculated for each of the 3 samples. From these values an average whisker density was calculated (figure 5.18).

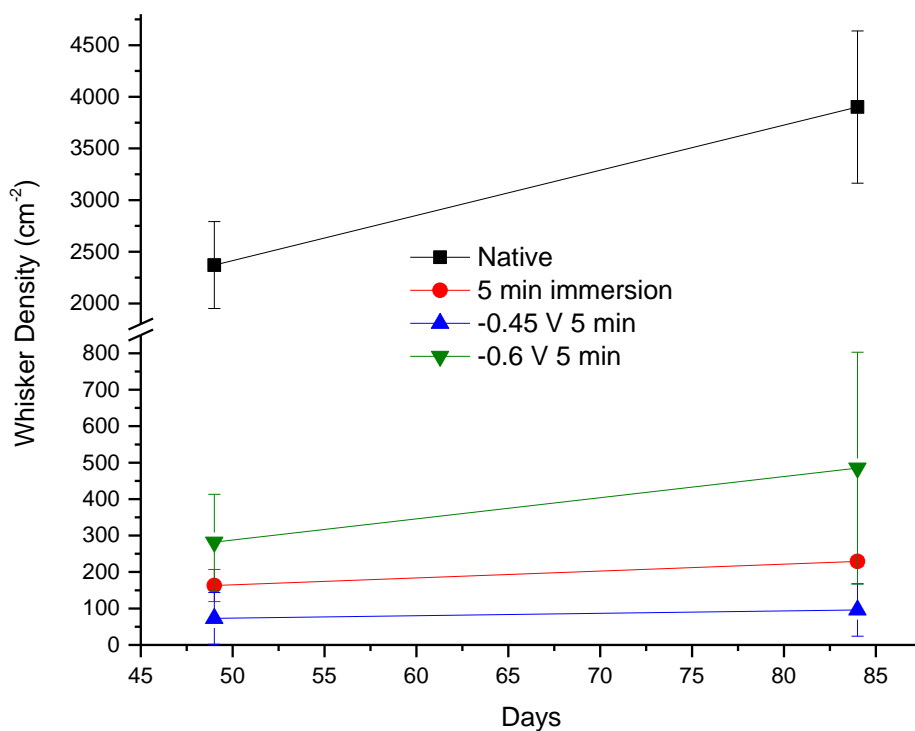


Figure 5.18 Data showing the effect of molybdate conversion coatings on whisker growth from electroplated Sn-Cu samples after storage at room temperature for ~7 and 12 weeks. The results from untreated samples are included for comparison. With the error bars representing the standard deviation between samples

Figure 5.18 shows the change in whisker growth from 7 weeks to 12 weeks at room temperature for the molybdate conversion coated samples, along with the growth results for untreated (native air-formed oxide) samples for comparison. The results show that all of the molybdate conversion coated samples significantly reduced whisker growth compared with a natural air-grown oxide. The results also show that the best molybdate coating (in terms of whisker reduction) was the -0.45 V sample which had less than 100 whiskers cm⁻² after 12 weeks of room temperature storage. Whereas the worst molybdate conversion coating (in terms of whisker reduction) was the -0.6 V sample which after 12 weeks of room temperature storage had an average whisker density of 485 whiskers cm⁻²; even though a molybdate conversion coating produced at -0.6 V vs. Ag/AgCl for 5 min is significantly thicker than that produced at -0.45 V vs. Ag/AgCl for 5 min (table 5.3). This difference in whisker density is most likely due to the high cracking density observed on molybdate conversion coatings produced at

-0.6 V vs. Ag/AgCl, compared with the molybdate conversion coating produced at -0.45 V vs. Ag/AgCl which had no visual cracks (figure 5.8).

The measured whisker densities in figures 5.17 (orange dotted line) and 5.18 shows that the 5 min immersion samples and those processed at -0.45 V vs. Ag/AgCl samples provided increased whisker mitigation compared with the electrochemically formed oxide. From figure 5.17 it can be determined that after 49 days the approximate ratio of whisker density for the untreated samples to the electrochemically oxidised samples was $\sim 8:1$, whereas the 5 min immersion, -0.45 V and -0.6 V samples had ratios of $\sim 15:1$, $\sim 32:1$ and $\sim 8:1$, respectively (figure 5.17). The improved whisker mitigation seen for the 5 min immersion and -0.45 V molybdate conversion coated samples may be due to the increased thickness of the oxide on those samples (given in table 5.3) providing more effective whisker mitigation.

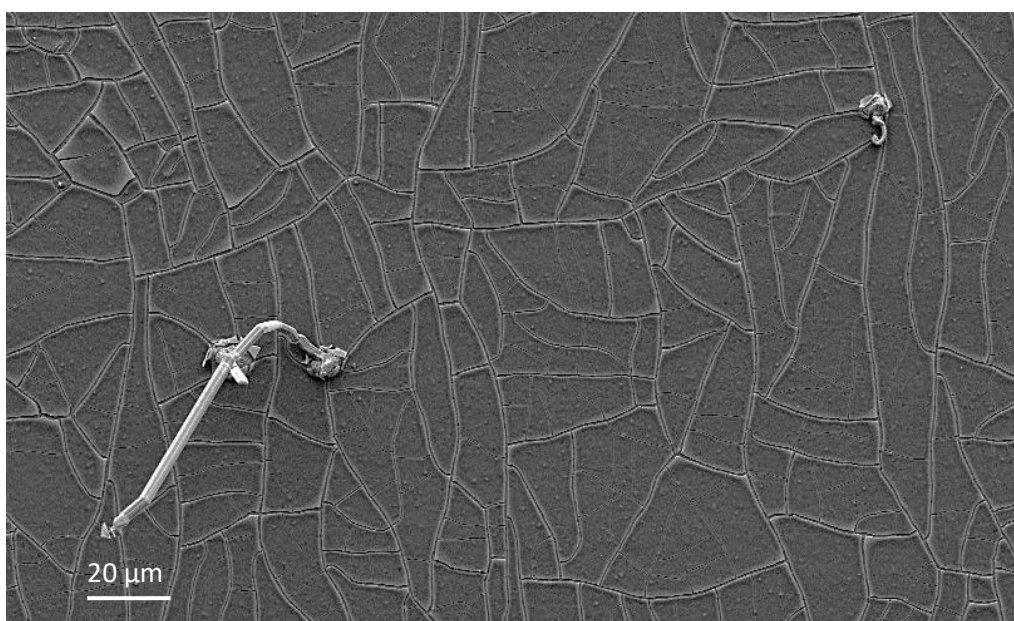


Figure 5.19 SE micrograph showing whiskers growing from cracks in the molybdate coating produced at -0.6 V vs. Ag/AgCl for 5 min on 2 μm thick Sn-Cu electroplate.

Although the molybdate sample produced at -0.6 V vs. Ag/AgCl showed increased whisker growth compared with the other two molybdate coatings, it still brought about a reduction in whisker growth (relative to the native air-formed oxide) comparable to that of an electrochemically oxidised surface produced at 2 V vs. Ag/AgCl for a charge passed of 60 mC cm^{-2} , i.e. a reduction of $\sim 8:1$. The reduced

effectiveness of the molybdate conversion coating produced at -0.6 V vs. Ag/AgCl is most likely due to the high density of cracks that are present (figures 5.9 and 5.19) since it was observed that all of the whisker growth initiated at cracks, as shown in figure 5.19. A similar observation was also reported by Chapaneri ¹⁵⁷, who observed that zinc whiskers would preferentially grow through cracks that were present in the chromate conversion coatings. However, Chapaneri also observed that for chromate conversion coatings with no cracks, the zinc whiskers would still grow through the chromate conversion coatings.

Figure 5.18 shows further that after 12 weeks of storage all the molybdate coatings are still effectively mitigating whisker growth and continuing to perform better than an electrochemically oxidised surface (figure 5.17). However, the -0.6 V molybdate samples show a slightly increased rate of whisker growth compared with the other two molybdate coatings; this is most likely due to the increased crack density present in these samples. No cracks or 'weak points' were observed in the other two molybdate coatings and the whisker density increases at a lower rate. However, compared with the untreated samples the molybdate sample produced at -0.6 V vs. Ag/AgCl was still mitigating whisker growth as effectively after 12 weeks as it did after 7 weeks, with a whisker density ratio of ~8:1 at both time intervals. The two other molybdate coatings produced using 5 min immersion and -0.45 V vs. Ag/AgCl both show a relative improvement in whisker mitigation compared with the untreated samples, with the whisker density ratios increasing from ~15:1 to ~17:1 for the 5 min immersion samples and from ~32:1 to ~41:1 for the -0.45 V vs. Ag/AgCl samples. The small increase in the whisker density ratio for the 5 min immersion samples may simply be due to slight variations in whisker density across the sample since the exact same areas weren't analysed at each time interval.

5.2.2 Studying the Effect of Tungstate Conversion Coatings on Tin Whisker Growth

For whisker growth studies, tungstate conversion coatings were produced using three different processing conditions: $\pm 10 \text{ mA cm}^{-2}$ for 45 cycles, $\pm 5 \text{ mA cm}^{-2}$ for 90 cycles and $\pm 5 \text{ mA cm}^{-2}$ for 150 cycles. Three samples were prepared for each coating treatment and twenty random areas were

analysed for each sample (after ~9 weeks of storage at room temperature), and the whisker densities were evaluated. An average whisker density for each set of processing conditions was calculated from these values (figure 5.20). It was observed that all of the conversion coated samples had significantly reduced whisker growth compared to the untreated samples. Comparison of the whisker density data given in figures 5.20 and 5.17 shows that the tungstate conversion coatings provided increased whisker mitigation compared with the electrochemically formed oxide sample. After 63 days the approximate ratio of whisker density for the untreated samples to electrochemically oxidised samples was ~5:1 (figure 5.17), whereas the least effective of the tungstate samples had a whisker density ratio of ~36:1 (figure 5.20).

Figure 5.20 shows that after 4 months of storage all of the tungstate coatings were still providing more effective whisker mitigation than the electrochemically oxidised surfaces (figure 5.17). The rate at which the whisker density has increased for both of the samples processed at $\pm 5 \text{ mA cm}^{-2}$ has reduced after 4 months of storage compared with untreated samples. Both coatings display a similar ability to mitigate whisker growth, despite there being a significant difference in coating thickness between them (table 5.4). This is most likely due to the cracking present in the coatings produced at $\pm 5 \text{ mA cm}^{-2}$ for 150 cycles, which introduces 'weak points' into the coating in the form of areas where the coating has completely flaked off (figure 5.9c and figure 5.21a); from which the majority of the whisker growth occurs for these samples (figure 5.21a). Areas where the coating had flaked away were also observed for the samples processed at $\pm 10 \text{ mA cm}^{-2}$ for 45 cycles, although a higher density of such features were observed.

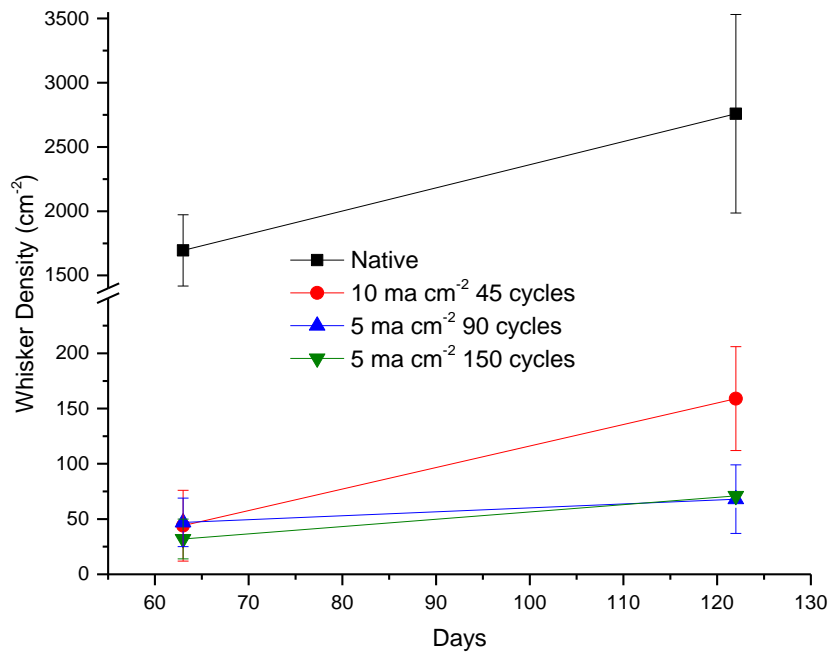


Figure 5.20 Data showing the effect of tungstate conversion coatings on whisker growth from electroplated Sn-Cu samples after storage at room temperature for ~9 weeks and 4 months. With the error bars representing the standard deviation between samples

In comparison, no cracking was observed on the samples produced at $\pm 5 \text{ mA cm}^{-2}$ for 90 cycles after 4 months of storage. The tungstate coatings produced at $\pm 10 \text{ mA cm}^{-2}$ for 45 cycles appears to become less effective with time, compared with the other two tungstate conversion coatings, which is most likely due to the high density of cracks and areas where the coating had flaked off present in those samples (figure 5.10a); such regions created 'weak points' from which whisker growth was able to occur (figure 5.21a). The tungstate conversion coated samples produced at $\pm 5 \text{ mA cm}^{-2}$ for 150 cycles also possessed regions where the coating thickness was reduced; however, these areas did not appear to be preferential sites for whisker growth after ~9 weeks of storage. This suggests that these regions were still sufficiently thick to mitigate whisker growth.

Comparison of the tungstate conversion coating processed at $\pm 5 \text{ mA cm}^{-2}$ for 150 cycles with the molybdate conversion coating, with similar a thickness, processed at $-0.6 \text{ V vs. Ag/AgCl}$ for 5 min, shows that the tungstate conversion coating mitigates whisker growth more effectively. After 122 days of room temperature storage the tungstate conversion coating had a whisker reduction ratio of

~39:1 (figure 5.20), whereas after only 84 days of room temperature the molybdate conversion coating had a whisker reduction ratio of ~8:1 (figure 5.18). This shows that for equivalent coating thicknesses, tungstate conversion coatings are better at whisker mitigation. This is most likely because at increased thickness the molybdate conversion coatings crack whereas the tungstate conversion coatings do not. This may be due to the processing parameters used and/or the different coating chemistries. For molybdate conversion coatings the coating is predominantly molybdenum oxide (figure 5.7), whereas for tungstate conversion coatings the coating is predominantly tin oxide (figure 5.10).

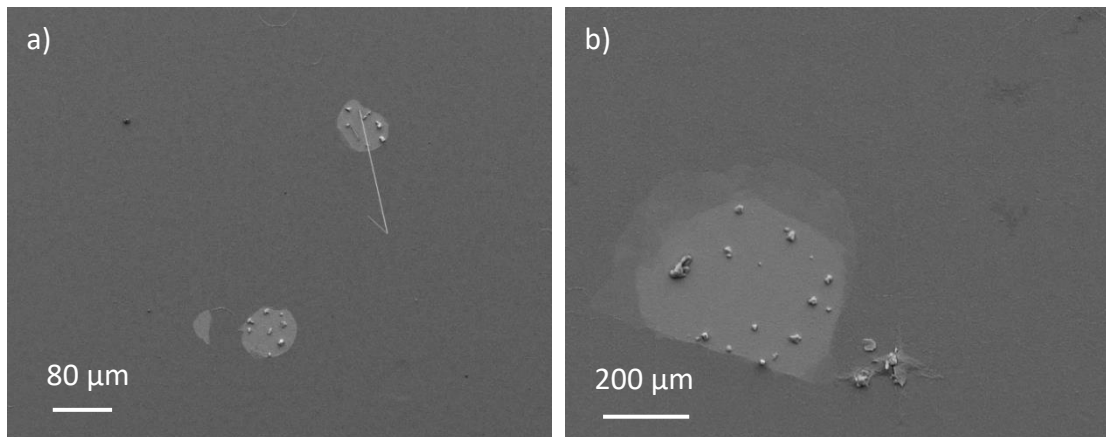


Figure 5.21 SE micrograph showing a high concentration of tin whisker growth at an area where no coating is present ('weak point') on a tungstate coating produced at a) $\pm 5 \text{ mA cm}^{-2}$ for 150 cycles on $2 \mu\text{m}$ Sn-Cu electroplate and b) $\pm 10 \text{ mA cm}^{-2}$ for 45 cycles on $2 \mu\text{m}$ Sn-Cu electroplate

5.3 Summary

5.3.1 Conversion Coating Optimisation

The results discussed in section 5.1 suggest that, for the molybdate conversion coating process, the solution needs to process a certain number of samples before consistent conversion coating thicknesses are produced. Results suggest that two samples should be processed for the solution for 4 min each before conversion coatings that will be used for whisker mitigation trials are produced. Molybdate conversion coating trials showed that increasing the immersion time from 1-9 min results in a progressive increase in the coating thickness; results also showed that reducing the pH of the bath from pH 4 to pH 2 also increases the thickness of the conversion coating. Further reduction in the pH

to pH 1 caused a reduction in the coating thickness, however, the amount of oxide mixing was increased, i.e. the molybdate coating was not a pure molybdate coating as it also contained tin oxide, so it can be said that the coating was a mixed oxide coating. This may be due to a more aggressive process occurring whereby the dissolution of tin may be occurring simultaneously with the deposition of the molybdate conversion coating, which may cause the dissolved tin to redeposit with of the molybdenum conversion coating to create a mixed oxide coating. It was also shown that increasingly thicker coatings could be produced by using electrochemical techniques.

For the tungstate conversion coatings, optimisation trials showed that increasing the total charge passed increases the coating thickness. Furthermore, coating at a current density of $\pm 10 \text{ mA cm}^{-2}$ produces a thicker coating, for an equivalent charge passed, than coating with current densities of $\pm 5 \text{ mA cm}^{-2}$ and $\pm 2.5 \text{ mA cm}^{-2}$. However, it was also shown that the use of higher current densities may result in poor coatings. To overcome this and produce thicker coatings with the fewest defects, lower current densities can be used for an increased number of cycles.

5.3.2 Whisker Growth Studies

The two thinnest molybdate coatings (5 min immersion and $-0.45 \text{ V vs. Ag/AgCl}$ for 5 min) both showed an improved ability to mitigate whisker growth compared to the electrochemically oxidised samples. This may be attributed to their increased thickness which enables them to physically block whisker growth more efficiently. Despite these coatings being thinner than that produced at $-0.6 \text{ V vs. Ag/AgCl}$, they showed improved whisker mitigation, due to the improved quality of the coating and the absence of cracks through which whiskers could grow.

Of the three tungstate samples investigated, that produced at $\pm 5 \text{ mA cm}^{-2}$ for 90 cycles mitigated whisker growth most effectively, even though x-ray photoelectron spectroscopy (XPS) depth profiling indicated that it was the thinnest coating; this is due to the absence of 'weak points' in the coating.

The molybdate samples produced at -0.6 V vs. Ag/AgCl and the tungstate samples produced at ± 5 mA cm^{-2} for 150 cycles were of similar thicknesses, however the tungstate samples had far lower whisker growth. This is due to the increased density of cracks in the molybdate conversion coating. This highlights that coating structure is equally as important as coating thickness with regards to the ability of the coating to mitigate whisker growth. The results show that it is likely that further improvement in whisker mitigation can be achieved by the optimisation of processing parameters.

Both the molybdate conversion coated sample produced at -0.45 V vs. Ag/AgCl for 5 min and the tungstate conversion coated sample produced at ± 5 mA cm^{-2} for 90 cycles had a similar whisker reduction ratio (at the second time interval) of $\sim 41:1$. However, the tungstate conversion coating was significantly thicker than the molybdate conversion coating, with the sputter times take to reach 50 % of the original oxygen content being 680 s (table 5.4) and 280 s (table 5.3), respectively. This may suggest that at certain process parameters the molybdate conversion coating is more efficient at whisker mitigation than a tungstate conversion coating. This shows that relatively thin molybdate conversion coatings will effectively mitigate whisker growth, however, thicker molybdate coatings will crack and are not as effective at mitigating whisker growth. Whereas, for tungstate conversion coatings thicker coatings can be achieved without many defects and will effectively mitigate whisker growth.

The results for whisker mitigation, discussed in section 5.2, are consistent to those observed by Su *et al*⁴², where it was observed that whiskers grew preferentially through pre-defined 'weak points' in the sputter-deposited tin oxide film.

6 Conformal Coating Studies

This chapter will present and discuss the results obtained for the electroplated Sn-Cu samples that had a conformal coating applied to them along with the electroplated Sn-Cu samples that had a dual-layer system. The electroplated Sn-Cu samples that had a dual-layer system, had an electrochemically formed oxide layer (produced at 2 V vs. SCE for a charge passed of 60 mC cm⁻²) with a conformal coating applied on top.

6.1 Dual-Layer Whisker Growth Studies

Before any whisker analysis was carried out, the conformal coating thickness was measured, using a Fischer Dual-Scope, to explain any anomalies that may occur due to differences in the thickness of the coatings, i.e. a sample with a thicker coating might be expected to have fewer whiskers than that with a thinner coating. Figure 6.1 shows the thickness for each of the samples from the initial whisker trial that had a conformal coating (including those that also had an electrochemically formed oxide). The figure shows sample 3, which didn't have an electrochemically formed oxide, had a significantly thicker conformal coating compared to the other samples. Therefore, it might be expected that the conformal coating on sample 3 would have mitigated whisker growth the most, due to the increased thickness. The figure also shows that the samples with the dual-layer system had conformal coatings that were of a similar thickness. The average thickness for all of the samples that only had a conformal coating was 5.8 μm and for all of the samples that had the dual-layer system the conformal coating average thickness was 6.4 μm.

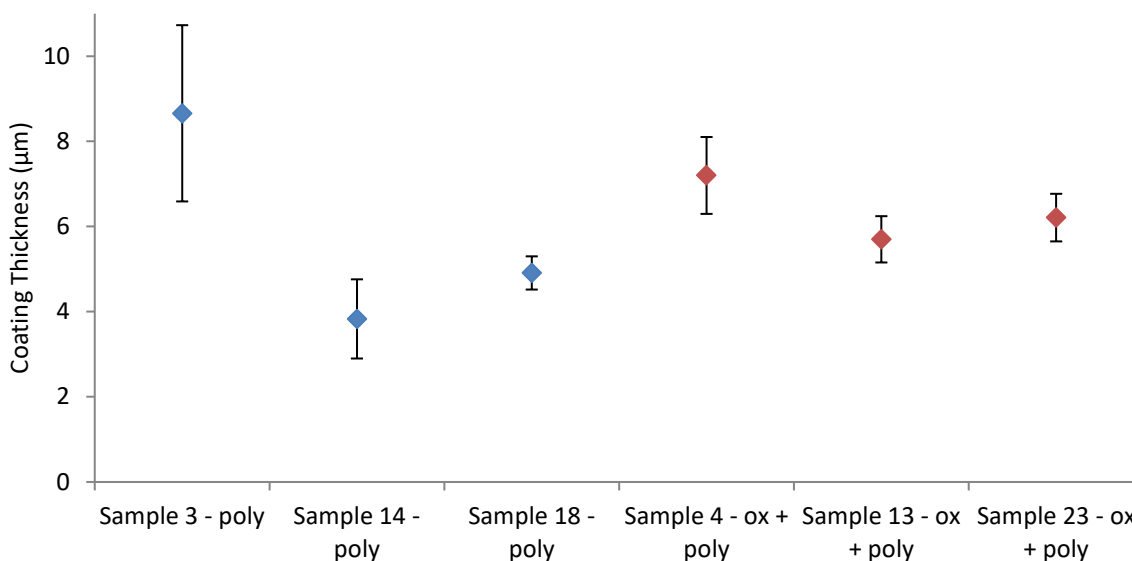


Figure 6.1 Data showing the average thickness for each conformal coated sample where 'poly' (blue) represents the samples that only had only a conformal coating and 'ox + poly' (red) represents the samples that had both an electrochemically formed oxide and a conformal coating. With the error bars representing the standard deviation between samples

6.1.1 Effect of Having a Dual-Layer System on Whisker Growth

The aim of this study was to investigate if whisker growth could be further reduced by combining a conformal coating with an electrochemical oxide. This was carried out by evaluating the whisker growth on four different sets of samples after ~9 weeks (figure 6.2a) and ~14 months (figure 6.2b) of room temperature storage. Three samples had a native air-formed oxide, three samples had an electrochemically formed oxide produced at a potential of 2.0 V vs. Ag/AgCl for a total charge passed of 60 mC cm⁻², three samples had an acrylic conformal coating only and three samples had both an electrochemically formed oxide and an acrylic conformal top coating (dual-layer coating).

Figure 6.2a shows the whisker growth data obtained after ~9 weeks of room temperature storage. The figure shows that for samples with an electrochemically formed oxide, the whisker density was reduced by 97.8 % compared to the untreated samples. For the conformal coated samples, the whisker density was reduced by 99.0 % compared to the untreated samples. For the dual-layer coated samples, the whisker density was reduced by 99.8 %. These results showed that after ~9 weeks, combining both an electrochemically formed oxide and a conformal coating will further improve whisker growth reduction compared to using the coating systems individually.

Figure 6.2b shows the whisker growth data obtained after ~14 months of room temperature storage. The figure shows that for samples with an electrochemically formed oxide, the whisker density was reduced by 79.0 % compared to the untreated samples. For the conformal coated samples, the whisker density was reduced by 96.1 % compared to the untreated samples. For the dual-layer coated samples, the whisker density was reduced by 84.2 %. The whisker density for all samples has increased compared with the figures for ~9 weeks. This was to be expected for the samples with an electrochemically formed oxide by observations noted in section 4.4, which suggested that the electrochemically formed oxide would generally reduce in effectiveness with increasing time. However, it was expected that the dual-layer system would still perform better than either of the coatings individually, which was not observed.

A possible reason for the higher than expected whisker density for the dual-layer coated samples could be the misinterpretation of some features, such as the 'bumps' shown in figure 6.3, i.e. these features that may have been counted as whiskers. One sample from each batch that had a conformal coating was stripped prior to whisker analysis for scanning electron microscopy (SEM) observation, which may have caused features to have been counted that wouldn't normally have been if the conformal coating was present, as the conformal coating may have prevented the observation of those features. Equally some of the samples with a conformal coating were very difficult to analyse under the optical microscope and it was difficult to distinguish what was and was not a whisker. This can be seen in figure 6.3, which shows that for the samples which had a conformal coating, large numbers of 'bumps' were observed which may or may not have been whiskers.

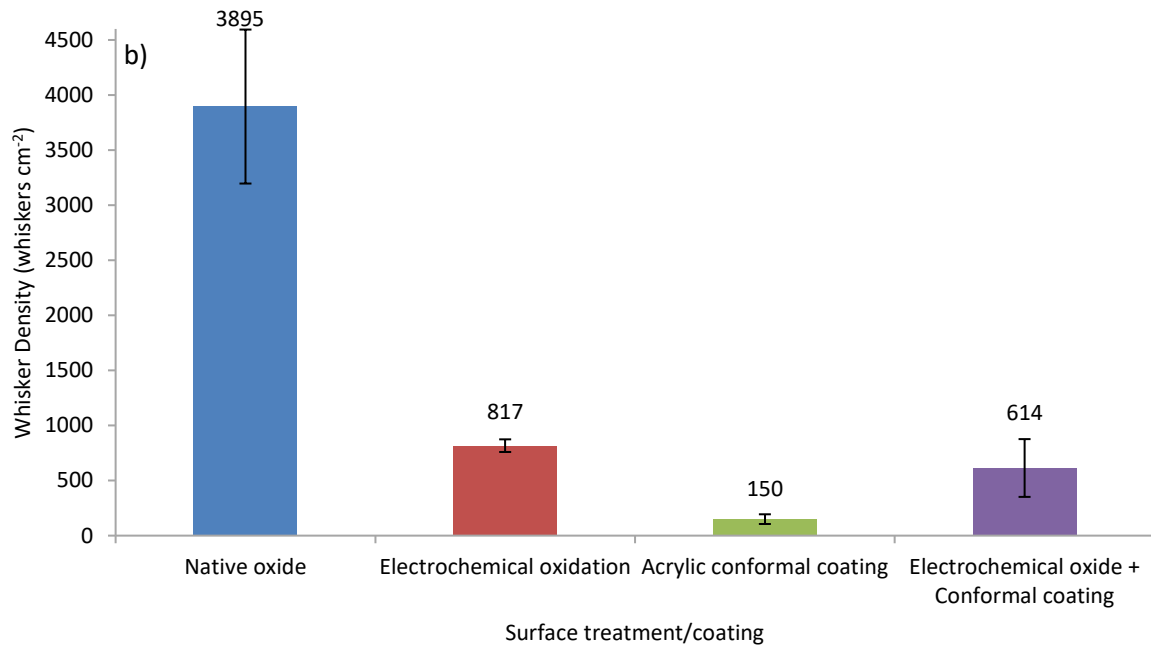
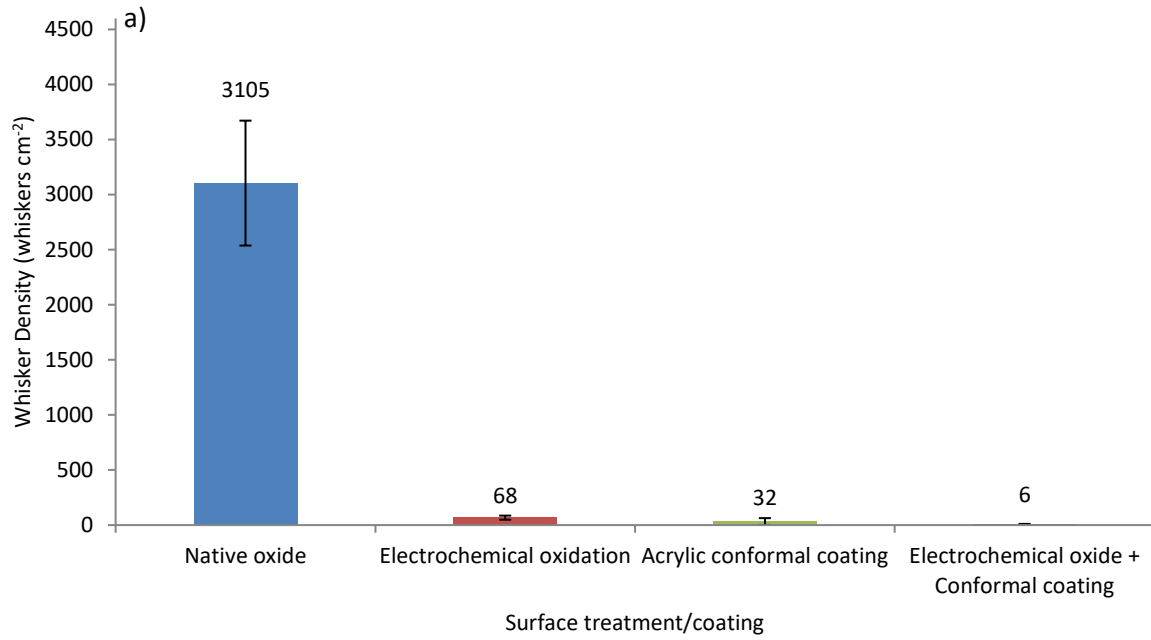


Figure 6.2 Data comparing whisker density after a) ~9 weeks and b) ~14 months of storage at room temperature between a native oxide, electrochemical oxide, conformal coating and a dual-layer coating. With the error bars representing the standard deviation between samples

SEM analysis was also carried out on a sample from each set of treatments along with an extra dual-layer coated sample and an extra conformal sample that had their conformal coatings stripped off using acetone to study the underlying surface. The samples that had a conformal coating on them were viewed at a tilt angle of 70 ° to improve the visualisation of any whisker growth. Figure 6.3 shows secondary electron (SE) micrographs, with all samples showing either nodule or eruption growth. It

can be seen from figure 6.3a and 6.3b that after the conformal coatings were stripped, the underlying surface for both the dual-layer coated sample and conformal coated sample were similar in appearance. Both samples had a similar number of eruptions and nodules, with a small number of filament-type whiskers. This, however, was unexpected, as the dual-layer coated sample had an underlying electrochemically formed oxide (2.0 V vs. Ag/AgCl for a total charge passed of 60 mC cm⁻²) and the conformal coated sample had an underlying native air-formed oxide. As with the previous results discussed in section 4.4, it would have been expected that the dual-layer coated sample to have reduced whisker growth compared to the conformal coated only samples, as the dual-layer coated samples had the addition of an electrochemically formed oxide to aid whisker mitigation. This could suggest that the conformal coating reduces whisker growth, not only by acting as a physical barrier, but by reinforcing 'weak points' in the oxide film, effectively nullifying the advantage of having an electrochemically formed oxide over a native air-formed oxide.

Figure 6.3 c and d, again, shows that both the dual-layer and the conformal coated samples were similar in appearance, in terms of them both containing a similar number of 'bumps'. These 'bumps' could be attributed to underlying whisker growth. However, the 'bumps' on the dual-layer coated sample appear to be shallower and wider compared to those on the conformal coated sample. This could suggest that the whisker growth on the conformal coated sample is more pronounced and more likely to be large eruption or a filament-type whisker trying to penetrate through the coating, which causes a tenting effect in the coating. However, the number of 'bumps' for both samples do not match the number of features that were observed on the samples that had their conformal coatings stripped away (figure 6.3 a and b). This suggests that some of the 'bumps' may be, in part, attributed to the coating itself; for example, the 'bumps' could be areas that had a higher concentration of solids content during the coating application process or the 'bumps' may be bubbles or solid inclusions within the coating; or equally it may just be variation from sample to sample.

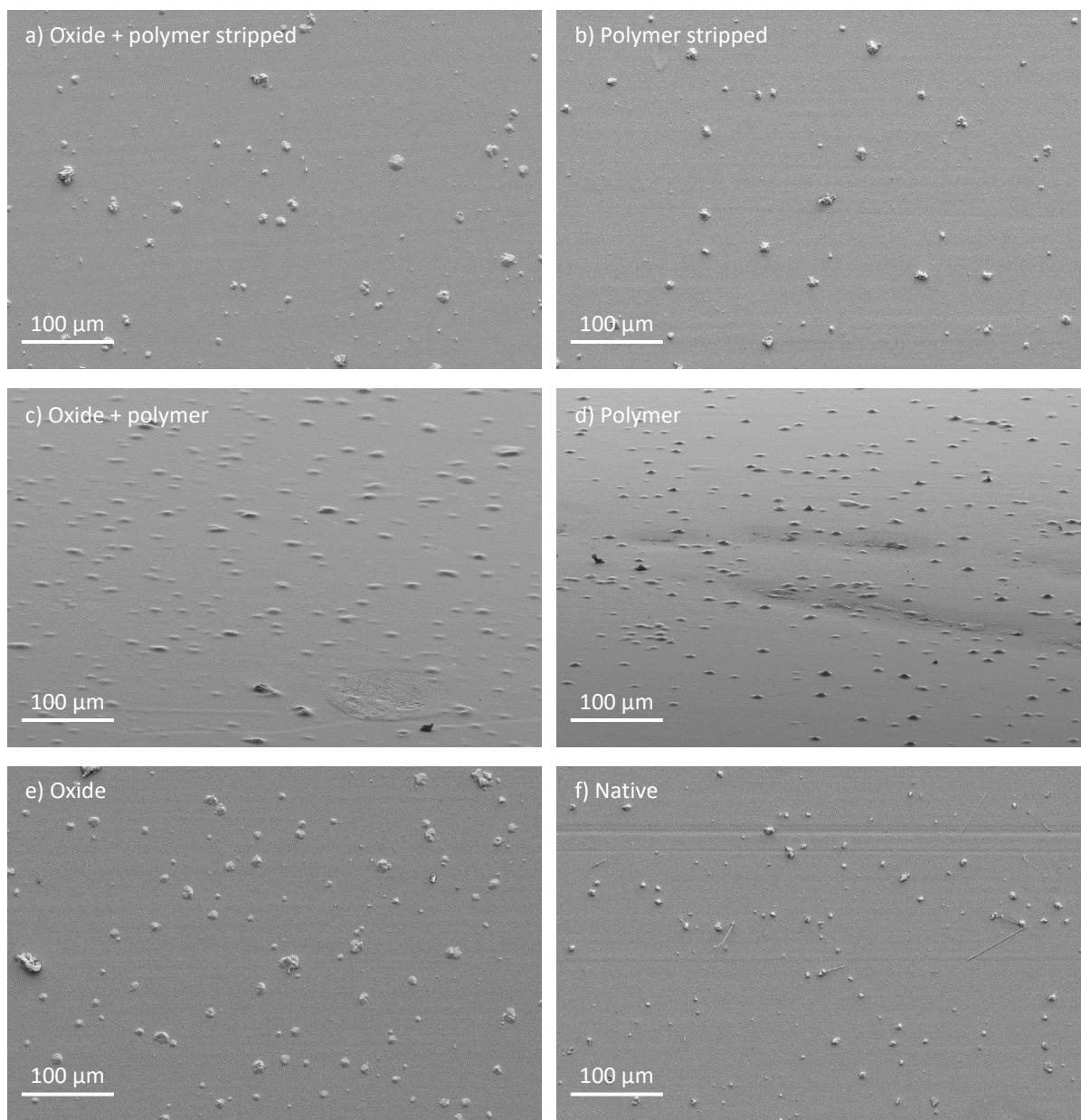


Figure 6.3 SE micrographs showing whisker formation after ~10.5 months of room temperature storage on electroplated 2 μm Sn-Cu on Cu with a) a sample that had a dual-layer system and the conformal coating stripped off, b) a sample that only had a conformal coating and had the coating stripped off, c) a sample that had a dual-layer system and was viewed at 70 ° to the stage, d) a sample that only had a conformal coating and was viewed at 70 ° to the stage, e) a sample with an electrochemically formed oxide produced at 2.0 V vs. Ag/AgCl for a charge passed of 60 mC cm⁻², and f) an untreated sample

Figure 6.3 e and f shows the whisker formation on an electrochemically oxidised (2.0 V vs. Ag/AgCl for a total charge passed of 60 mC cm⁻²) sample and a sample left to develop a native air-formed oxide, respectively. As expected, the figure shows that there are generally only eruptions on the electrochemically oxidised sample, with a small number of filament-type whisker; in contrast the untreated sample is shown to have many filament-type whiskers and not many eruptions. Comparing

figure 6.3a and 6.3e, it is shown that the dual-layer coated sample (figure 6.3a) has far fewer eruptions and nodules than the electrochemically oxidised sample (figure 6.3e). Comparing 6.3b and 6.3f, it is shown that the conformal coated sample (figure 6.3b) has fewer filament-type whiskers, eruptions and nodules than the sample left to develop a native air-formed oxide (figure 6.3f), which was, somewhat unexpected. As the sample shown in figure 6.3b also had a native air-formed oxide, so it may have been expected that growth would still occur, like with a sample that only had a native air-formed oxide, but underneath the coating.

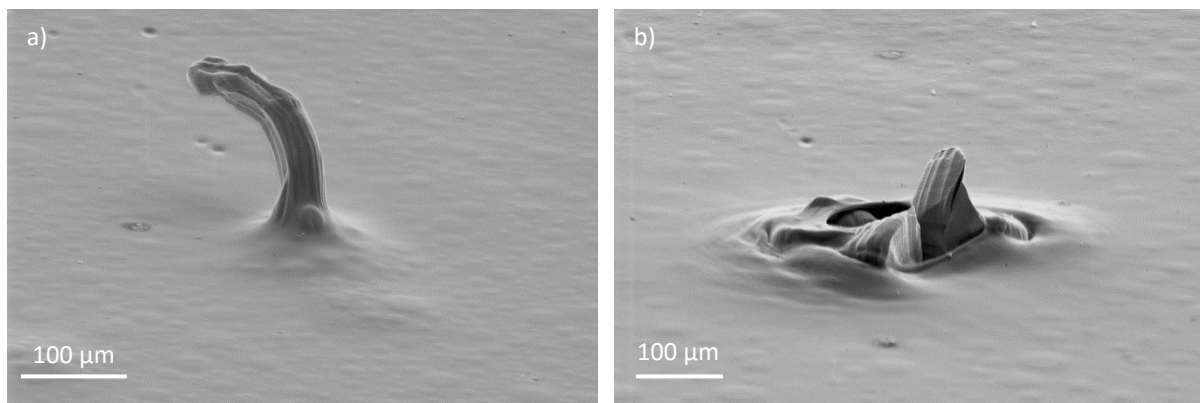


Figure 6.4 SE micrographs, taken at a tilt of 70 °, of how whiskers can interact with conformal coatings with a) a whisker growing but not penetrating the coating from a sample with a dual-layer system and b) an eruption breaking through the coating from a sample with only a conformal coating

Most of the whiskers and eruptions that were observed on the samples that had a conformal coating did not penetrate the coating. This caused the coating to stretch and effectively insulate the whisker growth, as shown in figure 6.4a. This is advantageous because if a whisker were to grow long enough on an electronic circuit to come into contact with another metal component then the whisker would be electrically insulated and would not cause a short circuit. However, some whiskers were found to have penetrated through the coating, as shown in figure 6.4b. This is disadvantageous as the whisker would no longer be electrically insulated and if it grew to a sufficient length, then it would cause a short circuit.

6.1.2 Effect of Coating Edge Coverage on Subsequent Whisker Growth

The aim of this study was to evaluate the effectiveness of the different coating systems for mitigating whisker growth at component and surface edges. This is because conformal coatings tend to suffer

from poor surface coverage at edges ¹⁴³, whereas it would be expected that an electrochemically formed oxide would be thicker at corners due to a higher current density that would be present at edges during formation ¹⁴⁴. Figure 6.5 shows the whisker growth data obtained after ~10.5 months of room temperature storage. The figure shows that for samples with an electrochemically formed oxide (2.0 V vs. Ag/AgCl for a total charge passed of 60 mC cm⁻²), the whisker density was reduced by 30.8 % compared to the untreated samples. For the conformal coated samples, the whisker density was reduced by 42.9 % compared to the untreated samples. For the dual-layer coated samples, the whisker density was reduced by 60.1 %.

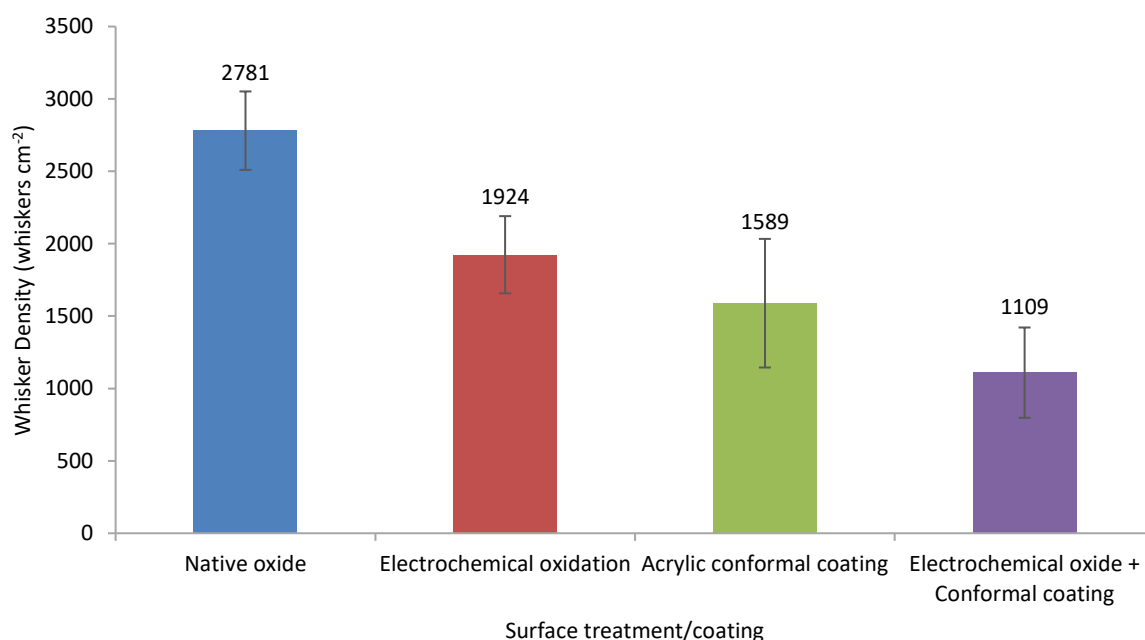


Figure 6.5 Data comparing whisker density on the edges after ~10.5 months of storage at room temperature between native oxide, electrochemical oxide, conformal coating and a dual-layer coating. With the error bars representing the standard deviation between samples

This lower than expected performance in whisker reduction may be due to several factors. One factor could be how the samples were prepared. Once the samples were cut to size (prior to electroplating) it was found that edges had a poor surface finish and were subsequently polished to obtain a flatter, higher quality finish. However, after inspection under the optical microscope this was not the case. Rather than the edges being perpendicular to the face and having one face, the edges appeared to have two different 'faces' which would have been due to poor polishing, most likely not occurring at 90 ° to the face. Polishing at an incorrect angle would have caused the edges to have varying angles

compared with each other. Another factor might have been how the whiskers were counted, in all the previous whisker growth studies each frame had an area of 0.00567 cm^2 , whereas in this study the area per frame was 0.00222 cm^2 . This suggests that smaller whiskers may have been counted that would not have been visible in the frame size used previously. This change in frame size was due to the need to use a different microscope, as the microscope that was used in the previous whisker studies was unable to view the edges due to the limitation of the working distance, therefore an inverted microscope was used which could view the edges.

As edge coverage is different for both an electrochemically formed oxide and a conformal coating, it would have been expected that the electrochemically oxidised samples would perform better at mitigating whisker growth than the conformal coated samples, however, figure 6.5 shows that this was not the case. This, somewhat, unexpected result may have been due to a thicker conformal coating being unintentionally applied which would have further reduced whisker growth. Although, the figure shows that the dual-layer coated samples performed better at mitigating whisker growth than the individual coatings did acting singularly.

7 Conclusions

7.1 Post-Electroplating Surface Treatments

7.1.1 Electrochemical Oxidation

The aim was to understand the oxidation and reduction reactions occurring on during cyclic voltammetry. The following conclusions may be made:

- An additional oxidation peak was observed during all subsequent cycles. This additional oxidation peak may suggest that an irreversible reaction is taking place during the anodic sweep of the first cycle.
- Equally, the additional oxidation peak may be the deposition of tin ions that were present in the solution due to dissolution during the anodic sweep of the first peak.
- The reduction area under the curve is much smaller than the oxidation area under the curve for the cyclic voltammograms cycled to and above 0 V vs. SCE. This may also suggest that an irreversible oxide is produced.
- The shorter cycles and the corresponding XPS data suggest that an irreversible oxide is produced within the range of 0 V – 0.6 V vs. SCE. This is shown by the presence 3rd peak in the cyclic voltammogram and the large oxide peak in the high resolution Sn3d scans.

The aim was to determine whether electrochemically formed oxides, formed at a range of potentials, were able to prevent whisker growth. The following conclusions may be made:

- The presence of an electrochemically formed oxide layer on both tin-copper deposits on copper and tin deposits on brass dramatically reduces the formation of whiskers and eruptions, compared with that of a native formed oxide.
- The thickness of the electrochemically formed oxide is greater than that of a native formed oxide.

- Electrochemical oxidation between potentials of -0.5 V – -0.83 V vs. SCE appeared to cause surface dissolution of the tin.
- The best performing electrochemically formed oxide, in terms of mitigating tin whisker growth, was produced at 2.0 V vs. SCE while passing a charge of 60 mC cm⁻².
- An electrochemical oxidation treatment not only reduces whisker density but also significantly reduces whisker length compared with an untreated surface.

The aim was to optimise the oxidation process for the potassium bicarbonate-carbonate solution and to produce the thickest oxide possible. The following conclusions may be made:

- The oxidising solution is electrochemically stable within the pH range of pH 7.87 – 9.88 and produces the same type and thickness of oxide when oxidising at 1.2 V vs. SCE.
- A freshly made solution produces the same thickness of oxide as a solution that is ~4 weeks old and has been used for ~6 samples.
- An increase in the total charge passed from 30 mC cm⁻² up to 60mC cm⁻² increased the thickness of the electrochemically formed oxide.
- Oxidation at potentials above 1.2 V vs. SCE (for an equivalent charge passed) increases the thickness of the electrochemically formed oxide. This suggests that increasing the oxidation potential above 1.2 V vs. SCE increases the efficiency of the oxidation process and also decreases the time needed.

7.1.2 Molybdate Conversion Coating

The aim was to improve the oxide thickness and improve whisker mitigation compared with the previously formed electrochemical oxides. The following conclusions may be made:

- Conversion coating treatments may be used to develop oxides that are significantly thicker than those that have been achieved to date by an electrochemical oxidation method.
- Two samples are needed to 'bed in' the bath. These two samples will then be discarded.

- Increasing the immersion time will further increase the coating thickness
- The optimum pH level of the bath for producing a thick coating is pH 2. However, a coating produced in a bath with a pH of 1 may produce a coating with a higher level of mixed oxides.
- Increased film thickness can be achieved by using electrochemical methods compared with simple immersion techniques.
- Initial observations show that molybdate conversion coatings provide improved whisker mitigation compared with electrochemically oxidised surfaces.
- Compared with the tungstate conversion coatings, an increased density of long, wide, deep cracks are formed on molybdate conversion coated samples produced at -0.6 V and -0.75 V vs. Ag/AgCl, which reduces their ability to mitigate whisker growth.
- Although the molybdate coatings produced at -0.6 V vs. Ag/AgCl had a high density of cracks, to date they mitigate whisker growth as effectively as an electrochemically formed oxide.
- A thicker coating doesn't necessarily provide improved whisker mitigation since the presence of defects within the coating will strongly influence its ability to mitigate whisker growth.

7.1.3 Tungstate Conversion Coating

The aim was to improve the oxide thickness and improve whisker mitigation compared with the previously formed electrochemical oxides. The following conclusions may be made:

- A tungstate conversion coating is much thicker than both the electrochemically formed oxides, produced at 2.0 V vs. SCE while passing a charge of 60 mC cm^{-2} , and the immersed molybdate coatings, produced at 9 minutes in a bath at pH 3.
- Increasing the total charge passed for the same current density will further increase the coating thickness.
- Increasing the total charge passed for samples produced at 10 mA cm^{-2} past a certain point will cause the coating to flake off. However, decreasing the current density while keeping the equivalent charge passed will improve the surface finish and reduce the number of defects.

- Initial observations show that tungstate conversion coatings provide improved whisker mitigation compared with electrochemically oxidised surfaces.
- Most whiskers were observed to grow from areas of the coating where the oxide was thinner or completely absent ('weak points'). Further optimisation of processing parameters (current density, number of cycles) is required to avoid the formation of 'weak points' in the oxide coating
- A thicker coating doesn't necessarily provide improved whisker mitigation since the presence of defects within the coating will strongly influence its ability to mitigate whisker growth.

7.2 Dual-Layer Trials

The aim was to improve on the whisker mitigation for both electrochemical oxide coatings and unmodified acrylic coatings. The following conclusion may be made:

- Whisker growth studies after ~9 weeks of room temperature storage showed that having both an electrochemically formed oxide and an unmodified acrylic coating further increased whisker mitigation compared with using the coatings singularly and gave a whisker reduction of 99.8 % compared to the untreated samples.
- Whisker growth studies after ~14 months of room temperature, however, showed that having a dual-layer system did not perform as well as a conformal coating by itself. Although, the dual-layer system still gave good whisker mitigation and reduced whisker growth by 84 % compared to the untreated samples.
- Studying the effect of edge coverage for coating systems on whisker growth after ~10.5 months of room temperature, showed that having a dual-layer system will perform better at mitigating whisker growth than using the coatings individually. However, the samples with only a conformal coating performed better than the electrochemically oxidised samples, which was unexpected.

8 Further Work

This chapter will focus on what work should be carried out in the future, to progress what has already been done in this study and why it should be carried out.

8.1 Post-Electroplating Surface Treatments

For the post-electroplating surface treatments the main aim for future work should be to further improve whisker mitigation. This may be achieved by increasing the coating thickness and/or improving the quality of the coating. The future work for both the electrochemical oxidation studies and the conversion coating studies will be discussed.

8.1.1 Electrochemical Oxidation

- Carry out the same 12 month experiment, analysing both the whisker growth and oxide growth, along with analysing the intermetallic compound (IMC) growth. The IMC growth analysis should be done on both pure tin on copper and tin-copper on copper; this is so to analyse the difference between the two electroplated coatings in terms of IMC growth, specifically how the copper alloying component effects IMC growth. This can be done by using both the focused ion beam scanning electron microscope (FIBSEM), to create and analyse a cross-section, as well as electrochemically stripping the tin to reveal the IMC growth across the entire sample. After stripping the sample, it can then be analysed using SEM and the micrographs obtained can be used to determine an estimated percentage of how much surface area is covered by IMC growth, at the interface between the electroplated coating and the substrate. This will show how the IMC growth changes with time and if the growth correlates with how the whisker growth changes with time, i.e. when the IMC growth begins to reduce, does the whisker growth also begin to reduce as the driving force for whisker growth will increase at a reduced rate. Repeating this experiment will also allow for the whisker growth and oxide growth to be analysed for the full amount of time. It was not

possible for this to be done in this study as Thermo-Scientific K-Alpha X-ray Photoelectron Spectrometer, used for x-ray photoelectron spectroscopy (XPS), was out of service for several months.

- Study the effects of increasing the oxidation potential and increasing the charge passed on the thickness of the electrochemically formed oxide and whisker growth. This will show whether the oxide thickness can be further increased compared what was used in this study. Increasing the thickness may further improve whisker mitigation. However, it was shown that increasing the potential from 1.2 V to 2.0 V vs. Ag/AgCl only slightly improved whisker mitigation, therefore the potential may, again, only slightly improve whisker mitigation.
- The results discussed in section 4.4.5 showed that storing samples at increased temperature and relative humidity will reduce whisker growth for samples with a native air-formed oxide, compared to those stored at room temperature; however, storing electrochemically oxidised samples will increase whisker growth, compared to those stored at room temperature. To further understand why this may be occurring, analysis of the intermetallic formation and oxide film growth should be carried out for samples that have been stored at room temperature and at elevated temperatures and relative humidity.
- The results discussed in section 5.1.2 showed that the tungstate conversion coatings were comprised primarily of tin oxide with only a small amount of tungsten present. This may suggest that a pure tin oxide coating could be produced to a similar thickness using the same reverse current pulse technique. The results discussed in section 5.2.2 showed that the tungstate conversion coatings mitigated whisker growth better than an electrochemically formed oxide produced at 2 V vs. Ag/AgCl for a charge passed of 60 mC cm^{-2} . These results may suggest the whisker mitigation may be further improved if a pure tin oxide can be produced, using the same parameters, to a similar thickness as the tungstate conversion coatings. To investigate this, the same potassium bicarbonate-potassium carbonate bath should be used to produce the coatings.

8.1.2 Conversion Coatings

- The results for both the molybdate and tungstate conversion coatings showed enhanced whisker mitigation compared with an electrochemically formed oxide. This could lead into further investigation into other conversion coating systems, such as zincates and chromates. Equally, different types of passivation treatments could be investigated such as anodisation. Anodisation of tin could potentially produce even thicker coatings compared with the conversion coatings that were produced in this study. An anodised coating may also improve adhesion for the application of a conformal coating on top, due to the microstructure of anodised surfaces¹⁵⁸. An anodised coating will differ from the electrolytic oxides produced in this work by using much higher potentials and purposely creating a porous structure so as to aid with adhesion, such as the coatings producing by Zaraska *et al*¹⁵⁸.
- It would be interested to see if a mixed conversion coating could be produced. The baths used for both molybdate and tungstate conversion coatings are based on sodium salts, which may suggest that the two could be combined and a mixed conversion coating, of molybdate and tungstate, could be deposited.
- The results discussed in chapter 5 showed that tungstate coatings have enhanced whisker mitigation compared with an electrochemically formed oxide. The results also showed that the quality and thickness of the coating could be improved by decreasing the current density. Further investigation should be carried out to optimise the parameters, so to produce the thickest coating possible while containing no visible defects. This should further improve whisker mitigation. Such optimisation may include, lowering the reverse current density to enable more charge to be passed, thus creating thicker coatings; varying the frequency, as this was not analysed during this study; and varying the maximum number of cycles further, for each of the reverse current densities used, so enabling an optimisation point for each reverse current density.

- The results discussed in chapter 5 showed that the best performing molybdate coating (in terms of whisker mitigation) was produced at -0.45 V vs. Ag/AgCl for 5 min; however, this was a relatively thin coating compared with the other molybdate conversion coatings. Further investigation should be carried out to see if the thickness of coating produced using this potential can be increased and without any visible defects. If so, this may improve whisker mitigation.

8.2 Developing Dual-Layer Systems

The main aim for future work of developing dual-layer systems should be to create the most efficient whisker mitigation system. This may be achieved by studying different coating pairs, such as studying the differences between using an electrochemically formed oxide to using a conversion coating as the bottom layer. The final aim should be, however, to successfully create a self-healing polymer that will be used in conjunction with the most efficient (in terms of whisker mitigation) post-electroplating surface treatment.

- The results discussed in chapter 5 showed that both conversion coatings mitigated whisker growth better than an electrochemically formed oxide. This may suggest that using a conversion coating instead of an electrochemically formed oxide in a dual-layer system will further enhance whisker mitigation compared with the results shown in chapter 6.
- The adhesion between the conformal coating and the bottom layer (either electrochemical oxide or conversion coating) should be studied. This can be done by carrying out a peel test to see how much force is needed to peel the conformal coating off the bottom coating. The adhesion can also be affected by the surface topography, whereby a rough surface will promote mechanical interlocking. However, if the roughness is on the nano-scale then the coating may not adhere as the surface may not be wettable. To study this, contact angle can be carried to measure the wettability of the bottom layer. A low contact angle will correlate

to good wetting and the coating will cover the sample easily, however, a high wetting angle will correlate to poor wetting and the coating may not cover the sample sufficiently.

9 References

1. Tu K-N. Irreversible processes of spontaneous whisker growth in bimetallic Cu-Sn thin film reactions. *Phys. Rev.* 1994;49(3):2030–2034.
2. Galyon GT. Annotated Tin Whisker Bibliography and Anthology. *Trans. on Elect. Pack. Manu.* 2005;28(1):94–122.
3. Cobb HL. Cadmium whiskers. *Monthly Rev. Am. Electroplaters Soc.* 1946;33(28):28–30.
4. Compton KG, Medizza A, Arnold SM. Filamentary growths on metal surfaces – whiskers. *Corrosion.* 1951;7(10):327–334.
5. Osterman M. Mitigation strategies for tin whiskers. CALCE EPSC. 2002 [accessed 2015 Jun 8]. <http://www.calce.umd.edu/tin-whiskers/TINWHISKERMITIGATION.pdf>
6. Wickham M, Lea D, Nottay J, Hunt C. Processability of lead-free component termination materials. 2001.
7. Boettinger WJ, Johnson C, Bendersky L, Moon K, Williams M, Stafford G. Whisker and hillock formation on Sn, Sn-Cu and Sn-Pb electrodeposits'. *Acta Materialia.* 2005;53(19):5033–5050.
8. Tu K-N, Zeng K. Reliability Issues of Pb-free Solder Joints in Electronic Packaging Technology. *Proceedings of the IEEE Electronic Components and Technology Conference.* 2002:1194–1200.
9. Tu K-N, Suh J, Wu AT-C, Tamura N, Tung C-H. Mechanism and Prevention of Spontaneous Tin Whisker Growth. *Mat. Trans.* 2005;46(11):2300–2308.
10. Tu K-N, Chen C, Wu AT. Stress analysis of spontaneous Sn whisker growth. *J. Mat. Sci.* 2007;18(1–3):269–281. doi:10.1007/978-0-387-48433-4_18
11. NASA. NASA Whiskers. [accessed 2015 Jun 8]. <http://nepp.nasa.gov/whisker/photos/index.html>
12. Speck T, Mülhaupt R, Speck O. Self-Healing in Plants as Bio-Inspiration for Self-Healing Polymers. In: Binder WH, editor. *Self-Healing Polymers From Principles to Applications.* Wiley-VCH Verlag GmbH;

2013. p. 61–90.

13. Lee MW, An S, Jo HS, Yoon SS, Yarin AL. Self-Healing Nano fiber-Reinforced Polymer Composites.

1. Tensile Testing and Recovery of Mechanical Properties. *Appl. Mat. & Interfaces*. 2015;7(35):19546–19554. doi:10.1021/acsami.5b05998

14. Döhler D, Michael P, Binder WH. Principles of Self-Healing Polymers. In: Binder WH, editor. *Self-Healing Polymers From Principles to Applications*. Wiley-VCH Verlag GmbH; 2013. p. 7–60.

15. Witze A. Seawater is the secret to long-lasting Roman concrete. *Nature*. 2017.

16. Van Tittelboom KV, Gruyaert E, Rahier H, De Belie N. Influence of mix composition on the extent of autogenous crack healing by continued hydration or calcium carbonate formation. *Construction and Building Materials*. 2012;37:349–359.

17. Bekas DG, Tsirka K, Baltzis D, Paipetis AS. Self-healing materials : A review of advances in materials, evaluation, characterization and monitoring techniques. *Composites Part B*. 2016;87(1):92–119. doi:10.1016/j.compositesb.2015.09.057

18. Brown EN, Kessler MR, Sottos NR, White SR. In situ poly (urea-formaldehyde) microencapsulation of dicyclopentadiene. *J. Microencapsulation*. 2003;20(6):719–730. doi:10.1080/0265204031000154160

19. Blaiszik B., Sottos NR, White SR. Nanocapsules for self-healing materials. *Composites Sci. & Tech*. 2008;68:978–986. doi:10.1016/j.compscitech.2007.07.021

20. Jackson AC, Bartelt JA, Marczewski K, Sottos NR, Braun P V. Silica-Protected Micron and Sub-Micron Capsules and Particles for Self-Healing at the Microscale a. *Macromol. Rapid Commun*. 2011;32:82–87. doi:10.1002/marc.201000468

21. Ashworth MA, Haspel D, Wu L, Wilcox GD, Mortimer RJ. An Investigation into the Effect of a Post-electroplating Electrochemical Oxidation Treatment on Tin Whisker Formation. *J. Electron. Mat*. 2015;44(1):442–456. doi:10.1007/s11664-014-3396-7

22. Haspel DM, Ashworth MA, Wu L, Wilcox GD, Mortimer RJ. Tin whisker mitigation by means of a post- electroplating electrochemical oxidation treatment. Transactions of the IMF. 2015;93(6):332–341. doi:10.1080/00202967.2015.1117258
23. Han S, Osterman M, Pecht M. Likelihood of Metal Vapor Arc by Tin Whiskers. SMT Magazine. 2012 Aug:48–56.
24. Van Westerhuyzen D, Backes P, Linder J, Merrell S, Poeschel R. Tin whisker induced failure in vacuum. In: Proc. of Inter. Sym. for Testing and Failure Analysis. 1992. p. 407–412.
25. Peach MO. Mechanism of growth of whiskers on cadmium'. J. Appl. Phys. 1952;23(12):1401–1403.
26. Koonce SE, Arnold SM. Growth of metal whiskers. J. Appl. Phys. 1953;24(3):363–366.
27. Williams M, Moon K, Boettinger W, Josell D, Deal A. Hillock and whisker growth on Sn and SnCu electrodeposits on a substrate not forming interfacial intermetallic compounds. J. Electron. Mat. 2007;36(3):214–219.
28. Yao ZX, Yin LM, Zhang LP, Zhou J. The Effect of Coating Thickness and External Force on the Growth of Tin Whisker. In: 15th International Conference on Electronic Packaging Technology. 2014. p. 1100–1103.
29. Bušek D, Vávra J, Dušek K. Whisker Growth and its Dependence on Substrate Type and Applied Stress. In: 39th International Spring Seminar on Electronics Technology (ISSE). 2016. p. 263–266.
30. Shin J, Chason E. Stress behavior of electroplated Sn films during the thermal cycling. J. Mat. Res. 2009;24(4):1522–1528.
31. Shin S-J, Kim J-J, Son YK. Analysis of plating grain size effect on whisker. J. Mech. Sci. & Tech. 2009;23(11):2885–2890.
32. Chason E, Jadhav N, Chan WL, Reinbold L, Kumar KS. Whisker formation in Sn and Pb-Sn coatings; Role of intermetallic growth, stress evolution, and plastic deformation processes. Appl. Phys. Lett. 2008;92(17):171901-171901–3.

33. Tu K-N. Interdiffusion and reaction in bimetallic Cu-Sn thin films. *Acta Metallurgica*. 1973;21(4):347–354.
34. Stuttle CJ, Ashworth MA, Wilcox GD, Mortimer RJ. Characterisation of tin-Copper intermetallic growth in electrodeposited tin coatings using electrochemical oxidation techniques. *Transactions of the IMF*. 2014;92(5):272–281. doi:10.1179/0020296714Z.000000000174
35. Dyson F, Anthony TR, Turnbull D. Interstitial Diffusion of Copper in Tin. *J. Appl. Phys.* 1967;38:3408.
36. He A, Ivey DG. Microstructural study of Sn films electrodeposited on Cu substrates: Sn whiskers and Cu₆Sn₅ precipitates. *J. Mat. Sci.* 2015;50(7):2944–2959. doi:10.1007/s10853-015-8859-6
37. Glazunova VK, Kudryavstev NT. An Investigation of the Conditions of Spontaneous Growth of Filiform Crystals on Electrolytic Coatings. *J. Appl. Chem. USSR*. 1963;36(3):543–550.
38. Sakuyama S, Kutami M. Substitute Materials for Complete Elimination of Hazardous Substances – Study of Whisker Growth on Lead-free Plating. *FUJITSU Sci. Tech. J.* 2005;41(2):217–224.
39. Ashworth MA, Wilcox GD, Higginson RL, Heath RJ, Liu C. An investigation into Zinc diffusion and tin whisker growth for electroplated tin deposits on brass. *J. Electron. Mat.* 2014;43(4):1005–1016. doi:10.1007/s11664-014-2983-y
40. Boguslavsky I, Bush P. Recrystallization Principles Applied to Whisker Growth in Tin. In: *Proc. of APEX Conference*. 2003.
41. Lee BZ, Lee DN. Spontaneous growth mechanism of tin whiskers. *Acta Materialia*. 1998;46(10):3701–3714.
42. Su C-H, Chen H, Lee H-Y, Liu CY, Ku C-S, Wu AT. Kinetic Analysis of Spontaneous Whisker Growth on Pret-treated Surfaces with Weak Oxide. *J. Electron. Mat.* 2014;43(9):3290–3295.
43. Kim KS, Yu CH, Yang JM. Tin whisker formation of lead-free plated leadframes. *Microelectronics Reliability*. 2006;46(1):1080–1086.
44. Illés B, Horváth B, Shinohara T, Harsányi G. Tin Whisker Growth from Sn-Cu (0-5 wt%) Surface

Finishes. In: IEEE 17th International Symposium for Design and Technology in Electronic Packaging (SIITME). 2011. p. 49–54.

45. Han S-W, Kim K-S, Yu C-H, Osterman M, Pecht M. Observations of the Spontaneous Growth of Tin Whiskers in Various Reliability Conditions. In: Proceedings of Electronic Components and Technology Conference. 2008. p. 1484–1490.

46. Chen K, Wilcox GD. Observations of the Spontaneous Growth of Tin Whiskers on Tin-Manganese Alloy Electrodeposits. *Phys. Rev. Lett.* 2005;94(6):66104-66104-4.

47. Illés B, Horváth B, Géczy A, Krammer O, Dušek K. Corrosion-Induced Tin Whisker Growth in Electronic Devices: A Review. *Soldering & Surface Mount Technology.* 2017;29(1):59–68.

48. Schroeder V, Alto P, Bush P, Williams M, Vo N. Tin Whisker Test Method Development. *IEEE Trans. on Elect. Pack. Man.* 2006;29(4):231–238.

49. Oberhoff P, Dittes M, Crema P, Su P, Yu E. Humidity Effects on Sn Whisker Formation. *IEEE Trans. on Elect. Pack. Man.* 2006;29(4):239–245.

50. Smetana J. Theory of Tin Whisker Growth: The End Game. *IEEE Trans. on Elect. Pack. Man.* 2007;30(1):11–22.

51. Nakadaira Y, Jeong S, Shim J, Seo J, Min S, Cho T, Kang S, Oh S. Growth of Tin Whiskers for Lead-Free Plated Leadframe Packages in High Humid Environments and During Thermal Cycling. *Microelectronics Reliability.* 2007;47(12):1928–1949.

52. Illés B, Horváth B, Harsányi G. Effect of Strongly Oxidising Environment on Whisker Growth From Tin Coating. *Surf. & Coat. Tech.* 2010;205(7):2262–2266.

53. Horváth B, Illés B, Shinohara T, Harsányi G. Copper-Oxide Whisker Growth on Tin-Copper Alloy Coatings Caused by the Corrosion of Cu₆Sn₅ Intermetallics. *J. Mat. Sci.* 2013;48(23):8052–8059.

54. Mathew S, Osterman M, Shibutani T, Yu Q, Pecht M. Tin Whiskers: How to Mitigate and Manage the Risks. In: Proc. IEEE Int. Sym. High Density Packag. Microsyst. Integr. 2007. p. 1–8.

55. Dittes M, Oberhoff P, Petit L. Tin whisker formation-results, test methods, and countermeasures. In: Proc. IEEE Electronic Components and Technology Conf. 2003. p. 822–826.
56. Zhang Y, Xu C, Abys J, Vysotskaya A. Understanding Whisker Phenomenon: Whisker Index and Tin/Copper, Tin/Nickel Interface. In: Proc. IPC SMEMA Council APEX. 2002.
57. Xu C, Zhang Y, Fan C, Abys JA. Driving Force for the Formation of Sn Whiskers: Compressive stress –Pathways for Its Generation and Remedies for Its Elimination and Minimization. IEEE Trans. On Elec. Pack. Manu. 2005;28(1):31–35.
58. Nicolet M-A. Ternary Amorphous Metallic Thin Films as Diffusion Barriers for Cu Metallization. Appl. Surf. Sci. 1995;91:269–276.
59. Chu JP, Huang JC, Jang JSC, Wang YC, Liaw PK. Tin Film Metallic Glasses: Preparations, Properties, and Applications. Journal of the Minerals, metals and Materials Society. 2010;62(4):19–24.
60. Chu JP, Jang JSC, Huang JC, Chou HS, Yang Y, Ye JC, Wang YC, Lee JW, Liu FX, Liaw PK, et al. Thin Film Metallic Glasses: Unique Properties and Potential Applications. Thin Solid Films. 2012;520(16):5097–5122.
61. Diyatmika W, Chu JP, Yen YW, Chang WZ, Hsueh CH. Thin Film Metallic Glass as an Underlayer for Tin Whisker Mitigation: A Room-Temperature Evaluation. Thin Solid Films. 2014;561:93–97.
62. Fukuda Y, Osterman M, Pecht M. The Effect of Annealing on Tin Whisker Growth. IEEE Trans. On Elec. Pack. Manu. 2006;29(4):252–258.
63. Leidecker H, Kadesch JS. Effects of Uralane Conformal Coating on Tin Whisker Growth. In: Proc. The 37th IMAPS Nordic Annual Conf. 2000. p. 108–116.
64. Kadesch JS, Brusse J. The Continuing Dangers of Tin Whiskers and Attempts to Control them with Conformal Coat. NASA's EEE Links Newsletter. 2001.
65. Woodrow T, Ledbury E. Evaluation of Conformal Coatings as a Tin Whisker Mitigation Strategy. In: IPC/JEDEC 8th International Conference on Pb-Free Electronic Components and Assemblies. 2005.

66. Woodrow T, Ledbury E. Evaluation of Conformal Coatings as a Tin Whisker Mitigation Strategy, Part 2. In: Proc. of SMTA International Conf. 2006.
67. Schetty R. Electrodeposited Tin Properties & Their Effect on Component Finish Reliability. In: Proc. IEEE Inter. Conf. on the Business of Electronic Product Reliability and Liability. 2004. p. 29–34.
68. Lal S, Moyer TD. Role of Intrinsic Stresses in the Phenomena of Tin Whiskers in Electrical Connectors. IEEE Trans. on Elect. Pack. Man. 2005;28(1):63–74.
69. Suganuma K, Kim KS, Yorikadol Y, Tsujimoto M, Yanada I. Prevention of Sn Whisker Formation by Surface Treatment off Sn Plating. In: 136th TMS Annual Meeting & Exhibition. 2007.
70. Takeuchi M, Kamiyama K, Suganuma K. Suppression of Tin Whisker Formation on Fine Pitch Connectors by Surface Roughening. J. Electron. Mat. 2006;35(11):1918–1925.
71. Wu L. A Study of the Oxide Chemistry and Whisker Growth on Tin Coatings using sequential Electrochemical Reduction Analysis. Loughborough University; 2012.
72. Haspel D. An Investigation of Electrochemical Oxidation as a Potential Strategy for the Mitigation of Tin Whiskers. Loughborough University; 2013.
73. Arnold SM. Repressing the Growth of Tin Whiskers. Plating. 1966;53(1):96–99.
74. The European Parliament and The Council of The European Union. Directive 2002/95/EC of the European Parliament and the Council of 27 January 2003 on the restriction of hazardous substances directive. Official Journal of the European Union. 2003;46(February):L37 19--23.
75. Zhang R, Zhang J, Evans J, Johnson W, Vardaman J, Fujimura I, Tseng A, Knight J. Tin-bismuth plating for component finishes. In: Proceedings - Electronic Components and Technology Conference. 2011. p. 2060–2066. doi:10.1109/ECTC.2011.5898801
76. Jordan M. The Electrodeposition of Tin and its Alloys. Eugen G. Leuze Publishers; 1995.
77. Akhlaghi S, Ivey D. Effect of processing parameters on the electroplating of Au-Sn solders. J. Plat. & Surf. Fin. 2003;90(7):36–39.

78. Samel MAF. The electrodeposition of tin and lead-tin based alloys. Loughborough University; 1984.
79. Dini JW. Electrodeposition: The Materials Science of Coatings and Substrates. First. Park Ridge, NJ: Noyes Publications; 1994. doi:10.1002/adma.19940060127
80. Reiger PH. Electrochemistry. Second. New York: Springer; 1994.
81. Solderability. [accessed 2015 Jun 9]. <http://www.efunda.com/materials/solders/solderability.cfm>
82. CES EduPack. 2012.
83. Díaz R, Díez-Pérez I, Gorostiza P, Sanz F, Morante JR. An Electrochemical Study of Tin Oxide Thin Film in Borate Buffer Solutions. *J. Braz. Chem. Soc.* 2003;14(4):523–529.
84. Callister WD. Materials and Engineering An Introduction. Seventh. John Wiley & Sons Inc; 2007.
85. Ganley J.C. High Temperature and Pressure Alkaline Electrolysis. *Inter. J. Hydrogen Energy.* 2009;34(9):3604–3611.
86. Gabe DR. Mixed oxide films on tin. *Surf. Tech.* 1977;5(6):463–478.
87. Andrienko D. Cyclic Voltammetry. 2008 [accessed 2015 Jun 8]. http://www2.mpip-mainz.mpg.de/~andrienk/journal_club/cyclic_voltammetry.pdf
88. Kissinger PT, Lafayette W, Heineman WR. Cyclic Voltammetry. *J. Chem. Edu.* 1983;6(9):702–706.
89. Alvarez P, Ribotta S, Folquer M. Potentiodynamic behaviour of tin in different buffer solutions. *Corr. Sci.* 2002;44(1):49–65.
90. Drogowska M, Ménard H, Brossard L. Electrochemical behaviour of tin in bicarbonate solution at pH 8. *J. Appl. Electrochem.* 1991;21(1):84–90.
91. Gervasi CA, Varela FE, Vilche JR, Alvarez PE. Investigations of the electroreduction process of anodic films grown on tin in carbonate-bicarbonate solutions. *Electrochimica Acta.* 1997;42(4):537–547.
92. Wilcox GD, Gabe DR, Warwick ME. The Development of Passivation Coatings by Cathodic

Reduction in Sodium Molybdate Solutions. *Corr. Sci.* 1988;28(6):577–586.

93. Zhang S, Yang B, Kong G, Lu J. Electrochemical analysis of molybdate conversion coating on hot-dip galvanized steel in various growth stages. *Surface and Interface Analysis*. 2017. doi:10.1002/sia.6210

94. da Silva CG, Margarit-Mattos ICP, Mattos OR, Perrot H, Tribollet B, Vivier V. The molybdate-zinc conversion process. *Corrosion Science*. 2009;51(1):151–158. doi:10.1016/j.corsci.2008.10.019

95. Wu L, Ashworth MA, Wilcox GD. Zinc Whisker Growth from Electroplated Finishes - A Review. *The Intern. J. Surf. Eng. & Coat.* 2015;93(2):66–73.

96. Arnold SM. The Growth and Properties of Metal Whiskers. In: 43rd Annual Convention of the American Electroplater's Society, Washington, DC, USA. 1956. p. 26–31.

97. Sugiarto H, Christie IR, Richards BP. Studies of Zinc Whiskers Formation and Growth from Bright Zinc Electrodeposits. *Trans. Inst. Met. Finish.* 1984;62:92–97.

98. European Parliament and Council. Directive 2000/53/EC of the European Parliament and the Council of 18 September 2000 on end-of life vehicles. *Official Journal of the European Union*. 2000;L269(34).

99. Van De Leest RE, Krijl G. A Tungstate Conversion Coating On Tin. *Thin Solid Films*. 1980;72:237–246.

100. Wilcox GD, Gabe DR, Warwick ME. The Role of Molybdates in Corrosion Prevention. *Corr. Rev.* 1986;6(4):327–365.

101. Wilcox GD, Gabe DR. Passivation Studis Using Group VIA Anions - Part IV: Cathodic Redox Reactions and Film Formation. *British Corr. J.* 1984;19(4):196–200.

102. Jahan F, Smith BE. Characterization of Molybdenum Black Coatings on Zinc Substrates. *J. Mat. Sci.* 1997;32(14):3869–3874.

103. Gabe DR, Gould SE. Black molybdate conversion coatings. *Surf. & Coat. Tech.* 1988;35:79–91.

104. Robertson WD. Molybdate and Tungstate As Corrosion Inhibitors and the Mechanism of Inhibition. *J. Electrochem. Soc.* 1951;98:94–100.
105. da Silva CG, Correia AN, de Lima-Neto P, Margarit ICP, Mattos OR. Study of Conversion Coatings Obtained from Tungsten-Phosphoric Acid Solution. *Corr. Sci.* 2005;47(3):709–722.
106. Wicks ZW, Jones FN, Pappas SP. *Organic Coatings: Science and Technology – Volume 1: Film Formulation, Components and Appearance.* John Wiley & Sons Inc; 1992.
107. Wicks ZW, Jones FN, Pappas SP. *Organic Coatings: Science and Technology Third Edition.* John Wiley & Sons Inc; 2007.
108. Kopeliovich D. Enhancement of adhesion. 2014 [accessed 2016 Jan 18]. http://www.substech.com/dokuwiki/doku.php?id=enhancement_of_adhesion
109. Wicks ZW, Jones FN, Pappas SP. *Organic Coatings: Science and Technology – Volume 2: Applications, Properties, and Performance.* John Wiley & Sons Inc; 1994.
110. Levinson SB. *Application of Paints and Coatings.* Federation of Societies for Coatings Technology; 1988.
111. Organic Chemistry. [accessed 2016 Jan 18]. <https://sites.google.com/site/chemistrysite/ch-8---organic-chemistry>
112. Beck F. Electrodeposition of polymer coatings. *Electrochimica Acta.* 1988;33(7):839–850.
113. Helmenstine AM. Functional Groups. [accessed 2016 Jan 18]. <http://chemistry.about.com/od/organicchemistry/ig/Functional-Groups/>
114. Smith RE, Boyd DW. No Title. *J. Coat. Tech.* 1988;60(756):77.
115. Miranda TJ. No Title. *J. Coat. Tech.* 1988;60(782):47.
116. iCVD. [accessed 2016 Jun 15]. <http://web.mit.edu/gleason-lab/iCVD.html>
117. oCVD. [accessed 2016 Jun 15]. <http://web.mit.edu/gleason-lab/oCVD.html>

118. Tenhaeff WE, Gleason KK. Initiated and Oxidative Chemical Vapour Deposition of Polymeric Thin Films: iCVD and oCVD. *Advance Functional Materials*. 2008;18(7):979–992.
119. IPC-HDBK-830: Guidelines for Design, Selection and Application Coatings.
120. Licari JJ, Hughes LA. *Handbook of Polymer Coatings for Electronics: Chemistry, Technology and Applications*. Noyes Publications; 1990.
121. Silicones. 2013 [accessed 2016 Jan 18].
<http://www.essentialchemicalindustry.org/polymers/silicones.html>
122. Pauling L. *Nature of the Chemical Bond*. Cornell University Press; 1960.
123. Polyurethanes. 2013 [accessed 2016 Jan 18].
<http://www.essentialchemicalindustry.org/polymers/polyurethane.html>
124. No Title. [accessed 2013 Dec 5]. <http://chem.chem.rochester/~chem424/ppx.htm>
125. What is Parylene? [accessed 2016 Jan 18]. http://www.conformal-coating.com/parylene_coating.htm
126. Han S, Osterman M, Meschter S, Pecht M. Evaluation of Effectiveness of Conformal Coatings as Tin Whisker Mitigation. *J. Electron. Mat.* 2012;41(9):2508–2518.
127. Hunt C, Wickham M. Mitigation Of Tin Whiskers With Polymer Coatings. In: 2010 Intern. Symp. on Adv. Pack. Mat. 2010.
128. Hong WS, Oh CM, Kim DS. Mitigation and Verification Methods for Sn Whisker Growth in Pb-Free Automotive Electronics'. *J. Electron. Mat.* 2012;42(2):332–347.
129. Samadzadeh M, Hatami Boura S, Peikari M, Kasiriha SM, Ashrafi A. A review on self-healing coatings based on micro/nanocapsules. *Progress in Organic Coatings*. 2010;68(1):159–164.
130. Zhang MQ, Rong MZ. Theoretical Consideration and Modeling of Self-Healing Polymers. *J. Poly. Sci. Prt. B. Poly. Phys.* 2012;50(4):229–241. doi:10.1002/polb.22387
131. Boiko YM, Homme REP. Surface Mobility and Diffusion at Interfaces of Polystyrene in the Vicinity

- of the Glass Transition. *J. Poly. Sci. Part. B. Poly. Phys.* 1997;36(4):567–572.
132. Wool RP, O'Connor KM. A theory of crack healing in polymers. *J. Appl. Phys.* 1981;52(10):5953–5963.
133. Wool RP. Self-healing materials: a review. *Soft Matter.* 2008;4(3):400–418. doi:10.1039/b711716g
134. Wu DY, Meure S, Solomon D. Self-healing polymeric materials: A review of recent developments. *Prog. Poly. Sci.* 2008;33(5):479–522. doi:10.1016/j.progpolymsci.2008.02.001
135. What is Biomimicry? [accessed 2016 Jun 2]. https://biomimicry.org/what-is-biomimicry/#.V1A43_krKUK
136. Benyus JM. *Biomimicry: Innovation Inspired by Nature.* William Morrow & Company; 2002.
137. White SR, Blaiszik BJ, Kramer SLB, Olugebefola SC, Moore JS, Sottos NR. Self-healing polymers and composites. *American Scientist.* 2011;99(5):392–399. doi:10.1146/annurev-matsci-070909-104532
138. Diesendruck CE, Sottos NR, Moore JS, White SR. Biomimetic Self-Healing. *Angew. Chem. Int. Ed.* 2015;54:10428–10447. doi:10.1002/anie.201500484
139. Nellesen A, Von Tapvicza M, Bertling J, Schmidt AM, Bauer G, Speck T. Self-healing in plants as a model for self-repairing elastomer materials. *Inter. Polym. Sci. & Tech.* 2011;38(9):1–4.
140. Clemetson KJ. Platelets and primary haemostasis. *Thrombosis research.* 2012 [accessed 2016 May 4];129(3):220–4. <http://www.thrombosisresearch.com/article/S0049384811006323/fulltext>. doi:10.1016/j.thromres.2011.11.036
141. Jackson AC. *Novel Encapsulation Technologies For Small Size-Scale Self-Healing Applications.* University of Illinois; 2011.
142. White SR, Sottos NR, Geubelle PH, Moore JS, Kessler MR, Sriram SR, Brown EN, Viswanathan S. Autonomic healing of polymer composites. *Nature.* 2001;409(1):794–797.

143. Hitchens L. Solving conformal coating problems in the application process. 2016.
144. Smyrl WH, Newman J. Current Distribution at Electrode Edges at High Current Densities. *J. Electrochem. Soc.* 1989;136(1):132–139.
145. Gervasi C a., Alvarez PE, Fiori Bimbi M V., Folquer ME. Comparative cyclic voltammetry and SEM analysis of tin electrodes in citrate buffer solutions. *J. Electroanalytical Chem.* 2007;601(1–2):194–204. doi:10.1016/j.jelechem.2006.11.019
146. Oxidation State Trends in Group 4. [accessed 2018 Feb 25]. <https://www.chemguide.co.uk/inorganic/group4/oxstates.html>
147. NIST. X-ray Photoelectron Spectroscopy Database. NIST Stand. Ref. Database 20, Version 20. [accessed 2015 Sep 3]. <http://srdata.nist.gov/xps/>
148. Simpson R, White RG, Watts JF, Baker MA. XPS investigation of monatomic and cluster argon ion sputtering of tantalum pentoxide. *Applied Surface Science.* 2017;405:79–87. doi:10.1016/j.apsusc.2017.02.006
149. Monatomic Depth Profiling. [accessed 2018 Feb 8]. https://xpssimplified.com/depth_profiling.php
150. Schetty R, Temp L, Temp H. Effects of Electrodeposited Matte Tin Crystal Orientation and Grain Structure on Tin Whisker Growth Propensity Using Stress-Inducing Test Methods. In: *Electrical Contacts (Holm)*, 2014 IEEE 60th Holm Conference on. 2014. p. 1–6.
151. Ashworth MA, Wilcox GD, Higginson RL, Heath RJ, Liu C, Mortimer RJ. The effect of electroplating parameters and substrate material on tin whisker formation. *Microelectronics Reliability.* 2015;55(1):180–191. doi:10.1016/j.microrel.2014.10.005
152. Woodrow TA, Works BP. Tracer diffusion in whisker-prone tin platings. *Proc. SMTA Int. Conf.* 2006;(1):24–28.
153. Driscoll TJ, McCormick LD, Lederer WC. Altered Layer Formation and Sputtering Yields for 5 keV

Ar⁺ Bombardment of MoO₃ and WO₃. *Surface Science*. 1987;187:539–558.

154. Mitchell DF, Sproule GI, Graham MJ. Sputter Reduction of Oxides by Ion Bombardment during Auger Depth Profile Analysis. *Surface and Interface Analysis*. 1990;15(March):487–497.

155. Lopez-Carreno LD, Benitez G, Viscido L, Heras JM, Yubero F, Espinos JP, Gonzalez-Eliphe a R. Oxidation of molybdenum surfaces by reactive oxygen plasma and O²⁽⁺⁾ bombardment: an Auger and XPS study. *Surface and Interface Analysis*. 1998;26(4):235–241. doi:10.1002/(sici)1096-9918(199804)26:4<235::aid-sia360>3.0.co;2-a

156. Brenner A. Electrodeposition of Alloys Containing Molybdenum and Nickel, Cobalt, Or Iron. In: *Electrodeposition of Alloys: Principles and Practice Volume II*. London: Academic Press Inc. (London) Ltd.; 1963.

157. Chapaneri R. A study of hexavalent and trivalent chromium conversion coatings on zinc surfaces. Loughborough University; 2010.

158. Zaraska L, Bobruk MB, Sulka GD. Formation of Nanoporous Tin Oxide Layers on Different Substrates during Anodic Oxidation in Oxalic Acid Electrolyte. *Advances in Condensed Matter Physics*. 2015;2015:1–11. doi:10.1155/2015/302560

159. Miller-Chou BA, Koenig JL. A review of polymer dissolution. *Progress in Polymer Science*. 2003;28(8):1223–1270. doi:10.1016/S0079-6700(03)00045-5

10 Appendix

10.1 Nanocapsule Production

Unfortunately, only the synthesis of the nanocapsules filled with the dicyclopentadiene (DCPD) reactive agent were undertaken as part of the self-healing polymer work. This was due to the undertaking of extra studies during the earlier parts of the PhD, which caused the self-healing polymer work to be pushed back.

10.1.1 Nano-Capsule Preparation

Two batches of nanocapsules were produced using an emulsion method to be used in conjunction with an acrylic conformal coating to produce a self-healing coating. One set of nanocapsules were produced to encapsulate dicyclopentadiene (DCPD) and the other set to encapsulate the Grubb's catalyst.

The nanocapsules filled with DCPD were produced using the method described by Brown *et al*¹⁸ and Blaiszik *et al*¹⁹:

1. Before beginning the capsule synthesis, the DCPD was vacuum distilled to separate it from the stabiliser, monomers and other unwanted oligomers. This was done by heating ~100 ml DCPD up to 40 °C using a silicon oil bath. The initial collected solution prior to and just after achieving 40 °C was discarded. This was because anything that had been collected up to that point were monomers and unwanted oligomers.
2. 200 ml of deionised (DI) water was placed in a 1000 ml beaker. 50 ml of 2.5 wt.% Poly(ethylene-alt-maleic anhydride) (EMA) solution was then added to the water. An overhead mixer blade was lowered into the beaker and set to 800 rpm.

3. Whilst mixing, 5 g of urea, 0.5 g of ammonium chloride and 0.5 g of resorcinol were added to the solution. Once the additions had dissolved, 60 ml of DCPD was added slowly to the solution along with 10 wt.% of hexadecane. The solution was then left to equilibrate for 10 min.
4. The solution was then sonicated for 3 min at 40 % intensity using a sonicator probe. After sonication, 12.67 g of 37 wt.% formaldehyde was added to the solution and the beaker was placed onto a hot plate and slowly heated up to 55 °C. The solution was then left for 4 h once the desired temperature was reached. After 4 h the heater was turned off and the pH was adjusted to 3.50 using 10 g l⁻¹ sodium hydroxide and 0.1 M hydrochloric acid.
5. The beaker was placed in an ice bath to ensure capsule dispersion stability and magnesium sulphate was added to the solution to act as a drying agent. Isopropyl alcohol (IPA) was then added remove any excess EMA surfactant. The resulting solution was then centrifuged to separate the capsules from the solution.
6. Multiple washes and centrifugation steps were necessary to remove excess water and surfactant. The resulting capsule mass was allowed to dry for 15 min at ambient conditions.

The nanocapsules filled with the Grubb's catalyst were produced using the method described by Jackson *et al*²⁰:

1. 0.4g of hexadecyltrimethylammonium bromide (CTAB) and 18 ml of 0.75 wt.% tetrabutylammonium fluoride (TBAF) solution was added to 120 ml of DI water and dissolved at room temperature (20°C). The solution was then mixed using an overhead mixer at 500 rpm.
2. In a separate beaker, 0.8 g of polystyrene, 0.4 g of poly(methyl methacrylate) and 0.08 g of Grubbs catalyst were dissolved in 16 ml of methylene chloride. This mixture was then added to the first solution and allowed to emulsify for 1 min. The sonicator probe was then placed in the emulsion and sonicated for 30 s at 40 % intensity.

3. The beaker was then returned to the overhead mixer and the emulsion was stirred overnight at 500 rpm to ensure all the methylene chloride had evaporated.
4. 1 ml of tetraethyl orthosilicate (TEOS) was then added to the solution and left to react for 1 day.
5. The final emulsion was centrifuged, and the resulting capsules were freeze dried for 4 days to obtain a dry powder.

10.1.1.1 Analysing the Compatibility of the DCPD Capsules with Different Solvents

Before the capsules could be incorporated into a polymer coating, compatibility between the capsules and the type of solvent used in the coating formulation was needed to be established, to ensure that the shell of the capsules was not dissolved. To investigate this, small vials (20 ml) were filled with a range of solvents that are currently used in commercial coating formulations, plus a small amount of capsules. The vials were then shaken and left overnight. After leaving overnight, they were shaken again to promote dispersion and inspected. If the solvent remained completely transparent it was inferred that the capsules had been dissolved; however, if the solvent was slightly opaque then this implied that the capsules were stable in that particular solvent. The solvents tested for compatibility were isopropanol (IPA), methylcyclohexane, xylene, toluene and butanone.

10.1.2 Results and Discussion

10.1.2.1 Analysis of the Synthesised Nanocapsules

The aim of this study was to successfully produce nanocapsules that were filled with the DCPD reactive agent and subsequently incorporate the nanocapsules into a conformal coating, along with the catalyst capsules, to create a self-healing conformal coating. The acrylic coating mixture that has previously been used is solvent based to improve flow and enable easier application, however, polymers are known to dissolve in certain solvents¹⁵⁹ and the nanocapsules have a polymeric shell. Therefore, the identification of a suitable coating mixture that will not dissolve the capsules needed to be undertaken. This was achieved by selecting several different solvents that are used in coating

mixtures and test their compatibility with the nanocapsules. The solvents that were chosen were methylcyclohexane, butanone, xylene, toluene and isopropanol (IPA). All these solvents, apart from IPA, are used in coating mixtures and IPA was chosen as it was used as a cleaning agent during nanocapsule production.

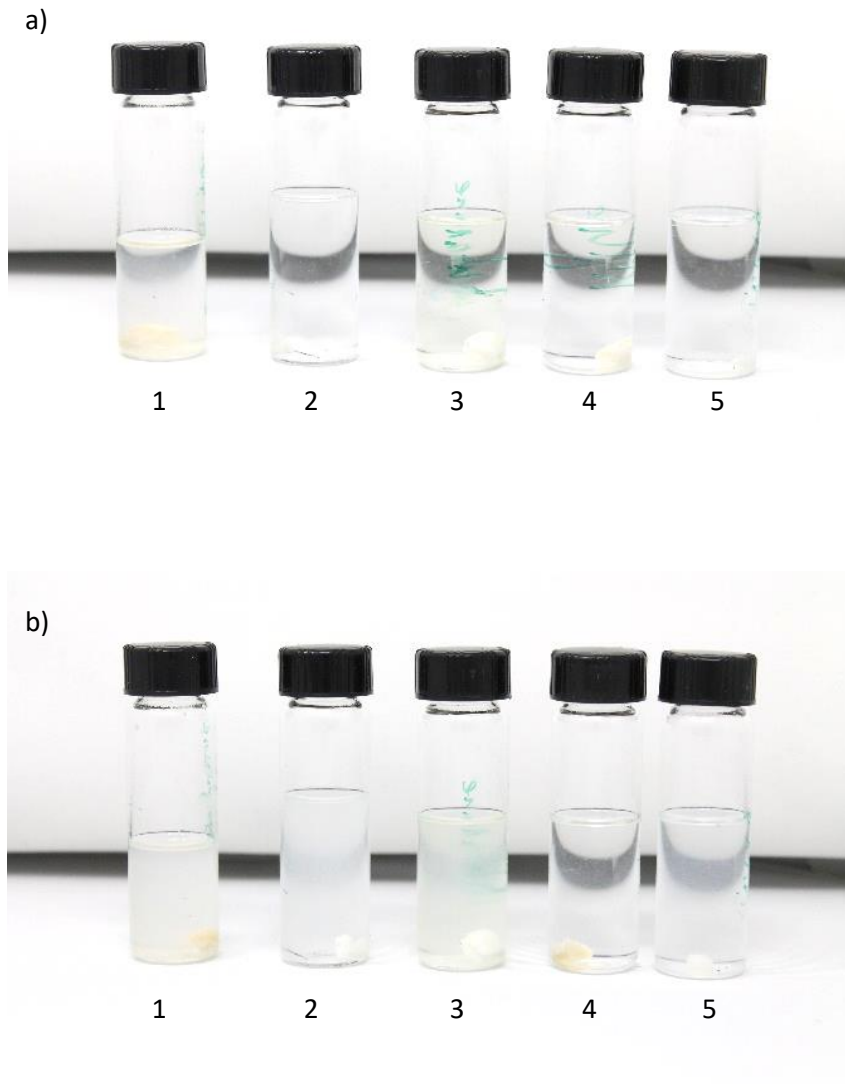


Figure 10.10.1 Photographs illustrating a) before and b) after agitation of nanocapsules in 1. methylcyclohexane, 2. IPA, 3. butanone, 4. xylene and 5. Toluene. Showing the compatibility of each solvent with the capsules, whereby a transparent solvent will be seen as compatible

Figure 10.1 illustrates the results obtained from this study, whereby if the solvent turned cloudy after agitation then this would show that that particular solvent was compatible as the cloudiness would have been due to the formation of a suspension of nanocapsules. The figure shows that after agitation (figure 10.1b) methylcyclohexane, IPA and butanone all became cloudy, which indicated that these

three solvents are compatible with the capsules and will not dissolve them. However, the capsules will dissolve in both xylene and toluene. Therefore, only coating mixtures that contained either methylcyclohexane or butanone should be used (IPA is used as a cleaning agent during processing and not used in coating mixtures).

Before the nanocapsules could be incorporated into a coating mixture, they were analysed using scanning electron microscopy (SEM) to confirm that nanocapsules had successfully been produced. Figure 6.7 shows secondary electron (SE) micrographs of nanocapsules, with figure 10.2a illustrating a low magnification micrograph and figure 10.2b illustrating a higher magnification micrograph. Before the nanocapsules were placed in the SEM it was apparent that they had agglomerated and formed large 'lumps' which can be seen in figure 10.2a. Further investigation of the nanocapsules showed that, in fact, the nanocapsules had a wide range of sizes from nanometre up to micrometre. These results showed that the capsules could not be incorporated into a coating mixture. This is because firstly the capsules formed very large agglomerates and secondly some of the capsules were too big to be incorporated into a conformal coating; due to the desired thickness of the conformal coating being $\sim 5\text{-}6\ \mu\text{m}$, to enable a better comparative analysis of whisker growth as a thinner coating would enable more whiskers to grow through. However, what the results did show was that spherical capsules could be successfully produced, albeit too large.

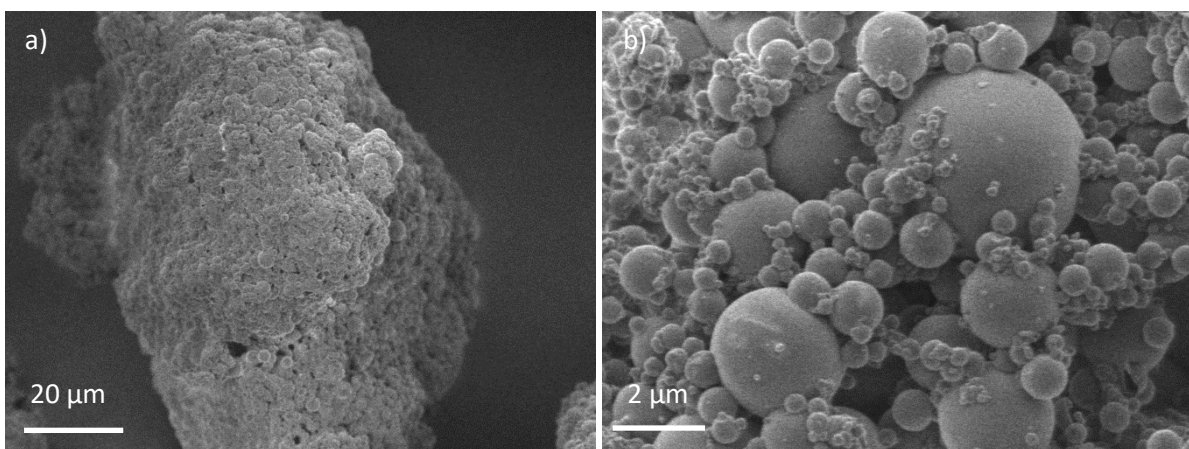


Figure 10.10.2 SE micrographs illustrating the DCPD filled capsules showing a) high agglomeration and b) wide range in capsule sizes

10.1.3 Conclusions

The aim was to successfully produce nanocapsules that were filled with dicyclopentadiene (DCPD) and to place them in a polymer coating to create a self-healing coating. The following conclusions may be made:

- Three solvents were identified as being compatible with the capsules, which were methylcyclohexane, isopropanol (IPA) and butanone. Both xylene and toluene are not compatible with capsules and will dissolve the capsules. Therefore, only coating mixtures that contained the three identified solvents can be used as the matrix.
- Capsules were successfully produced, however there was wide range of sizes from nano- up to microcapsules. Additionally, there was a high level of agglomeration which may have been due to the chemistry of capsules and the drying process.
- Due to the wide range of capsule size and the high degree of agglomeration, the first batch of capsules were not incorporated into a coating.

10.1.4 Future Work

The main aim for future work in self-healing polymers should be to successfully create a self-healing polymer coating. This may be achieved by using nano-capsules that contain healing agents or could be achieved by changing the polymer chemistry, i.e. using mechanophores that will react to a mechanical force to heal the polymer.

- The results discussed in this chapter showed that nano to sub-micron capsules could be produced, however, the capsules agglomerated too much which would cause poor dispersion in the polymer matrix. This could be overcome by carrying out an additional step during the synthesis of the capsules, as suggested by Blaiszik *et al*¹⁹. This extra step would add a silica outer layer to the particles which would reduce agglomeration, therefore improving dispersion. The silica layer would also mean that the capsules would be stable in a wider range of solvents, meaning that different conformal coating systems could be used.

- The dicyclopentadiene (DCPD) healing agent is fatal through inhalation and will give off fumes, therefore different healing agents should be researched to replace it and negate the risk.
- Different self-healing systems should be research to improve self-healing efficiency. Using capsules is the easiest and cheapest way to create self-healing polymers, however they aren't as efficient as microvascular self-healing systems, for example. This is because when using capsules, the same area can't be healed multiple times, whereas microvascular systems can.

10.2 Journal Papers

D.M.Haspel, M.A.Ashworth, G.D.Wilcox, X.Bao, R.J.Mortimer, **The Effect of Different Post-Electroplating Surface Modification Treatments on Tin Whisker Growth**, Submitted on 1st September 2017 to Journal of Electronic Materials

THE EFFECT OF DIFFERENT POST-ELECTROPLATING SURFACE MODIFICATION TREATMENTS ON TIN WHISKER GROWTH

D.M. Haspel^{1,3}, M.A. Ashworth¹, G.D. Wilcox¹, X. Bao¹ & R.J. Mortimer²

1.-Department of Materials, Loughborough University, Loughborough, Leicestershire, LE11 3TU, UK.

2.-Department of Chemistry, Loughborough University, Loughborough, Leicestershire, LE11 3TU, UK.

3.-e-mail: d.haspel@lboro.ac.uk

ABSTRACT

There are very few studies that have investigated directly the effect of an oxide film on tin whisker growth, since the 'cracked oxide theory' was proposed by Tu in 1994. The current study has investigated the effect of both a molybdate conversion coating and a tungstate conversion coating on tin whisker growth from Sn-Cu electrodeposits on Cu, and compared it with that from an electrochemically-formed oxide produced from a potassium bicarbonate-potassium carbonate electrolyte. X-ray photoelectron spectroscopy (XPS) has been used to investigate the effect of both immersion time and applied potential on the thickness and composition of the oxide film. The XPS studies show that the oxide film formed using either of the conversion coating baths is significantly thicker than that produced from the potassium bicarbonate-potassium carbonate bath. Initial observations suggest that both the tungstate-based conversion coatings and the molybdate-based conversion coatings significantly reduce whisker growth by over 80 % for all conversion coating systems compared with a native air-formed oxide and provide improved mitigation compared with the electrochemically formed oxides previously investigated.

Key words: Tin, conversion coating, molybdate, tungstate, electrochemical oxidation, electrodeposition, whisker growth

1 INTRODUCTION

A tin whisker is commonly a filamentary growth of pure tin, which will generally grow from thin tin electroplate, and can grow up to lengths of a few millimetres, though more commonly they will grow up to a few 100 μm 's [1]. Tin whiskers can cause major reliability problems in high value, long-life electronics, such as rocket guidance systems and aerospace systems, mainly due to them growing from one surface and coming into contact with another, adjacent surface, resulting in a short circuit and subsequent electronic

failure [2]. Electronics can also fail if whiskers are broken off and subsequently land across adjacent terminals. If the current in the circuit is high enough, the whisker can volatilise into a conductive metal gas, which could result in the creation of a metal vapour arc [3]. The metal vapour arc reaction can generate sufficiently high temperatures to melt metals and incinerate polymers.

One of the most significant problems is the unpredictability of whisker growth and their varying incubation periods, which causes concern with regards to the long-term reliability of electronic components [4]. Moreover, there is, currently, no one accepted whisker growth mechanism; though there are a number of theories and some commonly agreed factors that affect whisker growth [1,5,6].

Until recently, whisker growth was successfully mitigated through the alloying of tin with lead [7,8]. However, due to EU legislation (e.g. RoHS) [9], the use of lead has been restricted, therefore alternative strategies are required to mitigate whisker growth from both lead-free solderable surfaces and lead-free solid solders. Currently, there are a number of different strategies, including post-electroplating annealing, alloying (Sn-Ag and Sn-Bi [10]), applying a polymeric coating and the use of an electroplated underlayer to prevent intermetallic formation [11].

Until recently, there has been little research into the role of the oxide layer in whisker growth. Tu's cracked oxide theory [12–15] proposed that the tin oxide film played a crucial role in the growth of tin whiskers and that a very thick oxide would physically block the growth of whiskers by reducing the risk of localised oxide cracking at weak points in the film. If the protective oxide film is not sufficiently thick, it may be broken at certain weak points and it is from these locations that whiskers grow subsequently to relieve the stress [16,17]. In the absence of an oxide film, whisker growth would not occur as the deposit would be able to relieve stress by uniform creep [18], as demonstrated for by Chang and Vook [19] for hillock growth from aluminium. However, Moon *et al* [20] showed that whisker growth occurred on Sn-Cu electrodeposits that had been stored for 9 days under a vacuum following removal of the surface oxide by ion beam sputtering.

Evidence to support Tu's theory was provided by Su *et al* [21], [22] who produced samples with a 200 nm thick sputter deposit of tin oxide that was given a pre-defined array of circular-shaped 'weak spots' using lithography. It was observed that whiskers would preferentially grow from some, but not all, of these predefined 'weak points', demonstrating that although a weak oxide was necessary for whisker growth, the underlying grain structure was also important. Furthermore, results showed that an increased number of 'weak spots' resulted in increased number of whiskers, however, these were shorter than those developed on samples with fewer 'weak points'. Analysis of the residual stress levels with the coatings using

synchrotron radiation x-ray measurements revealed that the average compressive stress developed within the coatings because of intermetallic growth was independent of the number of weak points present in the coating. Wu and Ding [23] investigated the influence of a coating of tin oxide nano particles on whisker growth from surface treated electroplated tin films on copper. Their results showed that the nano particle coating introduced discontinuities (i.e. 'weak spots') into the native oxide film thereby promoting the growth of hillocks rather than long filament whiskers.

In previous studies by the current authors [24,25], it was observed that an electrochemically formed tin oxide greatly reduced the growth of whiskers and that increasing the thickness of the tin oxide film promoted further reductions in whisker growth.

Conversion coatings are a form of passivation treatment and consist of converting the substrate metal surface from an active to a passive state [26]. A conversion coating can also be thought of as a mixed oxide coating as it consists of a mixture of corrosion products from the substrate metal and reduced species from the ions in the electrolyte. Generally, conversion coatings are significantly thicker than a native air-formed oxide, however, they are prone to cracking and flaking. Two non-chromate conversion coatings specifically developed for tin surfaces are investigated in this paper; a molybdate-based conversion coating [26] and a tungstate-based conversion coating [27]. The effect of processes parameters on the composition and thickness of the conversion coatings was determined and the effect of the resultant oxide coatings on whisker growth investigated.

2 EXPERIMENTAL METHOD

2.1 Electrodeposition of Sn and Sn-Cu Alloy

For initial conversion coating trials, 5 μm of pure Sn was electrodeposited onto Cu substrates (Advent Research Materials, 99.9% purity, 0.4 mm thick) at a current density of 20 mA cm^{-2} , using a bright acid Sn electroplating bath. For subsequent whisker growth trials, a Sn-Cu alloy was electroplated onto Cu. The electroplating solution contained 60 g L^{-1} tin sulphate (Sigma Aldrich), 70 ml L^{-1} sulphuric acid (SG 1.83, Fisher Scientific) and 40 ml L^{-1} Tinmac Stannolyte (MacDermid), a propriety additive that acts as a brightener. For the electrodeposition of Sn-Cu alloys, the Sn electroplating bath was modified by the addition of Cu ions at a concentration of 10 mmol L^{-1} , using copper sulphate (Fisher Scientific). Electrodeposition of 2 μm Sn-Cu onto Cu was carried out at a current density of 10 mA cm^{-2} , which resulted in a uniform electrodeposit with a Cu content of ~1 wt.%.

Test coupons had dimensions of 2 x 4 x 0.04 cm and were masked with chemically inert tape, which resulted in an electroplated area of 2 x 2 cm. The coupons were used in their as-received condition with no additional grinding or polishing. Electrodeposition of pure Sn was carried out using a 99.95% Sn foil anode (Advent Research Materials, 0.25 mm), whilst electrodeposition of the Sn-Cu was carried out using a 50 x 50 mm platinised titanium mesh anode, 1 μm Pt coating (Ti-Shop). Prior to electrodeposition, all coupons were degreased with acetone (Fisher Scientific), cleaned using a detergent solution, rinsed with deionised water and dried using hot air. Immediately prior to electrodeposition, the coupon was pickled for 60 s in a 20% v/v solution of sulphuric acid (SG 1.83, Fisher Scientific), rinsed with deionised water and dried using hot air. Pickling was carried out just prior to electroplating.

2.2 Preparation of Electrolytes for Surface Modification Treatment

Three solutions were prepared for the post-electroplating surface modification treatments. One solution was for electrochemical oxidation and the other two solutions were used to generate conversion coatings. Electrochemical oxidation was carried out using a pH 8.9 potassium bicarbonate-potassium carbonate solution (0.75 mol L⁻¹ of potassium bicarbonate and 0.05 mol L⁻¹ of potassium carbonate, both Sigma Aldrich). The solution was prepared using deionised water and the pH was adjusted to 8.9, using additions of sodium hydroxide (Fisher Scientific).

For the molybdate conversion coating an acidic sodium molybdate solution (10 g L⁻¹ sodium molybdate, Sigma Aldrich) was used. The solution was prepared using deionised water and the pH was adjusted to ~3, using additions of hydrochloric acid (SG 1.18, Fisher Scientific).

For the tungstate conversion a sodium tungstate solution (0.1 mol L⁻¹ sodium tungstate and 10 g L⁻¹ sodium tetraborate, both Sigma Aldrich) was used. The solution was prepared using deionised water and the pH was not altered.

2.3 Surface Modification Treatment

All surface modification treatments were carried out immediately after electrodeposition of the Sn or Sn-Cu coating using, if required, a Solartron SI 1286 Electrochemical Interface potentiostat and the 3-electrode cell described previously [24,25].

2.3.1 Electrochemical Oxidation

Electrochemical oxidation treatments were carried out in the potassium bicarbonate-potassium carbonate solution. Following immersion of the coupon into the electrolyte solution, the Sn or Sn-Cu electrodeposit was initially held at a potential of -1.5 V vs. Ag/AgCl to reduce the pre-existing oxide. When hydrogen evolution was observed, the surface was agitated using a pipette filled with the electrolyte solution to remove any bubbles that were present and the potential was increased to 2 V vs. Ag/AgCl. For each test coupon a charge of 60 mC cm⁻² was passed.

2.3.2 Conversion Coatings

For molybdate conversion coatings, samples were immersed in solutions, with a pH of 3.13, for times of 1–10 minutes. Pulsed current trials were also carried out using the parameters shown in Table 1. Samples were also held at potentials ranging from -0.45 to -0.75 V vs. Ag/AgCl for 5 minutes.

For tungstate conversion coatings, a modified version of the pulsed current method used by Van De Leest and Krijl [27] was used. Pulsed current densities ranging from ± 2.5 to ± 10 mA cm⁻² were used at a frequency of 0.5 Hz for square wave cycles ranging in number from 30-300. Three sets of experiments were carried out to optimise the tungstate process and the full set of parameters used are given in Table 2.

2.4 Characterisation of Conversion Coatings

The effect of process variables on the composition and thickness of the molybdate and tungstate coatings was investigated by x-ray photoelectron spectroscopy (XPS) using a Thermo-Scientific K-Alpha x-ray photoelectron spectrometer. Sputter depth profiling was carried out using 1 keV argon ions with an estimated etch rate of ~ 0.28 nm s⁻¹ with respect to Ta₂O₅. XPS analysis was carried out within 24 hours of electrodeposition and conversion coating, unless otherwise stated. The sputter time taken to reach 50% of the surface oxygen content was used to compare the thickness of the oxide coatings produced by the different process variations.

The topography of the conversion coatings was investigated using scanning electron microscopy (SEM) and optical microscopy. SEM analysis was carried out using a Carl Zeiss Leo 1530 VP field emission gun SEM (FEGSEM) at an operating voltage of 10 kV and a working distance of ~ 11 mm. Optical microscopy was carried out using a Leica DMI8 optical microscope.

The thickness of the conversion coating and the microstructure of the electroplated Sn-Cu coating was investigated using a FEI Nova 600 Nanolab Dual Beam focussed ion beam milling scanning electron microscopy (FIB-SEM) using the method previously described [25].

2.5 Tin Whisker Growth Studies

The effect of the oxide coatings on subsequent tin whisker growth was assessed using 2 μm Sn-Cu electrodeposits on Cu. To study whisker growth on electrochemically formed oxides, 26 samples were produced, of which 13 were left to develop native air-formed oxides (untreated) and 13 were electrochemically oxidised. Periodically, three untreated samples and three electrochemical oxidised samples were randomly selected for analysis to investigate the time dependence of whisker growth and also to provide a benchmark for the conversion coated samples. The time dependent growth of the oxide film was also investigated by analysing both untreated and electrochemically oxidised samples at the same time intervals as the whisker growth samples. For each specific conversion coating treatment three identical test samples were prepared. In each case, uncoated control samples were left to develop native air-formed oxides (untreated) for comparison. After electrodeposition and the formation of the oxide coating, the samples were stored at room temperature ($\sim 20^\circ\text{C}$). The growth of the tin whiskers was studied periodically using both optical microscopy and SEM. The whisker density and the longest apparent whisker length (per frame) were measured using an optical microscope with an objective magnification of x20 and a frame area of $\sim 0.57\text{ mm}^2$. The method used to measure the apparent whisker length is shown in Fig.1, whereby Fig.1a shows the actual length of the whisker and Fig.1b shows the apparent whisker length.

3 RESULTS AND DISCUSSION

3.1 Characterisation of Molybdate Conversion Coatings

The depth profiles in Fig.2 (a) & (c) show that the conversion coating is comprised of molybdenum and oxygen with a region enriched in tin oxide present at the interface between the coating and the Sn metal. For the sample immersed for 5 min (Fig.2a), the oxygen and molybdenum contents suggest that the stoichiometry of the coating corresponds to MoO_2 whilst the outer surface of the conversion coating may correspond to MoO_3 . A similar change in oxidation state for molybdenum between the outer surface and the remainder of the coating was also observed previously [28–30]. This change in oxidation state is shown in Fig.2 (b) which plots the binding energy of the molybdenum peak as a function of sputter time. The binding energy of the molybdenum peak at the outer surface is 232.11 eV, which lies within the binding energy range given in the literature (232.1–233.25 eV) for MoO_3 [31]; whilst that within the remainder of

the coating (229.04-229.21 eV) lies within the reported range given in the literature (228.8-232.0 eV) for MoO₂ [31]. The binding energy data suggests that the molybdenum was further reduced to metallic Mo at the approximate position of the oxide-metal interface. The presence of Mo in the coating may not be valid as the coating being produced was a molybdate coating and not a metallic coating. The presence of pure Mo is most likely due to sputter induced reduction, which will be discussed later on. These depth profiles were typical for the majority of the molybdate coatings.

The coating thickness was seen to increase by ~15x for the sample produced at -0.75 V vs. Ag/AgCl in comparison with the sample immersed for 5 min (shown in Fig.2c), although a similar trend was observed in the binding energy of the molybdenum peak. However, there is a gradual reduction in the oxygen content up to ~1000 s of sputter, from ~60 at.% at the surface to ~50 at.% > 1000 s; beyond 1000 s the oxygen content remains constant, which would suggest a stoichiometry of MoO. This gradual reduction in oxygen content could be due to prolonged argon ion sputtering causing reduction of the molybdenum oxide. Molybdenum reduction, as a result of the prolonged sputter, is also reflected in Fig.2 (d) which shows that the molybdenum peak binding energy continually decreases throughout the thickness of the coating.

Table 3 shows that all of the molybdate conversion coatings are significantly thicker than the thickest electrochemical oxide previously produced [25]. Table 3 also shows that the molybdenum content within the oxide coating is similar for all the samples, however, for the sample produced at -0.75 V vs. Ag/AgCl the Mo content increases progressively through the bulk of the coating (Fig.2). This may be due to sputter induced reduction of the molybdenum oxide [28–30], which may also cause preferential sputtering of the oxygen. Table 3 also shows that there is a significant thickness difference between the two samples produced at the most cathodic formation potentials (-0.6 and -0.7 V vs. Ag/AgCl) and the rest of samples. Optical microscopy shows that both these coatings have a high density of cracking; shown in Fig.3 for the coating produced at -0.6 V vs. Ag/AgCl. The observed cracking may be due to increased tensile stress induced by film thickness and/or the drying process, as suggested by Zhang *et al* [32] and da Silva *et al* [33]. During the drying process the moisture is removed from the coating, which causes the coating to shrink; this shrinkage generates tensile stresses within the coating that can subsequently cause cracking.

3.2 Characterisation of Tungstate Conversion Coatings

The depth profile in Fig.4 shows that the coating consists mainly of tin oxide with only a small amount of tungsten present throughout; a slightly increased tungsten content (~4 at.%) is observed near the surface of the coating. All the tungstate depth profiles measured from the tungstate conversion coated samples were similar in appearance, irrespective of processing parameters, and the results are summarised in Table

4. It can be seen from Table 4 that as the current density is increased the thickness of the conversion coating is also increased, which is to be expected as the total charge passed increases. Table 4 also shows that as the number of cycles increases the thickness of the conversion coating increases. It might further be expected that passing an equivalent charge would result in conversion coatings of similar thickness, however, EC.3 was significantly thicker than EC.1 and EC.2, which were similar in thickness. This may arise from oxide formation at $\pm 10 \text{ mA cm}^{-2}$ being more effective at creating a thicker oxide layer than at either $\pm 2.5 \text{ mA cm}^{-2}$ or $\pm 5 \text{ mA cm}^{-2}$.

Table 4 shows that, although a higher current density is able to produce a thicker coating for an equivalent charge passed, there is a limit to how much charge can be passed before the coating quality deteriorates, as shown in Fig.5. At the higher current density, more gas bubbles were formed at the sample surface, compared with the lower current density, which may have hindered or prevented the deposition of the oxide coating and resulted in the formation of regions where the coating has either fully flaked off to expose the underlying tin or is thinner than the majority of the coating. Such regions can be considered as 'weak points' in the oxide coating. Results show that using a current density of $\pm 10 \text{ mA cm}^{-2}$ there is a limit of ~ 45 cycles before the coating quality is reduced, whilst the limit for a current density of $\pm 5 \text{ mA cm}^{-2}$ is between 150 and 180 cycles. This indicates that thicker coatings may be produced at lower current densities since increased charge may be passed before the coating quality deteriorates.

Optical microscope analysis was carried out on selected tungstate samples to study the surface of the coating. Fig.6 shows the appearance of the coating ~ 3 months after deposition, for samples processed at $\pm 10 \text{ mA cm}^{-2}$ for 45 cycles, $\pm 5 \text{ mA cm}^{-2}$ for 90 cycles and $\pm 5 \text{ mA cm}^{-2}$ for 150 cycles. As observed from Fig.5 the cycle limit for samples processed at $\pm 10 \text{ mA cm}^{-2}$ is 45 cycles and Fig.6a confirms that a high number of 'weak points' are present in the coating. In comparison the tungstate coating produced at $\pm 5 \text{ mA cm}^{-2}$ for 90 cycles (Fig.6b) showed no such 'weak points'. 'Weak points' were, however, present on the tungstate coating produced at $\pm 5 \text{ mA cm}^{-2}$ for 150 cycles (Fig.6c), though far fewer than were observed on the sample produced at $\pm 10 \text{ mA cm}^{-2}$ for 45 cycles. The impact of these 'weak points' on the ability of the coating to mitigate whisker growth is discussed in a later section.

SEM analysis was carried out on the tungstate samples to study the surface morphology of the coating in more detail. Fig.7 shows the appearance of the coating for samples processed using different conditions; Figs.6 (a) and (b), which were processed at $\pm 10 \text{ mA cm}^{-2}$ for 30 cycles and $\pm 5 \text{ mA cm}^{-2}$ for 60 cycles, respectively, both showed a uniform surface with no evidence of cracking. In comparison samples processed at $\pm 10 \text{ mA cm}^{-2}$ for 90 and 150 cycles (Fig.7 c and d respectively), both showed a surface with a

large number of cracks and areas, which varied in size, where the oxide was either thinner or completely flaked off to expose the underlying Sn (as shown in Fig.7e, $\pm 10 \text{ mA cm}^{-2}$ for 150 cycles). Compared with the cracking on the molybdate samples, that on the tungstate samples is much finer, in terms of crack width, (Fig.7 c and d) and not visible under the optical microscope at an objective magnification of x20.

3.3 Effect of Electrochemical Oxidation on Whisker Growth

Whisker growth has been evaluated using optical microscopy; three randomly selected samples for the electrochemically oxidised and untreated groups of samples were analysed at each analysis point and the average whisker density calculated. The graph in Fig.8 shows that, for both sets of samples, the whisker density increases progressively with time, however, the presence of the electrochemically formed oxide significantly reduces whisker growth compared with that from the untreated samples that were left to develop a native air-formed oxide.

Fig.8 shows that the whisker growth for the untreated samples rapidly increases between 14 and 84 days of storage; after which the whisker formation rate reduces. In comparison, the electrochemically oxidised samples showed an increased incubation period prior to the onset of whisker growth, with no significant increase in whisker density until the analysis after ~ 56 days storage. For both sets of samples there is a reduced rate of whisker initiation after ~ 84 days and most whiskers were formed between ~ 42 -84 days.

The graph in Fig.9 shows that the thickness of the oxide on the untreated samples steadily increases over time and becomes similar in thickness to that on the electrochemically oxidised samples after ~ 84 days of storage; Fig.9 also shows that the thickness of the oxide on the electrochemically oxidised samples remains relatively consistent over time with very little change over a period of 204 days. The increase in oxide thickness for the untreated samples may contribute to the reduced rate of whisker initiation observed after ~ 84 days. However, the reduced rate of whisker growth may also be due to a reduced rate of intermetallic compound (IMC) formation, which is a known driving force for whisker growth due to increased compressive stresses in the coating [1,17,34]. Stuttle *et al* [35] showed that after 1 day, IMC growth was observed for pure Sn on Cu, and after 55 days almost the entire copper surface was covered in IMC growth. This suggested that majority of the IMC growth would occur not long after 55 days, therefore slowing down the driving force for whisker growth; however, the IMCs may continue to grow along the grain boundaries. The coating used in this paper was a Sn-Cu alloy which may promote a more rapid formation of IMC due to the presence of copper in the coating itself. The increased incubation period prior to the onset of whisker growth for the electrochemically oxidised samples may be attributed to the increased thickness of the oxide, compared with the untreated samples.

The longest apparent length of whisker in each frame used to determine whisker density was measured at each time interval and is plotted in Fig.10. For the untreated samples, the results indicate that the whisker length increases gradually over the 220 days of storage but that the rate at which the whiskers grow progressively reduces with time. Compared with the untreated samples, the length of the longest whisker is significantly reduced for the electrochemically oxidised samples throughout the period analysed, with little apparent increase in whisker length between ~80 and ~220days.

Fig.11 shows the change in the distribution of the longest whisker per frame for both electrochemically oxidised and untreated samples, between 14 days and 119 days of storage. After 14 days (Fig.11a) all the measured whiskers were less than 100 μm in length for both the untreated samples and the electrochemical oxidised samples. Fig.11a also shows that not only were far fewer whiskers present on the electrochemically oxidised samples compared with the untreated samples but they were all less than 40 μm in length. After 119 days (Fig.11b), the whisker distribution for the untreated samples has shifted to much greater lengths and each frame analysed contained a whisker greater than 20 μm in length. The whisker length distribution for the untreated samples shows that the majority of the whiskers were greater than 100 μm in length after 119 days, whereas after 14 days, no whiskers were greater than 100 μm in length. In comparison, for the electrochemically oxidised samples, most of the whiskers were still less than 40 μm in length, although the maximum whisker length has increased compared with after 14 days of storage. Fig.11b shows that the whisker lengths on the electrochemically oxidised samples are greatly reduced compared with the untreated samples, thereby significantly reducing the risk of the whiskers bridging a gap between components or connections and causing a short circuit. The reduction in the number of long filament whiskers may be due to the increased incubation period for the electrochemically oxidised samples.

Alternatively, it may suggest that the electrochemical oxide influences the rate at the whiskers grow once the whisker has penetrated the oxide layer. It might be expected that when a whisker penetrates through the oxide film, the whisker would have a similar rate of growth to the untreated samples; therefore, the electrochemical oxide also appears to be having an influence on the driving force for whisker growth as well as inhibiting whisker initiation. It was shown previously that for Sn-Cu on Cu, IMC growth didn't appear to be influenced by the presence of the electrochemical oxide [25]. In the absence of an oxide film, the surface of the tin serves as a source for vacancies to facilitate tin diffusion through the coating, to support the growth of whiskers [36]. However, the presence of a sufficiently thick oxide may impede diffusion of tin atoms by reducing the number of available surface vacancies [13], therefore slowing the rate at which

whiskers may grow. This may suggest that whisker growth on the electrochemically oxidised samples is diffusion limited.

3.4 Effect of Molybdate Conversion Coatings on Whisker Growth

For whisker growth studies, molybdate conversion coatings were produced using three different conditions: 5 minutes immersion, -0.45 V vs. Ag/AgCl for 5 minutes, and -0.6 V vs. Ag/AgCl for 5 minutes. Whisker densities were evaluated for 3 samples from each coating treatment after ~7 weeks storage and an average whisker density was calculated (Fig.12). It was observed that all the conversion coatings significantly reduced whisker growth compared with the untreated samples. Comparison of Fig.12 with Fig.8 shows that both the 5 min immersion samples and that processed at -0.45 V vs. Ag/AgCl samples provided increased whisker mitigation compared with the electrochemically formed oxide. From Fig.8 it can be determined that after 49 days the approximate ratio of whisker density for the untreated samples to the electrochemically oxidised samples was ~8:1, whereas the 5 min immersion and -0.45 V samples had ratios of ~15:1 and ~32:1, respectively (Fig.12). This may be due to the increased thickness of the oxide on the molybdate conversion coated samples (given in Table 3) more effectively inhibiting whisker growth.

Although, the molybdate sample produced at -0.6 V vs. Ag/AgCl showed increased whisker growth compared with the other two molybdate coatings; however, it still brought about a reduction in whisker growth (relative to the native air-formed oxide) comparable to that of the electrochemically oxidised surface (i.e. a reduction of ~8:1). The reduced effectiveness of the molybdate conversion coating produced at -0.6 V vs. Ag/AgCl is most likely due to the high density of cracks that are present (Fig.3 and Fig.13). It was observed that all the whisker growth initiated at cracks, as shown in Fig.13.

Fig.12 further shows that after 12 weeks of storage all the molybdate coatings are still effectively mitigating whisker growth and performing better than an electrochemically oxidised surface (Fig.8). However, the -0.6 V molybdate samples show a slightly increased rate of whisker growth compared with the other two molybdate coatings; this is most likely due to the high crack density present in these samples (Fig.3 and Fig.13). No cracks or 'weak points' are observed in the other two molybdate coatings and the whisker density increases at a lower rate. However, compared with the untreated samples the molybdate sample produced at -0.6 V vs. Ag/AgCl is still mitigating whisker growth as effectively after 12 weeks as it did after 7 weeks, with a whisker density ratio of ~8:1 at both time intervals. The two other molybdate coatings produced using 5 min immersion and -0.45 V vs. Ag/AgCl both show a relative improvement in whisker mitigation compared with the untreated samples, with the whisker density ratios increasing from ~15:1 to ~17:1 for the 5 min immersion samples and from ~32:1 to ~41:1 for the -0.45 V vs. Ag/AgCl samples.

3.5 Effect of Tungstate Conversion Coatings on Whisker Growth

For whisker growth studies, tungstate conversion coatings were produced using three different conditions: $\pm 10 \text{ mA cm}^{-2}$ for 45 cycles, $\pm 5 \text{ mA cm}^{-2}$ for 90 cycles and $\pm 5 \text{ mA cm}^{-2}$ for 150 cycles. Whisker densities were evaluated for each of the 3 samples prepared for each coating treatment after ~ 9 weeks storage and an average whisker density calculated (Fig.14). It was observed that all the conversion coated samples had significantly reduced whisker growth compared with the untreated samples. Comparison of Fig.14 with Fig.8 shows that the tungstate conversion coatings provided increased whisker mitigation compared with the electrochemically formed oxide. After 63 days the approximate ratio of whisker density for the native samples to electrochemically oxidised samples was $\sim 5:1$ (Fig.8), whereas the least effective of the tungstate samples had a ratio of $\sim 36:1$ (Fig.14).

Fig.14 shows that after 4 months of storage the tungstate coatings are all still mitigating whisker growth more effectively than an electrochemically oxidised surface (Fig.8). The rate at which the whisker density increases for both $\pm 5 \text{ mA cm}^{-2}$ samples reduces after 4 months of storage compared with untreated samples. Both coatings display a similar ability to mitigate whisker growth despite there being a significant difference in coating thickness between them (Table.4). This is most likely due to the coatings produced at $\pm 5 \text{ mA cm}^{-2}$ for 150 cycles having 'weak points' (Fig.6c and Fig.15a), from which most of the whisker growth occurs for these samples (Fig.15a); similar observations were made for the samples processed at $\pm 10 \text{ mA cm}^{-2}$ for 45 cycles. There were still no 'weak points' observed on the samples produced at $\pm 5 \text{ mA cm}^{-2}$ for 90 cycles after 4 months of storage. The tungstate coatings produced at $\pm 10 \text{ mA cm}^{-2}$ for 45 cycles become less effective with time, which is most likely due to the high concentration of 'weak points' on the coatings (Fig.6a) from which whisker growth is able to occur (Fig.15a).

The tungstate conversion coated samples produced at $\pm 5 \text{ mA cm}^{-2}$ for 150 cycles also possessed regions where the coating thickness was reduced; however, these areas did not appear to be preferential sites for whisker growth after ~ 9 weeks of storage. This suggests that these regions were still sufficiently thick enough to mitigate whisker growth for these samples.

3.6 Summary of the Effect of Oxide Coatings on Whisker Growth

These results are consistent with those obtained previously [21,22,24,25] and provide further experimental evidence to support Tu's theory that the presence of a thicker oxide serves to mitigate whisker growth [12–15]. However, results for the conversion coated samples demonstrate that the quality of the coating is also important since thicker coatings were more likely to contain defects, which results in increased whisker

growth compared with thinner coatings with fewer or no defects. The study also indicates that the electrochemical oxide also significantly reduces the maximum and average whisker length, which would reduce the risk of a whisker bridging a gap in an electronic component and causing a short circuit. However, it was observed by Su *et al* [21] that the samples with the fewest pre-defined 'weak points' had longer whiskers compared with the samples with the greatest number of 'weak points'. An understanding of the stress distribution within the tin coating, particularly in the vicinity of whiskers, would be advantageous to elucidate the influence of the oxide coatings on stress generation and relaxation mechanisms within the coating. Synchrotron radiation X-ray studies have been used previously to investigate the development and distribution of compressive stresses within tin coatings [14,18,37–40].

FIB cross-sections were produced to study both the IMC growth in the Sn-Cu coating and the thickness of the conversion coating. The micrographs obtained from these cross-sections (Fig.16) show large area fractions of IMC formation for both a molybdate sample (Fig.16a) and a tungstate sample (Fig.16b), which would suggest that the conversion coatings have little effect on the IMC formation when comparing them to the results obtained previously [25]. This would suggest that they mitigate whisker growth simply by acting as physical barrier in the same way as an electrochemically formed oxide. The thickness for the molybdate conversion coating produced at -0.6 V vs. Ag/AgCl for 5 min is ~300 nm and the thickness for the tungstate conversion coating produced at 10 mA cm⁻² for 45 cycles is ~240 nm.

The two thinner molybdate coatings showed an improved ability to mitigate whisker growth compared with the electrochemically oxidised samples. This may be attributed to their increased thickness which enables them to physically block whisker growth. Despite being thinner, these two molybdate samples showed improved whisker mitigation compared with the -0.6 V molybdate samples, due to the improved quality of the coating and the absence of cracks through which whiskers could grow.

Of the three tungstate samples investigated, that produced at ±5 mA cm⁻² for 90 cycles mitigated whisker growth the most effectively even though it was the thinnest coating, due to the absence of 'weak points' in the coating.

The molybdate samples produced at -0.6 V vs. Ag/AgCl and the tungstate samples produced at ±5 mA cm⁻² for 150 cycles were of similar thicknesses, however the tungstate samples had far fewer whiskers compared with the molybdate samples. This is due to the molybdate samples having an increased density of cracks in the conversion coating, compared with the tungstate samples which had few 'weak points' in the conversion coating. This highlights that the coating quality is also important when mitigating whisker

growth. The results also show that the parameters to produce the coating can be optimised to maximise thickness whilst avoiding defects.

4 CONCLUSIONS

The following conclusions can be drawn from the results obtained in the current study:

- An electrochemical oxidation treatment has been demonstrated to provide continuous whisker mitigation over a period of 220 days for 2 μm Sn-Cu deposits on Cu.
- An electrochemical oxidation treatment not only reduces whisker density but also significantly reduces whisker length compared with an untreated surface.
- Conversion coating treatments may be used to develop oxides that are significantly thicker than those that have been achieved to date by an electrochemical oxidation method.
- Initial observations show that both molybdate and tungstate conversion coatings provide improved whisker mitigation compared with electrochemically oxidised surfaces.
- For the tungstate conversion coated samples, most whiskers were observed to grow from areas of the coating where the oxide was thinner or completely absent ('weak points'). Further optimisation of processing parameters (current density, number of cycles) is required to avoid the formation of 'weak points' in the oxide coating
- Compared with the tungstate conversion coatings, an increased density of long, wide, deep cracks are formed on molybdate conversion coated samples produced at -0.6 V and -0.75 V vs. Ag/AgCl, which reduces their ability to mitigate whisker growth.
- For both molybdate and tungstate conversion coatings, a thicker coating doesn't necessarily provide improved whisker mitigation since the presence of defects within the coating will strongly influence its ability to mitigate whisker growth.

5 ACKNOWLEDGEMENTS

The authors would like to thank both the UK EPSRC Innovative Electronics Manufacturing Research Centre for funding this research through the WHISKERMIT programme and the Loughborough University Materials Research School. The authors would also like thank Sabrina Yan at the Loughborough Materials Characterisation Centre (LMCC) for her assistance with FIB cross-sectioning.

6 REFERENCES

- [1] G.T. Galyon, *Trans. on Elect. Pack. Manu.* 28 (2005) 94–122.
- [2] S. Mathew, M. Osterman, T. Shibutani, Q. Yu, M. Pecht, in: *Proc. IEEE Int. Sym. High Density Packag. Microsyst. Integr.*, 2007, pp. 1–8.
- [3] S. Han, M. Osterman, M. Pecht, *SMT Mag.* (2012) 48–56.
- [4] K.G. Compton, A. Medizza, S.M. Arnold, *Corrosion* 7 (1951) 327–334.
- [5] E. Chason, N. Jadhav, F. Pei, E. Buchovecky, A. Bower, *Prog. Surf. Sci.* 88 (2013) 103–131.
- [6] P. Zhang, Y.M. Zhang, Z.M. Sun, *J. Mat. Sci. Tech.* 31 (2015) 675–698.
- [7] S.M. Arnold, *Plating* 53 (1966) 96–99.
- [8] W.J. Boettinger, C. Johnson, L. Bendersky, K. Moon, M. Williams, G. Stafford, *Acta Mater.* 53 (2005) 5033–5050.
- [9] The European Parliament and The Council of The European Union, *Off. J. Eur. Union* 46 (2003) L37 19-23.
- [10] M. Martin, D. Lea, J. Nottay, C. Hunt, *Processability of Lead-Free Component Termination Materials*, 2001.
- [11] M. Osterman, *CALCE EPSC* (2002).
- [12] K.-N. Tu, K. Zeng, *Proc. IEEE Electron. Components Technol. Conf.* (2002) 1194–1200.
- [13] K.-N. Tu, J. Suh, A.T.-C. Wu, N. Tamura, C.-H. Tung, *Mat. Trans.* 46 (2005) 2300–2308.
- [14] K.-N. Tu, C. Chen, A.T. Wu, *J. Mat. Sci.* 18 (2007) 269–281.
- [15] K.-N. Tu, *Phys. Rev.* 49 (1994) 2030–2034.
- [16] K.S. Kumar, L. Reinbold, A.F. Bower, E. Chason, *J. Mat. Res.* 23 (2008) 2916–2934.
- [17] B.Z. Lee, D.N. Lee, *Acta Mater.* 46 (1998) 3701–3714.

- [18] K.N. Tu, J.C.M. Li, *Mater. Sci. Eng. a-Structural Mater. Prop. Microstruct. Process.* 409 (2005) 131–139.
- [19] C.Y. Chang, R.W. Vook, *Thin Solid Films* 228 (1993) 205–209.
- [20] K.-W. Moon, C.E. Johnson, M.E. Williams, O. Kongstein, G.R. Stafford, C.A. Handwerker, W.J. Boettinger, *J. Electron. Mat.* 34 (2005) L31–L33.
- [21] C.-H. Su, H. Chen, H.-Y. Lee, C.Y. Liu, C.-S. Ku, A.T. Wu, *J. Electron. Mat.* 43 (2014) 3290–3295.
- [22] C.-H. Su, H. Chen, H.-Y. Lee, A.T. Wu, *Appl. Phys. Lett.* 99 (2011).
- [23] A.T. Wu, Y.C. Ding, *Microelectron. Reliab.* 49 (2009) 318–322.
- [24] M.A. Ashworth, D. Haspel, L. Wu, G.D. Wilcox, R.J. Mortimer, *J. Electron. Mat.* 44 (2015) 442–456.
- [25] D.M. Haspel, M.A. Ashworth, L. Wu, G.D. Wilcox, R.J. Mortimer, *Trans. IMF* 93 (2015) 332–341.
- [26] G.D. Wilcox, D.R. Gabe, M.E. Warwick, *Corr. Sci.* 28 (1988) 577–586.
- [27] R.E. Van De Leest, G. Krijl, *Thin Solid Films* 72 (1980) 237–246.
- [28] T.J. Driscoll, L.D. McCormick, W.C. Lederer, *Surf. Sci.* 187 (1987) 539–558.
- [29] D.F. Mitchell, G.I. Sproule, M.J. Graham, *Surf. Interface Anal.* 15 (1990) 487–497.
- [30] L.D. Lopez-Carreno, G. Benitez, L. Viscido, J.M. Heras, F. Yubero, J.P. Espinos, a R. Gonzalez-Elipe, *Surf. Interface Anal.* 26 (1998) 235–241.
- [31] NIST, NIST Stand. Ref. Database 20, Version 20 (n.d.).
- [32] S. Zhang, B. Yang, G. Kong, J. Lu, *Surf. Interface Anal.* (2017).
- [33] C.G. da Silva, I.C.P. Margarit-Mattos, O.R. Mattos, H. Perrot, B. Tribollet, V. Vivier, *Corros. Sci.* 51 (2009) 151–158.
- [34] K.-N. Tu, *Acta Metall.* 21 (1973) 347–354.
- [35] C.J. Stuttle, M.A. Ashworth, G.D. Wilcox, R.J. Mortimer, *Trans. IMF* 92 (2014) 272–281.

- [36] T.A. Woodrow, B.P. Works, Proc. SMTA Int. Conf (2006) 24–28.
- [37] W.J. Choi, T.Y. Lee, K.N. Tu, N. Tamura, R.S. Celestre, A.A. MacDowell, Y.Y. Bong, L. Nguyen, *Acta Mater.* 51 (2003) 6253–6261.
- [38] W.J. Choi, T.Y. Lee, K.N. Tu, N. Tamura, R.S. Celestre, A.A. MacDowell, Y.Y. Bong, L. Nguyen, G.T.T. Sheng, in: 52nd Electron. Components Technol. Conf. 2002 Proc., 2002, pp. 628–633.
- [39] H. Chen, H.Y. Lee, C.S. Ku, A.T. Wu, *J. Mater. Sci.* 51 (2016) 3600–3606.
- [40] J. Hektor, J.B. Marijon, M. Ristinmaa, S.A. Hall, H. Hallberg, S. Iyengar, J.S. Micha, O. Robach, F. Grennerat, O. Castelnau, *Scr. Mater.* 144 (2018) 1–4.

Table 1 Parameters used to produce molybdate conversion coatings using a pulsed current technique

Table 2 Parameters used for the optimisation of the tungstate conversion coating

Table 3 Summary of XPS depth profile measurements for molybdate conversion coated samples

Table 4 Summary of XPS depth profile measurements for tungstate conversion coated samples

Fig.1 Schematic showing how apparent length of whisker is viewed. a) shows the actual length of the whisker and b) shows the apparent length of the whisker

Fig.2 XPS depth profiles obtained from molybdate conversion coatings with respect to element concentration (top) and molybdenum peak binding energy (bottom): (a) & (b) 5 minutes immersion and (c) & (d) produced potentiostatically at -0.75 V vs. Ag/AgCl for 5 minutes. The pH of the conversion coating bath was 3.13

Fig.3 Optical micrograph of a molybdate conversion coating produced at -0.6 V vs. Ag/AgCl for 5 min on pure Sn after ~2 months of room temperature storage

Fig.4 XPS depth profile of a tungstate conversion coating formed by a pulsed current method at $\pm 5 \text{ mA cm}^{-2}$ for 150 cycles (EC.2)

Fig.5 Photographs of tungstate conversion coatings showing the coating quality. a) $\pm 10 \text{ mA cm}^{-2}$ 30 cycles, b) $\pm 5 \text{ mA cm}^{-2}$ 60 cycles, c) $\pm 10 \text{ mA cm}^{-2}$ 150 cycles d) $\pm 5 \text{ mA cm}^{-2}$ 150 cycles, e) $\pm 10 \text{ mA cm}^{-2}$ 90 cycles, f) $\pm 5 \text{ mA cm}^{-2}$ 180 cycles, g) $\pm 10 \text{ mA cm}^{-2}$ 45 cycles and h) $\pm 5 \text{ mA cm}^{-2}$ 90 cycles. All coatings were deposited onto $5 \mu\text{m}$ pure Sn

Fig.6 Optical images of tungstate conversion coatings on $2 \mu\text{m}$ Sn-Cu ~3 months after deposition: a) $\pm 10 \text{ mA cm}^{-2}$ 45 cycles, b) $\pm 5 \text{ mA cm}^{-2}$ 90 cycles and c) $\pm 5 \text{ mA cm}^{-2}$ 150 cycles. The arrows indicate 'weak points'

Fig.7 SEM micrographs of tungstate conversion coatings on $5 \mu\text{m}$ pure Sn. a) $\pm 10 \text{ mA cm}^{-2}$ 30 cycles, b) $\pm 5 \text{ mA cm}^{-2}$ 60 cycles, c) $\pm 10 \text{ mA cm}^{-2}$ 90 cycles, d) $\pm 10 \text{ mA cm}^{-2}$ 150 cycles and e) $\pm 10 \text{ mA cm}^{-2}$ 150 cycles showing examples of 'weak points' in the conversion coating

Fig.8 Graph comparing the evolution of whisker density with storage time for electroplated Sn-Cu samples left untreated and those electrochemically oxidised at 2 V vs. Ag/AgCl

Fig.9 Graph comparing the evolution of oxide thickness, measured using XPS, with storage time for electroplated Sn-Cu samples left untreated and those electrochemically oxidised at 2 V vs. Ag/AgCl

Fig.10 Graph comparing the longest measured apparent whisker length with storage time for untreated and electrochemically oxidised (2 V vs. Ag/AgCl) electroplated Sn-Cu samples

Fig.11 Graph showing the whisker distribution of untreated and electrochemically oxidised (2 V vs. Ag/AgCl) Sn-Cu electroplated samples after (a) 14 days and (b) 119 days of storage

Fig.12 Graph showing the effect of a molybdate conversion coating on whisker growth from electroplated Sn-Cu samples after storage at room temperature

Fig.13 SEM micrograph showing whiskers growing from cracks in the molybdate coating produced at -0.6 V vs. Ag/AgCl for 5 min on $2 \mu\text{m}$ thick Sn-Cu electroplate

Fig.14 Graph showing the effect of a tungstate conversion coating on whisker growth from electroplated Sn-Cu samples after storage at room temperature

Fig.15 SEM micrographs showing a high concentration of whisker growth from 'weak points' on tungstate coatings produced at a) $\pm 5 \text{ mA cm}^{-2}$ for 150 cycles on $2 \mu\text{m}$ Sn-Cu electroplate and b) $\pm 10 \text{ mA cm}^{-2}$ for 45 cycles on $2 \mu\text{m}$ Sn-Cu electroplate

Fig.16 FIB cross-section $2 \mu\text{m}$ Sn-Cu electrodeposits on Cu, a) molybdate conversion coating produced at -0.6 V vs. Ag/AgCl for 5 min after 19 weeks of room temperature storage and b) tungstate conversion coating produced at 10 mA cm^{-2} for 45 cycles after ~ 24 weeks of room temperature storage

Figure 1

[Click here to download Figure Fig1.tif](#)

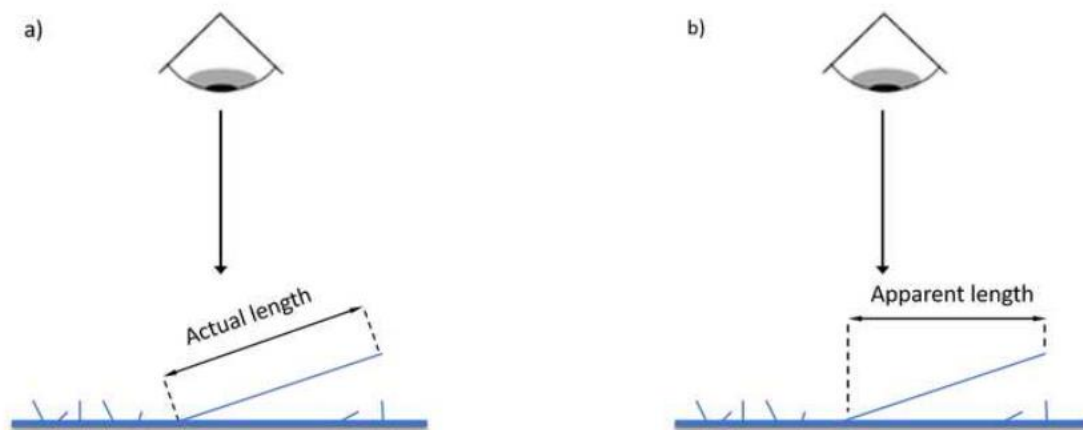


Figure 2

[Click here to download Figure Fig2.tif](#)

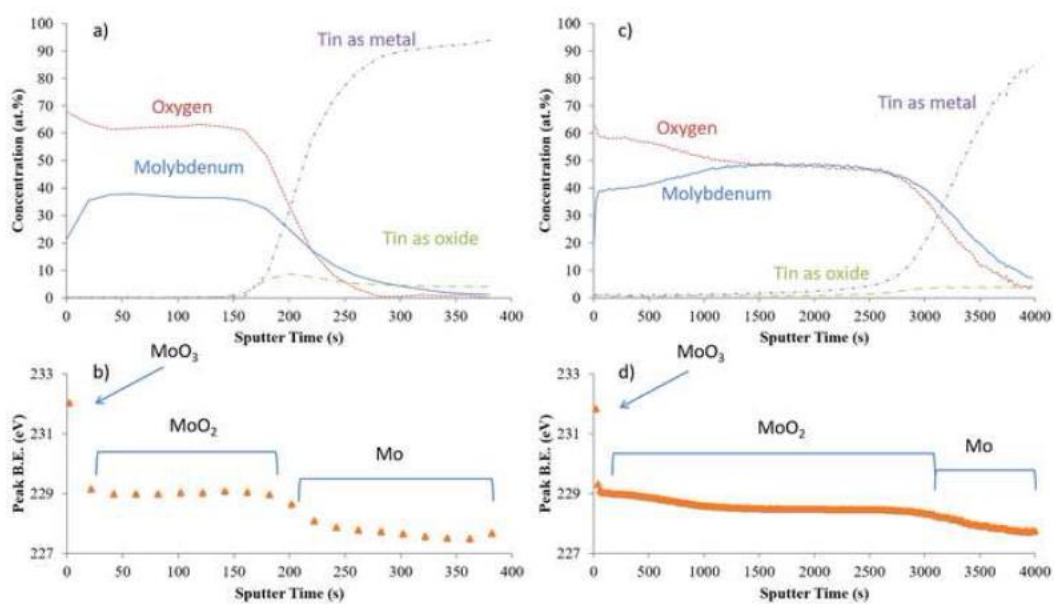


Figure 3

[Click here to download Figure Fig3.tif](#)

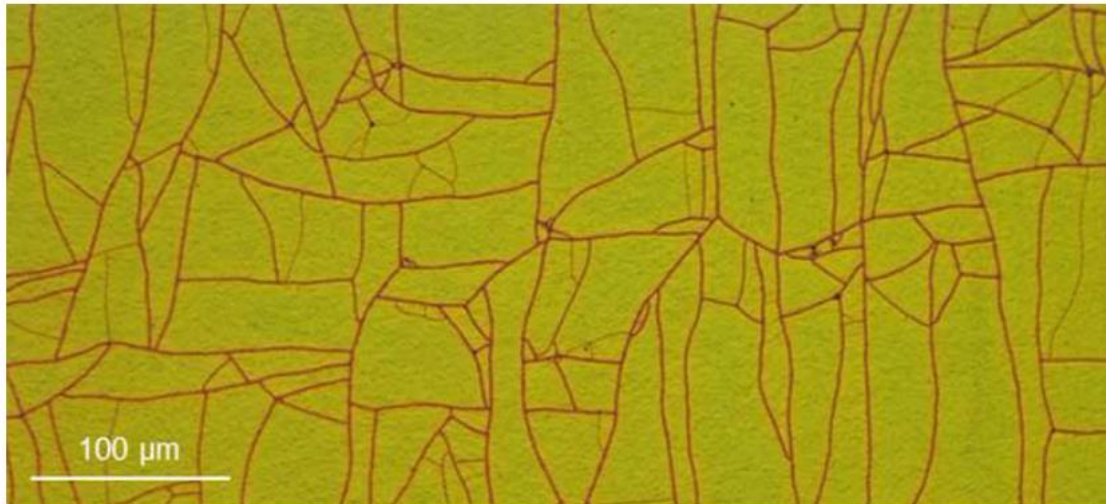


Figure 4

[Click here to download Figure Fig4.tif](#)

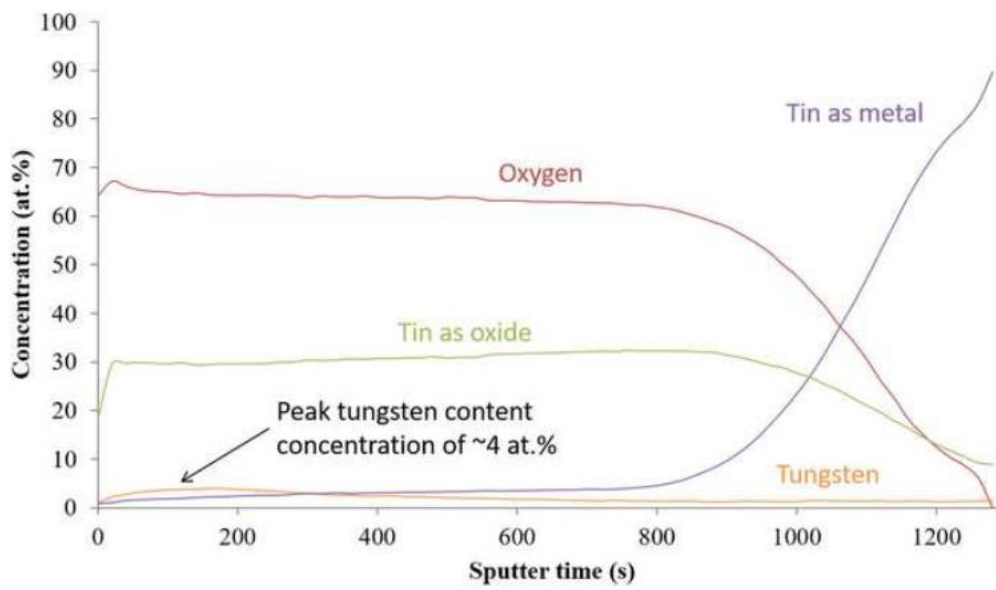


Figure 5

[Click here to download Figure Fig5.tif](#)

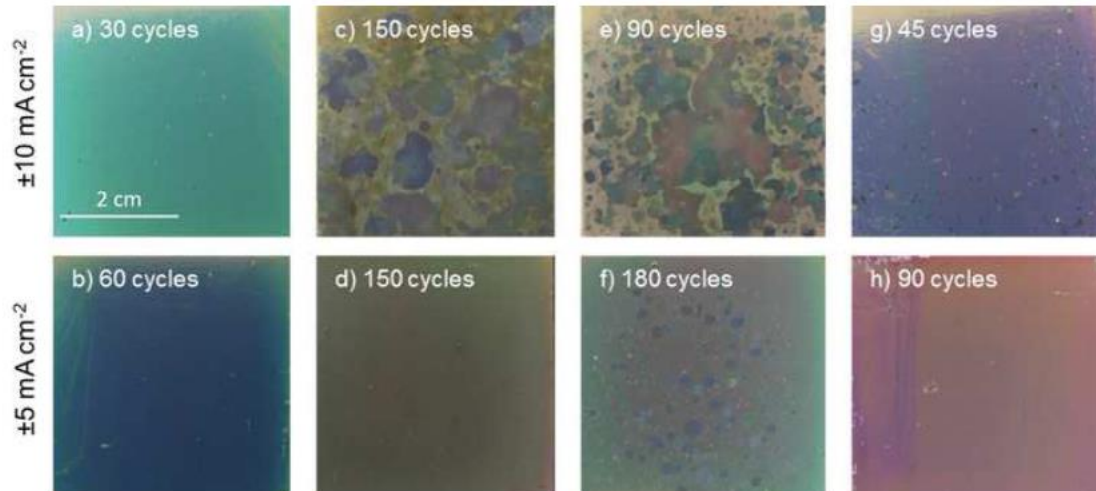
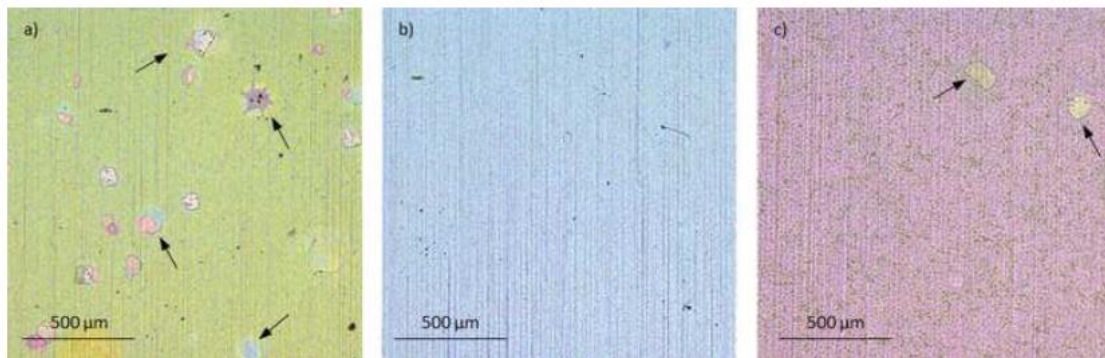


Figure 6

[Click here to download Figure Fig6.tif](#)



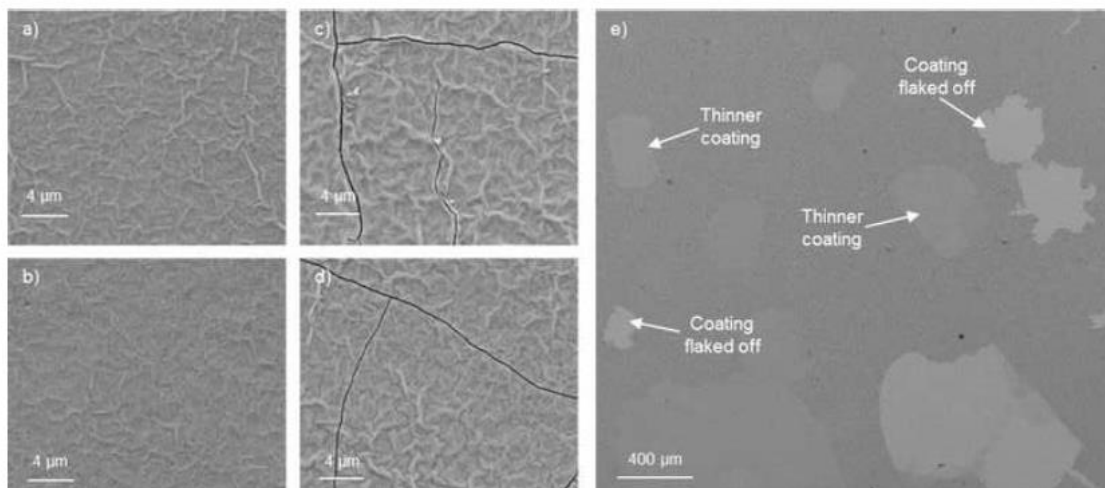


Figure 8

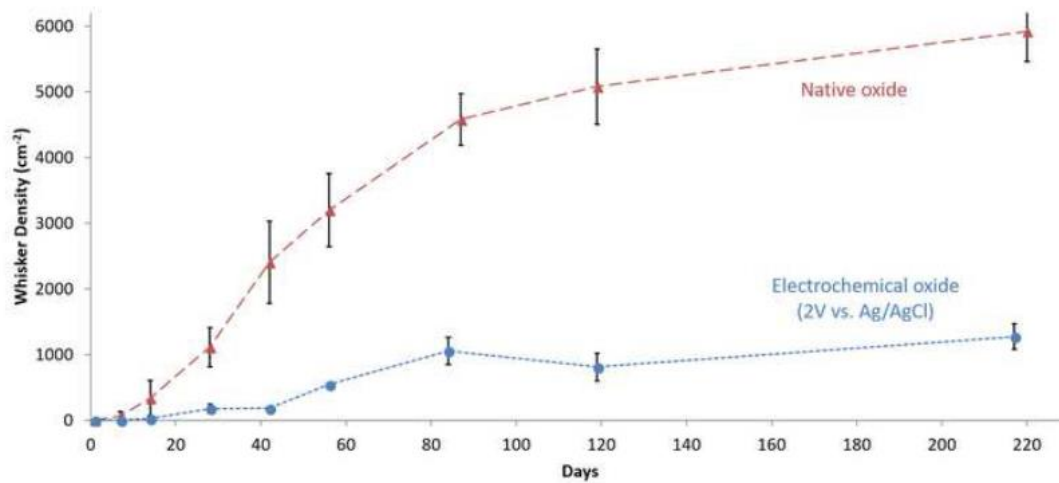


Figure 9

[Click here to download Figure Fig9.tif](#)

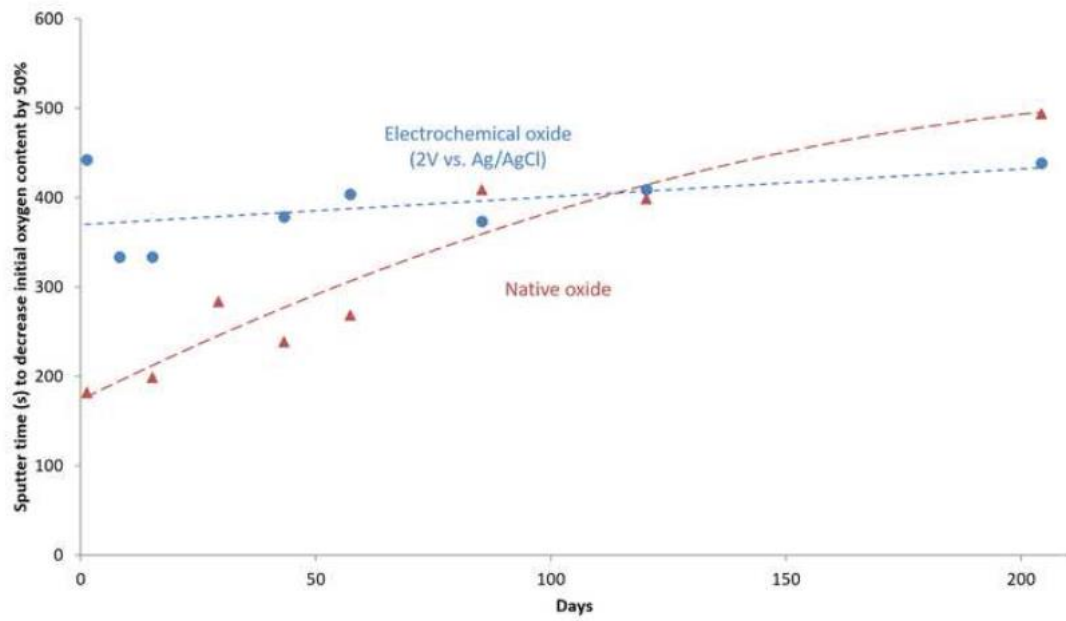


Figure 10

[Click here to download Figure Fig10.tif](#)

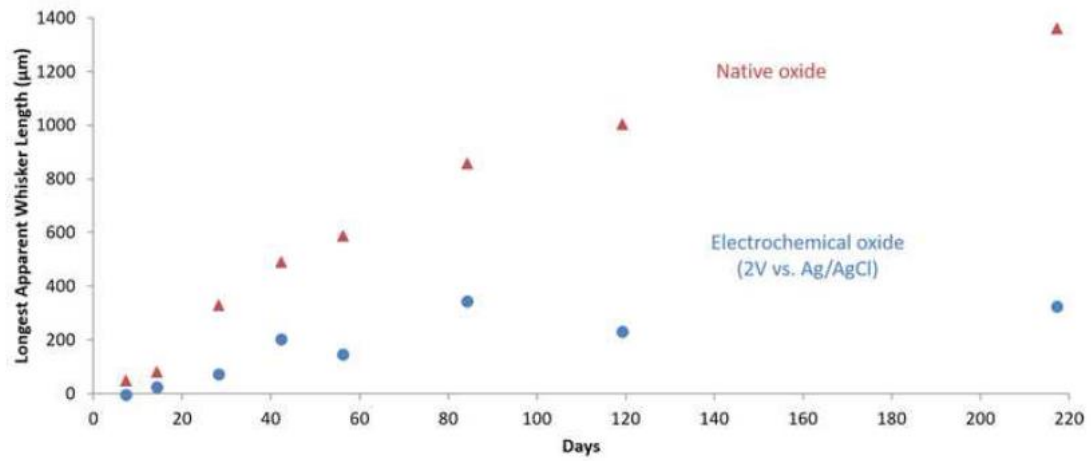


Figure 11

[Click here to download Figure Fig11.tif](#)

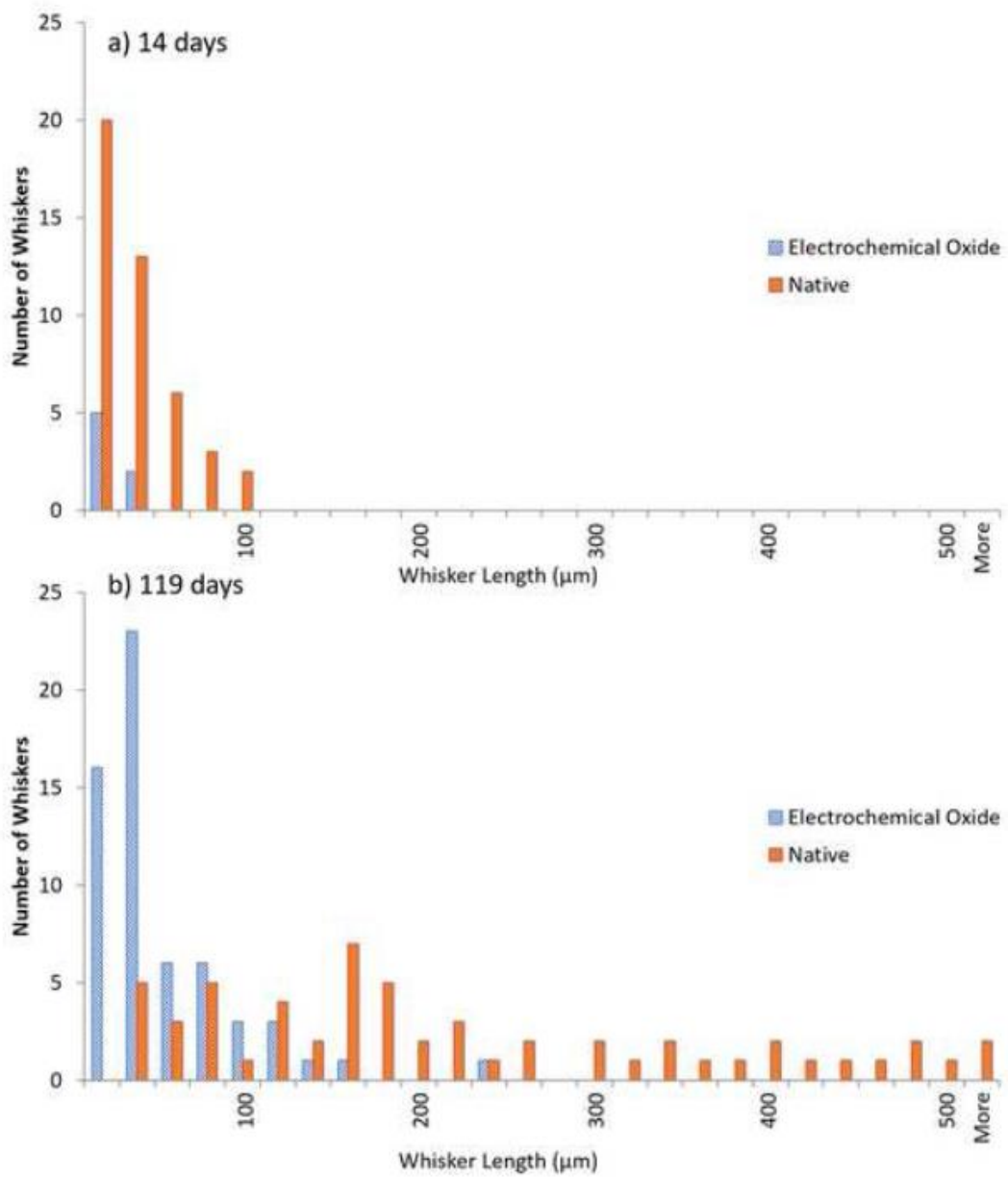


Figure 12

[Click here to download Figure Fig12.tif](#)

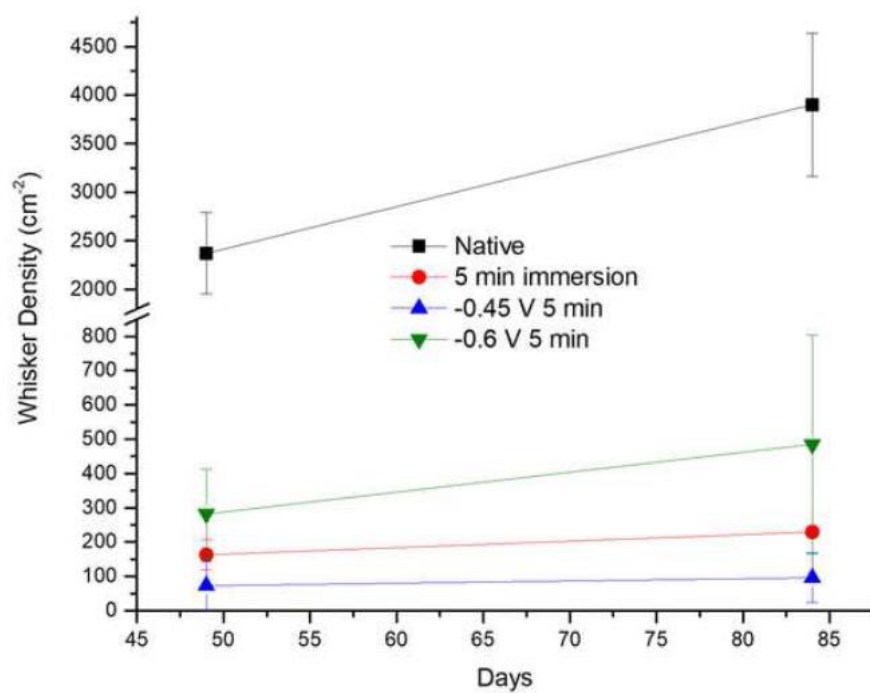


Figure 13

[Click here to download Figure Fig13.tif](#)

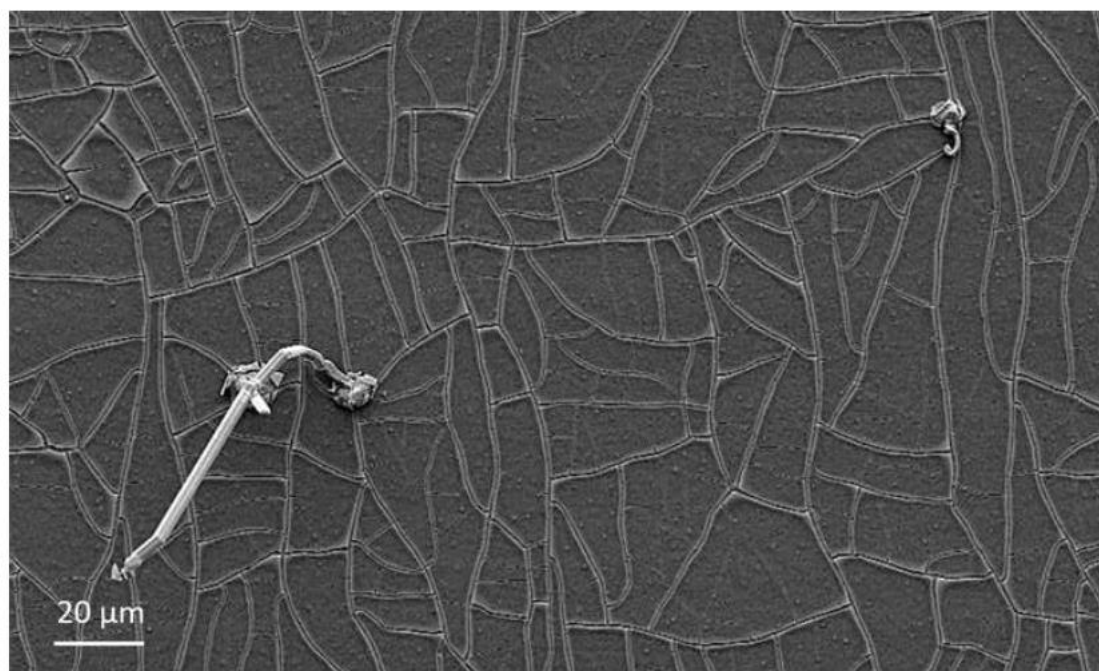


Figure 14

[Click here to download Figure Fig14.tif](#)

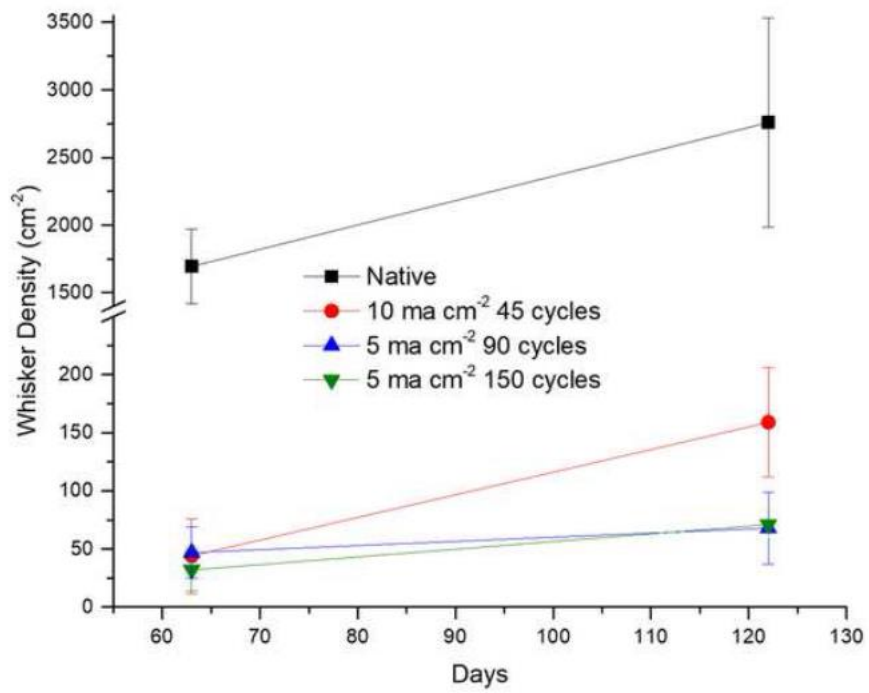
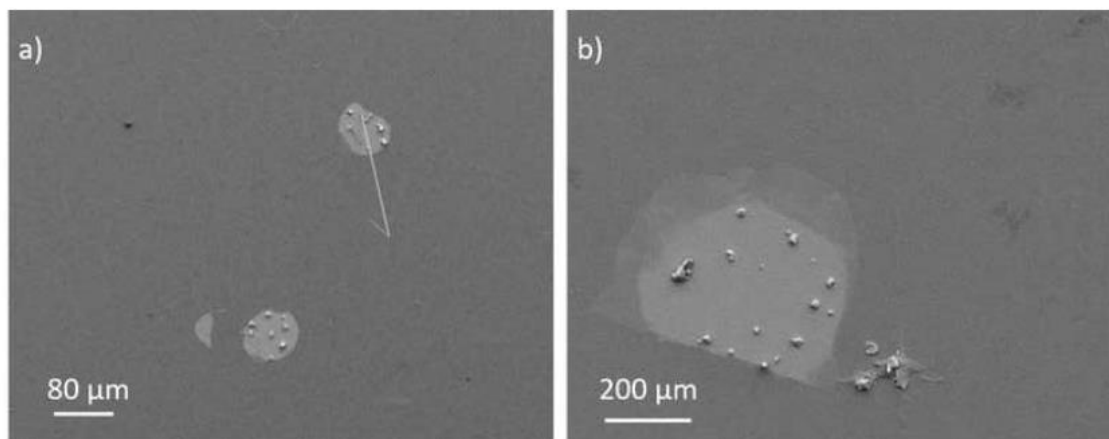


Figure 15

[Click here to download Figure Fig15.tif](#)



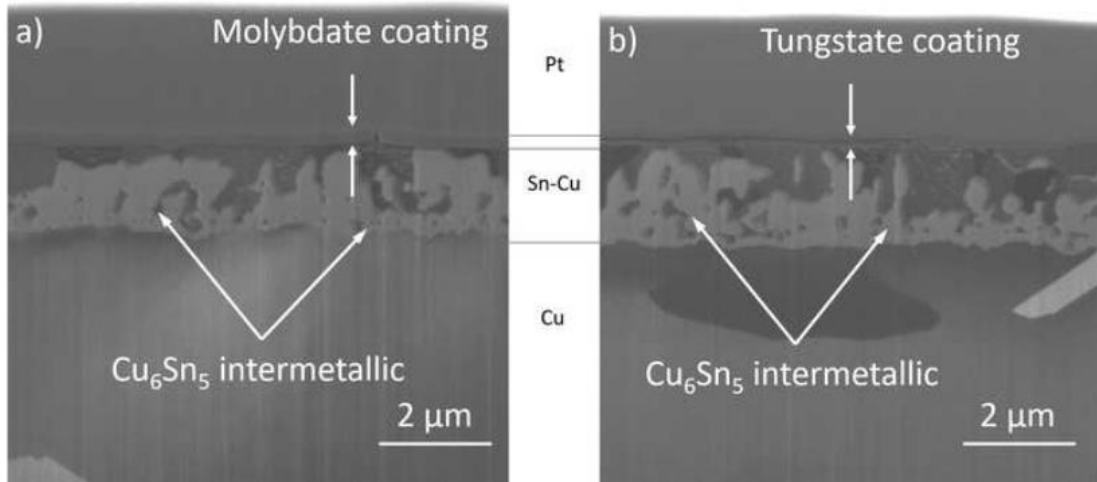


Table I

[Click here to download Table Table I.docx](#)

Current Density	Frequency	Number of Square Waves
$\pm 10 \text{ mA cm}^{-2}$	0.5 Hz	30
$\pm 5 \text{ mA cm}^{-2}$	0.5 Hz	30
$\pm 2.5 \text{ mA cm}^{-2}$	0.5 Hz	30
$\pm 2.5 \text{ mA cm}^{-2}$	0.5 Hz	120

Table II

[Click here to download Table Table II.docx](#)

Experiment	Trial Number	Current Density	Frequency	Number of Square Waves
Comparison of Current Density	CD.1	$\pm 2.5 \text{ mA cm}^{-2}$	0.5 Hz	30
	CD.2	$\pm 5 \text{ mA cm}^{-2}$	0.5 Hz	30
	CD.3	$\pm 10 \text{ mA cm}^{-2}$	0.5 Hz	30
Comparison of Number of Cycles	NC.1	$\pm 5 \text{ mA cm}^{-2}$	0.5 Hz	30
	NC.2	$\pm 5 \text{ mA cm}^{-2}$	0.5 Hz	90
	NC.3	$\pm 5 \text{ mA cm}^{-2}$	0.5 Hz	150
Comparison of Equivalent Charge Passed	EC.1	$\pm 2.5 \text{ mA cm}^{-2}$	0.5 Hz	300
	EC.2	$\pm 5 \text{ mA cm}^{-2}$	0.5 Hz	150
	EC.3	$\pm 10 \text{ mA cm}^{-2}$	0.5 Hz	75

Experiment	Sputter time to 50% oxygen content	Molybdenum content at plateau region
5 min immersion	200 s	~37 at.%
$\pm 5 \text{ mA cm}^{-2}$ 30 cycles	340 s	~36.5 at.%
$\pm 2.5 \text{ mA cm}^{-2}$ 30 cycles	215 s	~36 at.%
$\pm 2.5 \text{ mA cm}^{-2}$ 120 cycles	440 s	~37 at.%
-0.45 V 5min	280 s	~37 at.%
-0.6 V 5min	1085 s	~40 at.%
-0.75 V 5min	3095 s	~40-48 at.%
2V 60 mC cm ⁻² (potassium bath)	27 s	N/A

Tin whisker mitigation by means of a post-electroplating electrochemical oxidation treatment

D. M. Haspel^{1*}, M. A. Ashworth¹, L. Wu¹, G. D. Wilcox¹ and R. J. Mortimer²

There are very few studies that have investigated directly the effect of an oxide film on tin whisker growth, since the 'cracked oxide theory' was proposed by Tu in 1994 [K.-N. Tu: Phys. Rev., 1994, 49, (3), 2030–2034]. The current study has investigated the effect of an electrochemically produced oxide on tin whisker growth, for both Sn–Cu electrodeposits on Cu and pure Sn electrodeposits on brass. X-ray photoelectron spectroscopy (XPS) has been used to investigate the effect of the applied electrochemical oxidation potential on the oxide film thickness. Focused ion beam has been used to prepare cross sections from electrodeposited samples to investigate the influence of the electrochemically formed oxide film on deposit microstructure during long-term room temperature storage. The XPS studies show that the thickness of electrochemically formed oxide film is directly influenced by the applied potential and the total charge passed. Whisker growth studies show that the electrochemical oxidation treatment mitigates whisker growth for both Sn–Cu electrodeposits on Cu and pure Sn electrodeposits on brass. For Sn electrodeposits on brass, the electrochemically formed oxide greatly reduces both the formation of zinc oxide at the surface and the formation of intermetallic compounds, which results in the mitigation of tin whisker growth. For Sn–Cu electrodeposits on Cu, the electrochemically formed oxide has no apparent effect on intermetallic compound formation and acts simply as a physical barrier to hinder tin whisker growth.

Keywords: Tin, Electrochemical oxidation, Electrodeposition, Whisker growth, Intermetallic compounds

1. Introduction

A tin whisker is a growth of pure tin that is commonly in the form of a filament, which can grow up to a few millimetres in length, from a thin tin coating (around 0.5–50 µm thick) that has been electroplated onto a substrate.² The incubation period prior to the growth of a whisker is uncertain and it is this unpredictability that causes concern to the reliable operation of electronic components.³ At the current time, there is no one widely accepted mechanism for why and how whiskers grow; though there are a number of theories and some commonly agreed factors that affect the growth of tin whiskers.^{2,4,5}

Whisker growth has been shown to cause major reliability problems in high value, long-term electronics, such as satellites and rocket systems, mainly due to these whiskers growing from one surface and then coming into contact with another, adjacent, surface, resulting in a short circuit and subsequent electronic failure. Circuits can also short by long filament type whiskers breaking

off and landing across adjacent terminals. Both of these types of failures occur at low currents. At high currents the whiskers can volatilise, which causes a conductive metal gas, which in turn can create a metal vapour arc reaction.⁶ This metal vapour arc can generate such high temperatures that it can melt metals and incinerate polymers.

Until recently, whisker growth was successfully mitigated by alloying tin with lead.^{7,8} However, restrictions on the use of lead, as a result of EU legislation (RoHS), have led to a renewed interest in finding alternative mitigation strategies. There are a number of different mitigation techniques that are currently used to combat this problem, including post-electroplating annealing, alloying, applying a polymeric conformal coating to act as a physical barrier and the use of a nickel underlayer to prevent intermetallic formation.⁹

There has been very little research on the role of the oxide layer in whisker growth. The cracked oxide theory proposed by Tu^{1,10,11} suggested that the tin oxide film played a critical role in the growth of tin whiskers and that a very thick oxide would physically block the growth of filament whiskers or hillocks by reducing the risk of localised oxide cracking. For whiskers to grow, it is first necessary to break the oxide film at weak points and

¹Department of Materials, Loughborough University, Loughborough, Leicestershire LE11 3TU, UK

²Department of Chemistry, Loughborough University, Loughborough, Leicestershire LE11 3TU, UK

*Corresponding author, email d.haspel@lboro.ac.uk

from these, the whiskers will subsequently grow to relieve stress.^{12,13} It was suggested by Chang and Vook¹⁴ that no whiskers will grow in the absence of an oxide film as the deposit would be able to relieve internal stress by uniform creep of tin atoms to the deposit surface. However, Moon *et al.*¹⁵ later showed that whisker growth occurred on Sn–Cu electrodeposits that had been stored for 9 days under vacuum with the surface oxide initially removed by ion beam sputtering. A recent study carried out by Su *et al.*¹⁶ showed the importance of weak points in the oxide, by using 200 nm thick sputter deposited tin oxide films with pre-defined arrays of weak spots built into the oxide film using lithography. It was observed that an increased number of whiskers grew from samples that had a greater number of weak spots.

In a previous study¹⁷ the authors presented some initial results, which indicated that whisker growth could be reduced by the application of an electrochemical oxide film. The current paper builds upon this initial work to more fully investigate the influence of applied potential and charge passed on the oxide film developed and its effect on whisker growth. The effect of the electrochemical oxide treatment on the development of the deposit microstructure during long-term storage is also investigated to more fully understand the mechanism by which whisker growth is mitigated.

2. Experimental

2.1. Electrodeposition of tin

Pure Sn was electrodeposited onto both Cu (Advent Research Materials, 99.9%, 0.1 mm and 0.4 mm thickness) and brass (Goodfellow, 63% Cu/37% Zn, 0.38 mm thickness) substrates, using a bright acid Sn electroplating solution. A Sn–Cu alloy was also electrodeposited onto Cu for whisker growth trials. The tin electroplating solution contained 60 g L⁻¹ tin sulphate (Sigma Aldrich), 70 mL L⁻¹ sulphuric acid (Fisher Scientific) and 40 mL L⁻¹ Tinmac Stannolyte (MacDermid), a proprietary additive that acts as a brightener. Electrodeposition of 2 µm and 5 µm pure Sn onto Cu and brass was carried

out using a current density of 20 mA cm⁻². For the electrodeposition of Sn–Cu alloys the Sn electroplating bath was modified by the addition of Cu ions at a concentration of 10 mmol L⁻¹, using Cu sulphate. Electrodeposition of 2 µm Sn–Cu onto Cu was carried out using a current density of 10 mA cm⁻², which resulted in a uniform electrodeposit with a Cu content of ~1 wt%.

The test coupons used had dimensions of 2 × 4 cm and were masked with chemically resistant tape to result in an electroplated area of 2 × 2 cm. Larger test coupons with dimensions 4 × 6 cm and an electroplated area of 4 × 4.5 cm were used for whisker growth studies. The coupons were used in the as-supplied condition with no additional polishing or grinding. Electrodeposition of pure Sn was carried out using a 99.95% Sn foil anode (Advent Research Materials, 0.25 mm), whilst electrodeposition of the Sn–Cu was carried out using a platinised titanium mesh anode. Immediately prior to electrodeposition, all the coupons were degreased using acetone (Fisher Scientific), pickled for 60 s in a 20% v/v solution of sulphuric acid (SG 1.83, Fisher Scientific), rinsed in deionised water and dried using hot air. The thickness of pure Sn electrodeposits was 5 µm for cyclic voltammetry and electrochemical oxidation trials. The thickness of pure Sn and Sn–Cu electrodeposits was 2 µm for whisker growth studies.

2.2. Preparation of the electrolyte solution for tin oxidation

For the electrochemical oxidation of the Sn electrodeposits two solutions were selected, a pH 8.9 potassium bicarbonate–potassium carbonate solution (0.75 mol L⁻¹ of potassium bicarbonate, Sigma Aldrich, and 0.05 mol L⁻¹ of potassium carbonate, Sigma Aldrich) and a pH 8.4 borate buffer solution (9.55 g L⁻¹ sodium borate, Sigma Aldrich, and 6.18 g L⁻¹ boric acid, Sigma Aldrich). Both electrolyte solutions were prepared using deionised water and the pH was adjusted to the required value, using additions of sodium hydroxide (Fisher Scientific).

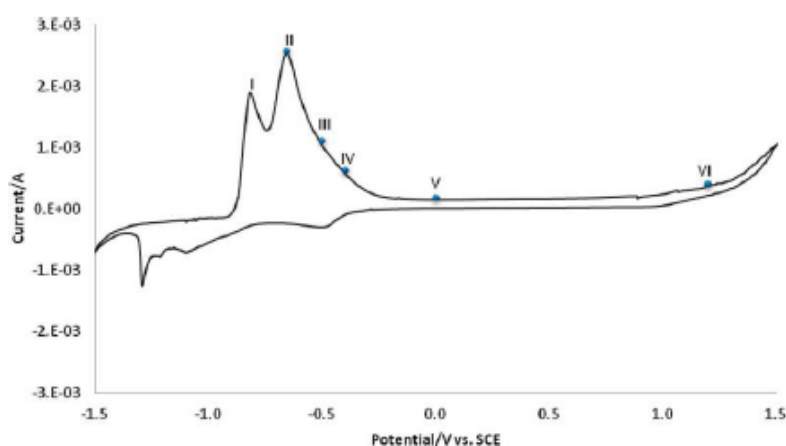


Figure 1 A cyclic voltammogram for electroplated tin on copper with a thickness of 5 µm in a potassium bicarbonate–carbonate oxidising bath at a scan rate of 10 mV s⁻¹

Table 1 The proportion of tin metal and tin oxide species constituting the Sn 3d_{5/2} peak as function of the applied electrochemical oxidation potential, showing the proportion of tin metal with tin oxide

Sample treatment V vs. SCE	Proportion of species	
	Tin metal %	Tin oxide %
Native air-formed	33	67
-0.66 V	23	77
-0.5 V	25	75
-0.4 V	20	80
0 V	16	82
1.2 V	4	96
1.6 V	2	98
2.0 V	1	99

2.3. Cyclic voltammetry

Cyclic voltammetry was carried out for Sn electrodeposits in naturally aerated pH 8.9 potassium bicarbonate–potassium carbonate solution to determine the location of the oxidation peaks. Analysis was carried out using a Solartron SI 1286 Electrochemical Interface potentiostat by means of a 3-electrode cell comprising a static Sn electrodeposit as the working electrode, a saturated calomel reference electrode (SCE) and a platinised titanium mesh counter electrode. The electrode potential was swept from a starting potential of -1.1 V down to -1.5 V, reversed up to 1.5 V and finally returned to -1.1 V (all vs SCE) using a linear scan rate of 10 mV s⁻¹.

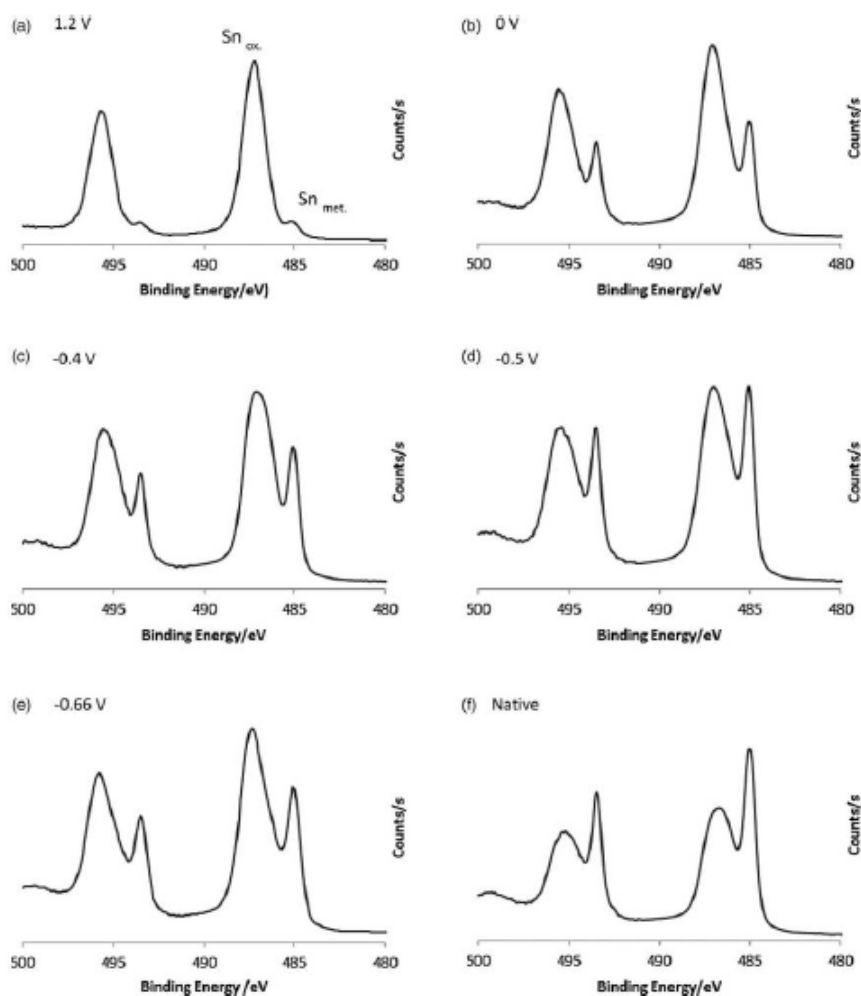


Figure 2 XPS high resolution Sn 3d scans of 5 μm tin electrodeposits on copper electrochemically oxidised in a potassium bicarbonate–carbonate solution that had been stored at room temperature for ~21 h. The charge passed was 30 mC cm⁻²: (a) 1.2 V vs. SCE (b) 0 V vs. SCE (c) -0.4 V vs. SCE (d) -0.5 V vs. SCE (e) -0.66 V vs. SCE (f) native air-formed oxide

2.4. Electrochemical oxidation of tin

Electrochemical oxidation was carried out immediately after tin electrodeposition using a Solartron SI 1286 Electrochemical Interface potentiostat using the 3-electrode cell previously described. Following immersion of the coupon into the naturally aerated electrolyte solution, the Sn electrodeposit was initially held at a potential of -1.5 V vs. SCE to reduce the pre-existing oxide. When hydrogen evolution was observed the surface was agitated using a pipette to remove the bubbles and the potential was increased to the desired value for oxidation.

2.5. Characterisation of electrochemically formed oxides

Two charges were set as limits, 30 mC cm^{-2} and 60 mC cm^{-2} . The effect of charge passed and oxidation potential on the composition and thickness of the oxide film was investigated by X-ray photoelectron spectroscopy (XPS) using a Thermo-Scientific K-Alpha X-ray photoelectron spectrometer. Sputter depth profiling was carried out using 200 eV argon ions with an estimated etch rate of $\sim 0.01 \text{ nm s}^{-1}$. XPS analysis was carried out within 24 h of electrodeposition and electrochemical oxidation, unless otherwise stated.

2.6. Characterisation of tin deposits

The effect of an electrochemical oxide film on the microstructural evolution of electrodeposited Sn and Sn-Cu alloys was investigated by means of cross sections that were prepared by focused ion beam (FIB) milling, using a FEI Nova 600 Nanolab Dual Beam FIB-SEM. Ion beam milling was carried out at a 52° tilt angle with 30 kV gallium ion beam. Initial trench milling was carried out at 20 nA and the final face milling was carried out at 3 nA with a tilt angle of 53.5° . Ion beam images were acquired using the gallium ion beam at a current of 30 pA .

2.7. Whisker growth studies

The effect of the electrochemically formed oxides on whisker growth was assessed using $2 \mu\text{m}$ Sn electrodeposits on brass and $2 \mu\text{m}$ Sn-Cu electrodeposits on Cu. For each electrochemical oxidation treatment three identical samples were prepared. After electrodeposition and electrochemical oxidation, the samples were stored at room temperature ($\sim 20^\circ\text{C}$). The growth of whiskers was studied using both optical microscopy and scanning electron microscopy (SEM). The density of whiskers was measured using an optical microscope with an objective magnification of either $\times 20$ or $\times 10$. SEM analysis was carried out using a Carl Zeiss Leo 1530 VP field emission gun SEM (FEGSEM) and an operating voltage of 10 kV .

3. Results and discussion

3.1. Development of the electrochemical oxide

Cyclic voltammetry was conducted using a standard potassium bicarbonate-carbonate electrolyte to identify suitable potentials for subsequent electrochemical oxidation trials (Fig. 1). Two oxidation peaks (I and II) were recorded at potentials of -0.83 V and -0.66 V vs. SCE respectively. Peaks I and II have been attributed previously to the two Sn oxidation states, Sn(II) and Sn(IV) respectively.^{18,19} However, Diaz *et al.*²⁰ have also suggested that oxidation peaks I and II both corresponded to the oxidation of Sn to Sn(II).

The potentials chosen for electrochemical oxidation studies, were -0.66 V (II), -0.5 V (III), -0.4 V (IV), 0 V (V) and 1.2 V (VI) (all vs. SCE). Oxidation peak I (-0.83 V vs. SCE) was not studied because it had previously been shown to produce an oxide film comparable to a native oxide.¹⁷ The electrochemical oxidation potentials -0.4 V and -0.5 V vs. SCE were chosen as they occurred upon the broad trailing slope of the second oxidation peak which would suggest large amounts of activity within this region and it was suggested by Drogowska *et al.*¹⁹ that this broad slope corresponds to a

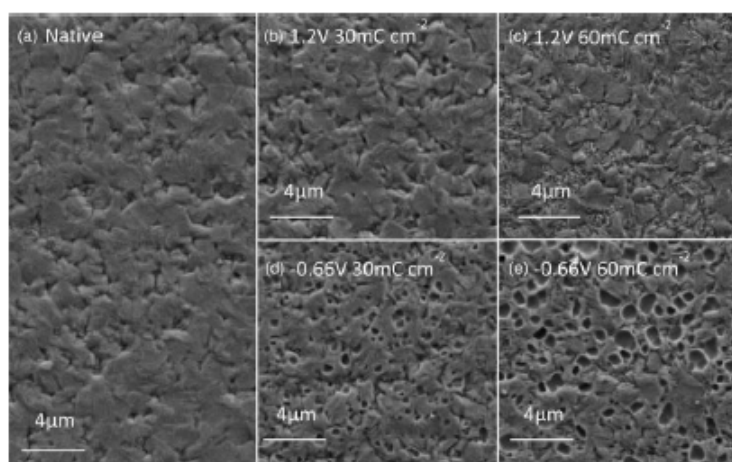


Figure 3 SEM micrographs showing the effect of electrochemical oxidation potential on the surface morphology of the electroplated tin, where (a) a native air-formed oxide (b) 1.2 V vs. SCE, 30 mC cm^{-2} , (c) 1.2 V vs. SCE, 60 mC cm^{-2} , (d) -0.66 V vs. SCE, 30 mC cm^{-2} , and (e) -0.66 V vs. SCE, 60 mC cm^{-2}

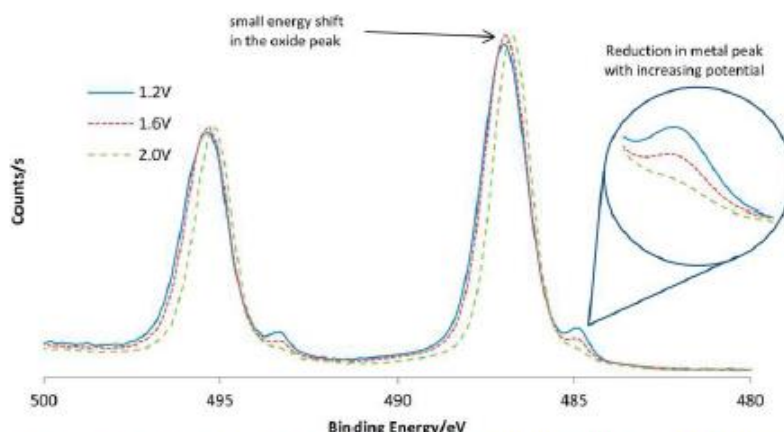


Figure 4 XPS high resolution scans of the Sn 3d peaks after electrochemical oxidation in a potassium bicarbonate-carbonate solution at potentials of 1.2 V (blue), 1.6 V (green) and 2.0 V (red) all vs. SCE

dehydration reaction that results in the formation of SnO₂. The electrochemical oxidation potential of 0 V vs. SCE was chosen as it occurred on the part of the voltammogram that had the lowest anodic current, which was suggested by Drogowska *et al.*¹⁹ to be the region of passivity. The electrochemical oxidation potential of 1.2 V vs. SCE was chosen as it was previously shown to produce a thick oxide film.¹⁷

The effect of electrochemical oxidation potential on the Sn oxide thickness, for a charge passed of 30 mC cm⁻², is shown in the XPS high resolution scans of the Sn 3d peak in Fig. 2; a high resolution Sn 3d scan of a native air-formed oxide is also shown for comparison. The relative intensity of the Sn oxide and Sn metal peaks, at ~487 eV and ~485 eV respectively, enables the comparative thickness of the oxide layer to be inferred. It is evident from Fig. 2 that the native air-formed oxide is very thin compared with oxide films that are formed electrochemically. Results show that the thickest electrochemical oxide film was produced at a potential of 1.2 V vs. SCE, which is

consistent with previous trials.¹⁷ The Sn oxide and Sn metal contributions as a function of electrochemical oxidation potential are summarised in Table 1, which clearly indicates that the thickness of the Sn oxide increases as the oxidation potential is increased.

Samples with electrochemically formed oxides were analysed using SEM to study the effect of electrochemical oxidation on the surface of the Sn electrodeposit. It is apparent from Fig. 3 that electrochemical oxidation at certain potentials (e.g. -0.66 V vs. SCE) can have a pronounced effect on the surface topography. However, the surface of samples electrochemically oxidised at a potential of 1.2 V vs. SCE (30 mC cm⁻² of charge passed) is indistinguishable from that of a native air-formed oxide. Increasing the amount of charge passed, increases the extent of the surface roughening for samples electrochemically oxidised at a potential of -0.66 V vs. SCE (Fig. 3c). This may suggest that a Sn dissolution reaction has occurred. The size and shape of the surface features are comparable to that of the Sn grains. Similar features

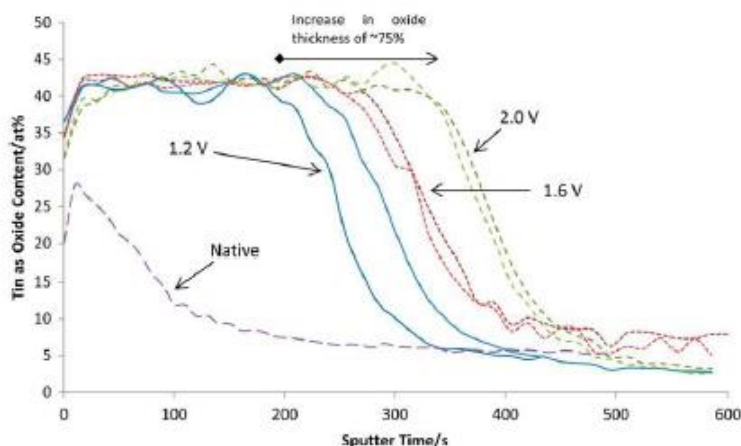


Figure 5 XPS depth profiles showing the distribution of Sn_{oxide} as a function of applied electrochemical oxidation potential

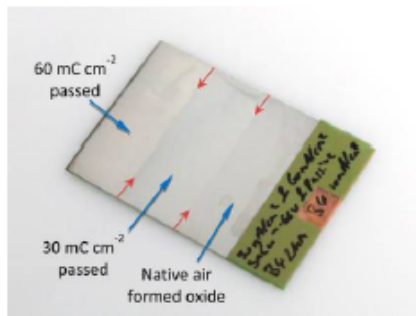


Figure 6 Test coupon used to investigate the effect of applied oxidation potential and charge passed on whisker growth

were also observed in an earlier study by Ashworth *et al.*¹⁷ for electrochemical oxidation at the same potential.

Further electrochemical oxidation trials were undertaken using the potassium bicarbonate-potassium carbonate solution, at potentials greater than 1.2 V *vs.* SCE, in an attempt to increase the electrochemical oxide film thickness. The observed reduction in the intensity of the Sn metal peak with increasing electrochemical oxidation potential (Fig. 4) suggests that the oxide film thickness is increased. This is consistent with previous trials by Ashworth *et al.*¹⁷ using the same potentials in a borate buffer solution. As the electrochemical oxidation potential was increased from 1.2 V to 2.0 V *vs.* SCE the binding energy of the Sn oxide peak shifted from 487 eV to 486.8 eV. However, this does not necessarily indicate a difference in the oxide formed as

the binding energies all fall within the binding energy range for SnO₂.²¹

Depth profiling was carried out on each sample to confirm that electrochemical oxidation at potentials above 1.2 V *vs.* SCE does increase the thickness of the oxide. The depth profiles in Fig. 5 confirm that the oxide film increases in thickness with increasing electrochemical oxidation potential. Results show that when electrochemical oxidation is carried out at a potential of 2.0 V *vs.* SCE the thickness of the oxide film increases by ~75% compared with a potential of 1.2 V *vs.* SCE. An increase in the thickness of the oxide film should have a beneficial effect on whisker mitigation.^{1,10,11}

The effect of electrochemical oxidation on whisker growth was studied using 2 μm Sn-Cu electrodeposits on Cu and 2 μm Sn electrodeposits on brass. The Sn-Cu electrodeposits were oxidised at potentials ranging between -0.66 V and 2.0 V *vs.* SCE in a potassium bicarbonate-carbonate solution. The Sn electrodeposits on brass were oxidised at potentials ranging between 1.2 V and 2.0 V *vs.* SCE. In each case, control samples were prepared and left to develop native air-formed oxide films.

3.2. Whisker growth studies

3.2.1. Sn-Cu electrodeposits on Cu

For whisker growth studies using Sn-Cu electrodeposits on Cu, electrochemical oxidation was carried out at potentials of -0.66 V, -0.5 V, -0.4 V, 0.0 V and 1.2 V (all *vs.* SCE). Large test coupons were used, which contained three different areas of oxide; two areas were electrochemically oxidised with a different charge passed applied in each area (achieved by sequentially lowering the test coupon into the electrolyte; the other area was left to develop a native air-formed oxide (Fig. 6). Whiskers were counted on each area after ~2

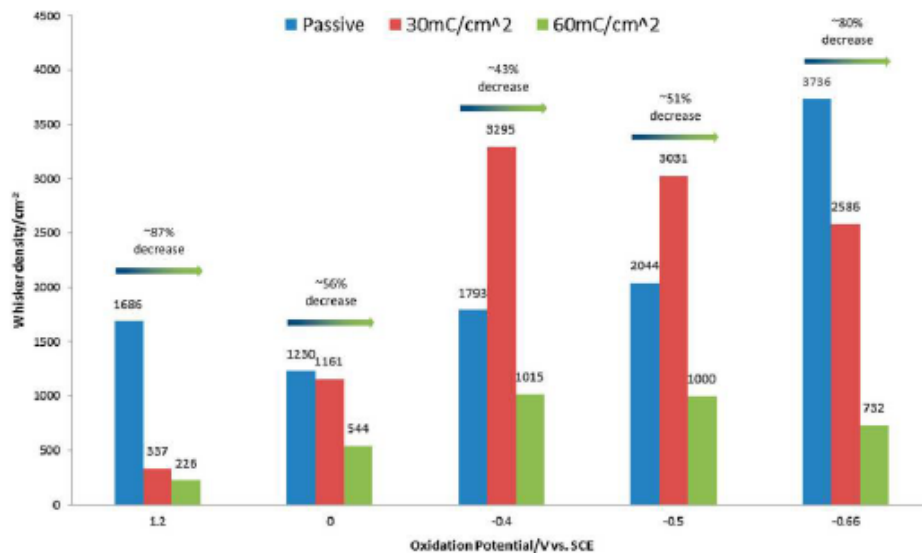


Figure 7 Graph showing the measured whisker density for electroplated tin samples electrochemically oxidised at different potentials after storage at room temperature for ~2 months

Table 2 Measured whisker densities for electrochemically oxidised 2 µm Sn–Cu electrodeposits on Cu after ~4 weeks of storage at room temperature

Oxidation potential V vs SCE	Average number of whiskers per cm ²	Number of frames with no whiskers (out of 60)
Native	264 ± 136	3
1.2 V	59 ± 65	23
1.6 V	37 ± 50	32
2.0 V	33 ± 49	34

months of storage and whisker densities were calculated (Fig. 7). An important observation is that there is a large difference in the whisker densities for the native oxides, ranging from ~1200 cm⁻² to ~3700 cm⁻². There are a number of possible explanations for this difference: firstly whisker growth is, by nature, unpredictable and sample to sample variations in whisker density are not uncommon.²² Secondly, there may be slight variations in the Cu content of the deposit, due to either Sn or Cu depletion since an inert counter electrode is being used and the electroplating bath is not being replenished with fresh metal ions.

For a charge passed of 30 mC cm⁻² electrochemical oxidation at 1.2 V, 0 V and -0.66 V vs. SCE (Fig. 7)

resulted in a reduction in whisker growth. However, electrochemical oxidation at potentials of -0.4 V and -0.5 V vs. SCE resulted in an increase in whisker density, despite the fact that the oxide film is thicker than that of the native oxide. Further work is planned to investigate the cause of the increased whisker growth.

For a charge passed of 60 mC cm⁻², all of the electrochemical oxide films significantly reduced the whisker density compared with the corresponding native oxide film (Fig. 7). This reduction in whisker density is mostly likely due to the presence of a thicker oxide film, which would be in agreement with Tu's cracked oxide theory,^{1,10,11} which proposed that a thicker oxide would reduce oxide cracking. The reduction in whisker density for samples electrochemically oxidised at potentials of -0.4 V and -0.5 V vs. SCE suggests that a minimum threshold charge has to be passed before a stable oxide is formed that can reduce whisker growth.

Results show that the greatest whisker mitigation is obtained for samples electrochemically oxidised at potentials of 1.2 V and -0.66 V vs. SCE, both these potentials reduced whisker density at each of the charges passed producing a reduction of over 80% compared with the corresponding native oxide

For electrochemical oxidation at potentials of 1.2 V, 1.6 V and 2.0 V (vs. SCE), samples with an electroplated

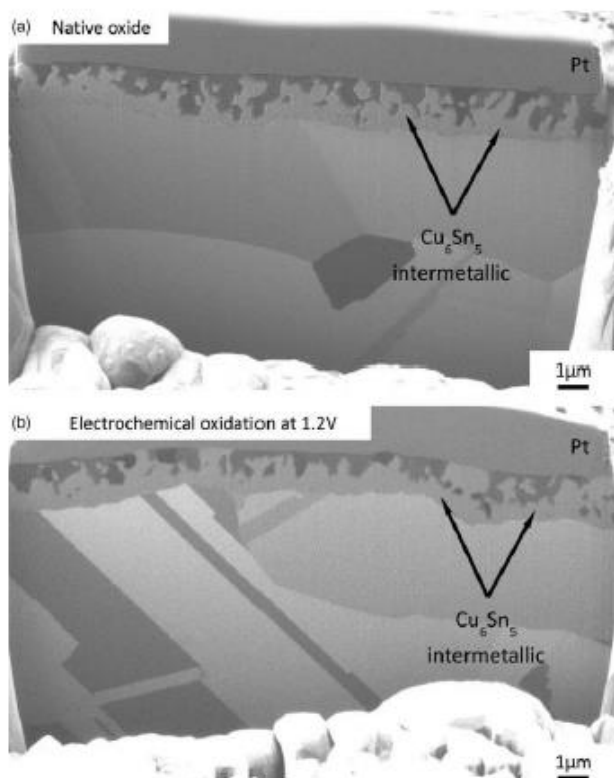


Figure 8 FIB cross sectioned 2 µm Sn–Cu electrodeposits on Cu after ~24 months of storage at room temperature, a native air-formed oxide and b oxide formed electrochemically at a potential of 1.2 V vs. SCE in potassium bicarbonate-carbonate

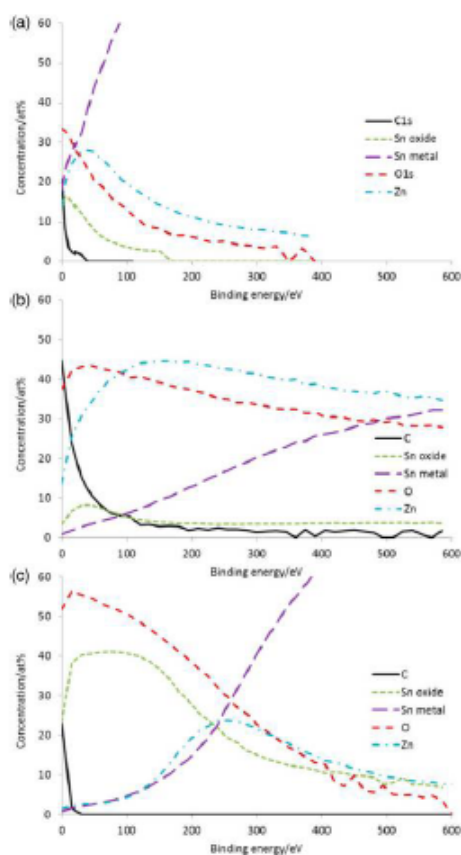


Figure 9 XPS depth profiles for Sn-Cu electrodeposits on Cu: a 1 day old native oxide, b native oxide after ~24 months storage, and c oxide formed electrochemically at a potential of 1.2 V vs. SCE in potassium bicarbonate-carbonate after ~24 months storage

area of 2×2 cm were used. Table 2 shows that as the applied oxidation potential is increased, from 1.2 V to 2.0 V vs. SCE, the whisker density is further reduced. The reduction in whisker growth can be directly related to the Sn oxide depth profiles in Fig. 5, which showed that oxidation at potentials greater than 1.2 V vs. SCE resulted in an increase in oxide thickness. Table 2 also

Table 3 Measured whisker densities for electrochemically oxidised $2 \mu\text{m}$ Sn electrodeposits on brass after ~36 months of storage at room temperature

Oxidation potential V vs SCE	Average number of whiskers per cm^2	Number of frames with no whiskers (out of 60)
Native	1489 ± 681	0
1.2 V	9 ± 21	50
1.6 V	7 ± 18	51
2.0 V	5 ± 16	54

shows that the number of frames (out of 60) where no whiskers were observed was considerably higher for the electrochemically oxidised samples and increased slightly with increasing oxidation potential. The large number of frames with no whiskers present results in a high standard deviation, relative to the measured whisker density, for the electrochemically oxidised samples.

To more fully understand the mechanism by which whisker mitigation is accomplished for the electrochemically oxidised samples, FIB analysis was carried on Sn-Cu electrodeposits on Cu after storage at room temperature for ~24 months.

Figure 8 shows FIB cross sections obtained from two Sn-Cu on Cu samples after storage at room temperature for 24 months; the first left to develop a native oxide (Fig. 8a) and the second electrochemically oxidised at 1.2 V vs. SCE in potassium bicarbonate-carbonate (Fig. 8b). It can be seen that extensive intermetallic formation has occurred in both samples, that is, the presence of the electrochemical oxide has had no observable effect on intermetallic growth, which is the primary driving force for whisker growth in these samples.^{8,23,24} This suggests that the reduced whisker growth observed for the electrochemically oxidised samples results from the thicker electrochemical oxide providing an enhanced physical barrier to the growth of whiskers rather than the driving force for whisker growth being reduced. This observation supports Tu's theory,^{1,10,11} which proposed that a thicker oxide will mitigate whisker growth by acting as a physical barrier and reduce the risk of localised cracking.

XPS depth profiles obtained from the surface of these samples are shown in Fig. 9, together with a one day old native oxide. After storage at room temperature for ~24 months the Sn oxide thickness is greatly increased for the sample left to develop the native oxide and is approaching the thickness of the electrochemically oxidised sample. The more gradual reduction in oxygen content with depth for the sample with the native oxide after ~24 months storage (Fig. 9b) indicates that significant inward diffusion of oxygen into the electrodeposit has occurred. In comparison, the oxygen content drops off more rapidly for the electrochemically oxidised sample. This suggests that the electrochemical oxide film may act as a diffusion barrier to prevent the inward diffusion of oxygen into the electrodeposit.

3.2.2. Sn electrodeposits on brass

For electrochemical oxidation at potentials of 1.2 V, 1.6 V and 2.0 V (vs. SCE), samples with an electroplated area of 2×2 cm were used. Table 3 shows that for Sn electrodeposits on brass, whisker growth is dramatically reduced by the electrochemical oxidation treatments. Furthermore, as the applied oxidation potential is increased the whisker density is further decreased. The slight reduction in whisker growth at the higher oxidation potentials can be directly related to the relative intensities of the Sn3d5 oxide and Sn3d5 metals peaks shown in previous work¹⁷ which indicated that oxidation at potentials greater than 1.2 V vs. SCE resulted in an increase in oxide thickness.

To more fully understand the whisker mitigation mechanism, FIB analysis was carried on Sn electrodeposits on brass after storage at room temperature for ~30 months

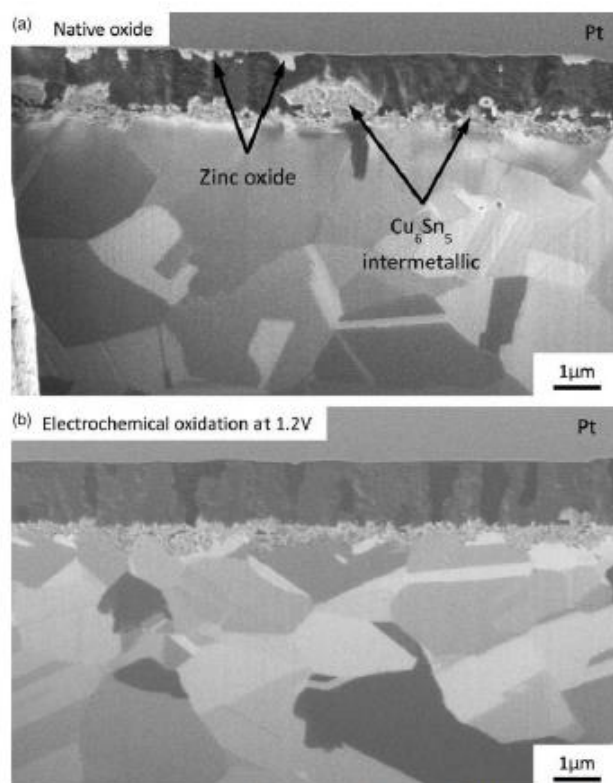


Figure 10 FIB cross sectioned 2 µm Sn electrodeposits on brass after ~30 months of storage at room temperature, a native air-formed oxide and b oxide formed electrochemically at a potential of 1.2 V vs. SCE in borate buffer

Figure 10 shows FIB cross sections of two Sn on brass samples, with the first left to develop a native oxide (Fig. 10a) and the second with an electrochemical oxide formed at 1.2 V vs. SCE in borate buffer (Fig. 10b). Figure 10a clearly shows both zinc oxide, at the deposit surface, and Cu_6Sn_5 intermetallic formation at the Sn-brass interface, both of which are known to cause whisker growth,^{8,17,23–25} by generating internal stresses within the electrodeposited coating. In comparison Fig. 10b shows that no zinc oxide formation has occurred at the surface of the electrochemically oxidised electrodeposit and only limited intermetallic formation has occurred at the Sn–Cu interface after ~30 months of storage.

XPS depth profiles obtained from the same samples are shown in Fig. 11 together with a depth profile, measured after ~24 h, from a tin electrodeposit on brass left to develop a native oxide (Fig. 11a). Comparison of the samples left to develop native oxides after 1 day and 30 months shows that the amount of zinc and oxygen present at the deposit surface greatly increases, which corresponds to the formation of zinc oxide at the surface. By comparison, zinc diffusion to the surface of the electrochemically oxidised deposit is prevented by the presence of the thicker Sn oxide film, which was produced shortly after the deposition of the Sn.¹⁷ Since high zinc concentrations are built up beneath the Sn oxide, but FIB

analyses suggest that no zinc oxide is present within the electrochemically oxidised Sn, it may be inferred that the electrochemically formed Sn oxide is preventing the inward diffusion of oxygen atoms into the electrodeposit.

These results demonstrate that the electrochemically formed oxide acts as a diffusion barrier and prevents the formation of zinc oxide at the electrodeposit surface, which prevents the development of internal stresses. The effect of the electrochemical oxidation treatment on the development of the Cu_6Sn_5 intermetallic is perhaps, more surprising, since it was not expected that the electrochemically formed oxide would have an influence on the Cu_6Sn_5 intermetallic growth.

4. Conclusions

The application of an electrochemical oxidation treatment has been demonstrated to successfully mitigate whisker growth for both Sn–Cu deposits on Cu and pure Sn deposits on brass.

For Sn–Cu deposits on Cu, the presence of the electrochemical oxide has no influence on the principal driving force for whisker growth, that is, intermetallic formation, and whisker mitigation is derived from the thicker electrochemical oxide providing an enhanced physical barrier. The presence of a thicker oxide layer mitigates whisker

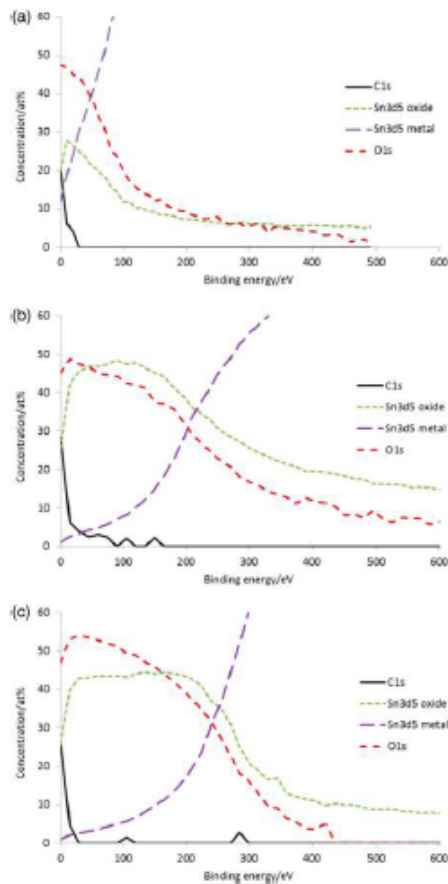


Figure 11 XPS depth profiles for 2 μm Sn electrodeposits on brass: a 1 day old native oxide, b native oxide after ~ 30 months storage at room temperature, and c oxide formed electrochemically at a potential of 1.2 V vs. SCE in borate buffer after ~ 30 months storage

growth by reducing the risk of localised cracking in the oxide film through which whiskers may subsequently grow.

For electrochemically oxidised pure Sn deposits on brass, whisker mitigation is achieved by preventing the formation of zinc oxide at the deposit surface and also by greatly reducing the growth of Cu_6Sn_5 intermetallic at the Sn–Cu interface, that is, the driving forces for whisker growth are diminished. The electrochemical oxide may also function as a physical barrier to whisker growth in a manner analogous to that observed for the Sn–Cu deposits.

The thickness of the electrochemically formed oxide film is directly related to the applied potential and the

total amount of charge passed. For an equivalent charge passed, the thickest oxide film, and most effective whisker mitigation, was obtained for samples electrochemically oxidised at the highest potentials studied, that is, 1.2–2.0 V vs. SCE.

Acknowledgements

The authors would like to thank both the UK EPSRC Innovative Electronics Manufacturing Research Centre for funding this research through the WHISKERMIT programme and the Loughborough University Materials Research School. This paper is based on a presentation given at EAST Forum 2015, Lund, Sweden, 25–26th June, 2015.

References

1. K.-N. Tu: *Phys. Rev.*, 1994, **49**, (3), 2030–2034.
2. G. T. Galvin: *Trans. Elect. Pack. Manuf.*, 2005, **28**, (1), 94–122.
3. K. G. Compton, A. Medina and S. M. Arnold: *Corrosion*, 1951, **7**, (10), 327–334.
4. E. Chason, N. Jadhav, F. Pei, E. Buchovecky and A. Bower: *Progr. Surf. Sci.*, 2013, **88**, (2), 103–131.
5. P. Zhang, Y. M. Zhang and Z. M. Sun: *J. Mat. Sci. Technol.*, 2015, **31**, (7), 675–698.
6. S. Han, M. Osterman and M. Pecht: 'Likelihood of metal vapor arc by tin whiskers', *SMT Magazine*, 2012, Aug., 48–56.
7. S. M. Arnold: *Plating*, 1966, **53**, (1), 96–99.
8. W. J. Boettinger, C. Johnson, L. Bendersky, K. Moon, M. Williams and G. Stafford: *Acta Materialia*, 2005, **53**, (19), 5033–5050.
9. M. Osterman: 'Mitigation strategies for tin whiskers'. CALCE EPSC 2002. available at: <http://www.calce.umd.edu/tin-whisker/TINWHISKERMITIGATION.pdf> (accessed 8 June 2015)
10. K.-N. Tu and K. Zeng: 'Reliability issues of Pb-free solder joints in electronic packaging technology', *Proceedings of the IEEE Electronic Components and Technology Conference*, 2002, 1194–1200.
11. K.-N. Tu, C. Chen and A. T. Wu: *J. Mat. Sci.*, 2007, **18**, (1–3), 269–281.
12. K. S. Kumar, L. Reinhold, A. F. Bower and E. Chason: *J. Mat. Res.*, 2008, **23**, (11), 2916–2934.
13. B. Z. Lee and D. N. Lee: *Acta Materialia*, 1998, **46**, (10), 3701–3714.
14. C. Y. Chang and R. W. Vook: *Thin Solid Films*, 1993, **228**, (1–2), 205–209.
15. K. W. Moon, C. E. Johnson, M. E. Williams, O. Kongstein, G. R. Stafford, C. A. Handwerker and W. J. Boettinger: *J. Electron. Mat.*, 2005, **34**, (9), L31–L33.
16. C. H. Su, H. Chen, H.-Y. Lee, C. Y. Liu, C.-S. Ku and A. T. Wu: *J. Electron. Mat.*, 2014, **43**, (9), 3290–3295.
17. M. A. Ashworth, D. Haspel, L. Wu, G. D. Wilcox and R. J. Mortimer: *J. Electron. Mat.*, 2015, **44**, (1), 442–456.
18. P. Alvarez, S. Ribotta and M. Eklauer: *Corr. Sci.*, 2002, **44**, (1), 49–65.
19. M. Drogowska, H. Ménard and L. Brossard: *J. Anal. Electrochem.*, 1991, **21**, (1), 84–90.
20. R. Diaz, I. Diez-Pérez, P. Gorostiza, F. Sanz and J. R. Morante: *J. Braz. Chem. Soc.*, 2003, **14**, (4), 523–529.
21. NIST X-ray photoelectron spectroscopy database. NIST Stand. Ref. Database 20, Version 20. available at: <http://rdata.nist.gov/xps/> (accessed 3 September 2015)
22. M. A. Ashworth, G. D. Wilcox, R. L. Higginson, R. J. Heath, C. Liu and R. J. Mortimer: *Microelectron. Reliab.*, 2015, **55**, (1), 180–191.
23. K.-N. Tu, J. Suh, A. T.-C. Wu, N. Tamura and C.-H. Ting: *Mat. Trans.*, 2005, **46**, (11), 2300–2308.
24. E. Chason, N. Jadhav, W. L. Chan, L. Reinhold and K. S. Kumar: *Appl. Phys. Lett.*, 2008, **92**, (17), 171901–171903.
25. M. A. Ashworth, G. D. Wilcox, R. L. Higginson, R. J. Heath and C. Liu: *J. Electron. Mat.*, 2014, **43**, (4), 1005–1016.

An Investigation into the Effect of a Post-electroplating Electrochemical Oxidation Treatment on Tin Whisker Formation

M.A. ASHWORTH^{1,3} D. HASPEL,¹ L. WU,¹ G.D. WILCOX,¹
and R.J. MORTIMER²

1.—Department of Materials, Loughborough University, Loughborough, Leicestershire LE11 3TU, UK. 2.—Department of Chemistry, Loughborough University, Loughborough, Leicestershire LE11 3TU, UK. 3.—e-mail: m.a.ashworth@lboro.ac.uk

Since the 'cracked oxide theory' was proposed by Tu in 1994,¹ there has only been a limited number of studies that have sought to investigate the effect of the Sn oxide on whisker growth. The current study has used electrochemical oxidation to produce oxide films, which has enabled the effect of the surface oxide thickness on whisker growth to be established. The effect of oxide thickness on whisker growth has been investigated for tin electrodeposits on both Cu and brass substrates. The influence of applied oxidation potential on the thickness of the Sn oxide film has been investigated using x-ray photoelectron spectroscopy (XPS) for potassium bicarbonate-carbonate and borate buffer electrolyte solutions. Whisker growth from electrochemically oxidised Sn-Cu deposits on Cu and Sn deposits on brass has been investigated and compared with samples left to develop a native air-formed oxide. XPS studies show that the thickness of the electrochemically formed Sn oxide film is dependent on the applied oxidation potential and the total charge passed. Subsequent whisker growth studies demonstrate that electrochemically oxidised Sn-Cu deposits on Cu and Sn deposits on brass are significantly less susceptible to whisker growth than those having a native oxide film. For Sn deposits on brass, the electrochemically formed Sn oxide greatly reduces Zn oxide formation at the surface of the tin deposit, which results in whisker mitigation. For Sn-Cu deposits on Cu, the reduction in whisker growth must simply derive from the increased thickness of the Sn oxide, i.e. the Sn oxide film has an important role in stemming the development of whiskers.

Key words: Tin, electrochemical oxidation, electrodeposition, whisker growth, zinc, diffusion

INTRODUCTION

The role of the surface oxide film in the growth of tin whiskers has not been widely reported in the literature. The cracked oxide theory put forward by Tu¹⁻³ proposed that the Sn oxide film played a critical role in the growth of tin whiskers by suppressing relaxation of the deposit via uniform creep of tin atoms to the surface of the deposit.⁴ Stress relaxation in deposits resulting from removal of the oxide layer was later demonstrated

experimentally.^{5,6} Lee and Lee⁷ also stated that, for whisker growth to occur, it was necessary to break the oxide at certain weak points on the surface, from which whiskers grew to relieve stress. It was also suggested that very thick oxides would physically block the growth of whiskers or hillocks.^{2,3} In the absence of an oxide film, no whisker growth was considered likely; this assumption was based on a study by Chang and Vook,⁸ which showed that, in the absence of a surface oxide, no hillock formation under compressive stress occurred on vapour-deposited aluminium films. However, whisker formation was later reported for Sn-Cu electrodeposits⁹ that had been stored for 9 days under vacuum, after

(Received January 30, 2014; accepted August 26, 2014)

Published online: 18 September 2014

initially removing the surface oxide by ion beam sputtering. Subsequent real-time focussed ion beam SEM (FIBSEM) studies by Jadhav et al.,¹⁰ however, indicated that removal of the oxide could relieve stress and hence reduce the driving force for whisker and hillock formation. Further evidence to suggest that the surface oxide plays an important role in whisker growth can be inferred from the observation of 'growth striations' on tin whiskers.¹¹ These were associated with discontinuous whisker growth as a result of repeated fracture and self-healing of the air-formed Sn oxide at the whisker base.

Further insight into the possible influence of the surface oxide on whisker formation may be obtained from a comparison of whisker growth rates during thermal cycling in air and vacuum environments. Suganuma et al.¹² showed that whisker growth was reduced for tin electrodeposits thermally cycled in air, compared with those tested under vacuum, which may indicate that whisker growth was more difficult on the samples thermally cycled in air due to the increased thickness of the Sn oxide layer.

Given the potential influence of the surface oxide on whisker growth, and the relative scarcity of research related to this phenomenon, the current study was undertaken to investigate the effect of electrochemical oxidation on whisker growth. Electrochemical oxidation is an ideal method for the development of Sn oxides, since other characteristic features of the tin deposit should be unaffected by the oxidation process, whereas the formation of Sn oxides at elevated temperatures is likely to be accompanied by other changes to the tin deposit (e.g. residual stress levels⁷ and intermetallic type and distribution¹³). Electrochemical oxidation has been performed in two different electrolyte solutions: a borate buffer solution^{14,15} and a potassium bicarbonate-carbonate solution.¹⁶ Initial cyclic voltammetry trials were performed in both electrolyte solutions to study the tin oxidation processes, followed by oxidation at selected potentials identified from the cyclic voltammograms. The thickness of the resultant Sn oxide films was determined by XPS depth profiling. The effect of the electrochemically formed oxide on whisker growth was established for both Sn deposits on brass and Sn-Cu deposits on Cu.

EXPERIMENTAL

Deposition of Tin

Pure Sn and Sn-Cu alloys were electrodeposited onto brass (63% Cu/37% Zn, 0.38 mm thickness) and Cu (99.9%, 0.1 mm thickness) substrates, respectively, using a bright acid Sn electroplating solution, which is comprised of 60 g L⁻¹ tin sulfate, 70 ml L⁻¹ sulphuric acid and 40 ml L⁻¹ Timmac Stannolyte, a proprietary additive (MacDermid). Electrodeposition of 2 μm pure Sn onto Cu and brass was carried out using a current density of 20 mA cm⁻² (corresponding to a deposition rate of

~1 μm min⁻¹). The Sn-Cu bath was prepared with a Cu²⁺ concentration of 10 mmol L⁻¹ by the addition of CuSO₄ to the pure Sn bath. For Sn-Cu electrodeposited onto Cu at 10 mA cm⁻², this resulted in a uniform deposit with a Cu content of ~1 wt%.

Test coupons with dimensions 2 × 4 cm were used with an electroplated area of 2 × 2 cm. The coupons were used in the as-supplied condition with no additional polishing or grinding operations. Electrodeposition of pure Sn was carried out using a 99.95% Sn foil anode (0.25 mm), whilst the Sn-Cu alloy was deposited using a platinised titanium anode. Immediately prior to deposition, all the substrates were degreased using acetone, pickled for 60 s in a 20% v/v solution of sulfuric acid (SG 1.83), rinsed in deionised water and dried using hot air. The thicknesses of the pure Sn and Sn-Cu deposits were 10 μm for cyclic voltammetry and electrochemical oxidation trials and 1 μm or 2 μm for whisker growth studies, the latter thin coatings being utilised to promote whisker growth.

Preparation of Electrolyte Solutions for Tin Oxidation

Two electrolyte solutions were selected for electrochemical oxidation of the Sn deposits: a pH 8.4 borate buffer (9.55 g L⁻¹ sodium borate and 6.18 g L⁻¹ boric acid; both Sigma-Aldrich) and a pH 8.9 potassium bicarbonate/potassium carbonate (75.09 g L⁻¹ of potassium bicarbonate and 6.91 g L⁻¹ of potassium carbonate; both Sigma-Aldrich). Both electrolyte solutions were prepared using deionised water and the pH was adjusted to the required level using additions of sodium hydroxide.

Cyclic Voltammetry

Cyclic voltammetry was carried out for Sn electrodeposited deposits in naturally aerated pH 8.4 borate buffer and pH 8.9 potassium bicarbonate/potassium carbonate electrolyte solutions to determine the location of the oxidation peaks. Analyses were conducted using an EG&G Princeton Applied Research model 263A potentiostat by means of a 3-electrode cell comprising of a static Sn electrodeposited as the working electrode, a saturated calomel reference electrode (SCE) and a platinised titanium counter electrode. The electrode potential was swept from -1.1 V up to 1.2 V, reversed to -1.5 V and then returned to -1.1 V (all versus SCE) using a linear scan rate of 10 mV s⁻¹. Multiple cycles were performed for each test and the second scan selected for analysis to reduce the influence of the pre-existing air-formed oxide on the results.

Electrochemical Oxidation of Tin

Electrochemical oxidation was performed immediately after Sn deposition using an EG&G Princeton Applied Research model 263A potentiostat and the 3-electrode cell described previously. After

immersion into the naturally aerated electrolyte solution, the tin deposit was initially held at a potential of -1.5 V versus SCE to reduce the pre-existing oxide. When hydrogen evolution was observed the potential was increased to the selected value for oxidation. The effect of oxidation potential on the thickness of the Sn oxide was investigated for both borate buffer and potassium bicarbonate-carbonate electrolyte solutions.

Characterisation of Electrochemical Oxides

The composition and thickness of the oxide films produced by electrochemical oxidation was determined by x-ray photoelectron spectroscopy (XPS) using a Thermo-Scientific K-Alpha x-ray photoelectron spectrometer. Sputter depth profiling was performed using 200 eV argon ions with an estimated etch rate of ~ 0.6 nm min^{-1} . XPS analysis was, unless otherwise stated, carried out 1 day after tin deposition and electrochemical oxidation.

Whisker Growth Studies

The effect of the electrochemical oxides on whisker growth was assessed using $2 \mu\text{m}$ tin deposits on brass and $1 \mu\text{m}$ and $2 \mu\text{m}$ Sn-Cu alloy deposits on Cu substrates. Typically, three samples were prepared for each electrochemical oxidation treatment. After deposition and electrochemical oxidation, the samples were stored at room temperature ($\sim 20^\circ\text{C}$). Whisker growth was evaluated using optical microscopy and scanning electron microscopy (SEM). Whisker densities were measured using an optical microscope with an objective magnification of $\times 20$. The analysed area was $\sim 1 \text{ cm}^2$ for samples electrochemically oxidised at 1.2 V versus SCE and 0.26 cm^2 for samples electrochemically oxidised at -0.66 V versus SCE. SEM analysis of the tin deposits was undertaken using a Carl Zeiss Leo 1530 VP field emission gun SEM (FEGSEM) equipped with an Oxford Instruments X-Max 80 mm^2 detector for energy dispersive x-ray spectroscopy (EDS). Details of the samples prepared for whisker growth studies are given in Table I.

RESULTS AND DISCUSSION

Electrochemical Oxidation and Characterisation

Cyclic voltammograms for the oxidation and reduction of electrodeposited Sn in borate buffer and potassium bicarbonate-carbonate solutions are shown in Fig. 1a and b. The cathodic current densities at the start of the potential sweeps were $\sim 2 \times 10^{-5} \text{ A cm}^{-2}$ and $1 \times 10^{-4} \text{ A cm}^{-2}$ for the borate buffer and potassium bicarbonate-carbonate electrolyte solutions, respectively. Two main oxidation peaks are evident in both electrolyte solutions. For the borate buffer electrolyte solution (Fig. 1a), oxidation peaks are evident at -0.82 V (peak I) and -0.64 V versus SCE, (peak II), while less clearly defined broad peaks are also observed at approximately 0 V (peak III) and 0.7 V versus SCE (peak IV). The increase in current density observed at ~ 1.1 V versus SCE is due to oxygen evolution (peak V). Two distinct reduction peaks are observed on the reverse sweep (labelled peaks VI and VII), together with other less clearly defined reduction peaks. For the potassium bicarbonate-carbonate electrolyte solution (Fig. 1b), oxidation peaks are evident at -0.83 V (peak I) and -0.66 V versus SCE (peak II), along with an increase in current density at ~ 1.1 V versus SCE due to oxygen evolution (peak III). Distinct reduction peaks are evident at approximately -0.6 V, -1.1 V and -1.4 V versus SCE, peaks IV, V, and VI, respectively.

Peak (I) has been associated previously with the active dissolution of Sn to Sn(II) whilst peak (II) has been attributed to the to the formation of Sn (IV).¹⁵⁻¹⁷ The broad, slowly decreasing slope on peak (II) observed for the potassium bicarbonate-carbonate electrolyte solution was considered by Drogowska et al.¹⁷ to correspond to a dehydration reaction that resulted, via multiple reaction steps, in the formation of SnO_2 . In a later study of Sn oxides formed in pH 7.5 borate buffer, Diaz et al.¹⁴ proposed that peaks (I) and (II) both corresponded to the formation of Sn (II) species.

On the basis of the cyclic voltammetry results, electrochemical oxidation of freshly prepared Sn

Table I. Summary of samples utilised for whisker growth studies

	Sn deposits on brass	Sn-Cu deposits on Cu	
Sn alloy	Pure Sn	Sn-Cu (10 mmol L^{-1} Cu)	
Substrate material	63% Cu/37% Zn	99.9% Cu	
Deposition current density	20 mA cm^{-2}	10 mA cm^{-2}	
Deposit thickness	$2 \mu\text{m}$	$2 \mu\text{m}$	$1 \mu\text{m}$
Electrolyte solution ^a	Solution 1	Solution 1 & 2	Solution 2
Oxidation potential (versus SCE)	1.2 V, 1.6 V and 2.0 V	1.2 V	-0.66 V

^aSolution 1: pH 8.4 borate buffer, solution 2: pH 8.9 potassium bicarbonate-carbonate.

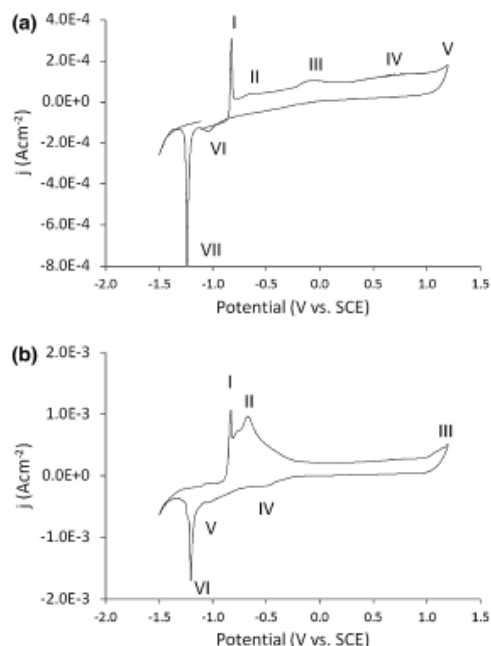


Fig. 1. Cyclic voltammetry for $10\ \mu\text{m}$ Sn electrodeposits on Cu at a sweep rate of $10\ \text{mV s}^{-1}$ in: (a) pH 8.4 borate buffer electrolyte solution and (b) pH 8.9 potassium bicarbonate-carbonate electrolyte solution.

deposits was performed in the potassium bicarbonate-carbonate solution at the following potentials; $-0.83\ \text{V}$ (peak (I)), $-0.66\ \text{V}$ (peak (II)), $-0.5\ \text{V}$, $0.35\ \text{V}$ and $1.2\ \text{V}$ versus SCE. The recorded current-time curves for oxidation at each of the potentials are shown in Fig. 2; in each case, the pre-existing oxide was first reduced by polarisation at $-1.5\ \text{V}$ until hydrogen evolution was observed, at which point the potential was increased to the appropriate value. For each oxidation potential, the total charge passed was $\sim 30\ \text{mC cm}^{-2}$. All the current-time curves were characterised by an initial rapid reduction in current density followed by a gradual reduction in current density throughout the duration of the experiment. The highest current densities were obtained for samples oxidised at potentials corresponding to peaks (I) and (II) in Fig. 1.

The effect of oxidation potential on the thickness of the Sn oxide film ($30\ \text{mC cm}^{-2}$ charge passed) is demonstrated by the high resolution XPS scans of the Sn 3d peak in Fig. 3; analysis of a native air-formed oxide, prepared at the same time, is also included for comparison. From the relative intensity of the Sn $3d_{5/2(\text{metal})}$ and Sn $3d_{5/2(\text{oxide})}$ peaks, at $\sim 485\ \text{eV}$ and $\sim 487\ \text{eV}$, respectively, it can be established that the thickness of the oxide film

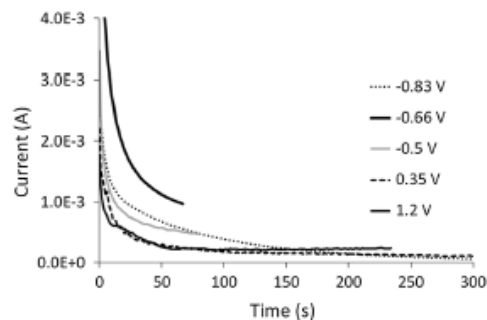


Fig. 2. Current-time curves for electrochemical oxidation of Sn deposits on Cu in potassium bicarbonate-carbonate electrolyte solution at different potentials (V versus SCE).

increases as the oxidation potential is increased from $-0.83\ \text{V}$ to $1.2\ \text{V}$ versus SCE. The proportion of $\text{Sn}_{(\text{oxide})}$ and $\text{Sn}_{(\text{metal})}$ species as a function of oxidation potential is shown in Table II, which also gives the binding energy of the metal and oxide peaks derived from curve fitting. From Table II, it is evident that the intensity of the oxide peak from the sample oxidised at $-0.83\ \text{V}$ versus SCE is comparable to that of the native air-formed oxide, which suggests that most, if not all, the charge passed results in Sn dissolution rather than the formation of a stable Sn oxide. Increasing the potential to $-0.66\ \text{V}$ and $-0.5\ \text{V}$ versus SCE results in a slightly increased oxide film thickness; only at the higher potentials investigated was the thickness of the oxide film increased notably. However, further trials demonstrated that considerably thicker oxides could be achieved at $-0.66\ \text{V}$ versus SCE by increasing the total charge passed. The oxygen depth profiles in Fig. 4 show that oxidation at $-0.66\ \text{V}$ versus SCE for 5 min (equivalent to $\sim 100\ \text{mC cm}^{-2}$ charge passed) resulted in an oxide thickness comparable to that of a sample oxidised at $1.2\ \text{V}$ versus SCE, and that further increases in oxide thickness were achieved if the charge passed was increased. However, oxidation at $-0.66\ \text{V}$ versus SCE was found to result in partial dissolution of the tin deposit. As shown in Fig. 4, the extent of the dissolution increased with increasing charge passed. The partial dissolution observed on the surface of the Sn deposits was most likely associated with individual Sn grains, and their specific growth orientation given that the scale of the features is comparable to the Sn grain size that results from electrodeposition at $10\ \text{mA cm}^{-2}$.¹⁸

The Sn $3d_{5/2}$ peaks shown in Fig. 3 could not be resolved into more than 2 peaks, suggesting that only a single Sn oxide species is present. In addition, Table II shows that there was no significant variation in the binding energy of the Sn $3d_{5/2}$ peak as a function of oxidation potential, i.e. the same oxide species is present in each case.

An Investigation into the Effect of a Post-electroplating Electrochemical Oxidation Treatment on Tin Whisker Formation

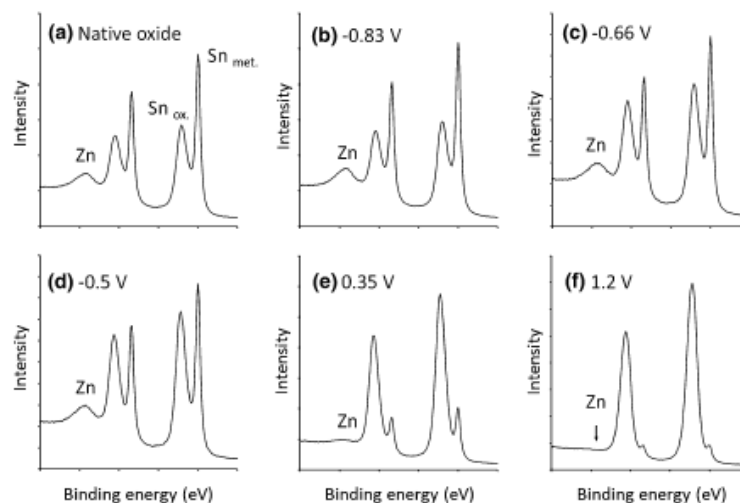


Fig. 3. High resolution XPS scans of the Sn 3d peak for 2 μm Sn on brass deposits 1 day after deposition and electrochemical oxidation in a potassium bicarbonate-carbonate electrolyte solution: (a) native air-formed oxide, (b) electrochemical oxidation at -0.83 V , (c) -0.66 V , (d) -0.5 V , (e) 0.35 V and (f) 1.2 V (versus SCE).

Table II. Analysis of Sn $3d_{5/2}$ peak as a function of oxidation potential

Sample treatment (V versus SCE)	Proportion of species		Binding energy of Sn $3d_{5/2}$ (eV)	
	Sn _(metal)	Sn _(oxide)	Sn _(metal)	Sn _(oxide)
Native	52	48		487.02
-0.83 V	53	47		486.95
-0.66 V	46	54	485.0	487.01
-0.5 V	43	57		487.13
0.35 V	19	81		487.21
1.2 V	7	93		487.22

Additional electrochemical oxidation trials were undertaken at higher potentials in a borate buffer solution to determine whether thicker oxide films could be obtained, without partial dissolution of the Sn deposit. The gradual reduction in the intensity of the metal peak observed as the potential is increased from 1.2 V to 1.6 V and 2.0 V versus SCE (Fig. 5) indicates that slightly thicker oxide films are obtained at higher oxidation potentials. The measured binding energies of the Sn $3d_{5/2}$ oxide peaks were 487.3 eV , 487.4 eV and 487.4 eV after oxidation at 1.2 V , 1.6 V and 2.0 V versus SCE, respectively, suggesting that the oxide species formed is the same at each potential and similar to those developed in the potassium bicarbonate-carbonate electrolyte solution (Table II).

The effect of electrochemical oxidation on whisker growth was investigated using $2\text{ }\mu\text{m}$ Sn-Cu deposits on Cu oxidised at 1.2 V versus SCE in both borate

buffer and potassium bicarbonate-carbonate electrolyte solutions. In addition, $2\text{ }\mu\text{m}$ Sn deposits on brass were oxidised at 1.2 V , 1.6 V and 2.0 V versus SCE in borate buffer. In each case, samples were prepared and left to develop a native air-formed oxide for comparison.

Sn Deposits on Brass: The Effect of Electrochemical Oxidation on Tin Whisker Formation

XPS depth profiles through the surface oxides of Sn deposits on brass, 1 day after Sn deposition and electrochemical oxidation at 1.2 V versus SCE in borate buffer and potassium bicarbonate-carbonate electrolyte solutions, are shown in Fig. 6a and b. A depth profile through a native air-formed oxide after 1 day is shown in Fig. 6c. Examination of Sn_(oxide) depth profiles indicates that, compared with the

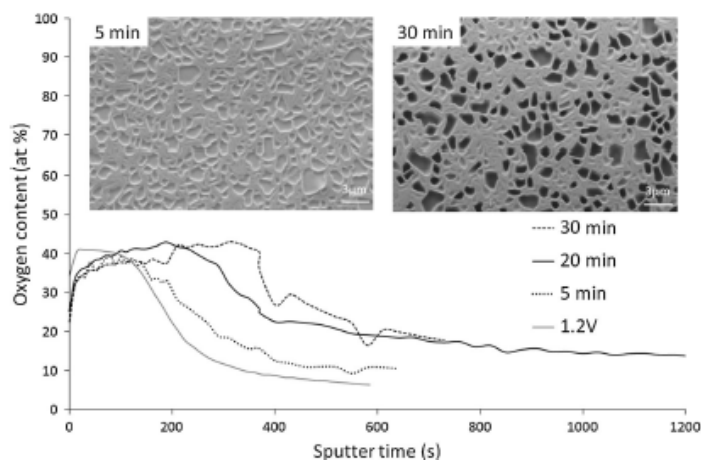


Fig. 4. XPS depth profiles for oxygen showing the effect of time on oxide thickness for Sn electrodeposits on copper oxidised in potassium bicarbonate-carbonate electrolyte solution at -0.66 V versus SCE. Inset secondary electron images show the effect of increasing oxidation time on the surface of the Sn deposit.

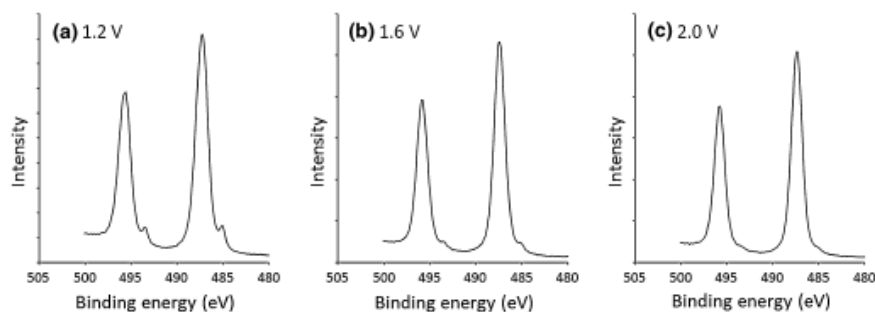


Fig. 5. High-resolution XPS scans of the Sn 3d peak for $2 \mu\text{m}$ Sn on brass deposits 1 day after deposition and electrochemical oxidation in a pH 8.4 borate buffer electrolyte solution: (a) 1.2 V versus SCE, (b) 1.6 V versus SCE and (c) 2.0 V versus SCE.

native oxide, the electrochemical Sn oxides are considerably thicker, which is consistent with the high-resolution scans in Fig. 3. The key feature of the depth profiles in Fig. 6 is the sub-surface enrichment of Zn; the position of the peak Zn concentration suggests that the Zn is located at the interface between the Sn oxide and the underlying Sn metal. Importantly, given the crucial role Zn diffusion plays in whisker formation for Sn deposits on brass, the peak Zn concentration was both reduced and located further from the surface of the deposit for the electrochemically oxidised samples (Fig. 6a and b) compared to the native air-formed oxide (Fig. 6c); the approximate sputter times at which the highest Zn contents (given in parentheses) were measured were 210 s (~ 18 at.% Zn), 170 s (~ 17 at.% Zn) and 45 s (~ 26 at.% Zn) for the potassium bicarbonate-carbonate, borate buffer and

native oxides, respectively. No copper signal was detected during depth profiling, which indicates that the Zn was present in the tin deposit as a result of diffusion rather than being detected from the underlying brass substrate.

The effect of storage time on the thickness and composition of the native oxide formed on $2 \mu\text{m}$ Sn deposits on brass is demonstrated by the electrochemical reduction curves in Fig. 7. The plateau at ~ -0.86 V versus SCE corresponds to the reduction of Sn oxide,¹⁹ whilst that at -1.2 V versus SCE was demonstrated experimentally, by electrochemical reduction analysis of the air formed native oxide on a Zn foil sample, to relate to the reduction of Zn oxide. The width of the plateaux (corresponding to the charge passed) is proportional to the thickness of the oxide film. Between 7 and 28 days, the thicknesses of both the Sn oxide and Zn oxide layers

An Investigation into the Effect of a Post-electroplating Electrochemical Oxidation Treatment on Tin Whisker Formation

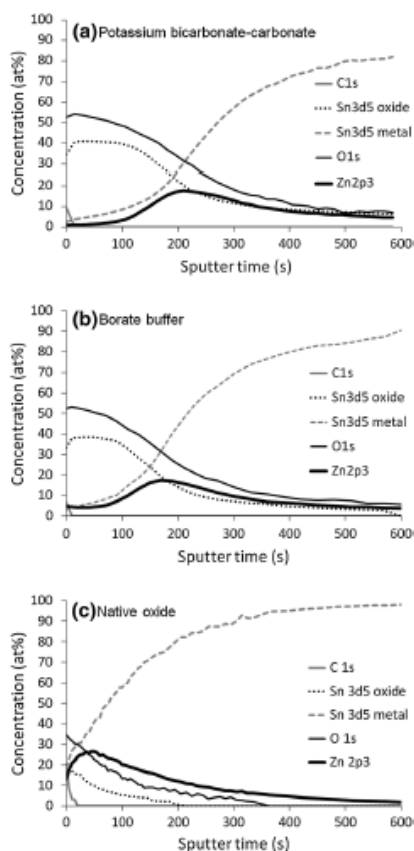


Fig. 6. XPS depth profiles showing the effect of sample treatment on oxide thickness and elemental distribution at the surface of 2 μm Sn deposits on brass 1 day after deposition: (a) electrochemical oxidation, at 1.2 V versus SCE in potassium bicarbonate-carbonate electrolyte solution, (b) electrochemical oxidation, at 1.2 V versus SCE in pH 8.4 borate buffer electrolyte solution and (c) a native air-formed oxide.

increase with increasing storage time. However, the increase in the thickness of the Zn oxide layer, in particular between 21 and 28 days, is more pronounced, i.e. Zn oxide is formed preferentially.

XPS depth profiles measured for samples with a native oxide and an oxide formed electrochemically in borate buffer, after storage for ~ 300 days at room temperature, are shown in Fig. 8. Comparing Figs. 8b and 6b, the elemental distribution at the surface of the Sn deposit having the electrochemically grown oxide (formed at 1.2 V versus SCE in borate buffer) is not changed significantly. By comparison, the surface composition at the surface of the deposit left to develop a native air-formed oxide is considerably changed; the thickness of the Sn

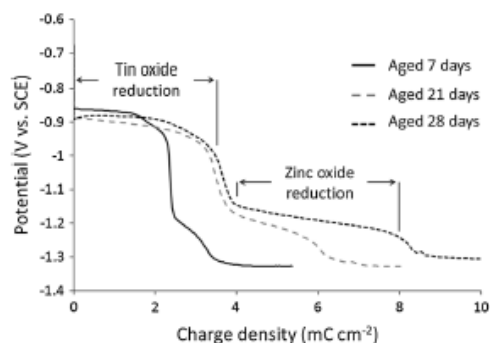


Fig. 7. Electrochemical reduction curves showing effect of storage time on the development of the surface oxide for 2 μm Sn deposits on brass. Electrochemical reduction in naturally aerated pH 8.4 borate buffer electrolyte solution at 60 $\mu\text{A cm}^{-2}$.

oxide film is only slightly increased but the measured Zn content at the interface between the Sn oxide and Sn metal has increased dramatically, from ~ 26 at.% to 45 at.%. The Zn (and oxygen) enrichment also extends much further into the Sn deposit. It is not easily established whether Zn is present in the metallic or oxidised state using XPS, since there is no discernible shift in binding energy.²⁰ However, the presence of the Zn Auger peak at a binding energy of ~ 499 eV in Fig. 3a-e shows that, in the case of Sn deposits with thin oxide films, either air-formed or electrochemically grown at low potentials, the Zn on the un-sputtered surface is present, at least in part, in the oxidised state.²⁰ For electrochemically oxidised surfaces with thicker oxide films (e.g. 1.2 V versus SCE in borate buffer; Fig. 3f), no Zn Auger peak is observed in the high resolution scans obtained prior to sputtering. However, for surfaces sputtered to the location at which the highest Zn content is measured, a Zn Auger peak corresponding to the oxidised state is clearly evident (Fig. 9). At this position, the total measured oxygen content is ~ 24 at.% whilst the $\text{Sn}^{(\text{oxide})}$ content is ~ 14 at.% and the Zn content is ~ 25 at.%; given the presence of ZnO, this suggests that Sn at this location is present as SnO. High-resolution XPS scans indicate a gradual slight reduction in the measured binding energy of the $\text{Sn}^{(\text{oxide})}$ peak from 487.0 eV at the outer surface to 486.7 eV at the location of the maximum Zn content.

The secondary electron images in Fig. 10 show a clear difference in surface appearance between samples with native air-formed oxides and those with oxides electrochemically formed in borate buffer (after 270 days storage at room temperature). The surface of the native air-formed oxide shows distinctive dark contrast regions at the grain boundaries of the Sn grains; as shown in Fig. 11, such features correspond to regions with high Zn and O contents. No such regions were evident on

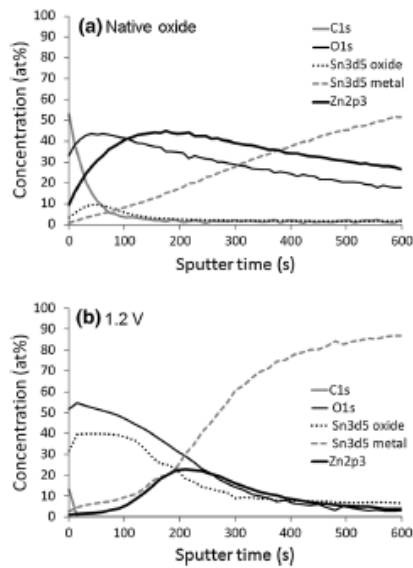


Fig. 8. XPS depth profiles showing the effect of electrochemical oxidation on oxide thickness and elemental distribution at the surface of $2\ \mu\text{m}$ Sn deposits on brass ~ 300 days after deposition: (a) native air-formed oxide and (b) electrochemical oxidation at $1.2\ \text{V}$ versus SCE in a pH 8.4 borate buffer electrolyte solution.

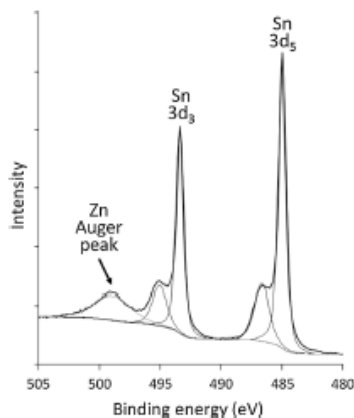


Fig. 9. High-resolution scan of the Sn 3d peak after sputtering for 210 s to the position at which the maximum Zn concentration is observed. XPS analysis ~ 300 days after deposition and subsequent electrochemical oxidation at $1.2\ \text{V}$ versus SCE in pH 8.4 borate buffer electrolyte solution.

samples with electrochemically formed oxides. Optical microscope and SEM analyses of these samples after 270 days storage at room temperature showed a dramatic difference in whisker growth. No

whiskers were observed on any of the Sn deposits on brass with electrochemically formed oxides. In comparison, long filament whiskers were observed on each of the samples left to develop air-formed oxides (Fig. 12). These results show that an electrochemically formed oxide, formed soon after deposition, is able to mitigate the formation of whiskers for Sn deposits on brass, by preventing the time-dependent formation of ZnO at the surface of the deposit, in particular at the Sn grain boundaries. This is accomplished by the electrochemically formed Sn oxide functioning as a barrier to the outward diffusion of Zn from the brass to the surface of the deposit. This explanation is supported by SEM/EDS analysis of regions of the Sn deposit surface that were Ar ion-sputtered during acquisition of XPS depth profiles ~ 300 days after Sn deposition and electrochemical oxidation. The EDS maps in Fig. 13, recorded ~ 90 days after sputtering (i.e. ~ 390 days after Sn deposition), show that outside of the sputtered area (region 1) there is no Zn enrichment or little evidence of whisker growth evident on the deposit surface. In comparison, within the sputtered area (region 2) Zn (and O) enrichment is apparent at the deposit surface, which has resulted in the growth of a significant number of whiskers (Fig. 13f).

Sn-Cu Deposits on Cu: The Effect of Electrochemical Oxidation on Tin Whisker Formation

To more fully explore the ability of electrochemically formed oxides to mitigate whisker formation, $2\ \mu\text{m}$ Sn-Cu deposits (containing $\sim 1\ \text{at.}\%$ Cu) on Cu were investigated; the addition of Cu to Sn has been shown to promote rapid whisker growth compared with pure Sn,²¹ which allows results to be obtained within a reasonably short time-frame. An important consideration was to establish whether Cu was incorporated into the electrochemically formed oxide film, which would potentially have complicated interpretation of the results. However, XPS of a sample electrochemically oxidised in a potassium bicarbonate-carbonate electrolyte solution indicated that Cu was not incorporated within the oxide film (Fig. 14).

XPS depth profiles for oxygen measured 21 days after Sn-Cu deposition for a native air-formed oxide and electrochemically formed oxides grown in borate buffer and potassium bicarbonate-carbonate solutions ($1.2\ \text{V}$ versus SCE, $40\ \text{mC cm}^{-2}$ charge passed) are shown in Fig. 15. Results indicate that at a given potential and with equivalent charge passed the resultant oxide thickness is similar for oxidation in either borate buffer or potassium bicarbonate-carbonate electrolyte solutions. Furthermore, the binding energy of the Sn $3d_{5/2(\text{oxide})}$ peak was $\sim 487.2\ \text{eV}$ in each case, i.e. identical to that formed on pure Sn deposits on brass. Figure 15 also shows that increasing the amount of charge passed to $160\ \text{mC cm}^{-2}$ in

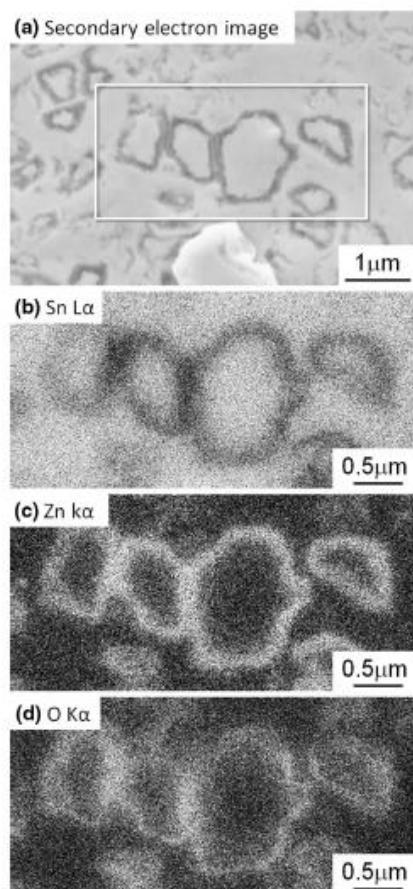


Fig. 11. SEM/EDS analysis of 5 μm Sn deposit on brass left to develop a native air-formed oxide. Analysis \sim 330 days after deposition: (a) secondary electron image of deposit surface, (b) Sn L α x-ray map, (c) Zn K α x-ray map and (d) O K α x-ray map.

considerable reduction in whisker density compared with the sample left to develop a native air-formed oxide. Furthermore, further reductions in whisker density were evident with increasing oxidation time. For regions of the sample electrochemically oxidised for 20 min and 30 min, whisker growth was often observed to be associated with areas of the Sn-Cu electrodeposit that appeared less oxidised than the surrounding regions; illustrated in Fig. 21. From Fig. 21, it is also evident that considerable dissolution of Sn has occurred during electrochemical oxidation at -0.66 V versus SCE. This is shown more clearly in Fig. 22. Comparison with regions of the surface left to develop a native air-formed oxide (Fig. 22a) indicates that the extent of the

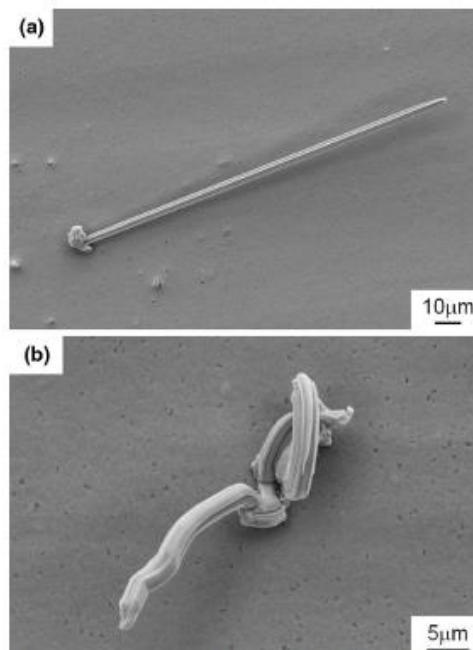


Fig. 12. Secondary electron images showing examples of whisker growth on a 2 μm Sn deposits on brass left to develop a native air-formed oxide. Analysis 300 days after deposition.

dissolution increases with increasing oxidation time and that the distribution of the preferential dissolution is related to the grain structure of the Sn electrodeposit.

These results indicate that the characteristics of the Sn oxide surface can have a profound effect on whisker growth during storage at room temperature.

DISCUSSION

Effect of Electrolyte Solution and Oxidation Potential on Sn Oxide Formation

XPS analysis of Sn deposits oxidised in both borate buffer and potassium bicarbonate-carbonate electrolyte solutions showed that, for a given charge passed, thickness of oxide achieved is a function of the applied oxidation potential, i.e. at higher oxidation potentials a thicker Sn oxide film is formed. Oxidation at the peak potentials, identified by cyclic voltammetry (Fig. 1), resulted in oxide films that were comparable in thickness to those present on samples left to develop a native air-formed oxide. From this, it may be inferred that, at least initially, oxidation at -0.83 V and -0.66 V versus SCE does not result in the formation of a stable passive film; Shah and Davies reported that at low potentials, for

An Investigation into the Effect of a Post-electroplating Electrochemical Oxidation Treatment on Tin Whisker Formation

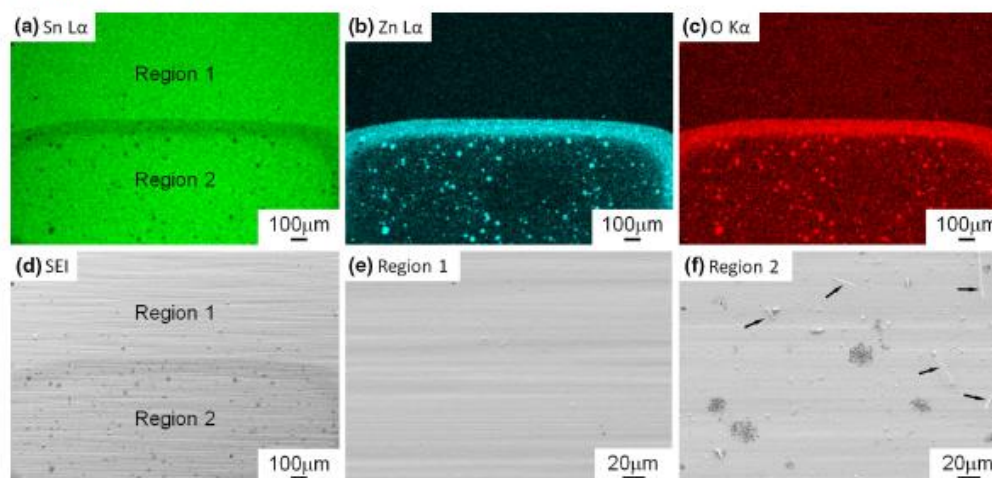


Fig. 13. SEM analysis of 2 μm Sn deposit on brass 90 days after Ar ion sputtering to remove the electrochemically oxidised surface (1.2 V versus SCE in borate buffer electrolyte solution): (a) Sn L α x-ray map, (b) Zn L α , (c) O K α , (d) secondary electron image of mapped region, (e) secondary electron image showing region 1 and (f) secondary electron image showing whisker growth in region 2 (sputtered area). Sputtering was performed 300 days after Sn deposition.

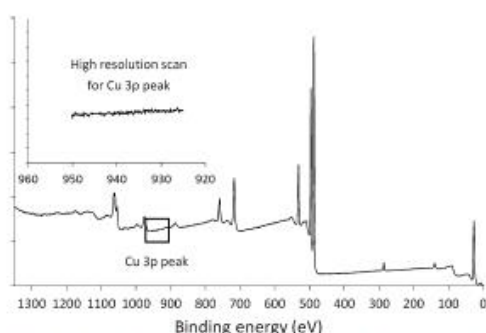


Fig. 14. XPS analysis of surface of a 2 μm Sn-Cu electrodeposit electrochemically oxidised at 1.2 V versus SCE in potassium bicarbonate-carbonate electrolyte solution after storage at room temperature for 21 days: (a) survey scan and inset (b) high-resolution scan of the Cu 3p peak.

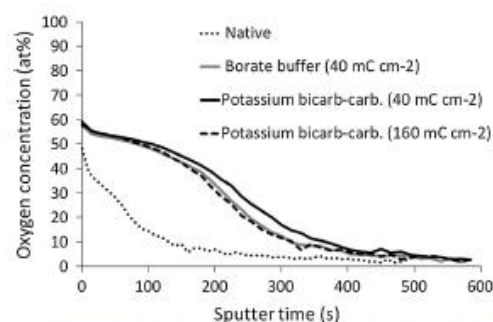


Fig. 15. XPS depth profiles for oxygen comparing the thickness of a native air-formed oxide with oxides formed electrochemically at 1.2 V versus SCE in borate buffer (pH 8.4) and potassium bicarbonate-carbonate electrolyte solutions. Analysis of Sn-Cu deposits on Cu, 21 days after electroplating and electrochemical oxidation.

anodic polarisation in 0.1 M sodium borate solution, half the current contributed towards stannous oxide (SnO) formation whilst the remainder resulted in Sn dissolution as stannite ions ($\text{Sn}(\text{OH})_3^-$).²² Above 0.2 V versus Ag/AgCl, no Sn dissolution was observed and stannic oxide (SnO_2) formation at the oxide/solution interface was inferred.²² Oxidation at -0.66 V for longer times was shown to result in significant thickening of the oxide film; however, this was accompanied by dissolution of the Sn deposit, the extent of which increased with increasing oxidation time (Fig. 4).

The thickness of Sn oxide films formed at 1.2 V versus SCE in borate buffer and potassium bicarbonate-carbonate solutions is comparable whilst attempts to develop thicker oxide films by increasing the charge passed (at 1.2 V versus SCE) were unsuccessful. On the basis of the XPS results, it cannot be established conclusively whether SnO or SnO_2 is formed during electrochemical oxidation due to the overlapping ranges of binding energy reported for Sn^{2+} and Sn^{4+} ,²³ or indeed whether a systematic change in the chemistry of the Sn oxide is evident as a function of applied oxidation

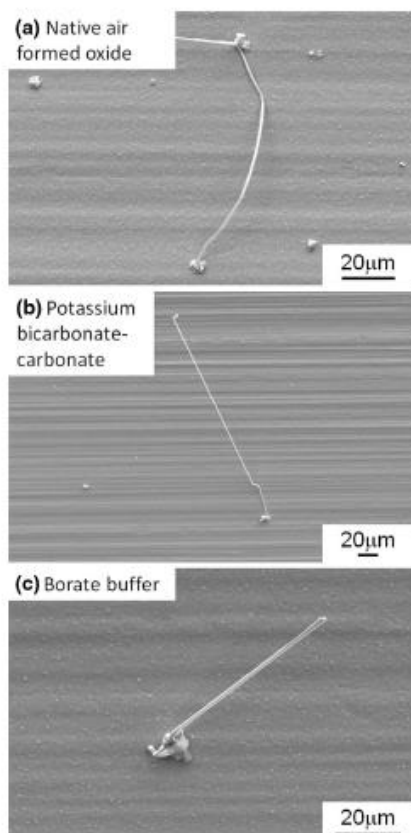


Fig. 16. Secondary electron images showing examples of filament whisker growth on $2\ \mu\text{m}$ Sn-Cu deposits on Cu: (a) sample left to develop a native air-formed oxide, (b) sample electrochemically oxidised in potassium bicarbonate-carbonate electrolyte solution at 1.2 V versus SCE and (c) sample electrochemically oxidised in borate buffer electrolyte solution at 1.2 V versus SCE. Analysis 48 days after Sn-Cu deposition.

potential; although Table II does indicate a slight increase in binding energy of the Sn $3d_{5/2(\text{oxide})}$ peak as the oxidation potential is increased. In general, the binding energies measured in this study for the Sn $3d_{5/2(\text{oxide})}$ peak (486.7–487.4 eV) lie within the range of values more typically associated with SnO_2 .^{23,24} The measured binding energy of the Sn $3d_{5/2(\text{oxide})}$ peak was comparable for Sn-Cu deposits on Cu and Sn deposits on brass.

Effect of the Electrochemical Oxide on Tin Whisker Growth

For Sn deposits on brass, the presence of the electrochemical oxide has a profound effect on whisker growth; to date, only limited whisker

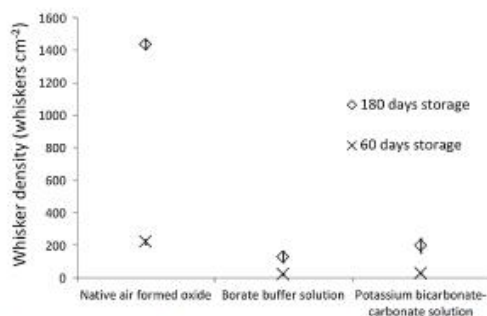


Fig. 17. Whisker growth data for $2\ \mu\text{m}$ Sn-Cu ($10\ \text{mmol L}^{-1}$ Cu) deposits on Cu, 60 days and 180 days after deposition and electrochemical oxidation at 1.2 V versus SCE in borate buffer and potassium bicarbonate-carbonate electrolyte solutions.

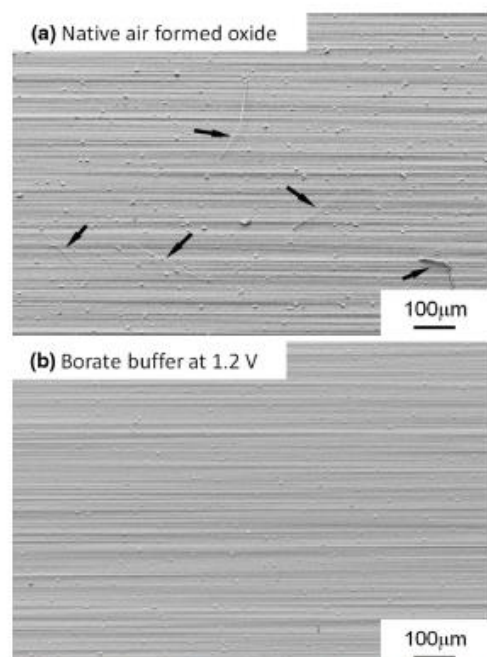


Fig. 18. Secondary electron images comparing whisker growth on $2\ \mu\text{m}$ Sn-Cu deposits on Cu: (a) sample left to develop a native air-formed oxide, (b) sample electrochemically oxidised in borate buffer electrolyte solution at 1.2 V versus SCE. Analysis ~150 days after Sn-Cu deposition.

growth has been observed on deposits electrochemically oxidised in a pH 8.4 borate buffer at 1.2 V, 1.6 V and 2.0 V versus SCE. For Sn deposits on brass, the main driving force for whisker growth is the diffusion of Zn to the surface of the Sn

An Investigation into the Effect of a Post-electroplating Electrochemical Oxidation Treatment on Tin Whisker Formation

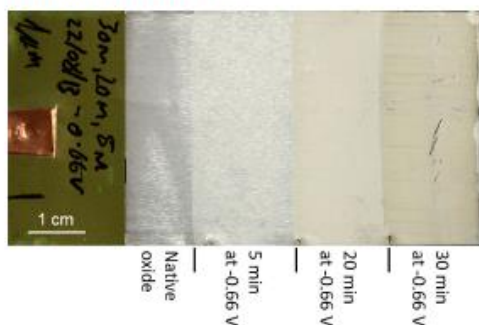


Fig. 19. The geometry and surface appearance of 1 μm Sn-Cu deposit on Cu after electrochemical oxidation in a potassium bicarbonate-carbonate electrolyte solution at -0.66 V versus SCE for 5, 20 and 30 min.

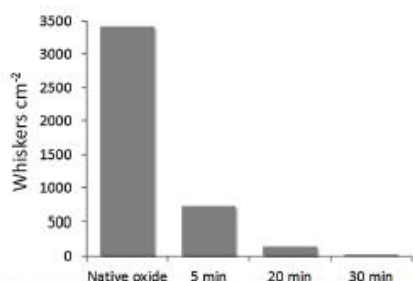


Fig. 20. Whisker densities measured after storage at room temperature for 60 days on a 1 μm Sn-Cu electrodeposit on Cu, electrochemically oxidised in potassium bicarbonate-carbonate electrolyte solution at -0.66 V versus SCE.

deposit.^{18,25,26} As shown in Figs. 3 and 6, Zn is evident on the surface of 2 μm Sn deposits on brass left to develop a native oxide, as a result of diffusion from the underlying brass substrate, within 1 day of deposition. In comparison, little Zn is detected on Sn deposits electrochemically oxidised at potentials of 1.2 V versus SCE and higher. Importantly, the measured surface Zn concentration does not increase with time after electrodeposition for electrochemically oxidised samples, thereby avoiding the formation of extended areas of Zn oxide at the Sn grain boundaries on the deposit surface observed in the current work (Figs. 10 and 11; Ref. 18) and a previous study.²⁷ Thus, Zn oxide formation is greatly reduced and whisker growth is suppressed, unless the electrochemically formed oxide is subsequently removed (e.g. by Ar ion sputtering).

For electrochemically oxidised Sn-Cu deposits on Cu, improved whisker resistance is derived by a different mechanism than for Sn on brass. In the case of Sn-Cu deposits, accelerated whisker growth results from the formation of Cu_6Sn_5 intermetallic,

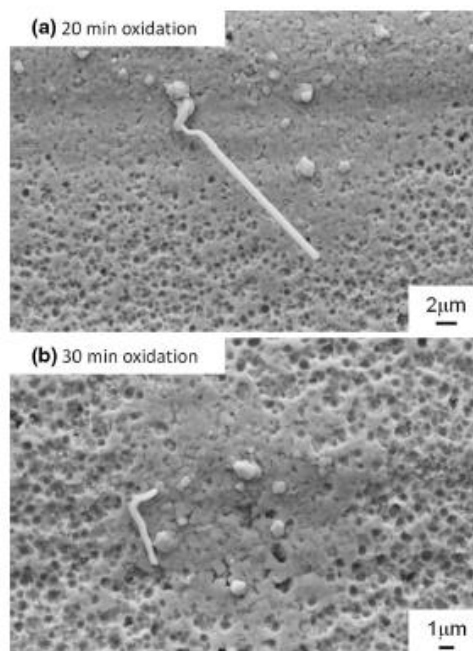


Fig. 21. Secondary electron images showing whisker growth from a 1 μm Sn-Cu electrodeposit on Cu, after electrochemical oxidation in potassium bicarbonate-carbonate electrolyte solution at -0.66 V versus SCE for (a) 20 min and (b) 30 min.

both at the interface with the Cu substrate²⁸ and throughout the thickness of the deposit.^{28,29} It is unlikely that the rate of intermetallic formation would be influenced by the electrochemical oxidation of the Sn. Therefore, any reduction in whisker growth rates observed on electrochemically oxidised Sn deposits must, on the basis of Tu's cracked oxide theory,¹ simply derive from an increase in the ability of the Sn oxide to resist the formation of localised cracks within the surface oxide. In Tu's model, whisker growth occurs where cracks are formed at localised sites in the surface oxide due to the build-up of compressive stresses within the deposit; this generates a source of vacancies whose flow is counterbalanced by the diffusion of Sn atoms, which provides the means for whisker formation and growth. On this basis, increased resistance to whisker formation may be derived from an increase in the thickness of the surface oxide, i.e. the increased thickness of the oxide film makes it more difficult for localised breakage of the oxide film to occur. Evidence that increased oxide thickness can make whisker growth more difficult has been observed in the current study from a 1 μm Sn-Cu deposit electrochemically oxidised for different times (Fig. 20). However, interpretation of the

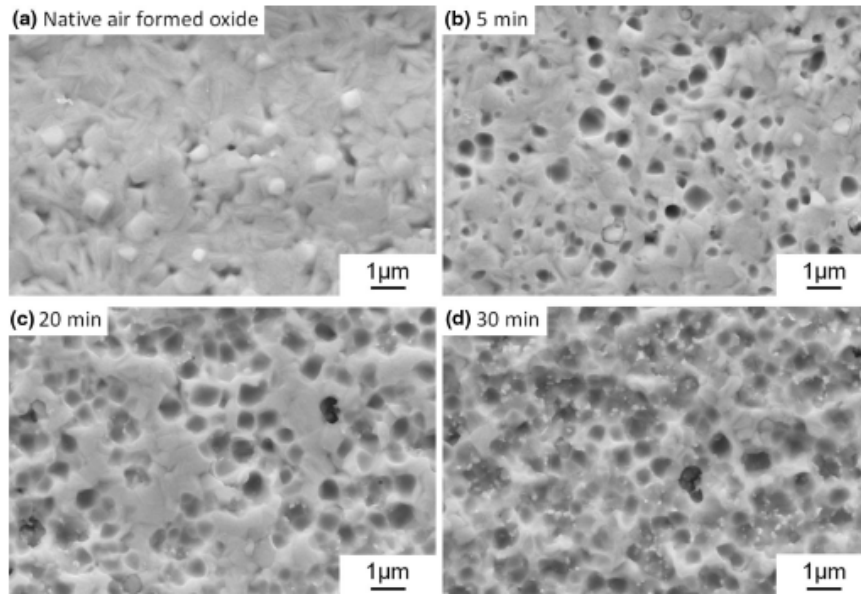


Fig. 22. Secondary electron images showing the surface of the $1\ \mu\text{m}$ Sn-Cu electrodeposit on Cu, after electrochemical oxidation and storage at room temperature for 60 days: (a) region left to develop native air-formed oxide, (b)–(d) regions electrochemically oxidised at $-0.66\ \text{V}$ versus SCE in potassium bicarbonate–carbonate electrolyte solution for 5 min, 20 min and 30 min, respectively.

results is potentially complicated by dissolution of the Sn deposit that occurred during electrochemical oxidation at $-0.66\ \text{V}$ versus SCE. This results in a reduction in the thickness of the Sn deposit, the extent of which increases with increasing oxidation time. A reduction in deposit thickness may potentially result in an increased susceptibility to whisker growth;^{18,30–32} however, at thicknesses $<1\ \mu\text{m}$, the effect on whisker growth is not so well established. Ideally, an electrochemical oxidation treatment that did not result in pronounced Sn dissolution would be preferable.

Although whisker densities were greatly reduced on all of the electrochemically oxidised samples, whiskers were still observed even on the samples oxidised for 30 min; however, as shown in Fig. 21, these were often growing from regions of the deposit that were discernibly less oxidised than the surrounding regions, i.e. areas that, potentially, represent a weak point within the oxide film. It may be inferred, however, that the increase in oxide thickness on the electrochemically oxidised Sn-Cu deposits on Cu, in particular those oxidised at $1.2\ \text{V}$ (versus SCE), results in fewer weak points in the surface oxide and hence a reduced propensity for whisker growth.

In terms of long-term whisker mitigation, the increased thickness of the oxide film may simply increase the incubation period prior to the onset of

whisker growth, since increased levels of compressive stress, brought about by intermetallic formation within the Sn-Cu coating²⁸ and at the coating–substrate interface,¹³ will be required to initiate oxide film cracking and subsequent whisker growth.¹ To address this issue, and also to further evaluate the comparative effectiveness of oxide films produced in borate buffer and potassium bicarbonate–carbonate electrolyte solutions, long-term whisker density measurements will be carried out.

CONCLUSIONS

For the first time, a direct correlation has been demonstrated between oxide thickness and whisker growth. Significantly reduced whisker growth has been observed for both pure Sn deposits on brass and Sn-Cu deposits on Cu that were electrochemically oxidised shortly after deposition.

For electroplated Sn on brass, whisker growth is mitigated by the formation of a comparatively thick Sn oxide on the surface of the Sn deposit, which prevents the formation of Zn oxide on the surface of the deposit, in particular at the Sn grain boundaries.

For Sn-Cu deposits on Cu, reduced whisker growth simply results from the increased thickness of the oxide film, which, potentially, makes localised cracking of the oxide film more difficult to achieve.

An Investigation into the Effect of a Post-electroplating Electrochemical Oxidation Treatment on Tin Whisker Formation

The thickness of the oxide films developed by electrochemical oxidation was dependent upon the applied potential and the total charge passed. Comparable reductions in whisker growth were observed for borate buffer and potassium bicarbonate-carbonate electrolyte solutions.

ACKNOWLEDGEMENTS

The authors would like to thank the UK EPSRC Innovative Electronics Manufacturing Research Centre for funding this research through the WHISKERMIT programme and also Loughborough University Materials Research School for provision of a student bursary for one of the authors (Dan Haspel).

REFERENCES

1. K.N. Tu, *Phys. Rev. B* 49, 2030 (1994).
2. K.N. Tu and K. Zeng, *Proceedings of IEEE Electronic Components and Technology Conference* (Piscataway, NJ, 2002), pp. 1194–1200.
3. K. Tu, C. Chen, and A.T. Wu, *J. Mater. Sci.* 18, 269 (2007).
4. K.S. Kumar, L. Reinbold, A.F. Bower, and E. Chason, *J. Mater. Res.* 23, 2916 (2008).
5. J.K. Shin and E. Chason, *J. Mater. Res.* 24, 1522 (2009).
6. E. Chason, N. Jadhav, W.L. Chan, L. Reinbold, and K.S. Kumar, *Appl. Phys. Lett.* 92, 171901 (2008).
7. B.Z. Lee and D.N. Lee, *Acta Mater.* 46, 3701 (1998).
8. C.Y. Chang and R.W. Vook, *Thin Solid Films* 228, 205 (1993).
9. K.W. Moon, C.E. Johnson, M.E. Williams, O. Kongstein, G.R. Stafford, C.A. Handwerker, and W.J. Boettinger, *J. Electron. Mater.* 34, L31 (2005).
10. N. Jadhav, E. Buchovecky, E. Chason, and A. Bower, *JOM* 62, 30 (2010).
11. B. Jiang and A.P. Xian, *Philos. Mag. Lett.* 86, 521 (2006).
12. K. Suganuma, A. Baated, K.-S. Kim, K. Hamasaki, N. Nemoto, T. Nakagawa, and T. Yamada, *Acta Mater.* 59, 7255 (2011).
13. K.N. Tu, *Acta Metall.* 21, 347 (1973).
14. R. Díaz, I. Díez-pérez, P. Gorostiza, F. Sanz, and J.R. Morante, *J. Braz. Chem. Soc.* 14, 523 (2003).
15. S.D. Kapusta and N. Hackerman, *Electrochim. Acta* 25, 1625 (1980).
16. P.E. Alvarez, S.B. Ribotta, M.E. Folquer, C.A. Gervasi, and J.R. Vilche, *Corros. Sci.* 44, 49 (2002).
17. M. Drogowska, H. Menard, and L. Brossard, *J. Appl. Electrochem.* 21, 84 (1991).
18. M.A. Ashworth, G.D. Wilcox, R.L. Higginson, R.J. Heath, and C. Liu, *Trans. Inst. Met. Finish.* 91, 260 (2013).
19. D. Morgan Tench, D.P. Anderson, and P. Kim, *J. Appl. Electrochem.* 24, 18 (1994).
20. G. Schon, *J. Electron Spectros. Relat. Phenom.* 2, 75 (1973).
21. K.W. Moon, M.E. Williams, C.E. Johnson, G.R. Stafford, C.A. Handwerker, and W.J. Boettinger, *Proceedings of PRICMA Forth Pacific Rim International Conference on Advanced Materials and Processing* (Honolulu, Hawaii, ed. S. Hanada, et al., 11–15 December 2001), pp. 1115–1118.
22. S.N. Shah and D. Eurof Davies, *Electrochim. Acta* 8, 663 (1963).
23. NIST, X-ray Photoelectron Spectroscopy Database, NIST Stand. Ref. Database 20, Version 4.1, <http://srdata.nist.gov/xps/> (n.d.).
24. W. Zhang and W. Ruythooren, *European Microelectronics and Packaging Conference (EMPC 2009)* (2009), vol. 1 2, pp. 597–600.
25. S.C. Britton and M. Clarke, *Trans. Inst. Met. Finish.* 40, 205 (1964).
26. B.D. Dunn, European Space Agency Representative. STR-223, European Space Agency (Paris, 1987).
27. S. Sakuyama and M. Kutami, *FUJITSU Sci. Technol. J.* 41, 217 (2005).
28. W.J. Boettinger, C.E. Johnson, L.A. Bendersky, K.W. Moon, M.E. Williams, and G.R. Stafford, *Acta Mater.* 53, 5033 (2005).
29. M.E. Williams, K.W. Moon, W.J. Boettinger, D. Josell, and A.D. Deal, *J. Electron. Mater.* 36, 214 (2007).
30. M. Dittes, P. Oberndorff, and L. Petit, *53rd Electronic Components and Technology Conference 2003 Proceedings* (2003), pp. 822–826.
31. J. Cheng, F. Yang, P.T. Vianco, B. Zhang, and J.C.M. Li, *J. Electron. Mater.* 40, 2069 (2011).
32. E.R. Crandall, Factors Governing Tin Whisker Growth (Ph.D. thesis, Auburn University, 2012).

10.3 Conference Presentations

D.M.Haspel, M.A.Ashworth, G.D.Wilcox, X.Bao, **The Use of Post-Electroplating Surface Modification**

Treatments to Mitigate Tin Whisker Growth, Electronic Materials and Processes for Space (EMPS)

Workshops, EMPS-8, European Space Agency, Noordwijk, The Netherlands, 10th-12th May 2017

Loughborough University

The Use of Post-Electroplating Surface Modification Treatments to Mitigate Tin Whisker Growth

D.M. Haspel, M.A. Ashworth, G.D. Wilcox & X. Bao
Department of Materials, Loughborough University, UK

Electronic Materials and Processes for Space (EMPS) Workshops
The Eighth Workshop, EMPS-8
ESA, Noordwijk, The Netherlands
10th-12th May 2017

#InspiringWinners since 1909

Loughborough University

Loughborough University

Contents

- Background
- Experimental
- Results
 - Electrochemical Oxidation
 - Tungstate Conversion Coating
 - Molybdate Conversion Coating
- Conclusions

Loughborough University

Loughborough University

Background

- Tu's 1994¹ theory suggested that a thicker oxide on tin would help prevent whisker growth
- Su *et al* 2014² later showed that whiskers would preferentially grow from pre-defined 'weak points' in the oxide film
- Our previous work³ showed that an electrochemical formed oxide would significantly reduce whisker growth

1 K.-N. Tu, Phys. Rev., vol. 49, no. 3, pp. 2030-2034, 1994.
2 C.-H. Su, H. Chen, H.-Y. Lee, C.-Y. Liu, C.-S. Ku, and A. T. Wu, J. Electron. Mat., vol. 43, no. 9, pp. 3290-3295, 2014.
3 D. M. Haspel, M. A. Ashworth, L. Wu, G. D. Wilcox, and R. J. Mortimer, Trans. IMF, vol. 93, no. 6, pp. 332-341, 2015.

Loughborough University

Loughborough University

Previous Work

Electrochemical oxidation at 1.2 V vs SCE

Whisker density (whiskers/cm²)

Oxygen Content (at.%)

Time (days)

Sputter Time (s)

Order of magnitude reduction in whisker growth

Native air formed oxide

Borate buffer solution

Potassium bicarbonate-carbonate solution

2 V vs Ag/AgCl 1 day

Native 1 day

Native

1.2V 60mC/cm²

Loughborough University

Loughborough University

Aims and Objectives

- Further reduce whisker growth by increasing the thickness of the oxide film
- Use conversion coatings to produce a thicker oxide coating
- Characterise conversion coatings using x-ray photoelectron spectroscopy (XPS), scanning electron microscopy (SEM) and optical microscopy
- Evaluate the whisker resistance of the conversion coatings

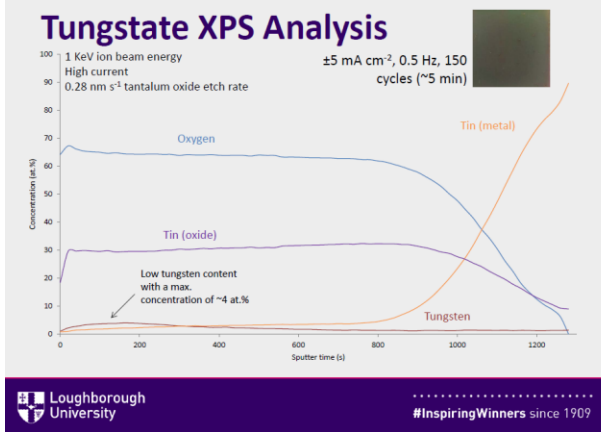
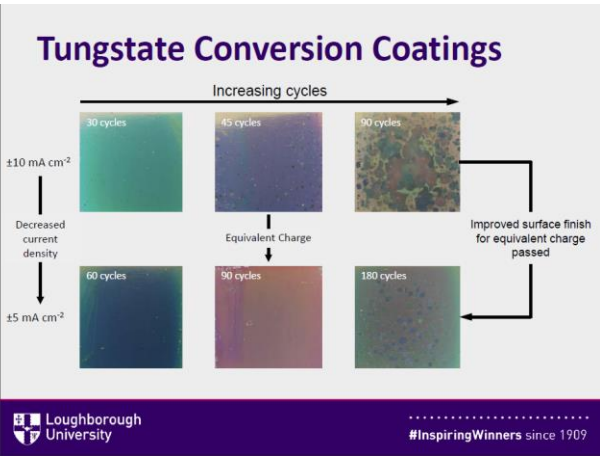
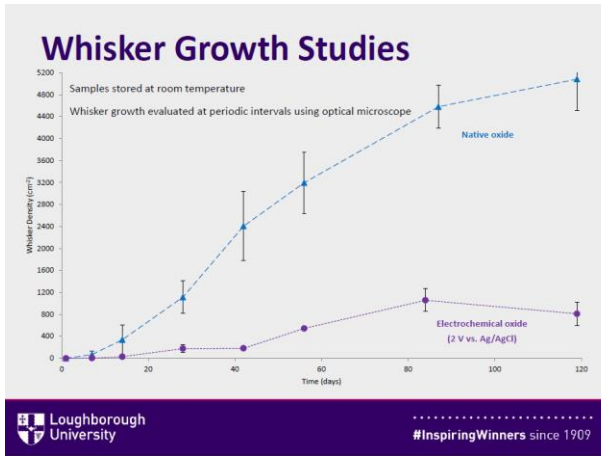
Loughborough University

Loughborough University

Experimental

- Electroplated Sn-Cu alloy on copper coupons
- Electrochemical oxidation
 - Potassium bicarbonate-potassium carbonate bath
 - 2 V vs. Ag/AgCl
 - Total charge passed of 60 mC cm⁻²
- Tungstate conversion coatings
 - Reverse current pulse, ranging between ±2.5 mA cm⁻² and ±10 mA cm⁻²
 - Square wave cycles ranging between 30 – 300 cycles
 - 0.5 Hz
- Molybdate conversion coatings
 - pH 3.13
 - 5 min immersion along with potentiostatic driven with potentials ranging between -0.45 to -0.75 V vs. Ag/AgCl
 - Reverse current pulse using similar parameters as tungstate conversion coatings

Loughborough University

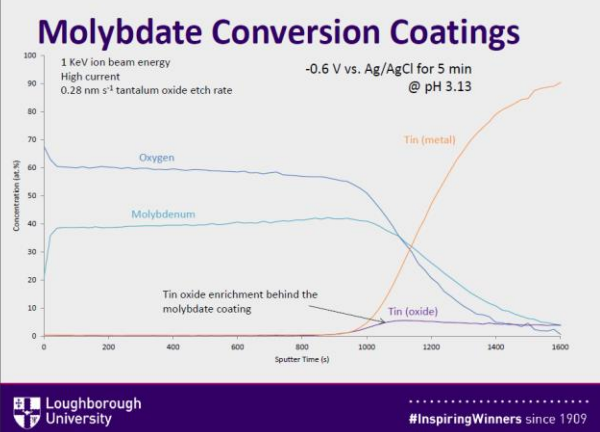
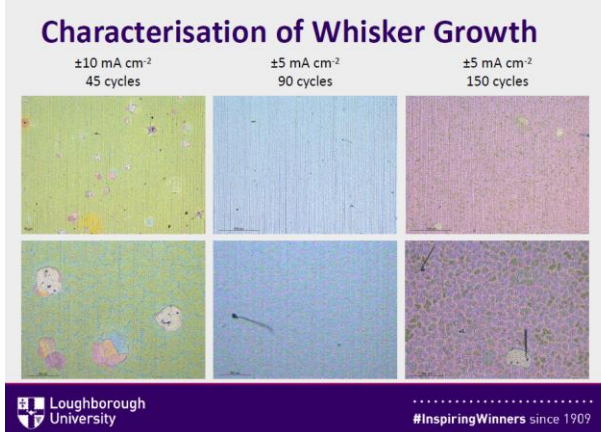
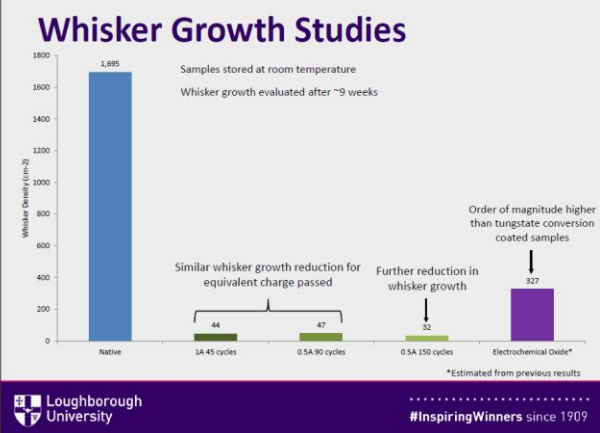
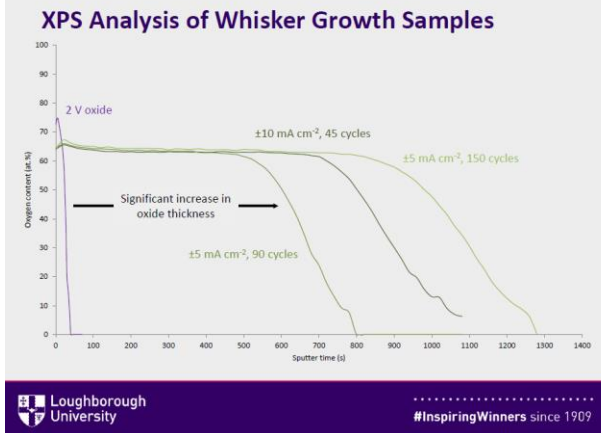


XPS Summary

Experiment	Current Density	Number of Square Waves	Sputter Time to 50% Oxygen Content
2 V vs. Ag/AgCl Electrochemical oxide	-	-	27
Comparison of Current Density	±2.5 mA cm ⁻²	30	130
	±5 mA cm ⁻²	30	280
	±10 mA cm ⁻²	30	550
Comparison of Number of Cycles	±5 mA cm ⁻²	30	275
	±5 mA cm ⁻²	90	680
	±5 mA cm ⁻²	150	1060
Comparison of Equivalent Charge Passed	±2.5 mA cm ⁻²	300	1085
	±5 mA cm ⁻²	150	1085
	±10 mA cm ⁻²	75	1410

Increased thickness for increased current density
Increased thickness for increased number of cycles
Constant thickness for equivalent charge
Thicker oxide for equivalent charge passed

Loughborough University #InspiringWinners since 1909



XPS Summary

Coating pH 3.13	Sputter time to 50% oxygen content	Molybdate content at plateau region
5 min immersion	195	~37 at.%
$\pm 5 \text{ mA cm}^{-2}$, 0.5 Hz, 30 cycles	340	~36.5 at.%
$\pm 2.5 \text{ mA cm}^{-2}$, 0.5 Hz, 30 cycles	215	~36 at.%
$\pm 2.5 \text{ mA cm}^{-2}$, 0.5 Hz, 120 cycles	440	~37 at.%
-0.45 V 5min	275	~37 at.%
-0.6 V 5min	1085	~40 at.%
-0.75 V 5min	3095	~40-48 at.%

NB. Tin content for the Mo plateau region is below ~1 at.%

Similar Mo content

Mo content increases with depth

XPS Summary

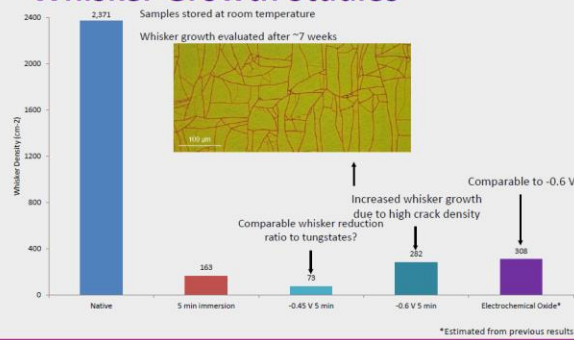
Coating pH 3.13	Sputter time to 50% oxygen content	Molybdate content at plateau region
5 min immersion	195	~37 at.%
$\pm 5 \text{ mA cm}^{-2}$, 0.5 Hz, 30 cycles	340	~36.5 at.%
$\pm 2.5 \text{ mA cm}^{-2}$, 0.5 Hz, 30 cycles	215	~36 at.%
$\pm 2.5 \text{ mA cm}^{-2}$, 0.5 Hz, 120 cycles	440	~37 at.%
-0.45 V 5min	275	~37 at.%
-0.6 V 5min	1085	~40 at.%
-0.75 V 5min	3095	~40-48 at.%

NB. Tin content for the Mo plateau region is below ~1 at.%

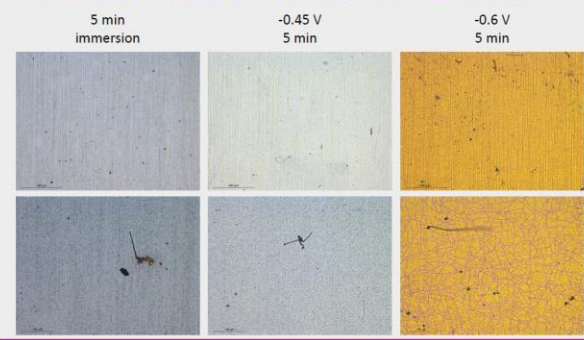
Similar thickness to simple immersion

Increased thickness for increased cathodic potential

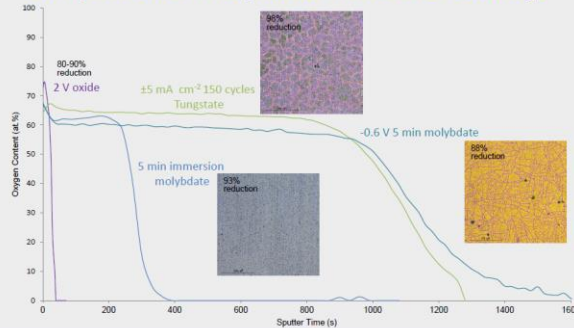
Whisker Growth Studies



Characterisation of Whisker Growth


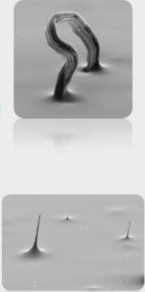


Comparison of Molybdate with Other Coatings



Conclusions

- An electrochemical oxidation treatment is able to provide continuous tin whisker mitigation
- Conversion coating treatments can be used to develop oxides that are significantly thicker than those achieved by electrochemical oxidation
- Both conversion coating treatments show enhanced whisker mitigation compared with an electrochemical oxidation treatment
- For the tungstate conversion coated samples most whiskers were observed to grow from 'weak points'
- For the molybdate conversion coated samples with a high density of cracking, all the whiskers grew from the cracks

<p style="text-align: right;">Tin Whisker Mitigation – Research into Mechanisms & Strategies</p> <p>M.A. Ashworth, G.D. Wilcox, H. Pearson and D. Haspel</p> <p>Tin Whisker Mitigation Methodologies Loughborough University 24th November 2016</p> <p style="text-align: right;">#InspiringWinners since 1909</p>	<p style="text-align: right;">Tin Whisker Mitigation - Research into Mechanisms & Strategies</p> <p>PART 1: EFFECT OF PLATING METHODOLOGIES</p> <p>PART 2: POST-PLATING MITIGATION METHODS</p> <p style="text-align: right;">#InspiringWinners since 1909</p>
<p>Part 2: Outline of presentation</p> <ul style="list-style-type: none"> • Introduction • Novel conformal coatings • Electrochemical oxidation • Atomic layer deposition • Summary 	<p>Introduction</p> <ul style="list-style-type: none"> • Although whisker growth may be reduced by choice of electroplating bath composition and optimisation of deposition parameters, such methods cannot be relied upon to fully mitigate whisker growth • Given the unpredictable nature of whisker growth, even the 'best' electroplated tin coatings should be considered 'whisker-resistant' rather than 'whisker-proof' • Additional control measures, in the form of surface coatings or treatments, are required to further suppress the growth of whiskers
<p style="text-align: right;">Post-plating mitigation methods</p> <p>1. NOVEL CONFORMAL COATINGS</p>	<p>Tin whiskers and conformal coatings</p> <ul style="list-style-type: none"> • Conformal coatings are applied to protect printed circuit boards and associated electronic components • Currently, tin whisker mitigation is attempted with conformal coatings that have not been designed to prevent whisker growth • WHISKERMIT 2 research programme aimed to develop novel conformal coatings specifically designed to mitigate whisker growth 
<p style="text-align: right;">#InspiringWinners since 1909</p>	<p style="text-align: right;">#InspiringWinners since 1909</p>

Research Aims and Objectives

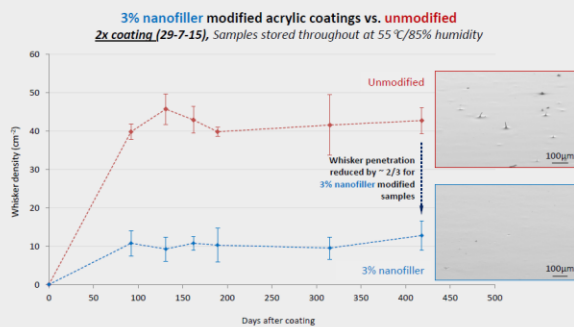
- Engender polymers with physical barriers to whisker growth through the inclusion of nano-fillers in the conformal coating polymer formulation.
- Apply concept to commercial conformal coatings that are currently used for environmental protection in electronic components
- Evaluate the microstructure, mechanical properties and whisker resistance of the modified coating formulations

Evaluation of whisker mitigation

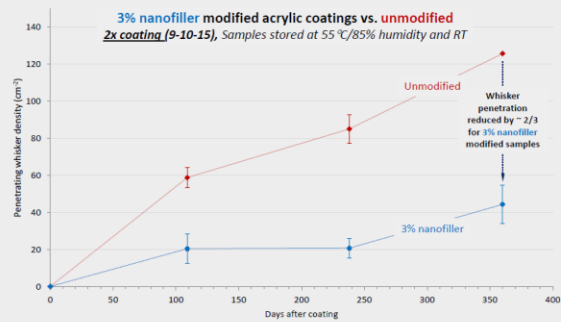
- Whisker growth has been investigated using brass coupons electroplated with $2 \mu\text{m}$ of bright tin at 10 mA cm^{-2}
- Modified coatings based on a HumiSeal acrylic formulation
- All conformal coatings applied by spraying
- Three sets of trials currently under evaluation (batches 1, 2 and 3)
- Samples stored in an environmental chamber at **55°C/85%** humidity
- Whisker growth evaluated at periodic intervals using a stereo microscope



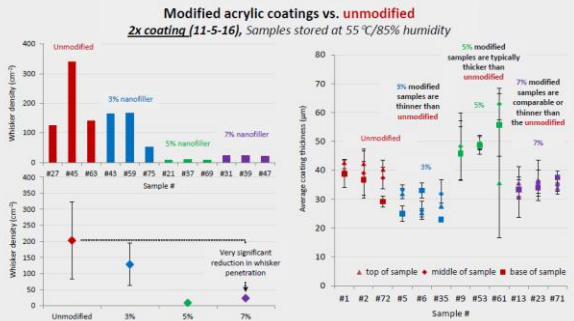
Evaluation of whisker growth: Batch 1



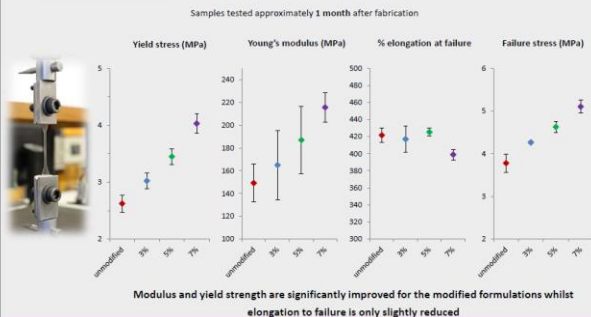
Evaluation of whisker growth: Batch 2



Evaluation of whisker growth: Batch 3



Batch 2: mechanical property data



Post-plating mitigation methods

2. ELECTROCHEMICAL OXIDATION

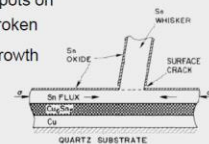
The role of the surface oxide in whisker growth

In 1994, Tu proposed his "cracked oxide theory"¹

- whisker growth occurs at certain weak spots on the surface where the oxide has been broken
- In the absence of an oxide no whisker growth would occur

Later adding² ...

- "if the surface oxide is very thick, it will physically block the growth of any hillocks and whiskers"



¹ Physical Review B 49, 2030, 1994

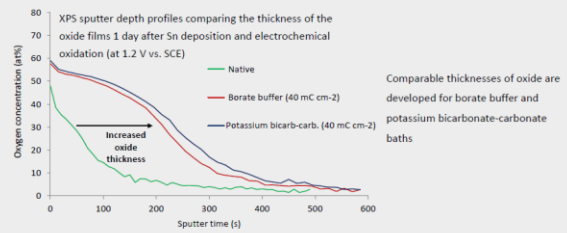
² Proceedings of the IEEE Electronic Components and Technology Conference, 2002 p1194-1200

Can we mitigate whisker growth by increasing the thickness of the surface oxide?

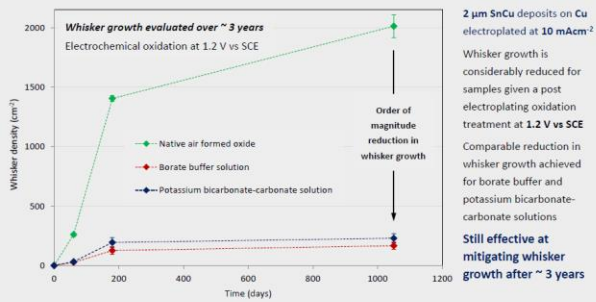
- Electrochemical oxidation in borate buffer and potassium carbonate/bicarbonate solutions used to develop thicker oxides
- Although the oxide film thickness is increased, other characteristics of the Sn coating (e.g. grain size, grain orientation and residual plating stresses) should be unaffected
- XPS analysis to evaluate the thickness and composition of the oxide layers formed
- Whisker growth evaluated using SEM and optical microscopy

Electrochemical oxidation

- Electrochemical oxidation can be used to develop oxide films that are much greater in thickness than a native Sn oxide

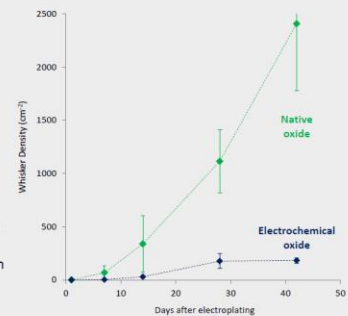


Effect of electrochemical oxide on whisker growth

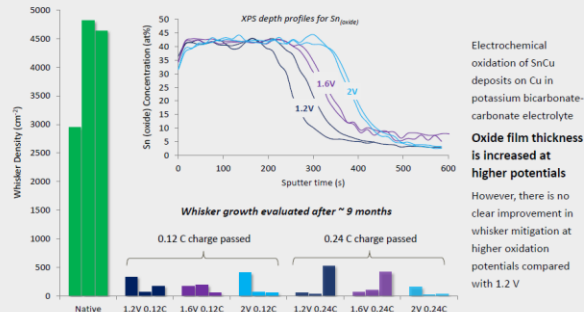


Whisker development with time

- Study underway to compare the growth of whiskers, and the development of the oxide film, on native and electrochemically oxidised deposits as a function of time
- 2 μm SnCu deposits on Cu
- Electrochemical oxidation at 2 V vs. SCE in potassium bicarbonate/carbonate solution



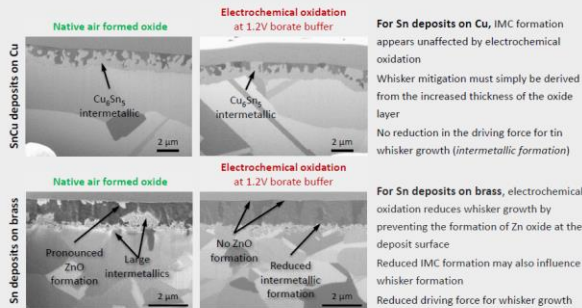
Electrochemical oxidation at higher potentials



Whisker mitigation: Sn deposits on brass



Whisker mitigation mechanisms



Post-plating mitigation methods

3. ATOMIC LAYER DEPOSITION

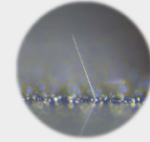
ALD as a whisker mitigation strategy

- Atomic layer deposition (ALD) has been investigated as a potential whisker mitigation strategy
- ESA funded collaborative research programme between Loughborough University, Picosun and Oy Poltronic Ab
- Initial studies to investigate the effect of coating process variables on whisker mitigation



Experimental approach

- Copper coupons electroplated with 2 μm Sn-Cu to promote whisker growth
- Electroplated coupons shipped to Picosun for ALD coating
- A range of pre-treatments and process conditions investigated
- Uncoated control samples included in each batch of ALD processed samples
- Whisker growth evaluated over ~12 month period using optical and scanning electron microscopy



Loughborough University

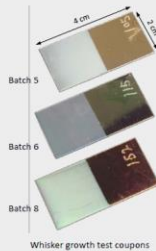
#InspiringWinners since 1909

Loughborough University

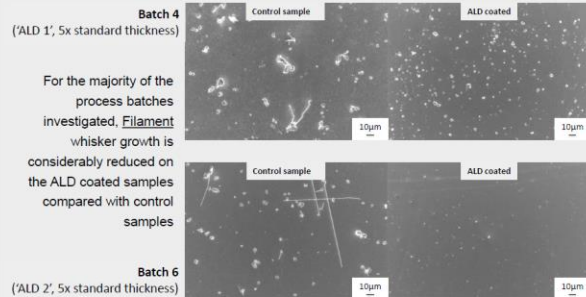
#InspiringWinners since 1909

ALD Coating Trials

Batch	Pre-treatment	Coating Material	Coating Thickness
1	Pre-treatment trials	'ALD 1'	'Standard'
2			5x 'standard'
3			'Standard'
4	-	'ALD 2'	5x 'standard'
5	-		'Standard'
6	-	'ALD 3'	5x 'standard'
7	-		'Standard'
8	-		5x 'standard'



Analysis of whisker growth



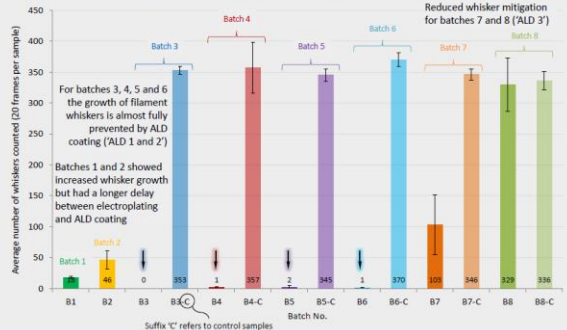
Loughborough University

#InspiringWinners since 1909

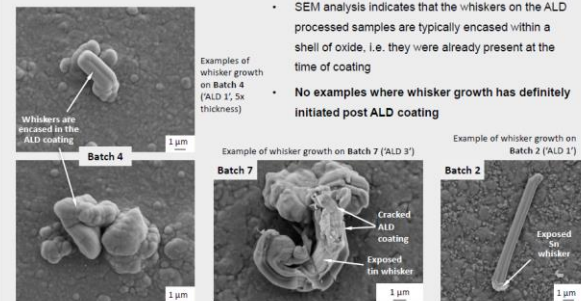
Loughborough University

#InspiringWinners since 1909

Effect of ALD coating on filament whisker growth



Whisker growth prior to coating?



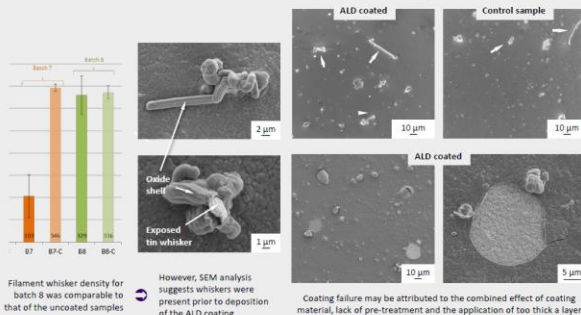
Loughborough University

#InspiringWinners since 1909

Loughborough University

#InspiringWinners since 1909

SEM analysis of batch 8 ('ALD 3')



Summary




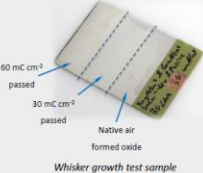


- **Conformal coating studies**
Novel conformal coatings are under development. Whisker growth studies show a significant improvement in whisker mitigation compared with unmodified coatings
- **Electrochemical oxidation treatment**
Electrochemical oxidation has been shown to provide long term whisker mitigation for both SnCu deposits on Cu and Sn deposits on brass
- **Atomic layer deposition**
Significant reductions in whisker growth have been achieved as a result of ALD processing

Loughborough University

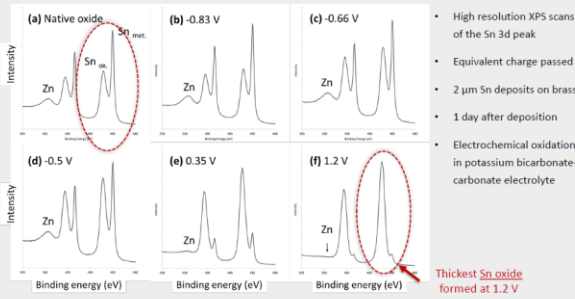
#InspiringWinners since 1909

Loughborough University

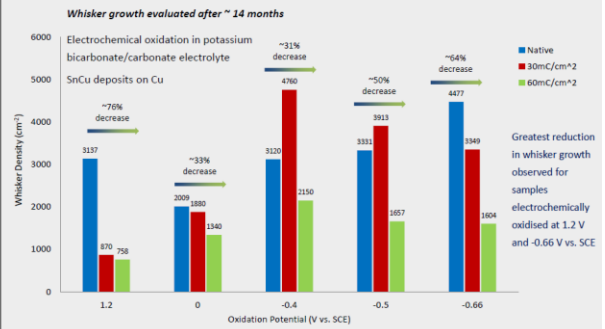
#InspiringWinners since 1909

<p> Loughborough University</p> <p>The Development of Post-Electroplating Surface Modification Treatments to Mitigate Tin Whisker Growth</p> <p>Dan Haspel, <u>Mark Ashworth</u>, Geoff Wilcox and Roger Mortimer</p> <p>Electronic Materials and Processes for Space (EMPS) Workshops The Seventh Workshop, EMPS-7 The University of Portsmouth, Portsmouth, UK 13th and 14th April 2016</p> <p>#InspiringWinners since 1909</p>	<h3>Outline of presentation</h3> <ul style="list-style-type: none"> • Background • Project objectives • Experimental approach • Results and discussion • Summary  <p> Loughborough University</p> <p>#InspiringWinners since 1909</p>
<h3>Factors that influence whisker growth</h3> <ul style="list-style-type: none"> • Electroplating bath chemistry <ul style="list-style-type: none"> – Pure tin or tin alloy (Sn-Pb, Sn-Bi, Sn-Cu etc) – Use of brighteners • Electroplating parameters <ul style="list-style-type: none"> – Current density, temperature, agitation • Deposit characteristics <ul style="list-style-type: none"> – Grain size and morphology, orientation, deposit thickness, Sn oxide • Substrate <ul style="list-style-type: none"> – Cu, brass, alloy 42 – Intermetallic formation, elemental diffusion from substrate • Environmental conditions <ul style="list-style-type: none"> – Temperature, humidity, thermal cycling, applied external stress 	<h3>The role of the surface oxide in whisker growth</h3> <ul style="list-style-type: none"> • In 1994, Tu proposed his “cracked oxide theory”¹ <ul style="list-style-type: none"> ▪ whisker growth occurs at certain weak spots on the surface where the oxide has been broken ▪ In the absence of an oxide no whisker growth would occur • Later adding² ... <ul style="list-style-type: none"> ▪ “if the surface oxide is very thick, it will physically block the growth of any hillocks and whiskers” • Can we mitigate whisker growth by increasing the thickness of the surface oxide?? <p><small>¹ Physical Review B 49, 2030, 1994 ² Proceedings of the IEEE Electronic Components and Technology Conference, 2002 p1194–1200</small></p>
<h3>Aims and objectives</h3> <p><i>Investigate the effect of post-electroplating surface treatments on whisker growth from tin and tin alloy electrodeposits</i></p> <ul style="list-style-type: none"> • Use electrochemical oxidation and conversion coating techniques to develop surface oxides • Evaluate the effect of process variables on oxide thickness • Evaluate the ability of the applied surface treatments to mitigate whisker growth 	<h3>Experimental approach</h3> <ul style="list-style-type: none"> • Surface modification treatments applied to electrodeposited Sn and Sn-Cu coatings <ul style="list-style-type: none"> – Electrochemical oxidation in pH 8.4 borate buffer and potassium carbonate/bicarbonate solutions – Application of a molybdate conversion coating • XPS analysis to evaluate effect of process variables on the composition and thickness of the oxide layers formed • Evaluate the effect of the surface modification treatment on whisker growth using SEM and optical microscopy 
<p> Loughborough University</p> <p>#InspiringWinners since 1909</p>	<p> Loughborough University</p> <p>#InspiringWinners since 1909</p>

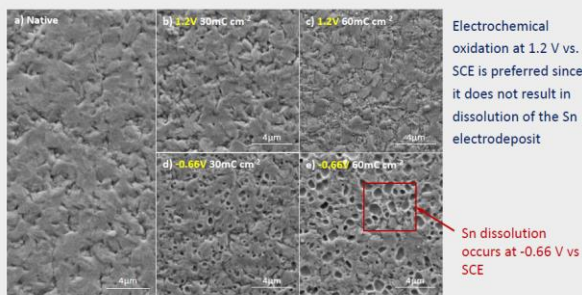
Effect of oxidation potential on oxide thickness



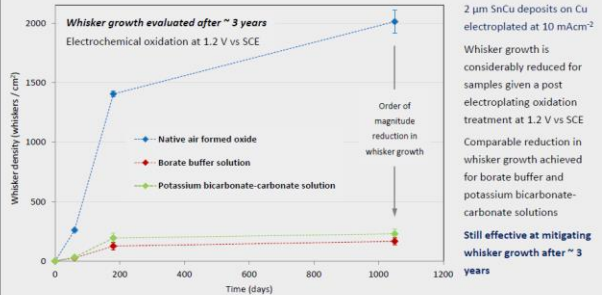
Effect of oxidation potential on whisker growth



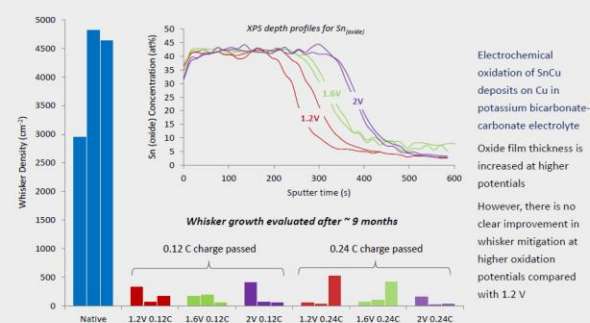
Optimisation of oxidation potential



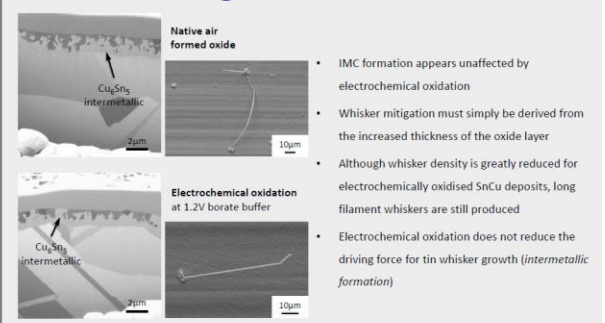
Effect of electrochemical oxide on whisker growth



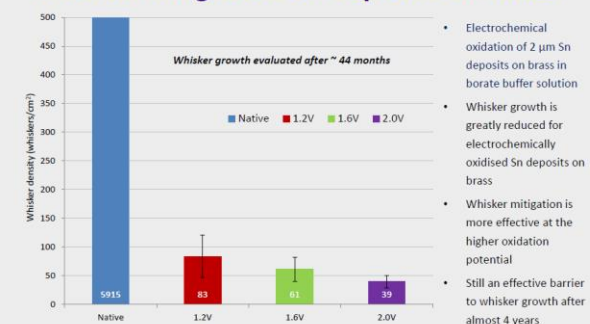
Electrochemical oxidation at higher potentials



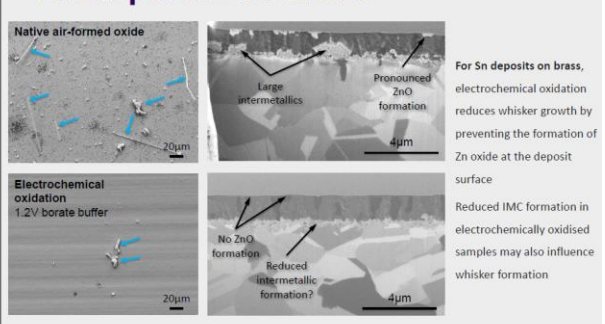
Whisker mitigation mechanism



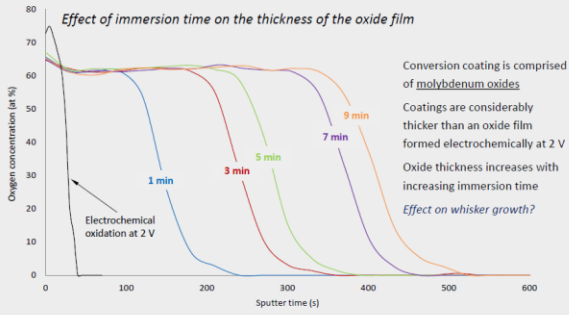
Whisker mitigation: Sn deposits on brass



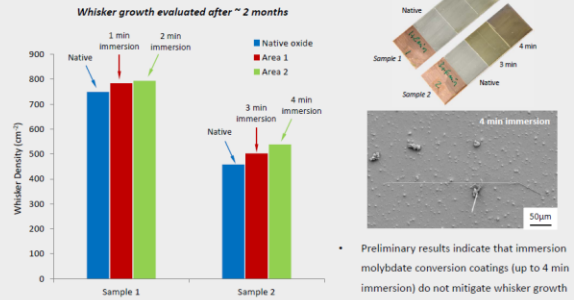
Sn deposits on brass



Molybdate conversion coatings



Effect of molybdate conversion coatings - preliminary whisker growth results



Summary

- Long term whisker mitigation (~ 3 years) has been demonstrated for electrochemically oxidised SnCu deposits on Cu
- Electrochemical oxidation also significantly reduces whisker growth for Sn deposits on brass
- The thickness of the oxide film developed by electrochemical oxidation is dependent upon the applied potential and charge passed.
- Comparable reductions in whisker growth were observed for deposits electrochemically oxidised in borate buffer and potassium bicarbonate-carbonate electrolyte solutions
- Initial results suggest that, although considerably thicker, molybdate conversion coatings formed by immersion are less able to mitigate whisker growth

Any questions?



We would like to thank the UK EPSRC Innovative Electronics Manufacturing Research Centre (IEMRC) for funding this research.

M.A.Ashworth, D.Haspel, L.Wu, G.D.Wilcox, R.J.Mortimer, **The Effect of a Post-Electroplating Electrochemical Oxidation Treatment on Tin Whisker Formation**, eastForum 2015, Lund, Sweden, 25th-26th June 2015

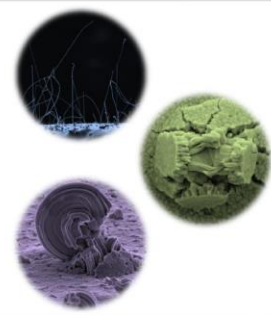
The Effect of a Post-Electroplating Electrochemical Oxidation Treatment on Tin Whisker Formation

M.A. Ashworth, D. Haspel, L. Wu,
G.D. Wilcox and R.J. Mortimer

eastForum 2015
25-26th June 2015, Lund, Sweden

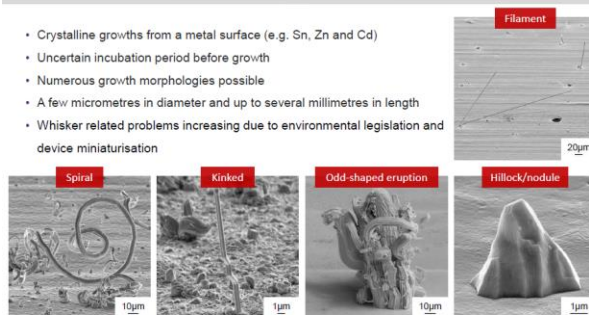
Outline of presentation

- Background
- Project objectives
- Experimental approach
- Results and discussion
- Summary





Background – what are metal whiskers?

- Crystalline growths from a metal surface (e.g. Sn, Zn and Cd)
- Uncertain incubation period before growth
- Numerous growth morphologies possible
- A few micrometres in diameter and up to several millimetres in length
- Whisker related problems increasing due to environmental legislation and device miniaturisation



Documented electronic failures due to tin whiskers



<http://nepp.nasa.gov/whisker/>

Factors that influence whisker growth...

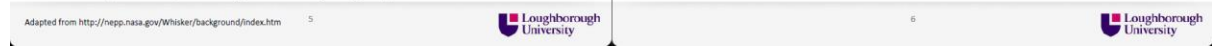
- Electroplating bath chemistry
 - Pure tin or tin alloy (Sn-Pb, Sn-Bi, Sn-Cu etc)
 - Use of brighteners
- Electroplating parameters
 - Current density, temperature, agitation
- Deposit characteristics
 - Grain size and morphology, orientation, deposit thickness, **Sn oxide**
- Substrate
 - Cu, brass, alloy 42
 - Intermetallic formation, elemental diffusion from substrate
- Environmental conditions
 - Temperature, humidity, thermal cycling, applied external stress

Adapted from <http://nepp.nasa.gov/Whisker/background/index.htm>

The role of the surface oxide in whisker growth

- In 1994, Tu proposed his “**cracked oxide theory**”¹
 - whisker growth occurs at certain weak spots on the surface where the oxide has been broken
 - In the absence of an oxide no whisker growth would occur
- Later adding² ...
 - “if the surface oxide is very thick, it will physically block the growth of any hillocks and whiskers”
 - *Can we mitigate whisker growth by increasing the thickness of the surface oxide??*

¹ Physical Review B 49, 2030, 1994
² Proceedings of the IEEE Electronic Components and Technology Conference, 2002 p1194-1200



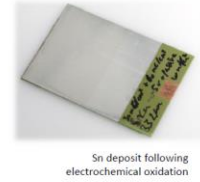
Aims and Objectives

- Investigate the effect of oxide thickness on whisker growth from tin and tin alloy electrodeposits
- Use electrochemical oxidation to develop thicker tin oxides
- Evaluate the effect of electrolyte and oxidation potential on oxide thickness
- Evaluate the ability of electrochemical oxides to mitigate whisker growth



Experimental approach

- Modify the thickness of the tin oxide layer by electrochemical oxidation
 - pH 8.4 Borate buffer and pH 8.9 potassium bicarbonate / potassium carbonate electrolytes
 - No effect on as-deposited structure of tin coating
- Characteristics of the oxide layer evaluated using XPS analysis
- Evaluate effect of electrochemical oxidation on whisker growth for **Sn-Cu deposits on Cu** and **Sn deposits on brass**



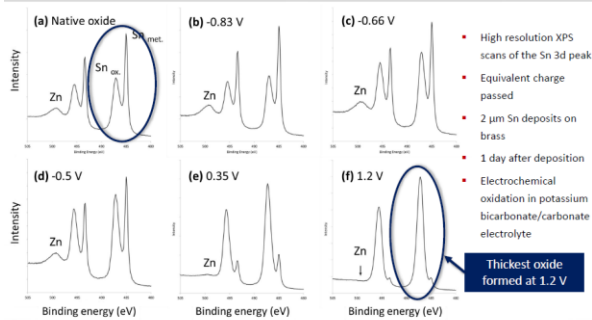
7



8



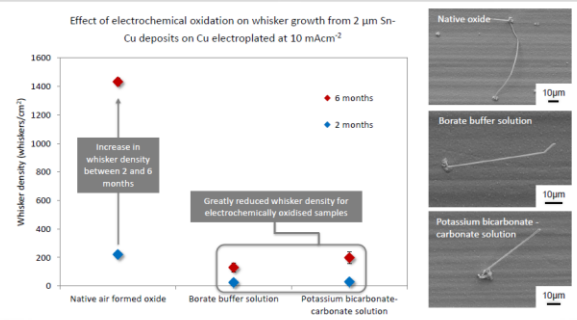
Evaluation of oxide thickness: XPS analysis



9



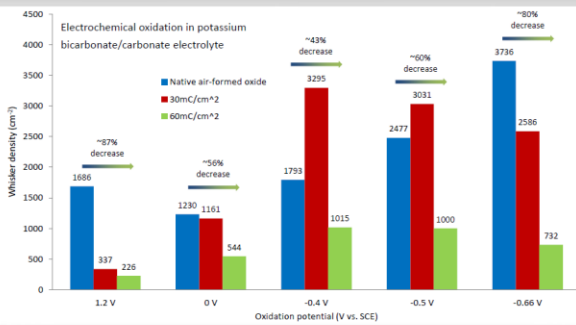
SnCu deposits on Cu: Electrochemical oxidation at 1.2V



10



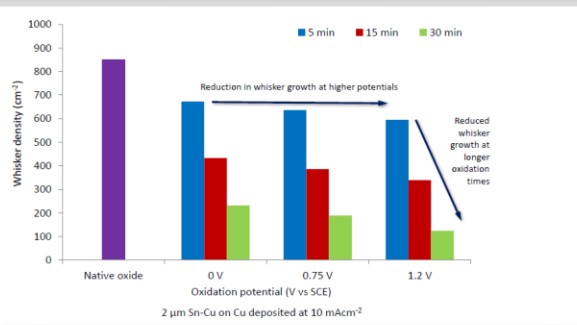
Whisker density after ~ 2 months storage



11



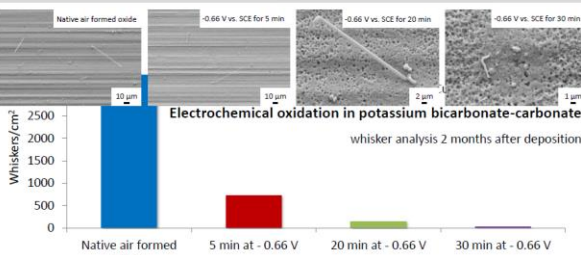
SnCu on Cu: oxidation in borate buffer



12



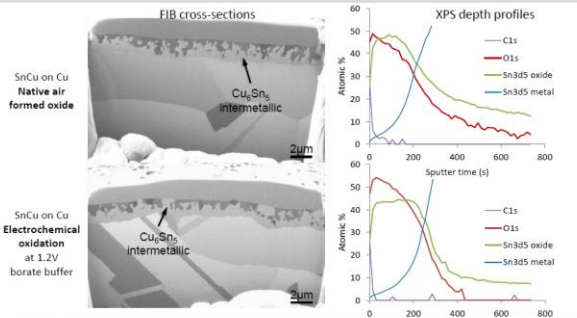
Effect of oxidation time: tin dissolution



13



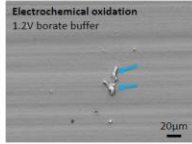
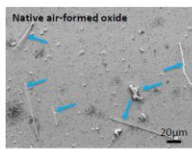
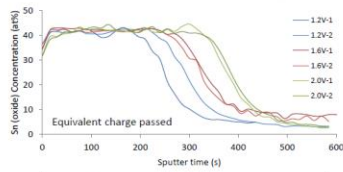
FIB/XPS analysis of SnCu deposits on Cu: ~2 years storage



14



Sn deposits on brass: whisker growth

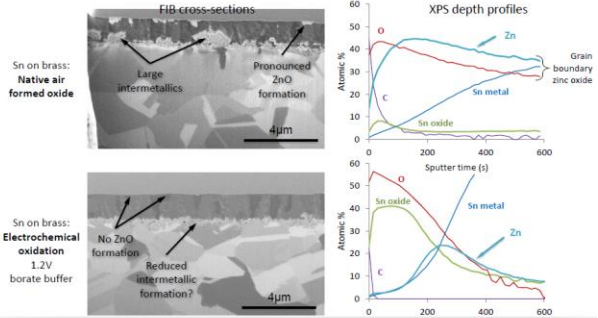


Number of whiskers on electrochemically oxidised deposits after 2 years storage (Sample area = 4cm ²)	
Oxidation potential [V vs SCE]	Average number of whiskers per sample
1.2 V	6 ± 2
1.6 V	2.5 ± 2
2.0 V	3 ± 2

Greatly reduced whisker growth for electrochemically oxidised deposits

15

FIB/XPS analysis of Sn deposits on brass: ~30 months storage



16

Whisker mitigation mechanism(s)

- For Sn(Cu) deposits on Cu, IMC formation appears unaffected by electrochemical oxidation and therefore whisker mitigation must simply be derived from the increased thickness of the oxide layer
- Although whisker density is greatly reduced for electrochemically oxidised SnCu deposits, long filament whiskers are still produced
- Electrochemical oxidation does not reduce the driving force for tin whisker growth (*intermetallic formation*)
- For Sn deposits on brass, electrochemical oxidation reduces whisker growth by preventing the formation of Zn oxide at the deposit surface
- Reduced IMC formation in electrochemically oxidised samples may also be an influence

17

Summary

- For the first time, a direct correlation has been demonstrated between oxide thickness and whisker growth.
- Greatly reduced whisker growth has been observed for electrochemically oxidised Sn-Cu deposits on Cu and pure Sn deposits on brass.
- The thickness of the oxide film developed by electrochemical oxidation is dependent upon the applied potential and charge passed.
- Comparable reductions in whisker growth were observed for deposits electrochemically oxidised in borate buffer and potassium bicarbonate-carbonate electrolyte solutions.

18

10.4 Conference Posters

leMRC 9th Annual and Final Conference, Loughborough University, February 2016



Tin Whiskers: The Effect of a Post-Electroplating Electrochemical Oxidation Treatment on Whisker Growth

D.M.Haspel, Dr M.A.Ashworth, Dr G.D.Wilcox & Prof. R.J.Mortimer

Introduction

The project aim was to mitigate tin whisker growth by means of an electrochemical oxide film. To date, no research has been carried out to investigate the effect of electrochemical oxide films on whisker growth, but Tu¹ suggests that when an oxide layer cracks whiskers will grow out of the cracks much like an extrusion; so having a thicker oxide film that would be more difficult to crack, would be advantageous. A tin whisker is a single crystal of pure tin that is in the form of a filamentary growth. Whiskers can grow up to a few millimetres and may be straight, kinked or curved as shown in figure [1]. Whiskers often cause problems in electronics by growing long enough to bridge between surfaces causing the circuit to short out, as shown in figure [2].

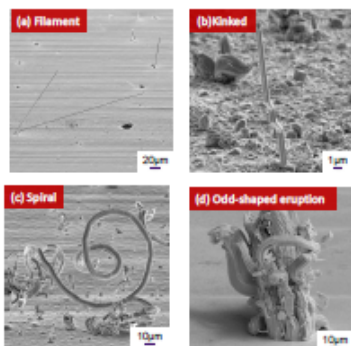


Figure [1] Examples of different whisker morphologies, (a) filament, (b) kinked, (c) spiral and (d) odd-shaped eruption

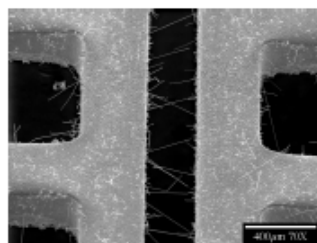


Figure [2] shows whiskers bridging a gap between two surfaces

Cyclic Voltammetry

Cyclic voltammetry was used to choose suitable oxidation potentials; a typical cyclic voltammogram is shown in figure [3]. The potentials chosen for oxidation in potassium bicarbonate-carbonate were -0.83V, -0.66V and 1.2V. These were chosen because they corresponded to the oxidation peaks, I & II (-0.83V & -0.66V vs. SCE, respectively), and 1.2V vs. SCE had been used in previous studies carried out in borate buffer solution. Further intermediate potentials were then selected to investigate how the oxide layer changes.

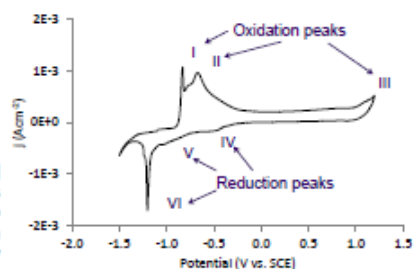


Figure [3] - cyclic voltammetry of tin in potassium bicarbonate-carbonate

Characterisation of Tin Oxides

Characterisation of the electrochemically formed tin oxides was carried out using XPS. Figure [4] shows that as the potential is increased the thickness of the electrochemically formed oxide is increased, for an equivalent charge passed. Depth profiles through these oxides were also carried out. Figure [5] shows that an oxide formed electrochemically at 1.2V vs. SCE, is much thicker than a native air formed oxide, which results in a dramatic reduction in whisker density (figure [6]). Increasing the duration of oxidation also increased oxide thickness, however this was at the expense of surface dissolution, which is illustrated in figure [7].

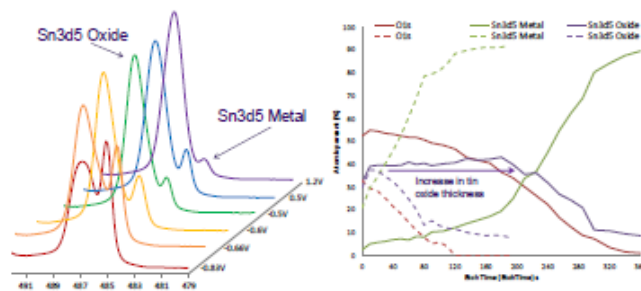


Figure [4] - high resolution scans of the Sn3d5 peak after oxidation at different potentials

Figure [5] - depth profiles comparing the (dashed) native air grown oxide and (solid) electrochemically formed oxide at a potential of 1.2V in potassium bicarbonate-carbonate

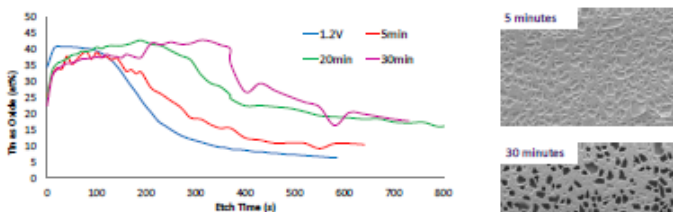


Figure [7] - depth profile showing how tin oxide thickness increases with time for samples oxidised at a potential of -0.66V vs. SCE. The micrographs (right) show the change in surface morphology with oxidation time

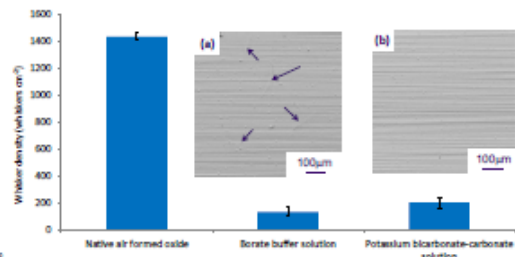


Figure [6] - graph showing a decrease in the number of whiskers present (after 6 months) after oxidation at 1.2V vs. SCE in both solutions and corresponding micrographs, taken ~150 days after deposition showing (a) surface of a native grown oxide and (b) surface of an electrochemically formed oxide at 1.2V vs. SCE in borate buffer, where the arrows are pointing to examples of whiskers.

Summary

- An electrochemical oxide formed at 1.2V vs. SCE is much thicker than a native air formed oxide
- Electrochemical oxides formed at 1.2V vs. SCE greatly reduces the number of whiskers
- Increasing oxidation time increases the thickness of the electrochemically formed oxide layer.
- Oxidising at -0.66V using the potassium solution results in tin dissolution.